University of Sheffield

Investigating novel approaches to stimulate oral soft tissue repair in medication-related osteonecrosis of the jaw

Krit Rattanawonsakul

A thesis submitted in partial fulfilment of the requirements for the degree of Doctor of Philosophy

The University of Sheffield
Faculty of Engineering
Department of Materials Science and Engineering

September 2023

Abstract

Medication-related osteonecrosis of the jaw (MRONJ) is characterised by exposed necrotic bone with persistent mucosal wounds in the oral cavity. The disease is found in patients receiving bisphosphonates for the treatment of osteoporosis, myeloma and bone metastasis. The current management of MRONJ remains challenging as existing therapies have inconsistent outcomes, are often ineffective and are unable to resolve the disease. Novel approaches, including geranylgeraniol (GGOH) and platelet-rich fibrin (PRF), have been introduced as potential solutions to enhance the healing of MRONJ wounds caused by bisphosphonate toxicity. However, the biological effects of these methods on oral soft tissue healing are yet to be fully understood.

The aim of this study was to evaluate the effects of GGOH and PRF, in particular a liquid-based, injectable formulation of PRF (I-PRF), on the behaviour of oral mucosa cells. We used two- (2D) and three-dimensional (3D) *in vitro* oral mucosa models to replicate MRONJ-like conditions. Zoledronate (ZA) and pamidronate (PA), the two bisphosphonates most commonly associated with MRONJ development, were used to induce oral mucosa toxicity as seen in MRONJ.

Our results revealed that both interventions produced some improvements in cellular activities linked to the healing process. A limited range of GGOH concentrations were able to reduce bisphosphonate toxicity in oral fibroblast, but were ineffective in keratinocytes. Combined treatment of GGOH and bisphosphonates led to a reduction of metabolic activity of oral mucosa cells.

I-PRF was shown to be biocompatible and demonstrated some positive effects on oral mucosal healing in the presence of bisphosphonates. I-PRF was shown to enhance cell proliferation and migration. I-PRF also partially protected the epithelial integrity of 3D oral mucosa models from ZA toxicity. We identified factors within I-PRF and suggest the potential role of these paracrine factors in mediating the cellular responses observed in this study.

The data presented here showed how cells from the oral mucosa responded to GGOH and I-PRF *in vitro*. These findings also demonstrated GGOH is unsuitable for the treatment of MRONJ given the narrow range of therapeutic concentrations and associated toxicity. In contrast results from this study highlighted the potential of I-PRF to support soft tissue repair in MRONJ treatment.

Acknowledgements

This thesis work could not be completed without the support of my lovely and dedicated supervisory team. First, I would like to express my gratitude and appreciation to my primary supervisor, Dr Vanessa Hearnden who offered me the invaluable opportunity to pursue my Ph.D. at The University of Sheffield. Her guidance, advice and support has been instrumental in shaping my academic journey.

I would also like to thank Dr Victoria Workman for her advice and encouragement during challenging moments, and for stepping into Vanessa's role during her maternity leave. Thanks also go to Professor Frederik Claeyssens, Dr Robert Bolt and Dr Simon Atkins for their specialised advice and support throughout the project. Special thanks also go to Dr George Bullock who was a mentor during my first year studying abroad and provided essential laboratory training for me.

I am extremely grateful for the financial support from the Faculty of Dentistry Mahidol University which has been crucial for the completion of this project. My appreciation also extends to Geistlich company for generously providing Mucograft® samples.

I would like to thank all those who provided the assistance throughout this work. Mrs Vanessa Singleton deserves special recognition for her support and suggestions on laboratory issues. I would also like to thank Sue and Kay from the Flow cytometry core facility for their support on the flow cytometer. Dr Chris Holland for rheometer training, Mrs Maggie Glover for her support with immunohistochemistry techniques.

I would also like to thank my colleagues in the Biomaterials and Tissue Engineering group at the Kroto Research Institute. Their support and encouragement are very vital to keep my mood and spirit high during the challenging time. Special acknowledgements go to Rachel Furmidge, Mina Aleemardani, Dr Samuel Higginbotham, and Dr Sanad Saad.

I would like to thank all my Thai friends, both in the UK and Thailand, whose always encourage and believe in my capabilities. Special thanks go to Ballad, Nam, Note, Mean, MD, Kim, Mook, June, Pukpik, Lhew and Bim.

Lastly, studying in the United Kingdom has been the longest and most distant period I have been away from my family. I would like to dedicate this achievement to my family – my mother, father, sister, and brother. Their love, faith, and constant support have been important in shaping me into who I am today. Their unwavering belief in me has been the greatest motivation force in my life and has driven me to complete this journey.

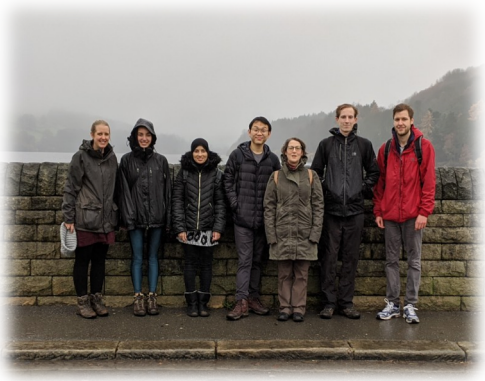

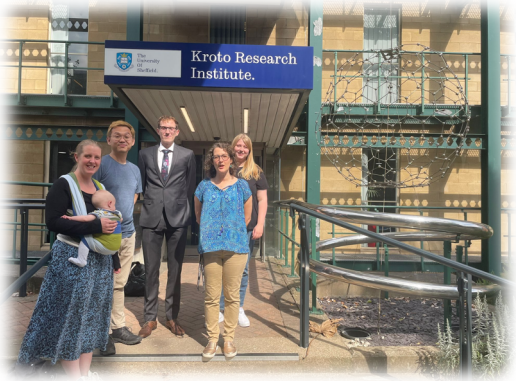

Outputs

Publications

- Rattanawonsakul K, Bullock G, Bolt R, Claeyssens F, Atkins S, Hearnden V. ***In vitro* Effect of Geranylgeraniol (GGOH) on Bisphosphonate-Induced Cytotoxicity of Oral Mucosa Cells.** Front Oral Health. 2022 Jun 20;3:892615. DOI: 10.3389/froh.2022.892615.

Oral Presentation

- **Identifying the mechanism of platelet-rich fibrin (PRF) on zoledronate-induced oral mucosa cell toxicity**. Post-Graduate Research Conference Day. Sheffield, United Kingdom (April 2022)
- **Platelet-rich fibrin protects epithelial layer of tissue engineered oral mucosa from zoledronate toxicity**. Biomaterials and Tissue Engineering Group Conference. York. United Kingdom (December 2022)
- **Platelet-Rich Fibrin Reduces Zoledronic Acid-Induced Oral Mucosa Toxicity *In Vitro.*** The Continental European Division together with the Scandinavian Division of the International Association for Dental Research (CED/NOF-IADR) Oral Health Research Congress (September 2023)

Poster presentations

- **The effect of Geranylgeraniol (GGOH) on zoledronate-induced toxicity on oral fibroblasts and keratinocytes**. Tissue and Cell Engineering Society (TCES) Conference (Virtual meeting), Edinburgh, United Kingdom (July 2021)
- ***In vitro* application of platelet-rich fibrin (PRF) in zoledronate-induced MRONJ on oral fibroblasts**. Biomaterials and Tissue Engineering Group (BITEG) Conference (Virtual meeting). Sheffield, United Kingdom (December 2021)
- **The Bioactivity of Platelet-rich fibrin (PRF) conditioned medium on Zoledronate-induced oral keratinocyte toxicity *in vitro*.** Tissue Engineering and Regenerative Medicine International Society (TERMIS)- European Chapter (In-person meeting). Krakow, Poland (June – July 2022)
- **Platelet-rich fibrin prevents the toxicity of pamidronate on oral fibroblasts.** Tissue Engineering and Regenerative Medicine International Society (TERMIS)-European Chapter (In-person meeting). Manchester, United Kingdom (March 2023)

Table of Contents

List of Abbreviations

2D	Two-dimensional
3D	Three-dimensional
α-SMA	Alpha-smooth muscle actin
°C	Degrees Celsius
µ	Micro
A-PRF/A-PRF+	Advanced-PRF/Advanced-PRF plus
AAOMS	American Association of Oral and Maxillofacial Surgeons
ADSCs	Adipose-derived stem cells
ALI	Air-liquid interface
ANOVA	Analysis of variance
ATP	Adenosine triphosphate
BDS	Broth Dilution Shaking
BMU	Basic Multicellular Units
BP	Bisphosphonate
BSA	Bovine serum albumin
$CaCl_2$	Calcium chloride
CFSE	Carboxy-fluorescein diacetate N-succinimidyl diester
cm^2	Square centimetre
CO_2	Carbon dioxide
CYP	Cytochrome P450
DAB	Diaminobenzidine
DED	De-epidermalised dermis
DMEM	Dulbecco's Modified Eagle Medium
DMSO	Dimethyl sulfoxide
ECM	Extracellular matrix
EDTA	Ethylenediaminetetraacetic acid
EGF	Epidermal growth factor
ELISA	Enzyme-linked immunosorbent assay
FBS	Foetal bovine serum
FGF	Fibroblast growth factor
FITC	Fluorescein isothiocyanate
FPP	Farnesyl pyrophosphate
FPPS	Farsenylpyrophosphate synthase
GAG	Glycosaminoglycan
GGOH	Geranylgeraniol
GGPP	Geranylgeranyl pyrophosphate
g	Gram
H&E	Haematoxylin and Eosin
H_2O_2	Hydrogen peroxide
HCl	Hydrochloric acid
HMG CoA	3-hydroxy-3-methylglutaryl coenzyme A

HRP	Horseradish-Peroxidase
HSCs	Haemopoietic Stem Cells
hTERT	Human Telomerase Reverse Transcriptase Enzyme
I-PRF	Injectable platelet-rich fibrin
i3T3	Irradiated mural fibroblasts
IGF	Insulin-like growth factor
IL	Interleukin
IMS	Industrial Methylated Spirit
IPP	Isopentenyl pyrophosphate
KGF	Keratinocyte growth factor
KSFM	Keratinocyte serum-free medium
L-PRF	Leucocyte-rich platelet rich fibrin
LLLT	Low-level laser therapy
LPS	Lipopolysaccharide
m	Milli, Metre
M	Molar
MFI	Mean fluorescence intensity
MMP	Matrix metalloproteinase
MRONJ	Medication-related osteonecrosis of the jaw
MSCs	Mesenchymal stem cells
MTS	3-(4,5-dimethylthiazol-2-yl)-5-(3-carboxymethoxyphenyl)-2-(4-sulfophenyl)-2H-tetrazolium
MTT	3-(4,5-dimethylthiazol-2-yl)-2,5-diphenyltetrazolium bromide
NaCl	Sodium chloride
NaOH	Sodium hydroxide
nm	Nanometre
NGF	Nerve growth factor
NO	Nitric oxide
NOFs	Primary oral fibroblasts
NOKs	Primary oral keratinocytes
OPG	Osteoprotegerin
P/S	Penicillin and Streptomycin
PA	Pamidronate
PBS	Phosphate buffered saline
PDGF	Platelet-derived growth factor
PI	Propidium iodide
PPARγ	Peroxisome proliferator-activated receptor gamma
PPP	Platelet-poor plasma
PRF	Platelet-rich fibrin
PRFR	Platelet-rich fibrin releasates
PRP	Platelet-rich plasma
RANK	Receptor activator of nuclear factor kappa-B
RCF	Relative centrifugation force

rhBMP-2	Recombinant human bone morphogenic protein-2
ROS	Reactive oxygen species
rpm	Revolutions per minute
SA-β-Gal	Senescence-associated beta-galactosidase
SD	Standard deviation
SIOX	Simple Interactive Object Extraction
SIRT	Sirtuin
T/T	3,3,5-Tri-iodothyronine /Apo-Transferrin
TBS	Tris buffered saline
TdT	Terminal deoxynucleotidyl transferase
TEOM	Tissue-engineered oral mucosa
TGF-β	Transforming growth factor-beta
TNF-α	Tumour necrosis factor-alpha
TRAP	Tartrate-resistant acid phosphatase
TUNEL	Terminal deoxynucleotidyl transferase-mediated dUTP nick end labelling
VEGF	Vascular endothelial growth factor
WST-1	Water soluble tetrazolium-1
ZA	Zoledronate

List of Figures

List of Tables

List of Equations

Declaration

I, the author, confirm that the Thesis is my own work. I am aware of the University's Guidance on the Use of Unfair Means (www.sheffield.ac.uk/ssid/unfair-means). This work has not been previously been presented for an award at this, or any other, university.

I would like to declare that the work in Chapter 4 has already been published in a peer-review journal with the details of contribution as indicated below:

Chapter 4

Rattanawonsakul K, Bullock G, Bolt R, Claeyssens F, Atkins S, Hearnden V. ***In vitro* Effect of Geranylgeraniol (GGOH) on Bisphosphonate-Induced Cytotoxicity of Oral Mucosa Cells.** Front Oral Health. 2022 Jun 20;3:892615. DOI: 10.3389/froh.2022.892615.

Author Contribution:

KR was the primary contributor responsible for designing and conducting the experiments, collecting, and analysing the data, and drafting the manuscript. All other authors contributed through supervision and revisions the manuscript.

CHAPTER 1

Introduction

1. Introduction

Medication-related osteonecrosis of the jaw (MRONJ) is an unwanted clinical condition defined when necrotic bone tissue in the maxilla or mandible becomes exposed and the oral mucosa breaks down and fails to maintain a protective barrier. This may lead to symptoms including infection, pain, and loss of function [1]. MRONJ is predominantly seen in patients receiving antiresorptive drugs called bisphosphonates which are primarily used to treat osteoporosis and bone malignancies [2]. However, the disease has also been observed in those receiving other medications including denosumab which is another antiresorptive agent, and antiangiogenic drugs such as sunitinib or bevacizumab [3]–[5].

As the number of patients receiving bisphosphonate therapy has escalated, millions of people worldwide are currently at risk of developing MRONJ [2]. In cancer patients receiving intravenous bisphosphonates, the risk of developing the disease is up to 18% [1]. It has been reported that approximately 10 patients per millions per year suffer from having MRONJ and the disease reduces their quality of life [6]. Unfortunately, current treatment strategies are not able to cure the disease [7]. Thereby, raising the importance of developing alternative strategies to manage the disease effectively.

Several approaches have been proposed including the use of geranylgeraniol (GGOH) and platelet-rich fibrin (PRF). Both treatments have demonstrated potential benefits in reducing the toxicity of bisphosphonates on the oral mucosa [8]–[10]. However, the effects remain unclear and the mechanisms of action of these interventions are questionable. Thus, it is important to gain more understanding of these potential therapies. This project aimed to develop and evaluate novel strategies for repairing soft tissue wounds in MRONJ.

This thesis begins with an extensive literature review addressing the biology of bone and oral mucosa. This is followed by the pharmacology of bisphosphonates as this class of drugs are the main cause of MRONJ development. Following this, details of MRONJ disease are described with a focus on the potential treatment approaches already explored in the literature.

The 1st experimental chapter (Chapter 4) focuses on the first potential method which is geranylgeraniol (GGOH). The effect of GGOH on oral mucosa cells and whether it can prevent or reduce the toxicity of bisphosphonates on oral mucosa has been examined.

Subsequently, another promising approach which is platelet concentrates, particularly PRF, will be explored. In the 2nd experimental chapter (Chapter 5), the method to prepare the injectable formulation of PRF, or I-PRF, is outlined. The paracrine factors present in the I-PRF have been identified and the effect of I-PRF on oral mucosa and oral wound healing with *in vitro* models has been assessed.

In the last experimental chapter (Chapter 6), the potential role of I-PRF on reversing bisphosphonate-induced soft tissue toxicity *in vitro* has been investigated. This is to provide details on the impact of I-PRF in curing MRONJ and to evaluate the effectiveness of I-PRF in the treatment of this disease.

CHAPTER 2

Literature Review

2. Literature Review

This literature review firstly describes the process of bone remodelling and the anatomy and physiology of the oral mucosa followed by the process of oral wound and socket healing since MRONJ affects both the soft and hard tissues of the oral cavity. The pharmacology of bisphosphonates will then be introduced and how these and other drugs cause the development of MRONJ will be explained. Following this, I will describe in detail what is known about the mechanism of MRONJ development, current treatment strategies and then review novel therapies which are being investigated.

2.1 Bone

2.1.1 Bone biology

Bone is a mineralised connective tissue that functions as a supportive and protective framework, mineral reservoir, potentiates haematopoiesis and facilitates locomotion of the human body [11], [12]. This specialised architecture is a highly dynamic organ that is constantly and continuously remodelled in order to preserve structural integrity and protect from mechanical forces or pathological damage [13].

The structure of bone consists of cells and extracellular bone matrix [14]. Four main cells are present in bone tissue: osteoblasts, osteoclasts, osteocytes and bone-lining cells; each cell type provides different functions for regulating bone homeostasis [15]. The chemical composition of the bone comprises inorganic components, which account for approximately 65%, while organic substances and water constitute approximately 35% [12]. The organic content of bone is composed of around 90% of collagen, in particular type I, while the remaining are the non-collagenous proteins such as osteocalcin, osteopontin, bone sialoprotein, and bone morphogenic proteins [16], [17]. The mineralised compartment is primarily made up of calcium and phosphate ions in the form of hydroxyapatite crystals [15]. Bone matrix materials contribute to the mechanical rigidity, elasticity, and flexibility of bone structure [16].

2.1.2 Physiology of bone remodelling

Bone remodelling is the continuous cycle of replacing old bone with newly formed tissue by a group of osteogenic cells called basic multicellular units (BMU) [18], [19]. Bone normally takes around 3-6 months to completely remodel [11], [20]. The overall process of bone remodelling is illustrated in Figure 2.1. The activation of the receptor activator of nuclear factor kappa-B (RANK) signalling pathway stimulates the fusion of mononuclear-macrophage progenitors (osteoclast precursors), forming multinucleated osteoclasts [15]. These polykaryotic cells then undergo polarisation creating the cytoskeleton reorganisation and ruffled border formation which is crucial for osteoclast adhesion and bone resorption activity [13], [15], [17], [21]. The ruffled border allows the release of protons (H^+) through a vacuolar proton pump (V-ATPase) and chloride ions (Cl^-) *via* chloride channels into the resorbing area causing the dissolution of hydroxyapatite minerals. The morphology of osteoclasts during bone resorption is shown in Figure 2.2. The ruffled border region also plays a part in degrading the organic component of bone by releasing several lysosomal proteases such as tartrate-resistant acid phosphatase (TRAP), cathepsins K and matrix metalloproteinases (MMPs) [13], [15], [22], [23]. After resorption, osteoblasts, which are derived from osteogenic mesenchymal stem cells (MSCs), play a significant role in bone formation by producing new osteoid matrices and processing bone mineralisation, shown in Figure 2.1. The remodelling process terminates when osteoblasts are embedded in the bone matrix and become osteocytes [13].

Abnormalities in osteogenic cell functions and activities cause an alteration in bone homeostasis and may lead to the development of several skeletal-related disorders such as osteoporosis, parathyroid-associated diseases, Paget disease of bone, osteogenesis imperfecta or osteopetrosis [24].

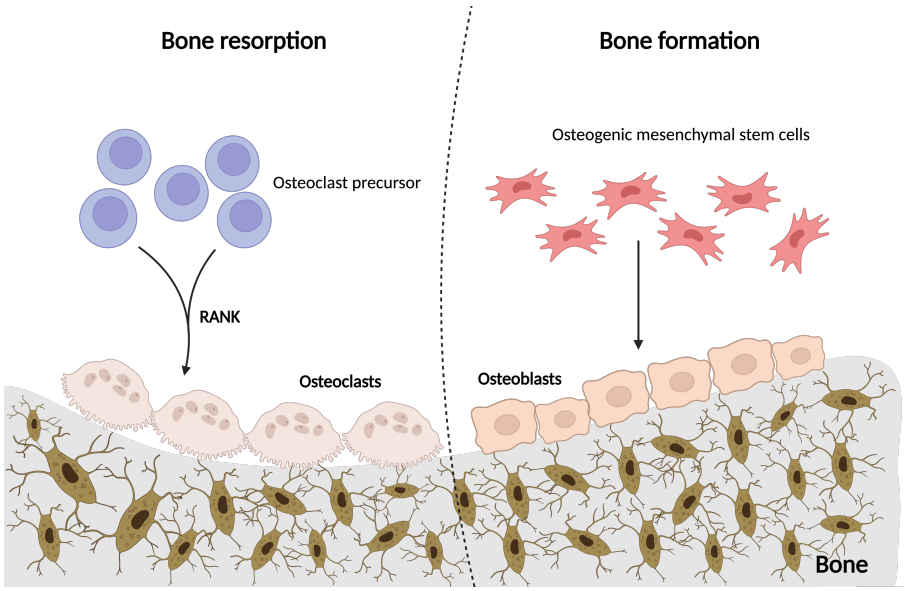

Figure 2.1 | ***Overview of the bone remodelling cycle.*** *This diagram illustrates the dual processes of bone resorption and formation in bone remodelling. On the left, is depicted bone resorption via RANK signalling activation, leading to mononuclear-macrophage progenitors fusing into multinucleated osteoclasts for bone resorption. On the right, osteoblasts, derived from mesenchymal stem cells are depicted engaging in bone formation. Figure created using Biorender.com. Abbreviations: RANK, receptor activator of nuclear factor kappa-B.*

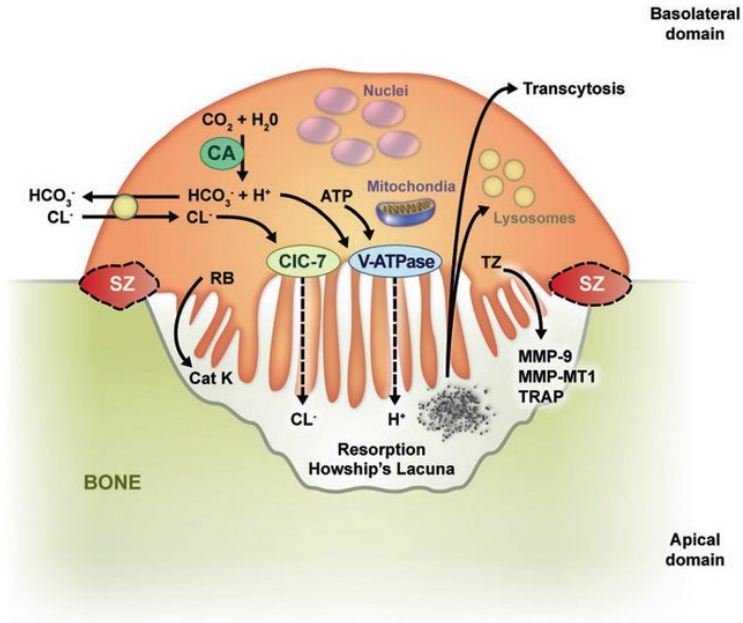

Figure 2.2 | ***Osteoclasts during bone resorption****. This schematic shows the process of bone resorption by osteoclasts, highlighting the ruffled border where CIC-7 and V-ATPase ion channels release chloride ions and protons, respectively, in order to dissolve hydroxyapatite in bone. Enzymes including Cathepsin K (Cat K), Tartrate-resistant acid phosphatase (TRAP) and various matrix metalloproteinases (MMPs) are also released for breaking down the organic components of bone. Figure reproduced with permission from Gasser et al., [23] under Copyright Clearance Centre Rights license number 5624951357125. Abbreviations: SZ, sealing zone; RB, ruffled border; TZ, transition zone; Cat K, cathepsin K; MMP, matrix metalloproteinase; TRAP, tartrate-resistant acid phosphatase.*

2.2 Oral mucosa

2.2.1 Anatomy

The oral mucosa is a moist and resilient soft tissue membrane covering the oral cavity. Its primary role is to protect underlying tissues from mechanical forces, chemical stimuli, and microorganism invasion. Furthermore, this mucous barrier also has function in taste sensation, touch perception, and salivary secretion [14]. The oral mucosa can be divided into three types based on their characteristics which are: lining mucosa, masticatory mucosa, and specialised mucosa. The more flexible lining mucosa covers most of the oral cavity areas including lips, buccal mucosa, alveolar mucosa, and floor of mouth. The hard palate and attached gingiva which are bound tightly with underlying tissues are considered as masticatory mucosa. Specialised mucosa is found at the dorsum surface of tongue [14], [25]. The location of each oral mucosa type is illustrated in Figure 2.3 [26]. This section covers the anatomy of lining mucosa and masticatory mucosa.

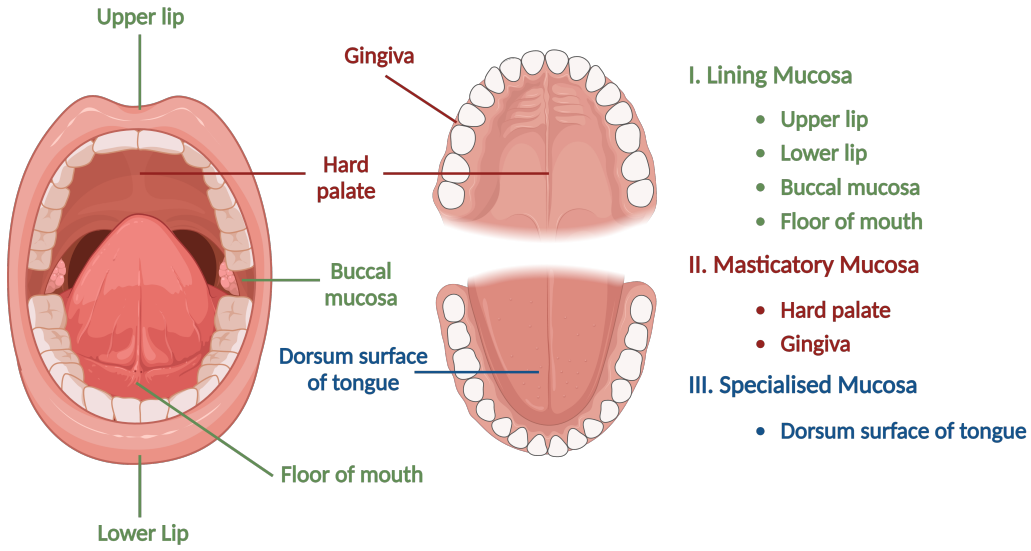

Figure 2.3 | ***Anatomical location of each type of oral mucosa***. *This schematic figure illustrates anatomical locations of the three distinct types of oral mucosa: lining, masticatory and specialised mucosa. Each type is mapped with a different colour to specific regions where it is found within the oral cavity. Figure created using Biorender.com.*

The oral mucosa comprises of an epithelium, a basement membrane, lamina propria, and submucosal tissue lying over muscle or bone [27]. Variation of cell layer patterns and thickness have been found in each type of oral mucosa depending on anatomical region and its functional demand [27], [28]. In general, buccal mucosa is approximately 500-800 µm in thickness while the other regions such as gingiva or sublingual mucosa measure between 100-200 µm [29]. The structure of oral mucosa with the layers of stratified squamous epithelium is demonstrated in Figure 2.4 and Figure 2.5, a haematoxylin and eosin (H&E) stained section of healthy oral mucosa.

The epithelial layer is a stratified squamous epithelium which is made up of several layers of proliferating and maturing keratinocytes [26]. The innermost epithelium layer, which rests above the basal lamina, is called the stratum basale. This basal layer consists of a single layer of cuboidal cells with a high proliferation capacity. These cells are connected to the underlying basement membrane *via* hemidesmosomes and focal adhesions while desmosomes provide attachment between adjacent keratinocytes [28]. On top of the basal layer, there are multiple rows of ovoid-shaped keratinocytes with spine-like projections, known as the spinous cell layer or stratum spinosum [28]. Around two-thirds of the epithelium thickness is composed of these two layers [14]. As cells continue migrating superficially in the layer called stratum granulosum, morphologies appear to be more flattened than spinous cells and basophilic keratohyalin granules can be observed [14]. The maturation of keratinocytes ends at the surface layer or keratinised layer. Cells are completely flat with no nucleus and no organelles, which is called ortho-keratinisation. This epithelium pattern is regularly found at the masticatory mucosa. The gingiva demonstrates a physiological variation called para-keratinisation where some cells in the most superficial layer still contain a shrunken nucleus [14]. In contrast, the lining mucosa is non-keratinised and exhibits different histological features from keratinised epithelium. The two innermost layers, the stratum basale and the stratum spinosum, retain similarities to the characteristics of keratinised epithelium. Instead of having a granular layer, the subsequent layer is termed the stratum intermedium or the intermediate layer, comprising of flattened keratinocytes containing dispersed tonofilaments and glycogen without keratohyalin granules. The outermost layer consists of flattened keratinocytes with prominent nuclei, known as the stratum superficiale [14].

The interface between the epithelium and underlying connective tissue is separated by a basement membrane which is a meshwork of type IV collagen, laminin V, and several glycoproteins [14], [28]. In this region, the structure is arranged in a “wavy” pattern due to the finger-like epithelial projections, which are termed rete ridges, that interdigitate with connective tissue papilla [28]. The structure creates a large surface area which provides good attachment and mechanical force dispersion [30].

The connective tissue located below the basement membrane is called the lamina propria. The majority of cells are fibroblasts which are responsible for fibres and extracellular matrix production. This matrix contains collagen (type I and III) and elastin fibres embedded in amorphous ground substances [14]. Underneath the lamina propria is a submucosa layer containing fatty tissue, salivary glands, blood vessels, and nerves that supply the oral mucosa. However, some regions such as attached gingiva and parts of hard palate do not have this layer. The lamina propria is directly attached to the underlying bone which is called the mucoperiosteum [14]. Figure 2.6 shows the comparison of tissue components in oral mucosa and mucoperiosteum [31].

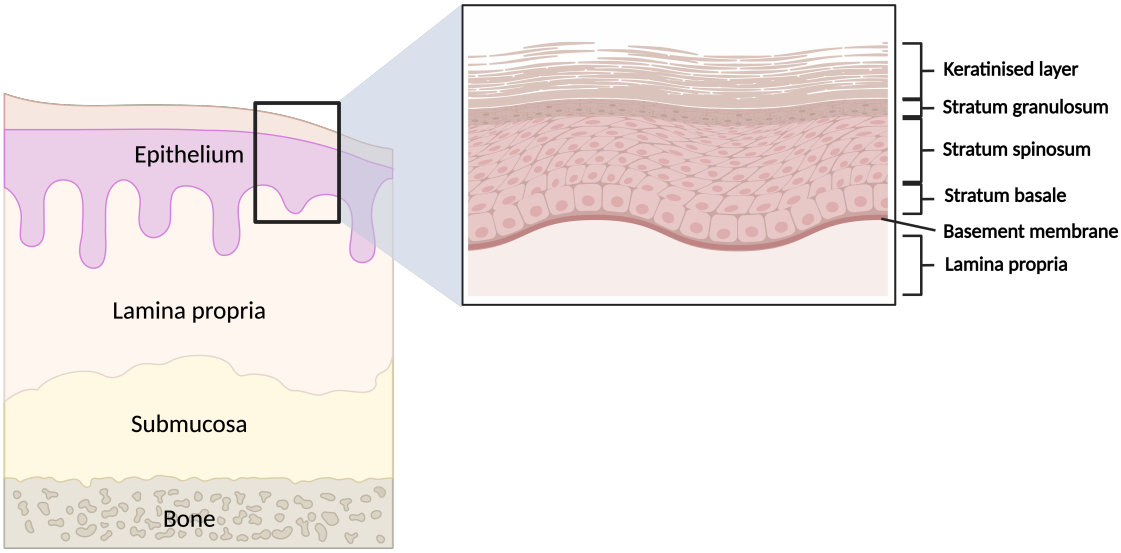

Figure 2.4 | ***The schematic structure of oral mucosa and the layers of stratified squamous epithelium***. *This figure illustrates the composition of oral mucosa, featuring the epithelium, lamina propria, submucosa and underlying bone. Four layers of the stratified squamous epithelium (stratum basale, stratum spinosum, stratum granulosum and keratinised layer) are detailed. The basement membrane is shown as a boundary between the epithelium and the lamina propria. Figure created using Biorender.com.*

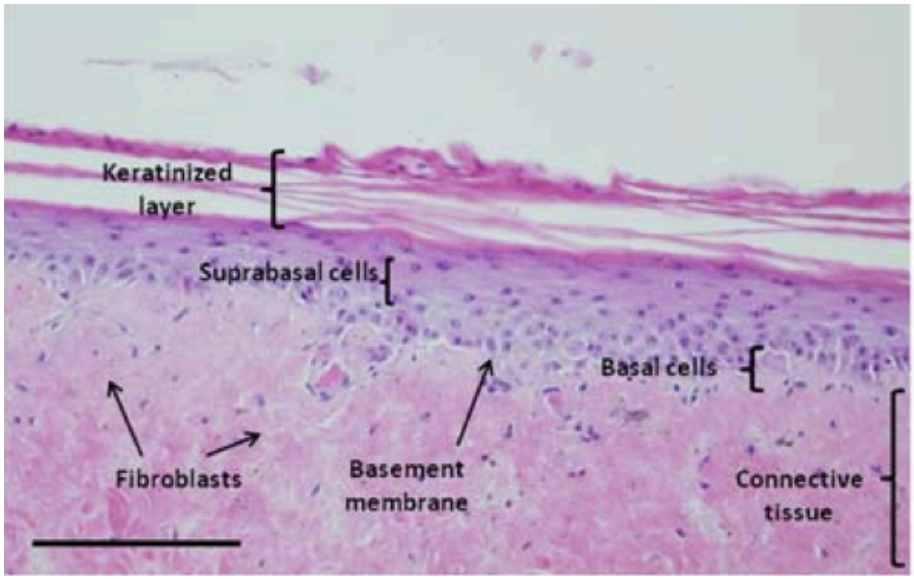

Figure 2.5 | ***Histological sections of healthy oral mucosa stained with haematoxylin and eosin.*** *The section illustrates the stratified squamous epithelium of oral mucosa, including basal and suprabasal layers, and the keratinised uppermost layer. The epithelium is supported by a connective tissue layer containing fibroblasts. Scale bar = 200 µm. Figure reproduced with permission from Hearnden et al.,* [32] *under Copyright Clearance Centre Rights license number 5624960970469.*

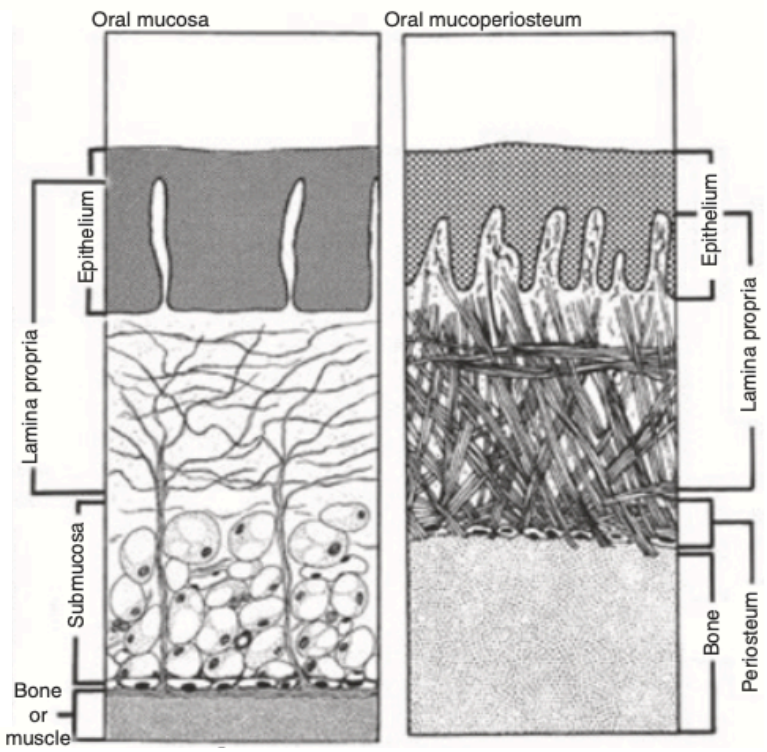

Figure 2.6 | ***Comparison of tissue components in oral mucosa and mucoperiosteum.*** *This figure illustrates the structural differences between oral mucosa (left) and mucoperiosteum (right). In oral mucosa, a submucosal layer is present between lamina propria and the bone while the lamina propria directly adheres to the underlying bone in mucoperiosteum. Figure reproduced with permission from Cruchley et al., [31] under Copyright Clearance Centre Rights license number 5626960515894.*

2.2.2 Physiology of oral wound healing

Since the oral mucosa is continuously subject to insults such as harmful substances, pathogens, and traumatic occasions [33], [34], the wound healing process plays an important role in reconstructing damaged tissues of the oral cavity. The healing procedure proceeds through a sequence of overlapping stages including the coagulation and inflammatory phase, proliferative or new tissue formation phase, and remodelling phase [35]. Multiple cell types including keratinocytes, fibroblasts, platelets, macrophages, and endothelial cells are involved during each stage of the healing process [36]. These cellular interactions are mediated by growth factors, cytokines, and inflammatory mediators which function in a coordinated manner to support the healing of wounds [37]. Figure 2.7 demonstrates the overall wound healing process [38].

The wound healing process begins by closing the wound with a newly formed blood clot which is a platelet plug embedded in a provisional extracellular matrix (ECM) made of fibrin and adhesion molecules such as fibronectin or vitronectin [35]. Platelets are degranulated and release chemotactic factors such as platelet-derived growth factors (PDGFs), transforming growth factor-beta (TGF-β) and epidermal growth factor (EGF) [37]. These mediators are responsible for recruiting inflammatory cells to the wound site [39], [40]. Neutrophils arrive first to counteract against bacteria invasion and remove necrotic tissues through their phagocytotic and protease secretion properties. This is followed by macrophages which appear within 24 hours to continue supporting the host defence, remove apoptotic cells and debris and prepare the wound for tissue regeneration [34], [35], [39], [41]. Pro-inflammatory cytokines such as interleukin-1 (IL-1), interleukin-6 (IL-6), tumour necrosis factor-alpha (TNF-α), and growth factors including fibroblast growth factor (FGF) are released from macrophages during the inflammatory phase of wound healing [37], [42]. This step lasts around 4 to 6 days after wounding [39].

The proliferative phase takes place 4 to 21 days after injury [39], [43]. This stage involves re-epithelialisation, vascular reconstruction, granulation tissue formation and connective tissue production [43]. Re-epithelialisation occurs when basal keratinocytes loosen their adhesions and migrate across the wound bed [33], [44]. The suprabasal cells also participate in the migration by rolling over the basal keratinocytes to form a new leading edge [45]. The migration continues until the leading cells from both wound edges

reach each other, known as contact inhibition [33]. The migratory activity of keratinocytes is mediated through a variety of signalling molecules including EGF, nitric oxide (NO), keratinocyte growth factor (KGF), insulin-like growth factor (IGF) and nerve growth factor (NGF) [43]. Meanwhile, the adjacent basal keratinocytes behind the migrating epithelium also proliferate to generate an adequate amount of cells for wound closure [46]. After the wound is covered by a layer of keratinocytes, cells stop dividing and start stratifying to reconstruct the epithelium [44], [47].

The vascular network is also restored to provide nutrients and oxygen during the healing process [43]. Activation of endothelial cells by angiogenic factors such as vascular endothelial growth factor (VEGF) or basic fibroblast growth factor (bFGF) allows them to migrate, proliferate and finally form new blood vessels [35]. During this process, fibroblasts simultaneously proliferate and migrate into the wounds under the control of FGF, TGF-β and PDGF [37], [43]. Fibroblasts are responsible for a variety of functions including MMP production, for dissolving the provisional fibrin-based framework, and the synthesis of ECM substances such as collagen, proteoglycans and hyaluronic acid [41], [43]. Fibroblasts, blood vessels and macrophages, along with collagen bundles, together form the granulation tissues which replace the temporary fibrin matrix [33], [41], [44]. This highly vascularised tissue becomes a scaffold for cell growth, adhesion, and differentiation in the wound healing process [41], [43]. In the later part of the proliferative phase, the presence of TGF-β promotes the differentiation of fibroblasts into myofibroblasts [35]. These differentiated fibroblasts, characterised by an increase of alpha-smooth muscle actin (α-SMA) expression, facilitate the contraction of wounds [43]. Oral fibroblasts express higher basal levels of α-SMA than dermal fibroblasts [48], resulting in a faster contraction and healing of the oral wounds compared to the skin.

The final stage of wound healing is the remodelling phase which occurs approximately 2-3 weeks after injury and can last for one year [44]. When wounds are completely matured and healed the majority of cells including myofibroblasts, fibroblasts, macrophages, and endothelial cells undergo apoptosis [34], [41]. Furthermore, the collagen component in ECM is converted from type III in the granulation tissues to type I which improves the tensile strength [43]. The production of new collagen and breakdown of old

collagen are mediated by TGF-β and PDGF, respectively [37]. Scar formation in skin is produced as a result of the interaction between myofibroblasts and collagen type I [49].

Although skin and oral mucosa share the same principles of healing process, there are significant differences between these two. Oral wounds demonstrate a faster healing rate and less scar formation when compared with dermal wounds [25], [34]. Several contributing factors have been reported to explain this phenomenon. Both oral keratinocytes and fibroblasts exhibit higher proliferation and migration capacity [50], [51]. In addition, it is proposed the expression of a foetal phenotype in oral fibroblasts leads to a similar healing pattern as foetal wounds, which exhibit minimal scarring [51]. Components in saliva such as peptides and growth factors also facilitate rapid wound closure in the oral cavity [52]. Oral wounds also express lower levels of TGF-β1 than the dermal wounds which is known as the indicator for scar formation [53]. In addition, oral fibroblasts exhibit resistance to the differentiation process into myofibroblast, which is mediated by TGF-β1 [54]. These all support a quicker healing process and reduced scarring in oral wounds.

The interplay between keratinocytes and fibroblasts plays a critical role in wound healing. These cellular activities are driven by numerous growth factors and cytokines which are released from a variety of sources such as platelets, serum of injured blood vessels, and the surrounding tissues [42]. Table 2.1 summarises growth factors and mediators involved in the wound healing process.

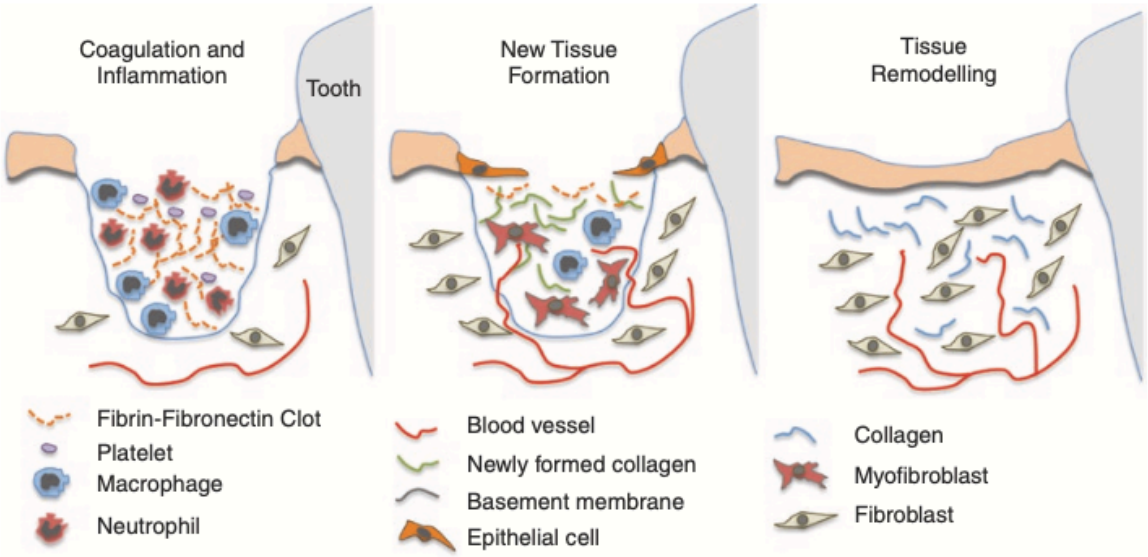

Figure 2.7 | ***Stages of the wound healing process.*** *The primary stages of the wound healing process are shown (coagulation and inflammation, new tissue formation or proliferative, and tissue remodelling phases), highlighting the key cellular elements involved in each phase. Figure reproduced with permission from Smith et al.,* [38] *under Copyright Clearance Centre Rights license number 5624961143875.*

Table 2.1 | ***Growth factors and mediators involved in the wound healing process*** [37], [42], [55]–[59]

Growth factors and mediators	Source	Function(s)
PDGF	Platelets, Keratinocytes, Macrophages, Endothelial cells, Fibroblasts	• Initiate the inflammatory responses during the early healing stages and recruit neutrophils, monocytes, and fibroblasts to the wound sites • Stimulate the granulation tissue formation • Regulate re-epithelialisation • Stimulate fibroblast proliferation • Regulate ECM production and remodelling
TGF-β	Platelets, Macrophages, Lymphocytes, Fibroblasts, Keratinocytes	• Recruit inflammatory cells and fibroblasts to the wound sites • Facilitate granulation tissue formation • Promote fibroblast proliferation and migration • Induce keratinocyte migration and proliferation • Stimulate angiogenesis • Stimulate collagen production
EGF	Platelets, Macrophages, Fibroblasts	• Promote keratinocyte migration and proliferation during re-epithelialisation stage • Stimulate granulation tissue formation
KGF-1 (FGF-7)	Fibroblasts, Endothelial cells	• Enhance epithelial cell proliferation and migration during re-epithelialisation stage • Stimulate neovascularisation
IGF	Liver, Macrophages, Fibroblasts	• Regulate epithelial cell migration
NGF	Fibroblasts, Epithelial cells, Endothelial cells	• Stimulate nerve ingrowth • Stimulate epithelial cell proliferation and inhibit cell apoptosis • Stimulate fibroblast migration

Abbreviations: PDGF, platelet-derived growth factor; TGF-β, transforming growth factor-beta; EGF, epidermal growth factor; KGF-1, keratinocyte growth factor-1; IGF, insulin-like growth factor; NGF, nerve growth factor.

Table 2.1 (continued) | Growth factors and mediators involved in the wound healing process

Growth factors and mediators	Source	Function(s)
VEGF	Platelets, Neutrophils, Epithelial cells, Macrophages, Fibroblasts	• Promote angiogenesis • Regulate the formation of the granulation tissues
bFGF (FGF-2)	Endothelial cells, Macrophages, Fibroblasts, Keratinocytes,	• Regulate granulation tissue formation • Promote keratinocyte migration during re-epithelialisation • Promote fibroblast migration • Regulate ECM synthesis and deposition
IL-1	Neutrophils, Monocytes, Macrophages, Keratinocytes	• Stimulate inflammatory responses • Stimulate keratinocyte and fibroblast proliferation
IL-6	Macrophages, Neutrophils	• Stimulate inflammatory responses
IL-10	Macrophages	• Anti-inflammatory cytokines • Regulate the growth of keratinocytes, endothelial cells, and immune cells
TNF-α	Macrophages, Lymphocytes,	• Facilitate keratinocyte migration and proliferation

Abbreviations: VEGF, vascular endothelial growth factor; bFGF, basic fibroblast growth factor; IL, interleukin; TNF-α, tumour necrosis growth factor-alpha.

2.2.3 Physiology of extraction socket healing

The process of extraction socket healing after tooth extraction follows the same sequences of soft tissue healing described above with the additional involvement of bone healing [33]. After tooth removal, the socket space is immediately filled with blood and the injured vessels are sealed by a blood clot to stop bleeding [60]. The healing process continues with re-epithelisation and granulation tissue formation within the first week [33], [61]. The next stage, during the subsequent week, is the formation of a provisional matrix consisting of mesenchymal cells, collagen and blood vessels to replace the granulation tissue, followed by the beginning of bone mineralisation [62], [63]. The woven bone with finger-like projections is firstly developed within two weeks and completely remodelled into the lamella bone and bone marrow tissues after 9 to 12 months [60], [63].

2.2.4 Tissue-engineered oral mucosa (TEOM)

A shift from *in vivo* research to *in vitro* testing has been occurring across various scientific fields [64]. This transition is in accordance to the principle of the 3Rs proposed by Russell and Burch, aiming to replace the use of animal studies, reduce the number of animals used, and minimise the potential discomfort resulting from experimentation [65]. *In vitro* investigations also help overcome the possible ethical concerns from clinical studies in humans. For this reason, *in vitro* models that closely resemble a physiological environment *in vivo* are needed to gain more understanding in the process of wound healing [66].

The simplest technique which has been widely used is a monolayer or two-dimensional (2D) cell culture to investigate the responses of oral mucosa cells to substances [67]. However, this technique fails to mimic the three-dimensional (3D) structure, behaviour, and microenvironment of native tissues [32], [64]. Advancements in tissue engineering have led to the development of tissue-engineered oral mucosa (TEOM) which is more relevant to native characteristics of the oral mucosa [68].

TEOM was originally developed by Masuda and colleagues in 1996 [69]. Human oral keratinocytes isolated from the gingiva were seeded on top of contracted collagen gel containing gingival fibroblasts which resembled the lamina propria layer of the oral mucosa. TEOM was cultured at an air-liquid interface (ALI) and found to demonstrate

normal characteristics of oral mucosa including stratified epithelial layers with well-differentiated keratinocytes. Throughout the years, the protocol for TEOM construction has been optimised and modified with three key elements involved (i) cells, (ii) culture medium, and (iii) scaffolds [70].

Keratinocytes and fibroblasts, the two main cellular components of the oral mucosa, are used to produce the TEOM. Most TEOM models are currently constructed by co-culturing primary oral keratinocytes on top of a scaffold containing oral fibroblasts at an ALI [64]. Fibroblasts play a pivotal role in supporting the growth and differentiation of the overlying epithelium of TEOM through the modulation of keratinocyte behaviour [71], [72]. The ALI culture method additionally encourages keratinocyte ability to proliferate and differentiate, forming a multilayer stratified structure that closely resembles the native oral epithelium [32].

Primary cells isolated from oral tissues such as hard palate, gingiva, or buccal mucosa, were originally used [70]. However, several drawbacks have been mentioned, particularly for primary keratinocytes, since cell supply depends on each donor. Primary cells also have limited proliferative capacity and batch-to-batch variability [64]. The use of immortalised cell lines substituted these cells to construct TEOM. However, some keratinocyte cell lines such as TR146 could not fully differentiate. TR146 cells are buccal carcinoma cell lines, thereby they are not a good representative for normal oral keratinocyte in terms of the morphology and characteristics [73].

Later studies have used immortalised keratinocytes with an overexpression of human telomerase reverse transcriptase enzyme (hTERT) in the fabrication of TEOM. The hTERT enzyme help elongates the telomeres, thereby allowing cells to continue dividing and prolonging the lifespan of cells [74]. As a result, cells are unable to enter the stage of senescence or undergo cell death, making these cells immortalised [75]. Two immortalised oral keratinocytes cell lines, OKF6/TERT-2 which were originally derived from the floor of mouth, and FNB6/TERT isolated from the buccal mucosa, have been reported in the literature to successfully produce TEOM [64], [76]. The histological appearance of TEOM produced by either cell line demonstrated a multilayer epithelium [64], [77], [78]. However, it was shown that the epithelium of TEOM containing OKF6/TERT-2 was poorly differentiated [78], [79]. Work by Jennings *et al.*, demonstrated a well-differentiated

stratified epithelium of TEOM using FNB6/TERT cells [64]. They also found that the expression of cytokeratins and pro-inflammatory gene profile in TEOM constructed from FNB6/TERT cells resembles those made up from primary cells [64], thereby suggesting more favourable characteristics for using FNB6/TERT cells over the OKF6/TERT-2 cell lines in TEOM construction.

In terms of culture medium, the most common medium used for TEOM construction is a mixture of Dulbecco's Modified Eagle Medium (DMEM) and Ham's F12 nutrient solution with a variety of supplements including foetal bovine serum (FBS), L-glutamine, adenine, insulin, transferrin, tri-iodothyronine, hydrocortisone, epidermal growth factor (EGF), penicillin and streptomycin (P/S), amphotericin B, and cholera toxin. The use of a serum-free medium to produce the TEOM has also been reported [70]. Izumi *et al.*, indicated that the aim was to reduce the exposure xenogenic DNA or viruses that could potentially exist in serum, as a result they were able to produce a multi-layered epithelium TEOM, with an increased number of proliferative keratinocytes [80].

Another important essential element for TEOM construction is a scaffold which resembles the lamina propria layer of the native tissues and provides a supportive structure for cells [70]. A variety of naturally-derived materials including collagen, gelatin, and fibrin have been utilised to successfully produce *in vitro* models of TEOM [70]. Most of these models are based on a collagen matrix embedded with fibroblasts. For example, Jennings *et al.*, produced and characterised TEOM using rat tail collagen. Their models demonstrate a similar histological and immunohistochemical appearance to the native oral mucosa as previously described [64]. These materials; however, have been reported as having poor mechanical properties [70]. In addition, the amount of ECM produced from fibroblasts in the collagen gel was limited [81].

Later, modifications of these natural-based materials have been made by combining with other substances such as chitosan, glycosaminoglycan (GAG), chitin, hyaluronic acid, or elastin with the goal to improve the biological, mechanical, and chemical properties of the scaffolds [70]. Black *et al.*, and Kinikoglu *et al.*, both utilised a porous scaffold composed of collagen, GAG, and chitosan to successfully develop well-differentiated skin and oral mucosa equivalents [82], [83]. It has also been demonstrated

that fibroblasts cultured in this compound matrix express higher levels of collagen production compared to the collagen gel alone [81].

Overall, these materials are biocompatible; however, they demonstrate a major drawback in terms of variability as they were obtained from humans or animals [70]. It is also difficult to obtain the projection pattern of rete ridges which are naturally present in the oral mucosa (Figure 2.8A) using these materials.

Acellular dermal matrix derived from cadaveric skin (Alloderm™) or a split-thickness skin graft, known as de-epidermalised dermis (DED), were also used for establishing 3D models of oral mucosa. DED is prepared from skin grafts by detaching the epidermal layer and removing fibroblasts from the dermis layer using a hypertonic solution such as sodium chloride (NaCl) [84]. Colley *et al.*, developed a full-thickness TEOM using DED containing primary oral fibroblasts and keratinocytes which was similar to the native oral mucosa in terms of histological morphology [85] (Figure 2.8). Bullock *et al.*, have also produced a multi-layered epithelium from DED-based TEOM whilst using an immortalised keratinocyte cell line (OKF6/TERT-2) [78]. DED offers several advantages including good durability and low antigenicity [70]. DED also maintains the distinctive characteristics of rete ridges of the native tissue. In addition, the expression of basement membrane proteins such as collagen IV and laminin, which help facilitate the adhesion of keratinocytes in TEOM, are still present in DED [32], demonstrating the advantageous properties of DED to be used as a suitable scaffold for TEOM construction.

TEOM has become an important tool for *in vitro* studies with various applications reported in the literature. TEOM has been used to examine drug toxicity, drug delivery, material biocompatibility and immune responses [78], [86]–[88]. These models have also been to be used to study a variety of oral diseases including wounds and ulcers, cancer progression, *Candida albicans* infections, or lichen planus [73], [78], [85], [86].

Using TEOM as an *in vitro* representative of the oral mucosa provides deeper insights into epithelium biology and wound healing. TEOM also offers more robust data on the tissue responses to substances or stimuli that are closer to an *in vivo* scenario.

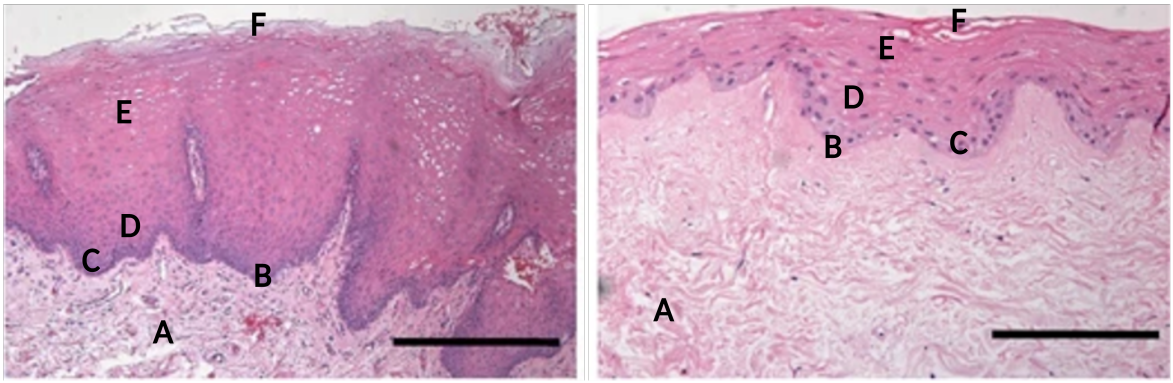

Figure 2.8 | ***Histological sections of native oral mucosa and tissue-engineered oral mucosa.*** *This figure presents the histological resemblance between native oral mucosa (left) and tissue-engineered oral mucosa (right), which was cultured for 14 days at an air-liquid interface. Each layer is annotated as follows: (A) lamina propria, (B) basement membrane, (C) basal cell layer, (D) spinosum layer, (E) granulosum layer, and (F) keratinised layer. Scale bar = 200 µm. Figure modified with permission from Colley et al.,* [85] *under Creative Commons License (CC-BY-NC-SA 3.0).*

2.3 Bisphosphonates

2.3.1 General information and properties

Bisphosphonates are antiresorptive drugs which have been widely used to treat excessive bone resorption disorders such as osteoporosis, Paget's disease, multiple myeloma, bone metastasis and also osteogenesis imperfecta in children [89]. Bisphosphonates were first developed in the 19th century but became more popular for therapeutic purposes after the 1960s [90].

Bisphosphonates structurally resemble inorganic pyrophosphate molecules, a common by-product of human metabolism [91]. Natural pyrophosphate structures contain two phosphonate molecules attached to an oxygen (O) atom, while bisphosphonates, synthetic analogues, have carbon (C) as a geminal atom [92], [93]. The general structure of pyrophosphates and bisphosphonates are illustrated in Figure 2.9.

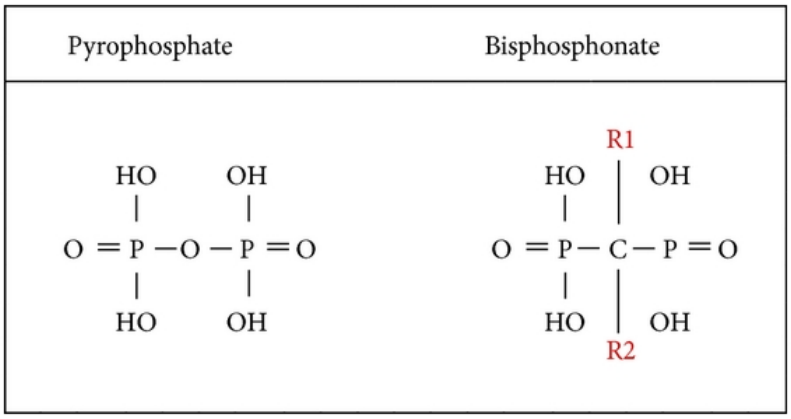

Figure 2.9 | ***Generic bisphosphonate structure.*** *Figure reproduced with permission from Rasmusson et al.,* [94] *under Creative Commons Licenses (CC BY-NC 3.0).*

Each part of the structure accounts for different properties of bisphosphonates. The P-C-P backbone plays a major part in bisphosphonate's pharmacological actions. Carbon linkage helps protect the drug from enzymatic and chemical degradation [95], while both phosphonate molecules function as "bone hooks" which are important for binding tightly with hydroxyapatite crystals, the major inorganic component of bone. Phosphonates also produce an inhibitory effect towards osteoclasts at a cellular level resulting in impairment of bone resorption. The remaining two functional groups

represented by R_1 and R_2 primarily regulate calcium binding ability and potency of bisphosphonates respectively [89].

The R_1 side chain of bisphosphonates is either a hydroxyl group (OH^-) (most bisphosphonates), chloride (Cl^-) (clodronate), or a hydrogen atom (H) (tiludronate). Binding affinity between calcium ions and hydroxyl groups is the strongest bonding among other molecules due to the presence of three binding sites [96]. The chemical component and structural configuration of the R_2 group determine the antiresorptive efficacy of drugs. Nitrogen-containing bisphosphonates provide stronger potency than non-nitrogen containing analogues [91]. Furthermore, the optimum distance between nitrogen and bisphosphonate backbone (P-C-P) with specific spatial configuration determines the potency of bisphosphonate actions [92].

The R group of bisphosphonates dictates their relative potency. Compared to etidronate, a prototype molecule, bisphosphonates with a heterocyclic aromatic amine (e.g. risedronate, zoledronate) provide the strongest potency around 10,000 times greater than etidronate while the nitrogen-containing alkyl chain such as alendronate and pamidronate are 10-100 fold more potent [90], [97], [98]. The side chain structures, both R_1 and R_2, and the relative potencies of each bisphosphonate molecule are summarised in Table 2.2.

Table 2.2 | ***Structures of the R_1 and R_2 side chains of bisphosphonates and relative potencies.*** *Modified with permission from Piper Jr. et al.,* [98] *under Creative Commons Licenses (CC BY-NC 3.0) and Catterall et al.,* [99] *under Copyright Clearance Centre Rights license number 5625560995208.*

Agents	**R_1 side chain**	**R_2 side chain**	**Relative potencies (compared to etidronate)**
Etidronate	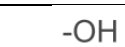	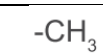	1x
Clodronate			10x
Tiludronate	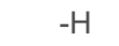		10x
Pamidronate		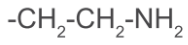	100x
Neridronate	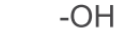	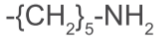	100x
Olpadronate		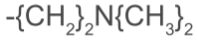	>100x – <1,000x
Alendronate		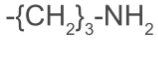	>100x – <1,000x
Ibandronate	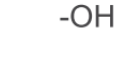	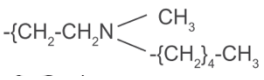	>1,000x – <10,000x
Risedronate	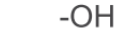	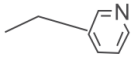	>1,000x – <10,000x
Zoledronate	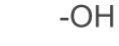	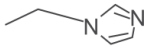	>10,000x

2.3.2 Pharmacokinetics of bisphosphonates

The pharmacokinetic profile of bisphosphonates is remarkable and strongly influences its mechanism of action and clinical use. Oral bisphosphonates are poorly absorbed with low bioavailability in the range between 0.3-6% compared with 100% of intravenous administration [100].

Bisphosphonate levels rapidly decrease in the bloodstream after administration [101] with a half-life in plasma of around 1-2 hours [94]. Around 50% of administered bisphosphonates are selectively distributed into the skeleton, especially in the jawbones which have a high bone remodelling rate while the remaining bisphosphonates are eliminated unchanged *via* the kidney [102]

Bisphosphonates are tightly bound to calcium in bone and retained inactive in the skeleton [91]. The exact bisphosphonate quantity in bone is difficult to estimate because of several factors such as renal function, bone turnover rate, and dosing regimen [91]. Marolt *et al.,* suggested the estimated concentration of pamidronate in human bone is around 0.2 – 2 mM [103]. A prolonged use of higher affinity bisphosphonates to the bone could increase the concentrations of bisphosphonate found in the bone.

The acidic environment during osteoclast-mediated bone resorption helps dissolve bone minerals causing the release of bisphosphonates into the resorption space [104]. These non-bound bisphosphonates then get internalised into osteoclasts by endocytosis [97]. Most bisphosphonates are readily able to inhibit the bone resorption effects of osteoclasts, however, etidronate, clodronate and tiludronate require metabolism by intracellular enzymes before exerting their effects [92], [105]. Despite the uptake into osteoclasts, bisphosphonates can also be recycled and adsorbed back to bone surfaces which extend its half-life in the bone [105]. Literature has reported that the half-life of bisphosphonates in bone can vary from 1 to over 10 years [106], resulting in long term effects on bone resorption.

2.3.3 Mechanism of action of bisphosphonates

Bisphosphonates can be classified into two major groups based on the presence of nitrogen atoms where each group has its specific modes of action [90]. The non-nitrogen containing bisphosphonates are taken up and metabolised into cytotoxic analogues of adenosine triphosphate (ATP) [90]. The nitrogen-containing bisphosphonates, such as zoledronate (ZA) and pamidronate (PA), inhibit farsenyl pyrophosphate synthase enzyme (FPPS), a key regulator in the mevalonate pathway [97] which disrupts the generation of isoprenoids such as farnesyl pyrophosphate (FPP) and geranylgeranyl pyrophosphate (GGPP) [97], [102], [107]. These intermediates are important for the prenylation of small signalling proteins (GTPase), a post-translational modification process that adds the isoprenoid group (FPP or GGPP) to a cysteine group on proteins [97]. This is especially true for the geranylgeranylated proteins which are associated with various osteoclast activities including cell growth, differentiation, ruffled border formation, and cytoskeleton arrangement [93], [107], [108]. Loss of prenylated proteins mainly inhibits osteoclast synthesis, impairs osteoclast function and induces osteoclast apoptosis [109], [110]. The mechanism of bisphosphonates associated with the mevalonate pathway is demonstrated in Figure 2.10. Bisphosphonates are also known to have an effect on osteoblasts by interfering with RANK signalling which in turn blocks osteoclast maturation and survival [111].

In addition to their known effects on bone, both ZA and PA have been shown to adversely affect various cell types within the oral mucosa, including fibroblasts, keratinocytes and endothelial cells [2], [112].

Studies focusing on both individual and co-culture studies have revealed that ZA and PA significantly reduced the viability of oral keratinocytes and fibroblasts [2]. Toxic doses for fibroblasts range from 5 to 60 µM for PA, and 0.16 to 50 for the more potent ZA [2], [78]. In keratinocytes, doses of ZA between 1 to 20 µM have been observed to decrease cell viability, with PA showing similar effects at concentrations ranging from 1 to 100 µM [2], [78]. However, there is notable variation in the reported dosages and evaluation time points associated with toxicity induction.

The mechanism affecting cell viability possibly involves apoptosis induction, as both ZA and PA have been implicated in triggering apoptosis pathways. *In vitro* studies have

shown increased apoptosis levels in oral fibroblasts and epithelial cells following treatment with ZA and PA, causing the impairment of soft tissue integrity in the oral cavity [2], [9], [113], [114]. Cozin *et al.* and Zafar *et al.*, reported the induction of caspase activity in fibroblasts by PA and ZA, respectively [9], [114]. Pabst *et al.*, also showed an increase of apoptosis rate in human normal keratinocytes after treatment with either PA or ZA [10], [115]. Scheper *et al.*, revealed that ZA treatment not only activated caspase activity but also inhibited *SURVIVIN* gene expression, an important inhibitor of the apoptosis pathway in both human gingival fibroblast and oral epithelial (HaCat) cell lines [113]. However, Landesberg *et al*., found that the number of apoptotic cells did not increase after being treated with PA [116]. Thereby, the cellular viability could also possibly be affected through other pathways. The precise mechanism by which bisphosphonates impact the viability of oral mucosa cells remains unclear. Disruptions in the mevalonate pathway, similar to those observed in osteoclasts, could lead to a depletion of prenylated proteins, which are associated with cell survival [110].

There is some evidence that bisphosphonates may induce oxidative stress in oral soft tissue cells. Tanigushi *et al.*, demonstrated that bisphosphonates induced the production of reactive oxygen species (ROS) in oral fibroblasts leading to oxidative damage and inflammation, which can slow the growth of fibroblasts [117]. The induction of ROS production contributes to cell damage, inflammation, and apoptosis. highlighting the complexity of cellular responses to bisphosphonates.

In addition to the effect on cell viability, studies have shown that both PA and ZA at various doses markedly impaired the migration of oral mucosa cells [2], a fundamental process in oral wound healing. This inhibitory effect of these bisphosphonates is likely due to their impact on the mevalonate pathway, leading to disruptions in downstream signalling pathways including those involving Rho GTPases [118]. These GTPase molecules are critical in controlling actin cytoskeleton, a crucial component for cellular dynamics [119]. Thereby, disruption to these molecules could impair cellular movements, particularly cell migration.

The inhibitory effects of PA and ZA on the proliferation of oral mucosa cells, another key aspect in oral wound healing, have also been widely documented [2]. Notably, most studies assessing cell proliferation have utilised the MTT assay, it is crucial to recognise that

this assay primarily measures metabolic activity rather than direct cell proliferation. A number of studies have employed other methods such as CFSE staining [120], Ki-67 staining [121], or cell counting [79] to provide a more accurate assessment of cell proliferation. Despite different methodologies, the consensus indicates the inhibitory effect of bisphosphonates on oral mucosa cell proliferation.

Several mechanisms underlying this inhibition have been proposed. Hemmi *et al.*, demonstrated that ZA suppressed the expression of fibroblast growth factor-2 (FGF2) and connective tissue growth factor (CNTF), which are both pivotal for fibroblast growth [122]. Research has also indicated that the regulation of the cell cycle appears to be another contributing mechanism. Ohnuki *et al.* and Kim *et al.,* found that PA and ZA induced cell cycle arrest in keratinocytes and fibroblasts at the non-mitotic phase, thereby reducing essential protein synthesis required for cell proliferation [123], [124].

The remodelling phase of wound healing is also adversely affected by nitrogen-containing bisphosphonates. Manzano-Moreno *et al.*, showed that ZA treatment disrupted the expression of *DECORIN* and *FIBRONECTIN* genes in fibroblasts, suggesting a possible detrimental effect on collagen and ECM production [125]. In addition, work by Hemmi *et al.*, also reported the direct effect of ZA treatment on the expression of *COL1* gene expression in fibroblasts [122]. Thereby, the remodelling process in soft tissue healing has also been shown to be compromised.

The integrity and functionality of oral mucosa are significantly influenced by vascularisation and an adequate blood supply. This has directed research towards investigating the effects of bisphosphonates, particularly ZA and PA, on endothelial cell behaviour and vascular formation. These bisphosphonates have been observed to negatively impact endothelial cells, a finding consistent with their previously documented effects on fibroblasts and keratinocytes. A number of studies have reported the adverse effects of both PA and ZA on the viability of human umbilical vein endothelial cells (HUVECs) [126]–[131]. These studies highlight the variability in doses and time points required to induce toxicity, with toxic doses ranging between 2.06 – 160 µM. Notably, Misso *et al*., determined that the half-maximal inhibitory concentration (IC_{50}) of ZA on HUVECs at 72 hours is 64.46 µM [129].

The viability of endothelial cells is negatively affected by both ZA and PA through a variety of cell death pathways, predominantly *via* apoptosis. This is confirmed by markers such as TUNEL assay [130], [132], [133] and Annexin V staining [126], [132]. Studies have explored the molecular mechanism behind PA and ZA-induced endothelial cell apoptosis. Jung *et al.*, demonstrated an increase of Caspase 3/7 activity, a hallmark of apoptosis [127]. Lang *et al.*, showed the decrease of phosphorylation of AKT, which normally controls apoptosis [126]. Furthermore, Lu *et al.*, reported that ZA induces endothelial cell death through the Beclin-1 pathway [134], highlighting the negative impact of ZA on endothelial cell survival.

Despite the impact on cell viability, both PA and ZA have also been shown to adversely affect the proliferation and migration of HUVECs [126], [127], [132], [133], [135]. Ziebart *et al.*, revealed that bisphosphonates inhibit the proliferation of endothelial progenitor cells, thereby disrupting angiogenesis [133]. The effect is potentially linked to the mechanism of nitrogen-containing bisphosphonates on the mevalonate pathway as Hasmim *et al.*, reported that ZA inhibited the expression of Ras and the translocation of RhoA in HUVECs [76]. This finding is correlated with a study from Lang *et al.*, which also demonstrated a reduction in ERK1/2 phosphorylation [126], suggesting that the inhibition of these prenylation molecules by bisphosphonates potentially leads to the decrease in cell proliferation.

As described, these bisphosphonates inhibit a key enzyme in the mevalonate pathway (Figure 2.10), leading to a reduction in prenylated protein production. The disruption is critical, affecting essential cellular functions including viability, migration, proliferation of cellular compartments of the oral mucosa, ultimately impairing wound healing in the oral soft tissues [2]. These studies collectively contribute to a deeper understanding of the molecular interactions and cellular effects of bisphosphonates, specifically in the context of oral mucosa.

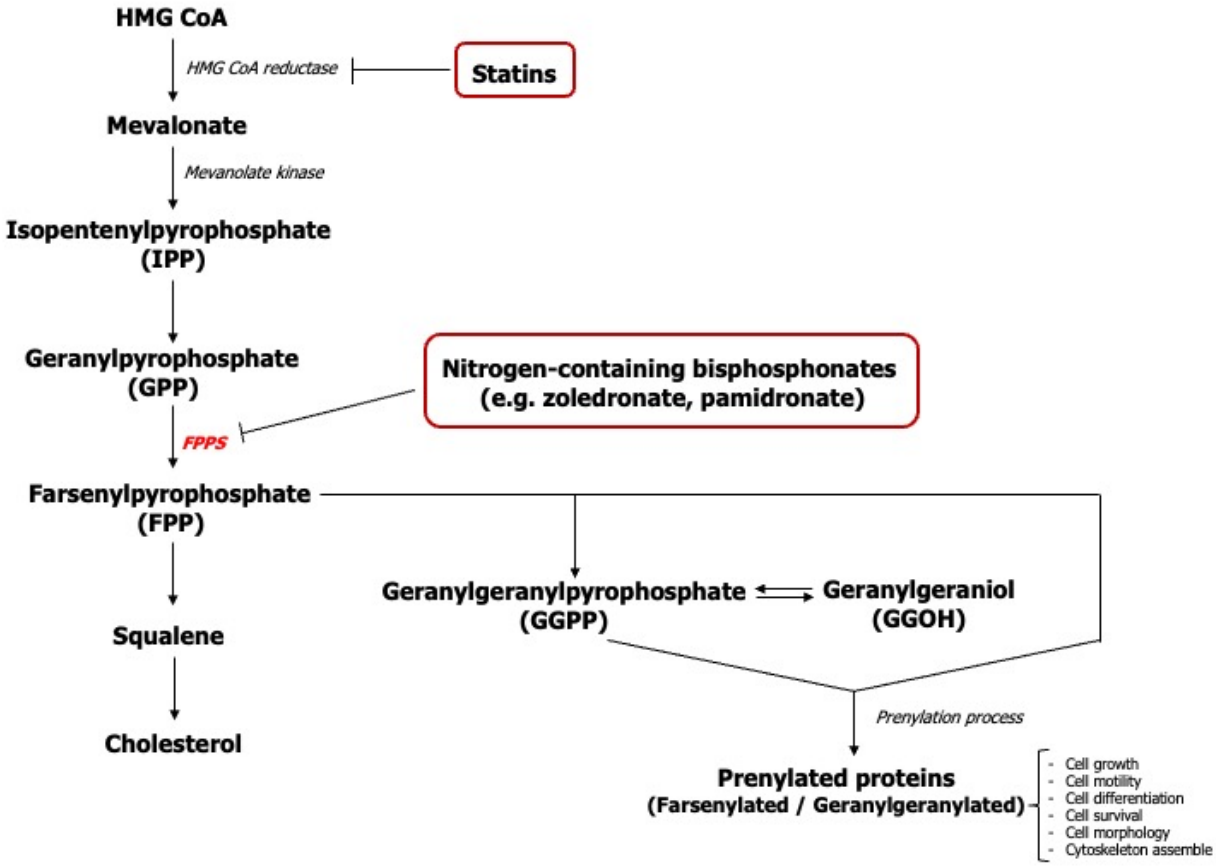

Figure 2.10 | The mevalonate pathway. *Abbreviations: HMG CoA, 3-hydroxy-3-methylglutaryl coenzyme A.*

2.3.4 Clinical usage

Bisphosphonates are currently used in oral or intravenous forms with different dosing regimens depending on the type and severity of diseases [96], [105]. Low-dose oral bisphosphonates such as alendronate or risedronate are typically used either once daily or weekly to manage postmenopausal osteoporosis. In contrast a yearly ZA or three-month dose of ibandronate infusion can be used as an alternative [136]. In contrast, high dose intravenous bisphosphonates are approved for bone malignancy with the recommended dose at 4 mg of ZA or 90 mg of PA every 3-4 weeks [137].

2.3.5 Adverse effects

Although bisphosphonate therapy is safe and well-tolerated in most patients, these antiresorptive agents may develop some concerning side effects [109]. Oral bisphosphonates have been shown to cause gastrointestinal toxicity such as oesophageal irritation or ulceration [138], [139]. However, more serious events are potentially caused by intravenous dosage forms due to higher potency and prolonged treatment duration [140]. The most concerning adverse effect during recent years is osteonecrosis of the jaw (ONJ) which occurs more frequently in multiple myeloma or breast cancer patients receiving high-dose nitrogen bisphosphonates [141], [142]. Despite this, other possible effects that can be found include bone pain, arthralgia, influenza-like symptoms, and renal toxicity [143].

2.4 Medication-related osteonecrosis of the jaw (MRONJ)

2.4.1 Definition

According to an American Association of Oral and Maxillofacial Surgeons (AAOMS) report in 2022, MRONJ is defined as “necrotic exposed alveolar bone or probe-able bone through fistula which lasts longer than eight weeks in patients who have currently or previously received antiresorptive or antiangiogenic drugs with no history of radiotherapy in head and neck region” [1]. However, recent consensus from the European task force has described some limitations of the AAOMS definition, staging, risk factors, and treatment strategies. The European task force have suggested that MRONJ criteria should include patients who have non-exposed necrotic bone which has been confirmed by histopathological results. Furthermore, the 8-week length of bone exposure in the definition is not observed with all MRONJ cases and may delay prognosis and negatively affect treatment outcomes [144]. Risk factors and treatment strategies for MRONJ will be discussed later.

2.4.2 Clinical presentation and staging of MRONJ

MRONJ can be detected through a wide range of signs and symptoms starting from asymptomatic and non-specific symptoms such as pain, soft tissue swelling, erythema through to severe bone exposure with the presence of infection and extraoral fistula [108], [145]. The primary clinical features are the exposure of necrotic bone with mucosal breakdown [146]. An example of an MRONJ case is illustrated in Figure 2.11. MRONJ staging has been divided into five stages based on symptoms, clinical presentations, and radiographic findings which are shown in Table 2.3

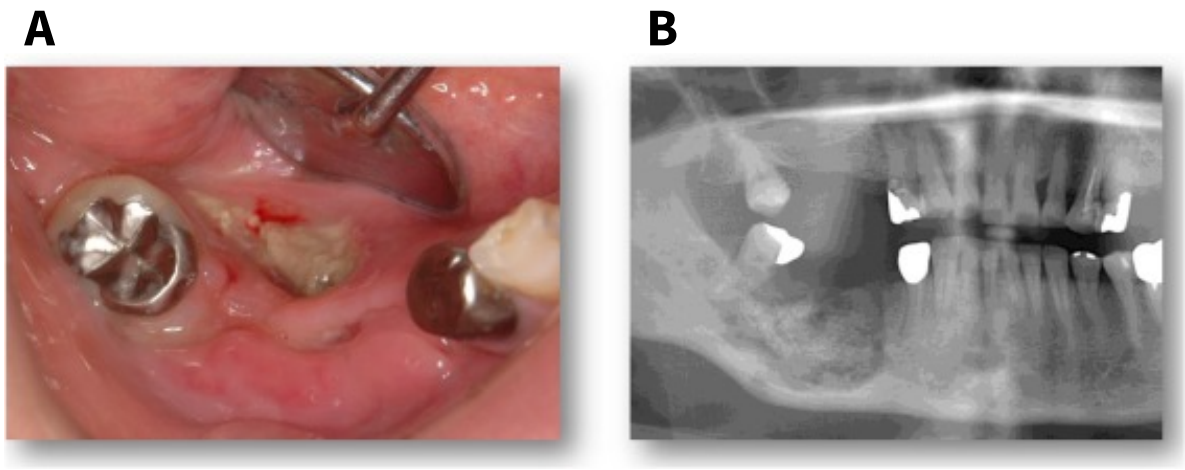

Figure 2.11 | ***Clinical appearance and radiographic image of MRONJ.*** *(A) displays the clinical appearance, while (B) shows a radiographic image highlighting the necrotic bone (sequestrum) of MRONJ. Figure reproduced with permission from Kishimoto et al.,* [147] *under Creative common license (CC BY-NC-ND 4.0).*

Table 2.3 | ***Staging of MRONJ*** *[1].*

Stage	Signs and Symptoms
At risk	No apparent necrotic bone in asymptomatic patients who are treated with antiresorptive or antiangiogenic agents
0	No clinical evidence of necrotic bone but nonspecific symptoms, clinical or radiographic, are detected
I	Exposed and necrotic bone or probeable bone from fistula in patients who have no symptoms and evidence of infection or inflammation
II	Exposed and necrotic bone or probeable bone with evidence of infection and associated symptoms such as pain and erythema
III	Same as stage II and one or more of these additional conditions: - Exposed necrotic bone extending beyond the region of alveolar bone - Pathologic fracture - Extraoral fistula - Oroantral or oronasal communication - Osteolysis extending to the inferior border of the mandible or sinus floor

2.4.3 Risk factors and prevalence

Several groups of factors have been reported for their association with MRONJ leading to difficulties in carrying out MRONJ epidemiological studies [148]. Common factors that have been reported are age, gender, smoking status, steroid use, and concomitant systemic diseases [137], [149], [150].

Focusing on medication aspects, cumulative dosage, administration route, and length of drug therapy all appear to be related to MRONJ. These factors should be considered together in order to determine the risk of MRONJ development [144]. The estimated incidence of MRONJ is mostly considered in 2 groups which are high dose antiresorptive therapy for cancer treatment and low dose for osteoporosis [149]. The cumulative risk of MRONJ among oncology patients receiving ZA (intravenous bisphosphonates) is less than 5% (estimates varied between 0% and 18%) and ranged from 0% to 6.9% for denosumab. An incidence between 0.02-0.05% is found in patients taking low dose bisphosphonates for osteoporosis treatment [1]. Longer exposure significantly increases the risk of MRONJ occurrence in cancer patients [151]. The incidence of MRONJ in cancer patients treated with either ZA or PA for four years is approximately 4-fold higher compared to a one-year exposure group [151]. The risk of MRONJ also increased over time from 0.5% to 1.1% in patients exposed to denosumab for 1 and 3 years respectively [152]. In contrast, the effect of time was unclear in users receiving bisphosphonates to treat osteoporosis. A study by Lo *et al.,* demonstrated that MRONJ frequency was increased in patients having 4 years or more of oral bisphosphonate therapy (0.21%) compared to the prevalence of nearly 0% in a group having lower than 4 years [153]. A recent study by Black *et al.,* reported that there was no significant difference to the risk of developing MRONJ for patients receiving ZA to treat osteoporosis between 6 or 9 years [154].

The anatomical location is also another factor affecting the risk of MRONJ development. Typically, the jawbones especially the lower jaw are prone to develop MRONJ more than any other skeletal structures [155], [156]. Osteonecrosis mostly affects single jawbones which the highest frequency, around 73%, is found at the mandible followed by 22.5% in the maxilla, and the remaining (4.5%) affected on both jaws [157]. The susceptibility of alveolar bone can be explained by bisphosphonate accumulation in areas with high bone turnover rate [158]. As the masticatory process occurs regularly in jawbones,

they are likely to develop repetitive microdamage which requires more rapid bone remodelling [108]. An animal study also confirmed that the bone turnover rate in jaws is 10 times higher than long or flat bones [107].

When MRONJ was first described it was widely thought that dental extractions were the main trigger for the disease since around 62% to 82% of MRONJ cases are correlated with tooth extraction events [1]. The incidence of jaw necrosis following tooth extraction in cancer patients receiving intravenous bisphosphonates has been reported to be between 1.6% and 14.8% [149]. Other traumatic events in the oral cavity such as dental implant placement or wearing poor-fitting dentures have also been linked with the occurrence of MRONJ [159]–[161].

However, alternative theories are now being explored as more patients develop MRONJ without extraction and the majority of cancer patients receiving bisphosphonates who had undergone extraction demonstrated normal wound healing and a low incidence of jaw necrosis development [162], [163].

The underlying reason for tooth extraction is usually infection and inflammation of the tooth which is preceded by poor oral hygiene, dental or periodontal diseases [1]. As a result, it is infection and inflammation which are now thought to be the primary risk factor which possibly trigger MRONJ development instead of the surgical procedures themselves [144]. Poor dental health and periodontal status has been observed in MRONJ patients when compared to patients without bone necrosis [164]. Almost 50% of cancer patients who developed MRONJ were reported to have existing oral infection [157]. The role of infection will be further described in the pathophysiology section (Section 2.4.4).

2.4.4 Pathophysiology

Although MRONJ has been studied for a period of time, the exact pathophysiology of this condition has not been fully clarified. According to the latest position paper of AAOMS in 2022, MRONJ may be described as a multifactorial disease resulting from several contributing mechanisms which are dysfunctional bone remodelling, angiogenesis inhibition, the presence of inflammation or infection, immune dysfunction, and genetic factors [1].

Bisphosphonates primarily impair osteoclast-mediated bone resorption in the bone remodelling process by suppressing osteoclast differentiation, inhibiting bone adhesion, and inducing cell apoptosis [94], [110], [165]. Despite the effects on osteoclasts, bisphosphonates are also reported for their effects on other osteogenic cells [166]. Bisphosphonates can induce osteoprotegerin (OPG) synthesis and inhibit the RANK ligand in osteoblasts which impairs osteoclast differentiation [94], [167]. ZA also directly inhibits osteoblast proliferation, migration, and viability [130], [168], providing the concept of bisphosphonate-induced bone remodelling imbalance in the pathogenesis of MRONJ. Figure 2.12 summarises the effects of bisphosphonates on osteogenic cells.

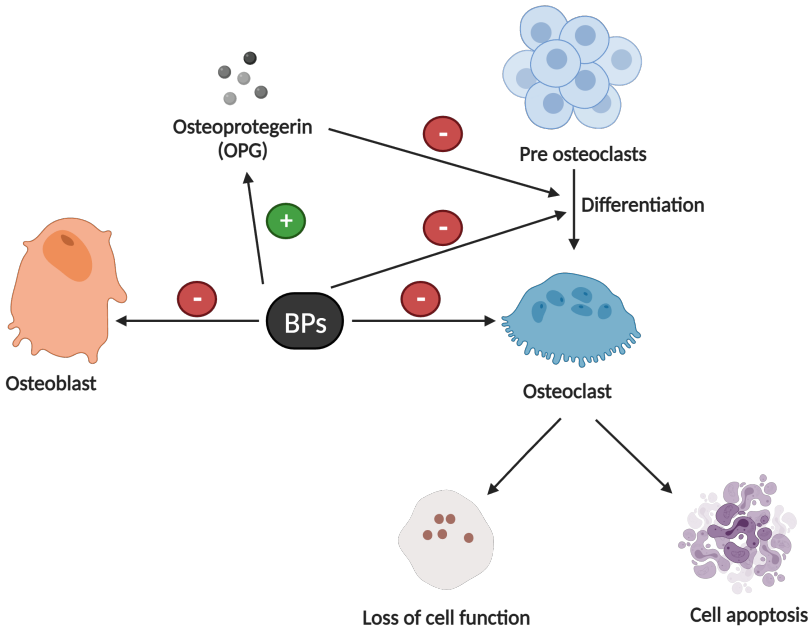

Figure 2.12 | ***Effects of bisphosphonates (BPs) on osteogenic cells.*** *The diagram illustrates how bisphosphonates impair osteoclast function and induce apoptosis. Bisphosphonates also inhibit the differentiation of preosteoclasts by promoting of osteoprotegerin synthesis. Additionally, bisphosphonates negatively impact osteoblast function. Figure created using Biorender.com. Abbreviations: + (Stimulatory effect); - (Inhibitory effect).*

Inadequate blood supply is frequently exhibited in necrotic bone tissue leading to the possible contribution of angiogenesis inhibition in the development of MRONJ [149]. Both *in vitro* and *in vivo* experiments have demonstrated the negative impacts of nitrogen-containing bisphosphonates especially ZA on new blood vessel formation by reducing endothelial cell proliferation, migration, adhesion and the production of capillary tubes [127], [128], [132], [133], [135]. Clinical studies have shown that ZA significantly lowers serum VEGF which is a key growth factor responsible for promoting angiogenesis [169]. In addition, the presence of osteonecrosis in patients who are exposed to anti-angiogenic drugs such as bevacizumab and sunitinib can explain the association between jaw necrosis and angiogenesis impairment [4], [5].

Oral infection is implicated as significant in the pathogenesis of jaw necrosis [149]. Histological results demonstrated polymicrobial biofilms in necrotic bone specimens obtained from patients exposed to bisphosphonates [170], [171]. *Actinomyces sp.* have been identified as the most common microorganisms found in MRONJ lesions [172], [173]. Other bacterial species that have been found in MRONJ bone cultures include: *Porphyromonas*, *Streptococcus, Enterobacter, Staphylococcus,* and *Fusobacterium sp.* [174]–[176]. An *in vivo* study by Aguirre *et al.*, on periodontitis-induced jaw necrosis in rats suggested a significant correlation between infection and MRONJ [177]. It is believed that jawbones are vulnerable to infection because they are only protected from the large number of microbes in the oral cavity by thin mucosal tissues [178]. Bisphosphonates themselves can also create a favourable bone surface for bacterial adhesion [179]. Furthermore, bisphosphonates also impair the immune system which increases the possibility of infection-mediated jaw necrosis [180].

Inflammation is also considered to be one of the contributing mechanisms of MRONJ. Bisphosphonates can induce inflammation by disrupting the balance between pro-inflammatory and anti-inflammatory cytokines [181]. ZA-induced MRONJ in mice models demonstrated higher levels of inflammatory cytokines such as IL-1β, IL-6, and TNF-α at the extraction sites compared to other areas [182]. Another study reported that mice with systemic inflammatory disorders such as rheumatoid arthritis developed more severe MRONJ conditions with more inflammatory cell infiltration and larger areas of necrotic bone observed [183], suggesting the role of inflammation in the pathogenesis.

Immune dysfunction and genetic variations are also proposed as possible mechanisms in the pathogenesis. Higher risks and prevalence of developing MRONJ were reported in patients with systemic diseases such as diabetes mellitus, multiple myeloma, bone malignancies or those who are immunocompromised [1]. Furthermore, evidence has shown that variations of genes such as sirtuin-1 (*SIRT1*), *TGFβ, PPARγ, VEGF*, or *CYP2C8*, are reported to be associated with the risks of developing MRONJ [184], [185]. However, more evidence is still needed to confirm the association of both mechanisms with the development of MRONJ. Thus far, all these hypotheses are considered as a part of the pathophysiology of MRONJ.

Soft tissue toxicity induced by bisphosphonates was previously included in the possible mechanisms of MRONJ in the AAOMS 2014 position paper but it was not presented in the latest version in 2022 [1], [149]. Despite this it is well established that lack of mucosal covering impedes resolution of the disease.

Bisphosphonates reside in the bone and it is likely that they are released into surrounding tissues following the primary inhibitory effect on osteoclasts (Section 2.3.2 and Figure 2.12). This local tissue release is then thought to induce oral mucosa toxicity. The presence of infection and chronic inflammation, which is now considered a key contributing factor for MRONJ development, also impede the ability of the oral epithelium to heal [2]. This implies that the mucosal breakdown and incomplete soft tissue healing seen in MRONJ could be a result of the combined effects of bisphosphonates and the underlying oral disease.

A review by Bullock *et al.*, summarised the toxic effects of bisphosphonates on oral fibroblasts and keratinocytes. Bisphosphonates have been shown to inhibit cell growth, migration, and proliferation and increase apoptosis in both oral keratinocytes and fibroblasts in culture [2]. Disrupting these processes causes soft tissue damage and impairs wound healing.

Since the clinical hallmark of MRONJ is a loss of mucosa with bone exposure, this highlights the significance of the impact of bisphosphonates on soft tissues, and highlights the need to consider this aspect as a part of MRONJ research. Therefore, we will primarily focus on the toxicity of bisphosphonates on oral mucosal tissues in this thesis.

2.4.5 Treatment strategies

The definitive treatment for MRONJ is still a challenging issue due to inconclusive underlying mechanisms and clinical outcomes [108]. Preventive strategies such as regular oral examination and treatment planning before initiating bisphosphonates use are recommended in order to reduce the incidence of MRONJ [186], [187]. Besides oral check-ups, the concept of a drug holiday, temporarily stopping patients from using bisphosphonates before undergoing any invasive dental surgeries, was proposed by AAOMS in 2008 as a choice of treatment [188]. It was hoped this particular approach could reduce bisphosphonate exposure time and minimise the risk of osteonecrosis development; however, its effectiveness in clinical studies has not been demonstrated [149]. Provisional drug cessation is considered to be ineffective because the ability of bisphosphonates to reside in bone for almost 10 years results in an extended effect from the exposure period [94], [186]. Clinical data demonstrated that discontinuing the use of bisphosphonates is correlated with the cumulative risk of osteoporosis occurrence [189]. Therefore, a drug holiday is not suitable for MRONJ patients.

Control of pain and infection, soft tissue healing, and bone necrosis management are the main focus for patients with exposed MRONJ [1], [190]. AAOMS has produced treatment guidance based on the disease severity which is described in Table 2.4. Conservative treatments such as oral hygiene maintenance, analgesics, systemic antibiotics or antibacterial mouth rinse (e.g. chlorhexidine) were considered as the first-line approach for patients, while resection surgery and tissue debridement were suggested for more advanced stages or in cases where the conservative therapies fail because of patient's morbidity and quality of life [94], [191].

Surgical procedures in patients receiving bisphosphonates were previously avoided because of their perceived role in triggering jaw necrosis [107], [149]. However, studies have demonstrated that surgical approaches resulted in higher success over non-surgical therapies [144]. It is recommended that uncovered bone with irregular sequestrum is removed and followed by full-thickness flap coverage in order to avoid infection and inflammation [192]. Socket closure by mucoperiosteal flap was shown to prevent alendronate-induced osteonecrosis of the jaw in rats [193]. 59% of malignant patients undergoing sequestrectomy and local flap procedures demonstrated complete oral

mucosa healing with no presence of necrotic bone [194]. Resection surgery resolved oral wound healing problems in patients receiving either oral or intravenous bisphosphonates in nearly 90% of cases [195], [196]. In addition, the European task force suggested that early surgical procedures could delay the progression of MRONJ and also facilitate the healing of oral mucosa [144].

Despite the supporting evidence, surgical treatment for patients with MRONJ is still being questioned with concerns raised over its damage to patients and the reliability of studies. Therefore, investigating novel treatment strategies with the aim of preventing or reducing the onset of MRONJ should be the topic of further investigation.

Table 2.4 | ***MRONJ treatment strategies*** [149]

Stage	Treatment Strategies
At risk	- No treatment is required - Patient education about signs, symptoms, and risks of MRONJ development
0	- Conservative management for local factors such as caries and periodontal diseases - Pain medication and antibiotics
I	- Antibacterial mouth rinse - Quarterly clinical follow-up - Patient education and review of indications for continued bisphosphonate therapy
II	- Oral antibiotics - Oral antibacterial mouth rinse - Pain control - Debridement and infection control
III	- Antibacterial mouth rinse - Antibiotic therapy and pain control - Surgical debridement or resection

2.4.6 Novel treatment strategies for MRONJ

Despite the recent approaches, there are no reliable guidelines for MRONJ management [7]. Research has been focused on other potential strategies which can be used for improving patient's quality of life. The restoration of overlying oral mucosa is thought to be a key factor to resolve the disease [144]. Restoring the soft tissue barrier can help prevent the progression of bone exposure and also reduce the risk of infection. This part of the review provides a summary of novel MRONJ therapeutic methods being investigated including stem cells, growth factors, laser technologies, antimicrobials, and hydroxyapatites.

2.4.6.1 Stem cell therapies

Cell-based approaches for MRONJ treatment have demonstrated promising benefits in a number of studies, especially the use of mesenchymal stem cells (MSCs). Administration of allogenic bone marrow MSCs intravenously has been shown to improve oral wound healing and bone reconstruction in MRONJ-like rodent and minipig models [197], [198]. MSCs have been selected for their immunomodulatory properties and the ability to secrete cytokines and growth factors for tissue regeneration [192]. However, systemic MSC infusions can cause serious adverse events by increasing the risk of cancer and recurrence and intravascular thrombosis [199]. Current studies are more focused on local administration rather than systemic application. Topical MSCs suspended in a gel were shown to significantly enhance alveolar bone healing in ZA-induced MRONJ rats [200]. A case-report of a stage III MRONJ patient also showed clinical and radiographic improvement after receiving autologous MSC treatment locally [201]. As well as bone marrow derived MSCs, other stem cells such as adipose-derived stem cells (ADSCs) have also been reported for their potential in curing MRONJ. Zang and colleagues demonstrated that ADSCs in combination with hydroxyapatite disc transplantation promoted gingival healing after tooth extraction and also prevented osteonecrosis in MRONJ-induced rabbits [199]. Studies conducted by Alonso-Rodriguez *et al.,* and Barba-Recreo *et al.,* using ADSC-based therapies both demonstrated favourable results improving bone regeneration and reducing MRONJ occurrence in rats [202], [203]. Therefore, the concept of cellular therapy in MRONJ management may be considered as an alternative method; however, further

observation and larger scale randomised controlled trials are still required to support clinical use.

2.4.6.2 Growth factors

The ability of growth factors to stimulate tissue regeneration, promote angiogenesis and improve wound healing for MRONJ treatment has also been investigated [204]–[208].

TGF-β is a commonly known cytokine involved in fibroblast migration and fibronectin and collagen production which are essential for hard and soft tissue healing [206], [207] which has been found to be decreased in gingival tissues obtained from MRONJ lesions [199]. This growth factor has been examined for its contribution and possible therapeutic effects in MRONJ. Zang *et al.*, discovered that the ability of ADSCs to promote gingival healing in MRONJ-like rabbits was caused by an upregulation of *TGF-β* and *fibronectin* expression. Furthermore, Komatsu *et al.*, demonstrated the positive effects of TGF-β on gingival fibroblast migration was diminished in the presence of ZA, further supporting the hypothesis that TGF-β may be beneficial [208].

Other growth factors including PDGF-BB and EGF have also been studied for their possible role in improving the cellular mechanisms in the healing process, which are negatively affected by bisphosphonate treatment. Cozin *et al.*, investigated the ability of PDGF-BB to reverse ZA and PA toxicity on oral fibroblasts. In this study, they showed PDGF-BB restored the proliferation of PA-treated fibroblasts after 1 week, while a slight increase was observed from ZA-treated conditions during a 72-hour time point [9]. EGF treatment also appeared to significantly improved the migration of keratinocytes which had been negatively affected by ZA [209].

Although there is supporting evidence on the therapeutic effects of growth factors, more investigation is required.

2.4.6.3 Laser therapies

The use of laser technologies especially low-level laser therapy (LLLT) as a supportive treatment for MRONJ have been introduced over the past years [210]. The mechanism of LLLT for oral tissue healing was hypothesised to be as a result of its biostimulatory effects on bone and mucosa cells [192]. Two studies have investigated the influence of LLLT on cell

viability [211], [212]. Walter *et al.*, applied LLLT to four cell types: keratinocytes, fibroblasts, endothelial cells, and osteoblasts in the presence of bisphosphonates. They observed an increase in viability in all cell lines after diode laser exposure [211]. Other work by Basso *et al.,* also demonstrated the positive effects of LLLT on epithelial cells and gingival fibroblasts treated with ZA [212]. Besides the *in vitro* studies, clinical applications of LLLT in MRONJ patients have been described as well. Results across the literature indicated clinical improvement in MRONJ patients receiving LLLT with either surgical procedures, antibiotics, or in combination, which led them to conclude that it should be used as a key approach in the early stages of MRONJ [210].

Though the success of using laser therapy has been reported, there are only a few studies and the mechanism of action remains unclear. Furthermore, there is a lack of strong, reliable evidence to support the use of LLLT as a single treatment for MRONJ.

2.4.6.4 Antimicrobials

As infection plays a significant role in MRONJ pathogenesis, antimicrobial agents are commonly prescribed to MRONJ patients for different purposes based on the severity of the disease. Antibiotic prophylaxis was recommended for stage 0 patients before tooth extraction in order to prevent the occurrence of MRONJ; while patients in stage II and III received antibiotic treatment to eliminate local infection [1]. Despite this, no standard protocols for antimicrobial use in MRONJ have been established. In general, penicillin-based antibiotics such as amoxicillin or amoxicillin/clavulanic acid are frequently used as a single treatment or in combination with metronidazole [213]. Clindamycin is given as an alternative choice for patients who are allergic to penicillin [205], [214]. These drugs have broad spectrum properties which can counteract against MRONJ-associated pathogens. It is difficult to indicate the individual effect of antibiotics because most studies reported the improvement of MRONJ lesions in patients who were prescribed antibiotics in combination with other treatment procedures such as surgical intervention or laser therapies as described earlier.

In addition to the regular regimens, AAOMS has also highlighted the successful treatment of MRONJ using quinolones and doxycycline [188]. Studies have examined how these antimicrobial agents can control the local infection and wound healing process.

Ikeda *et al.*, treated 20 patients who had been defined as stage II or III MRONJ with Sitafloxacin, a fluoroquinolone antibiotic, alone or in combination with surgical treatment as necessary. 95% of patients showed no signs of infection and an improvement in wound healing after a 2-10 weeks treatment course [215]. Capar *et al.*, evaluated the efficacy of a doxycycline sponge on ZA-induced MRONJ in Wistar rats. They applied a sponge with control-released doxycycline into the socket immediately after the tooth extraction and covered it with the buccal mucoperiosteal flap. Clinical wound healing was significantly improved in doxycycline-treated rats and histological findings also showed a lower percentage of necrotic bone and inflammation in comparison to the group that received only a flap closure [216]. It is clear antimicrobial treatment is an important aspect for the management of MRONJ lesions and further study is ongoing into the bacterial species present and the optimum treatment strategies.

2.4.6.5 Hydroxyapatite

The use of calcium-based materials especially hydroxyapatite [$Ca_{10}(PO_4)_6(OH)_2$] as a potential option in MRONJ management has been examined in several studies. The hypothesis behind these studies was that the binding between bisphosphonates and calcium may be able to reduce the bioavailability of bisphosphonates in MRONJ and subsequently decrease the toxicity to the bone and oral mucosa [78], [217], [218]. Paolo *et al.*, investigated the potential effect of biphasic calcium ceramics, Adbone®, consisting of 75% hydroxyapatite and 25% beta-phosphate tricalcium on protecting human gingival fibroblasts from bisphosphonate toxicity. They suggested that the adsorption ability of calcium phosphate ceramics limited the toxic effect of ZA on fibroblast viability and migration [217]. This was correlated with work by Bullock *et al.*, who examined the effects of hydroxyapatite granules on oral mucosa cells in the presence of nitrogen-containing bisphosphonates (ZA and PA). The metabolic activity of oral keratinocytes and fibroblasts was restored when the media containing bisphosphonates was pre-treated with hydroxyapatite. Furthermore, the addition of hydroxyapatite granules improved the metabolic activity and epithelial morphology in 3D oral mucosa models treated with ZA [78]. The protective role of hydroxyapatite has also been studied *in vivo*. Another work by Paolo *et al.*, applied the Adbone® ceramics into the extraction socket of ZA-treated rats

immediately following tooth removal. Healed soft tissues and signs of bone formation were observed clinically and histologically at the extraction site in rats receiving hydroxyapatite treatment [218], supporting the possibility of using hydroxyapatite for MRONJ prevention and treatment. This may be another interesting scope of research to be explored in the future.

2.5 Geranylgeraniol (GGOH)

Besides the previously outlined potential strategies for the treatment of MRONJ, another method which has been studied to reverse bisphosphonate toxicity is through the use of GGOH. This part of the literature review summarises what GGOH is and the possibility for use as a novel therapeutic substance for MRONJ.

2.5.1 General information

GGOH is a natural isoprenoid molecule which plays critical roles in several biological processes in animal and plants [219]. It is converted from GGPP *via* dephosphorylation [220]. The structure of GGOH is illustrated in Figure 2.13. GGOH is chemically classified as a diterpene. The structure is made up from 20 carbon atoms with a substitution of methyl (CH_3-) and hydroxyl (OH^-) group in the molecule at specific locations [220], [221].

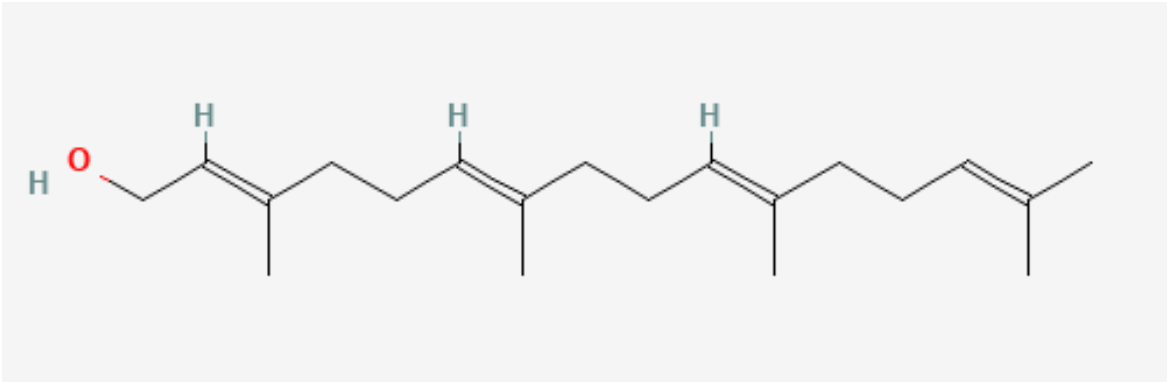

Figure 2.13 | ***Chemical structure of geranylgeraniol (GGOH).*** *Figure reproduced with permission from PubChem database* [221].

2.5.2 GGOH effect on reversing bisphosphonate toxicity

GGOH is commonly recognised as a substrate for GGPP, which is an intermediate product in the mevalonate pathway of cholesterol synthesis (Figure 2.10) [219], [222]. It has previously been shown that bisphosphonates inhibit protein geranylgeranylation through this mevalonate pathway [97]. GGOH has been shown to counteract bisphosphonate induced cell effects and restore cell viability, proliferation and adhesion in numerous cell types [9], [10], [222]–[224]. As bisphosphonate-induced soft tissue toxicity is an important component of MRONJ and the scope of our research, this section mainly focuses on the rescue effect of GGOH on oral mucosa cells in both *in vitro* and *in vivo* studies.

2.5.2.1 In vitro - cell viability

Studies have assessed the potential benefits of GGOH on reversing bisphosphonate toxicity on cell viability and proliferation using various assays including 3-(4,5-dimethylthiazol-2-yl)-2,5-diphenyltetrazolium bromide (MTT), 3-(4,5-dimethylthiazol-2-yl)-5-(3-carboxymethoxyphenyl)-2-(4-sulfophenyl)-2H-tetrazolium (MTS), and resazurin assays. A study by Pabst *et al.*, simultaneously incubated human oral keratinocytes with four bisphosphonates and GGOH for 72 hours. This study indicated that 10 µM GGOH significantly improved cell viability in the presence of nitrogen-containing bisphosphonates (PA and ZA) [10]. Work by Kim *et al.*, used a lower GGOH concentration (0.5 µM) for investigation. They found that GGOH partially restored cellular proliferation of PA-treated keratinocytes after 144 hours of treatment [124].

In fibroblast studies, a wide range of GGOH concentrations have been examined. Hagelauer *et al.*, found that all tested GGOH concentrations from 10 to 100 µM rescued the viability of ZA-treated fibroblasts over a 72 hour period [223]. This work was supported by two further studies which also investigated the same time point. Zafar *et al.*, demonstrated that both 10 and 50 µM GGOH antagonised the ZA effect on gingival fibroblasts [114], while work by Ziebart *et al.*, showed positive effects on viability using 10 µmol GGOH [224]. Cozin *et al.*, also investigated a longer incubation period to test the effects of GGOH. They reported that a 50 µM GGOH concentration could neutralise the inhibition at low concentrations of PA only, while broader effects were seen in all concentrations of ZA after 7 days [9].

2.5.2.2 In vitro - cell migration

Several studies, also mentioned above (Section 2.5.2.1), describe GGOH effects on cellular migration in the wound healing process [9], [223]–[225]. Keratinocyte migration was investigated using a Boyden chamber and scratch wound assay by Pabst *et al.*, and results showed an improvement in migration and wound closure after cells were co-treated with GGOH compared to bisphosphonates alone [225].

The effect on fibroblasts has also been determined. Results were consistent among the literature even at different exposure lengths. Cozin *et al.*, showed a similar effect with GGOH able to close a scratch wound completely in ZA-treated fibroblasts, while a partial recovery was found after PA exposure for 1 week [9]. Migration rates over 72 hours and 48 hours were observed in studies by Ziebart *et al.*, and Hagalauer *et al.*, respectively. The first work indicated a significant increase in cell migration after adding GGOH in the presence of three bisphosphonates tested (Ibandronate, Pamidronate, and Zoledronate) [224]. The other study showed that significant healing started at 24 hours in fibroblasts receiving a combination treatment of GGOH and ZA [223].

2.5.2.3 In vitro - cell death

Incomplete soft tissue healing in MRONJ patients may be caused by oral mucosal cell death. Bisphosphonate-triggered cell death *via* the apoptosis pathway has been reported in several studies [9], [113], [209], [226]. However, there is no work directly investigating whether GGOH could antagonise bisphosphonate effects on oral mucosa cells. A study by Kim *et al.*, proposed that the mechanism underlying keratinocyte cell death involves the induction of early senescence. Treatment with GGOH led to a reduction in the expression of senescence-associated beta-galactosidase (SA-β-Gal), a marker for senescence, which had been induced by PA. Their data suggested a potential role of GGOH on mitigating cell death *in vitro* [124].

2.5.2.4 In vivo

The *in vivo* effect of GGOH on counteracting bisphosphonate toxicity has been examined in two studies. Work by Koneski *et al.*, evaluated GGOH function on MRONJ-like lesions in Wistar rats. The rats were injected with 0.06 mg/kg ZA intraperitoneally once a week for 5 weeks and an extraction socket was created by removing a lower molar tooth on day 21 of the experiment in order to develop MRONJ. Following the tooth extraction, 5 mM GGOH was administered locally into the socket every day for 2 weeks. Lower levels of inflammation in the tissues and signs of osteonecrosis were observed clinically in rats receiving GGOH with ZA; while bone exposure with impaired soft tissue healing was found in the group which was solely treated with ZA [227]. Figure 2.14 demonstrates the clinical wound healing of the two experimental groups. The histological sections of GGOH-treated rats (shown in Figure 2.15) also showed favourable signs of granulation tissue formation and tissue remodelling when compared to the rats without GGOH, suggesting the potential effect of GGOH on reducing bisphosphonate toxicity [227].

Other work by Nagaoka *et al.*, analysed bone mineral density and deposition using micro-computed tomography (micro-CT) in the presence of GGOH in bisphosphonate-induced MRONJ-like mice. ZA was administered into mice twice a week for 2 weeks. At the beginning of the third week, an upper molar tooth was extracted and GGOH was injected in combination with ZA for another 4 weeks. GGOH application was partially able to recover bone deposition and increase bone mineral density from ZA effects [228].

In summary, the favourable effects of GGOH on counteracting bisphosphonate negativity have been demonstrated. However, further investigation is still required because of the variability in results and variability of experimental conditions including concentrations, treatment length, and type of cells used.

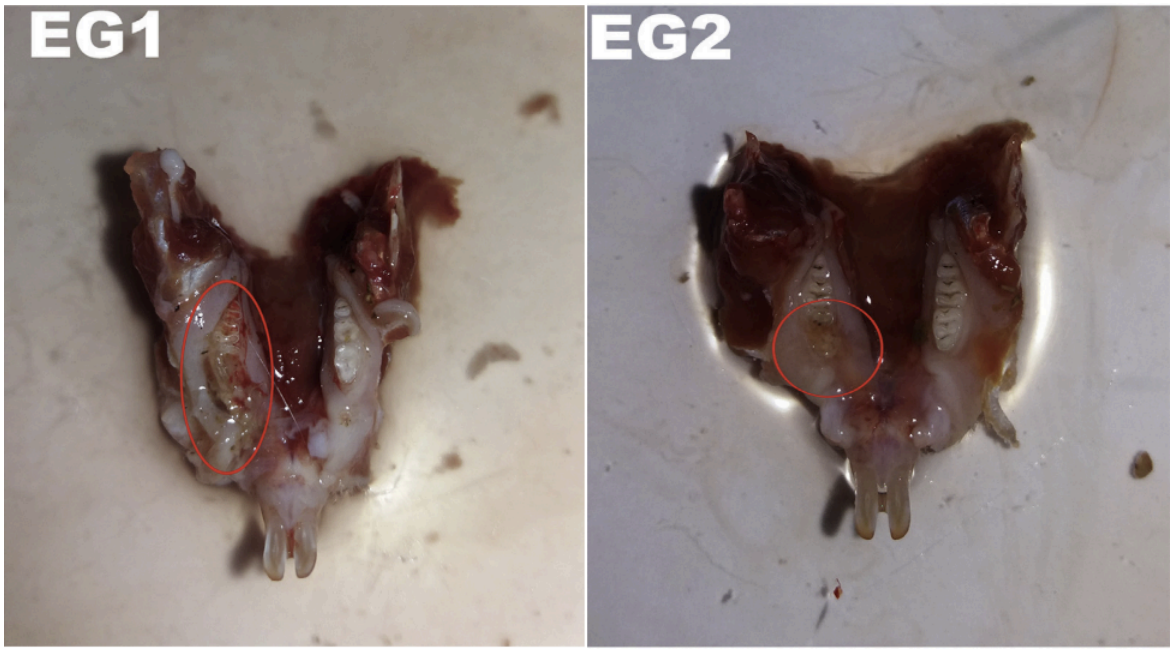

Figure 2.14 | ***Jawbones of zoledronate-treated Wistar rats (EG1) without GGOH or (EG2) with GGOH.*** *Figure reproduced with permission from Koneski et al.,* [227] *under Copyright Clearance Centre Rights license number 5624970242553.*

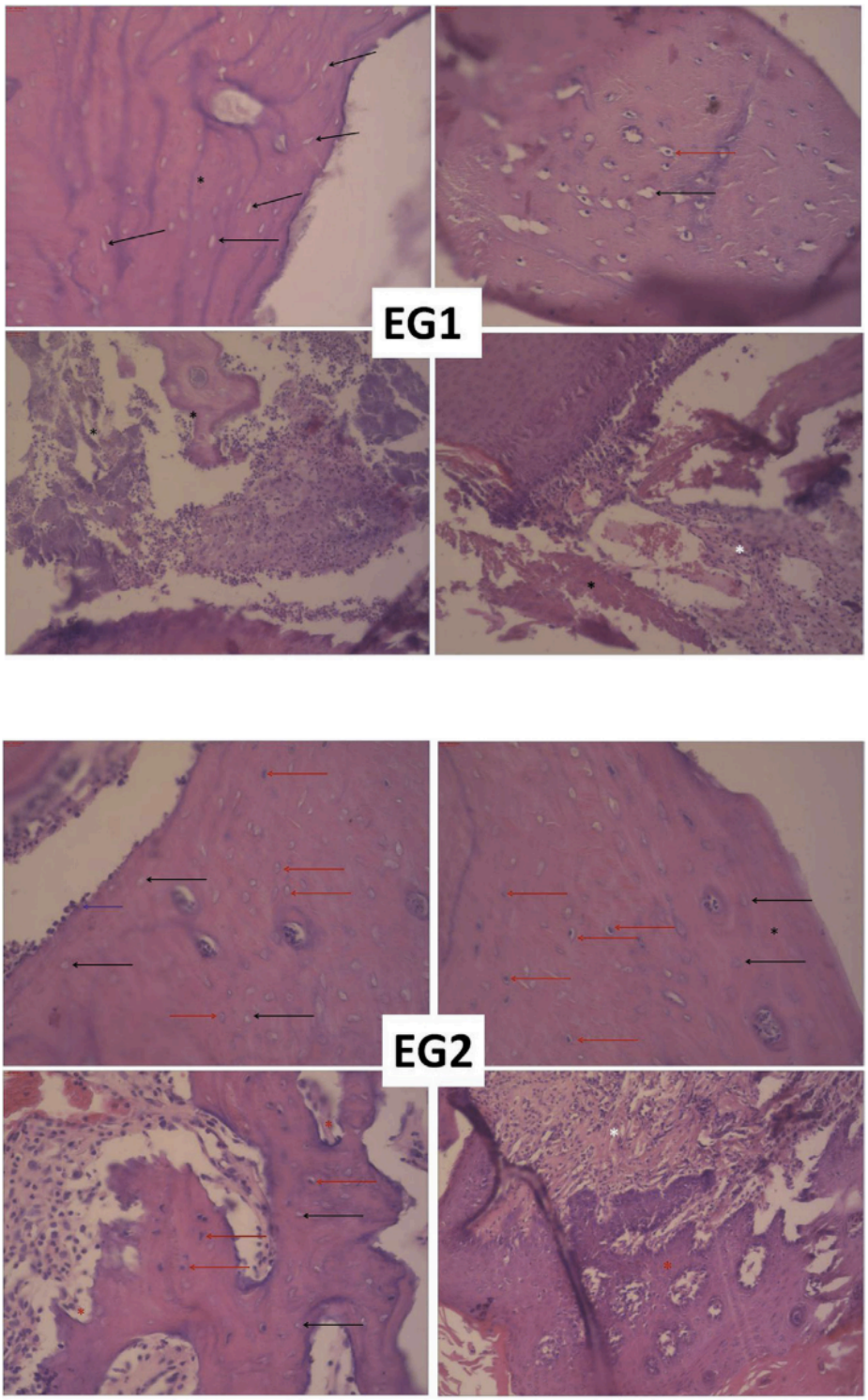

Figure 2.15 | ***Histological sections obtained from tissues adjacent to the extraction socket of zoledronate-treated Wistar rats (EG1) without GGOH or (EG2) with GGOH.*** *Figure reproduced with permission from Koneski et al., [227] under Copyright Clearance Centre Rights license number 5624970242553. Symbols: Red, black, and white asterisk represent vital bone, necrotic bone, and inflammatory cell infiltration respectively. Black arrows highlight empty lacuna while red arrows indicate a lacuna with osteocytes.*

2.5.3 GGOH effect on oral mucosa cells

Besides the desirable effects of GGOH on bisphosphonates, the cytotoxicity needs to be evaluated to determine the drug safety profile. Previously referenced studies have also reviewed the individual effect of GGOH without bisphosphonates on oral mucosa cells. In terms of keratinocytes, studies by Kim *et al.*, and Pabst *et al.*, used two GGOH concentrations which were 0.5 and 10 µM respectively. Both demonstrated no negative effects on oral keratinocyte viability [10], [124].

Inconsistent results have been reported among studies on fibroblasts. A previously mentioned work by Hagelauer *et al.*, also investigated the impact of GGOH without bisphosphonates. They found cytotoxicity occurred at 10 µM GGOH while the higher concentrations, 25, 50, and 100 µM, had no effects [223]. In contrast, work by Ziebart *et al.*, indicated an increase of cell viability from the same GGOH concentration of 10 µM [224]. Two studies by Cozin *et al.*, and Zafar *et al.*, did observe the effects in the presence of 50 µM GGOH for 168 and 72 hours, respectively. The first work demonstrated that GGOH had no effect on fibroblast proliferation at any time point while the later work showed a lower percentage of viable cells after 72 hours of treatment [9], [114].

With unclear effects of GGOH towards oral mucosa, more research needs to be done in order to clarify the GGOH cytotoxicity before further applications are pursued.

2.5.4 Additional therapeutic effects of GGOH

Besides the effects on bisphosphonate related toxicity, GGOH has also demonstrated other therapeutic effects associated with the pathogenesis of MRONJ such as antimicrobial and anti-inflammatory activities.

As infection plays an important role in MRONJ development, the antimicrobial activities of GGOH may help determine the success of MRONJ treatment. As described in Section 2.4.4, infection-related MRONJ contains diverse bacterial strains such as *Actinomyces*, *Porphyromonas*, and *Staphylococcus sp.* [173], [176]. Only a few studies have reported the effects of GGOH on bacterial growth. Inoue *et al.*, investigated the inhibitory effects of GGOH against *Staphylococcus aureus* growth using multiple microbiological methods including broth dilution shaking (BDS) and K^+ leakage assays. Biphasic effects of GGOH on bacterial growth were observed with the most effective inhibitory concentration at 1.25 μg/mL while the higher concentrations produced less growth inhibition. They also indicated the inhibitory mechanism of GGOH was from its ability to disrupt bacterial cell membranes causing the leakage of intracellular potassium ions [229]. This work was supported by Togashi *et al.*, who also examined the effects of aliphatic terpene alcohols and demonstrated the similar growth-inhibitory pattern of GGOH [230]. However, there is no evidence on other MRONJ-associated bacteria which provide an area of study for elucidating the antimicrobial activities of GGOH and further use for prevention and treatment of MRONJ.

The anti-inflammatory effect of GGOH in the presence of bisphosphonates has also been investigated. Work by Marcuzzi *et al*., used alendronate to induce inflammation in mice. They found that inflammatory markers in serum were decreased after injecting the mice with 250 mg/kg GGOH once daily for 2 days [231]. However, this is the only study using bisphosphonates to induce inflammation. Besides, studies have examined the therapeutic effect of GGOH in lipopolysaccharide (LPS)-induced inflammation model. Ohsaki *et al.*, observed lower expression of the *IL-6* gene in LPS-treated human monocytic cell line (THP-1) when pre-treated with GGOH for 24 hours [232]. This was consistent with work by Giriwano *et al.*, who also indicated that pre-treatment with 10 μM GGOH suppressed the expression of inflammatory-related genes including *IL-1β*, *IL-6*, and *TNF-α* in the same cells [233]. Giriwano *et al.*, also conducted an animal experiment to confirm the anti-

inflammatory activity of GGOH. Wistar rats were fed with a GGOH-supplemented diet for 10 days before injecting LPS intraperitoneally. Moderate and high doses of GGOH supplementation significantly reduced serum inflammatory cytokines [234], suggesting that GGOH may inhibit inflammation. This could be another interesting field of study to explore which could also contribute to MRONJ treatment.

2.6 Platelet Concentrates

Platelet concentrates have been highlighted for their benefits in tissue regeneration in various fields including orthopaedics, plastic surgery, dermatology and dentistry [235]. The application of platelet concentrates in the oral and maxillofacial region was first demonstrated in 1998 by Marx *et al.*, who showed an increase in bone density in mandibular defects after treatment with platelet-rich plasma in combination with bone grafts [8], [236].

Difficulties in management and unpredictable outcomes from existing MRONJ therapies have led to the development of complementary strategies [8], [237]. The use of platelet concentrates has been proposed to promote and restore tissue healing caused by bisphosphonate toxicity [8], [238]. A market analysis project that I participated in 2021 reported a high level of interest from dentists who have experiences with MRONJ patients with using platelet concentrates as a potential therapy. Clinical studies on the effect of platelet concentrates on MRONJ have been reported during the past years; however, most were reported cases with only a few randomised controlled trials [6]–[21]. In addition, *in vitro* evidence regarding the cellular responses and the effectiveness of platelet concentrates on MRONJ-like conditions is limited [252]–[254], leading to another interesting field in MRONJ research. This section covers the biology of platelet concentrates and their potential for use as an alternative treatment method for MRONJ patients.

2.6.1 General information and classification

Platelet concentrates are autologous blood fractions containing high quantities of platelets [255]. Platelet concentrates contain numerous growth factors such as platelet-derived growth factor (PDGF), transforming growth factor-beta (TGF-β), vascular endothelial growth factor (VEGF), fibroblast growth factor (FGF), epidermal growth factor (EGF) and insulin growth factor (IGF) which are released following platelet activation and are present within these blood-derived products [238], [256], [257]. Leukocytes and fibrin matrix proteins are also found in varying amounts in platelet concentrates [255], [258]. The importance of leukocytes in platelet concentrates has been determined in the regulation of immune cells and preventing infection [258]. Furthermore, leukocytes are an additional source of growth factors and cytokines which play a significant role in wound healing [259]. The fibrin matrix structure is also known to be important in the healing process as it acts as

a scaffold to trap and regulate the release of growth factors from platelet concentrates while also providing structure [260].

Platelet concentrates are mainly classified into two types: (i) platelet-rich plasma (PRP) and (ii) platelet-rich fibrin (PRF) consisting of a low or high density of fibrin network, respectively [258]. The presence or absence of leukocytes is used to further sub-categorise PRP and PRF into four categories outlined in Table 2.5 [258]. Various preparation techniques (summarised in Table 2.5) have been proposed during the past decades but platelet concentrates are generally isolated either by gravitational centrifugation or automatic cell separators [258].

Table 2.5 | ***Classification of platelet concentrates with preparation protocols*** [258].

Types	Subtypes	Preparation protocols	Techniques
1. PRP	P-PRP	Automated separators	• Cell separator PRP • Vivostat PRF
		Centrifugation	• Anitua's PRGF • Nahita PRP
	L-PRP	Automated separators	• PCCS PRP • SmartPReP® PRP • Magellan PRP • GPS PRP
		Centrifugation	• Curasan9 PRP • Friadent PRP • Regen PRP • Plateltex PRP • Ace PRP
2. PRF	P-PRF	Centrifugation	Fibrinet PRFM
	L-PRF	Centrifugation	• Choukroun's PRF • Modified L-PRF - A-PRF/A-PRF+ - i-PRF

Abbreviations: P, Leukocyte-poor; L, Leukocyte-rich; A-PRF/A-PRF+, Advanced PRF/Advanced PRF plus; I-PRF, Injectable PRF.

2.6.2 Platelet-rich plasma (PRP)

PRP, the first generation of platelet concentrate, was developed in the 1990s and used in bone augmentation surgery [236], [261]. PRP is produced from 2-stage centrifugation of blood containing anticoagulants, as outlined in Figure 2.16 [262]. Variability in the relative centrifugation force (RCF) and spinning time for PRP preparation have been reported [255], [262]. In general, the first spin segregates collected blood into three compartments: red blood cells, buffy coat, and platelet-poor plasma (PPP) located from the bottom to the uppermost portion, respectively. The upper two layers are further processed through a second high speed centrifugation to obtain a liquid formulation of PRP containing concentrated platelets and plasma fibrinogen [262]. The prepared product is later mixed with bovine thrombin or calcium chloride ($CaCl_2$) to stimulate growth factor release and form a gel-like PRP before use [255], [261].

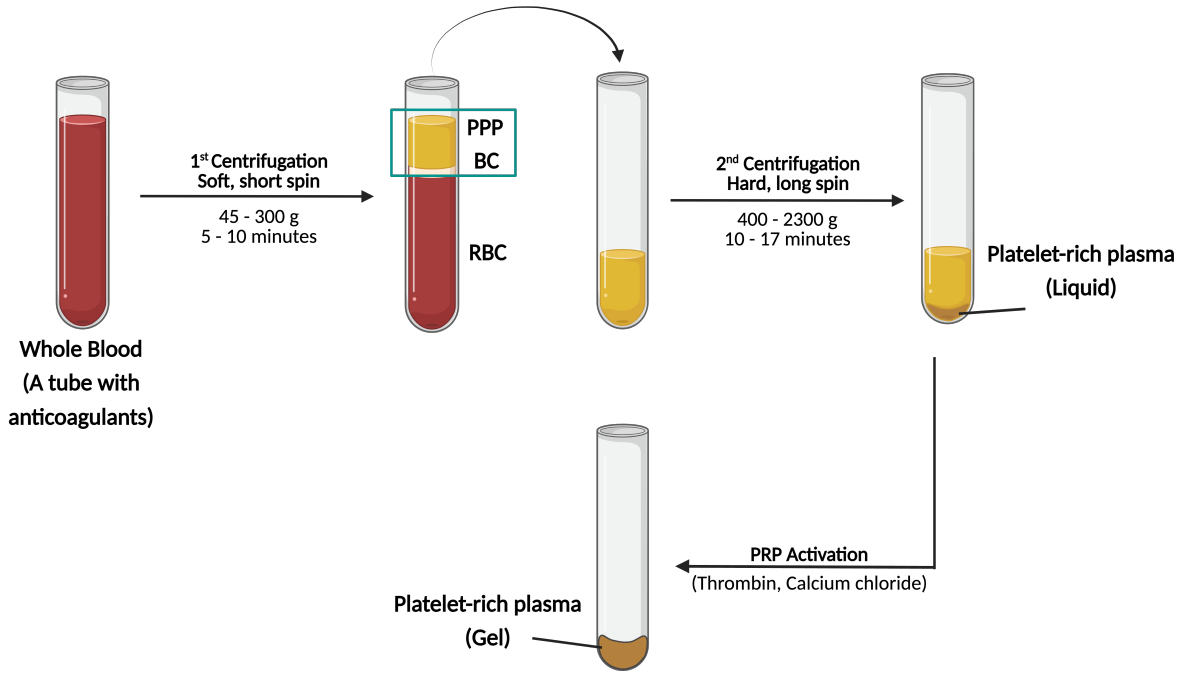

Figure 2.16 | ***Platelet-rich plasma (PRP) preparation process.*** *The diagram outlines the PRP preparation method, starting with the collection of whole blood into an anticoagulant-coated tube. The initial soft and short centrifugation separates the blood into three fractions. The upper yellow layer and buffy coat are collected and subjected to a harder, longer centrifugation to obtain liquid-PRP. PRP is activated to transition from a liquid to a gel formulation with the addition of thrombin and calcium chloride. Figure created using Biorender.com. Abbreviations: PPP, platelet-poor plasma; BC, buffy coat; RBC, red blood cells.*

The *in vitro* effects of PRP on oral wound healing and tissue repair have been examined and positive effects have been observed in many cellular responses including viability, proliferation, migration, and adhesion [263]–[266]. These data suggest PRP has potential for soft tissue regeneration, however, current results are based on experiments with fibroblasts obtained from gingiva and periodontal ligament with no results reported yet for oral keratinocytes.

In these studies, cell culture medium was incubated or mixed with PRP to generate what is described as 'conditioned media'. The procedure allows the paracrine factors from platelet concentrates to be released into the medium. These conditioned media are then used to investigate the bioactivity of not only PRP but also PRF in *in vitro* studies. Therefore, this term will be used throughout this thesis.

Though PRP has demonstrated remarkable effects on tissue regeneration, several concerns have been raised including the complexity and inconsistency of preparation protocols and the use of anticoagulants and bovine thrombin in the preparation [261], [267]. Anticoagulants in PRP from the preparation process may interfere with native tissue wound healing and the regeneration processes [268]. Furthermore, the addition of bovine thrombin to stimulate fibrin clot formation has previously been shown to lead to life-threatening coagulopathies [269].

2.6.2.1 PRP in MRONJ research

As soft tissue toxicity and the failure of the oral mucosa to cover defects is one of the most important contributing mechanisms of MRONJ, PRP has been investigated both *in vitro* and *in vivo* for its potential to repair MRONJ wounds. Steller *et al.*, studied the effectiveness of PRP in the form of PRP-derived conditioned medium on ZA-induced toxicity in oral fibroblasts. The PRP-derived conditioned media, fibroblast growth media containing 2.5% PRP by volume, was applied to oral fibroblasts treated with ZA and an improvement on cell migration was seen compared to cells not exposed to PRP factors [252].

Animal studies have also been conducted to evaluate the effects of PRP. Sakarat *et al.*, applied PRP directly into the extraction socket of ZA-induced osteonecrosis in rats to evaluate its ability to treat MRONJ wounds [254]. The amount of vital bone was significantly higher in the PRP-treated groups but there was no difference in epithelial, blood vessel, and sequestrum formation. Toro *et al.*, hypothesised that PRP could prevent the occurrence of MRONJ [253]. In their study, 100 µg/kg of ZA was injected into senile female rats every 3 days for 7 weeks. The first lower left molar was extracted after 3 weeks, and PRP was immediately applied into the extraction socket and covered by suturing the surrounding mucosa. The epithelium and connective tissue both healed over the extraction site in the PRP-treated group, however, those only treated with ZA developed MRONJ like wounds with exposed bone. Histological sections of rats receiving PRP also demonstrated a higher amount of newly formed bone and lower amounts of non-vital bone, as shown in Figure 2.17. The improvements in tissue repair also correlated with a lower expression of inflammatory markers including TNF-α and IL-1.

The combined use of autologous platelets with stem cells has been investigated by Barba-Recreo *et al.*, they found a synergistic effect on MRONJ prevention in rats treated with PRP and ADSCs [203]. These data prove that MRONJ development after tooth extraction could be prevented through the use of local PRP administration immediately following extraction, which warrants further investigation.

The clinical effects of PRP have been investigated primarily in combination with other treatment approaches such as surgical debridement, bone resection, laser therapies, or cell-based treatment. Studies in a small number of patients have shown improvements to wound healing following administration of PRP in combination with other treatments;

either surgery or laser therapy [205], [206], [245], [246]. Adornato *et al.*, demonstrated that a PRP membrane in combination with marginal resection promoted wound healing in almost 85% of cases (Total patients = 12) [245]. This work was supported by Longo *et al.*, and Curi *et al.*, who both successfully treated MRONJ patients with a combination of bone resection and PRP (Total patients = 72 and 3, respectively) [205], [246]. Mauceri *et al.*, studied the treatment outcomes from using PRP with surgery and Er,Cr:YSGG laser treatment in breast cancer patients exposed to bisphosphonates. An improvement in wound healing was found in 80% of cases (Total cases = 10) [206].

Though evidence has shown that PRP improves wound healing in MRONJ patients, more randomised controlled studies with larger sample sizes are still needed to build the strength of evidence to change clinical practice. In addition, both *in vitro* and *in vivo* investigations on the individual effects of PRP alone without other interventions is also required to confirm the effectiveness of PRP and to further understand the mechanism of action. Drawbacks of PRP, including the use of exogenous additives, anticoagulants and platelet activators, and the variability in preparation procedures, need to be taken into consideration when investigating the potential of PRP for MRONJ treatment.

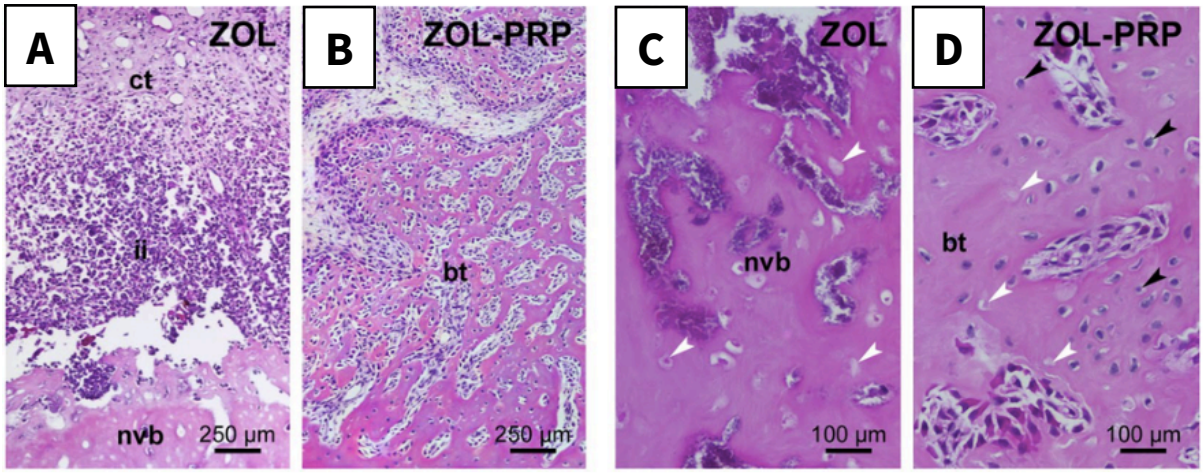

Figure 2.17 | ***Histology of tooth extraction sites after zoledronate treatment with platelet-rich plasma in rats.*** *This figure shows histological sections from tissues surrounding the tooth extraction areas of rats receiving zoledronate alone (A, C) or zoledronate with platelet-rich plasma (PRP) (B, D). (A, B) and (C, D) use 100x and 250x magnification, respectively. Modified with permission from Toro et al.,* [253] *under Creative Common license (CC BY 4.0). Abbreviations: ct, connective tissue; ii, inflammatory infiltrate; bt, bone tissue; nvb, non-vital bone. Symbols: Black arrows indicate osteocytes; white arrows indicate empty lacuna or necrotic osteocytes.*

2.6.3 Platelet-rich fibrin (PRF)

Platelet-rich fibrin (PRF), a second-generation platelet concentrate, was first introduced in 2001 by Choukroun *et al.*, who aimed to develop platelet concentrate without using any anti-coagulating substances [268], [270]. PRF consists of a three-dimensional fibrin meshwork structure enriched with concentrated platelets, growth factors, cytokines, and leukocytes, providing a favourable environment for cell recruitment to support wound healing and tissue regeneration processes [258], [271]–[273]. PRF has been widely used for a variety of regenerative procedures in dentistry including the management of periodontal defects, sinus floor lifting, alveolar bone preservation, and wound closure [273], [274].

PRF has significant advantages over PRP as its preparation requires just one centrifugation step [275]. To prepare PRF, whole blood is immediately centrifuged which induces a natural fibrin clot formation, meaning no additional anticoagulants are required [274]. This fibrin matrix provides a slow continuous and steady release of growth factors over 10 days, offering a more prolonged effect than PRP which has been demonstrated to release the majority of growth factors during the first hour after activation [276], [277]. PRF offers good stability and degradation has been observed over 10-14 days *in vivo* [278]. PRF has also been demonstrated to be non-immunogenic and biocompatible as it is purely obtained from an autologous source unlike PRP which requires the addition of biochemical additives such as anticoagulants in blood tubes and bovine thrombin or $CaCl_2$ for platelet activation [274].

The original PRF, later defined as leucocyte-rich platelet rich fibrin (L-PRF), was produced in a gel formulation after centrifuging blood samples at 400 – 700 g for 10 to 15 minutes [272], [279], [280]. Since then, advancements in PRF preparation have been demonstrated using low-speed (between 44 and 300 g) and shorter centrifugation time (3 to 14 minutes) with the aim of increasing the number of cellular components and growth factors released [271]. These improvements resulted in the development of other PRF formulations including advanced-PRF (A-PRF) and injectable or liquid-PRF (I-PRF/liquid-PRF) [274], [277] (Table 2.5). Figure 2.18 illustrates the preparation process of each type of PRF.

To identify which PRF formulation is most suitable for the treatment and prevention of MRONJ, the following section reviews the *in vitro* studies which have measured the

impact of each PRF formulation on oral soft tissue healing, which is summarised in Table 2.6.

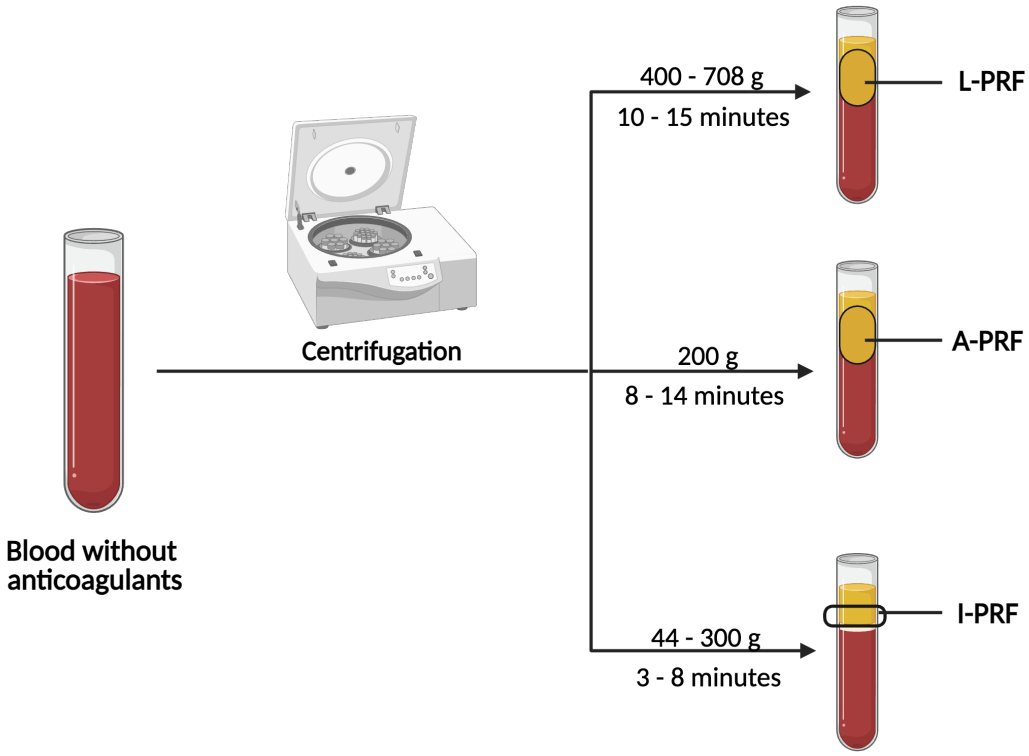

Figure 2.18 | ***Platelet-rich fibrin (PRF) preparation process.*** *This figure illustrates the process of preparing three PRF formulations (L-PRF, A-PRF, and I-PRF) using varying centrifugation speeds and times. Figure created with Biorender.com. Abbreviations: L-PRF, Leukocyte-rich PRF; A-PRF/A-PRF+, Advanced-PRF/Advanced-PRF plus; I-PRF, Injectable-PRF.*

Table 2.6 | Summary of research investigating the in vitro effect of PRF on oral mucosa cells

Cells	Type of PRF	Cellular activities				References
		Viability	**Migration**	**Proliferation**	**Adhesion**	
Keratinocytes	**L-PRF**				↑	[272]
Fibroblasts	**L-PRF**			↑ Cell count		[281]
		↑ (24 hours) ↓ (48,72 hours) MTT				[282]
		--- Live-dead assay	↑	↑ MTT		[283]
		--- Annexin V-Dead cell Assay	↑	↑ Cell count		[284]
	A-PRF	---	↑	↑ MTT		[283]
		--- Annexin V-Dead cell Assay	↑	↑ Cell count		[284]
	I-PRF/ liquid-PRF	---	↑	↑ MTS		[274]
		--- Live-dead assay	↑	↑ WST-1	---	[285]
		--- Live-dead assay	↑	↑ CellTiter-Glo®		[278]
				↑ MTT		[286]

--- = No effect, ↑ = Increase, ↓ = Decrease

2.6.3.1 Traditional PRF (L-PRF)

Traditional PRF or L-PRF presented in a gel formulation, shown in Figure 2.19, is prepared by centrifugation of whole blood using speeds between 400 g and 708 g for 12 to 15 minutes [271], [272], [280]. Several studies have investigated the *in vitro* effects of L-PRF on oral keratinocyte or fibroblast activities as these cells are central to the healing process of the oral mucosa. The only previous study on keratinocytes was conducted by Kasnak *et al.*, who found an increase in epithelial cell adhesion after treating gingival keratinocytes with L-PRF-derived conditioned medium for 24 hours [272]. While this is interesting this study is not directly relevant to the physiological characteristics of oral soft tissues because adhesion was examined on titanium and hydroxyapatite surfaces rather than adhesion to the lamina propria.

Burnorf *et al.*, measured the proliferation of primary gingival fibroblasts using an automated cell counter and found that substances released from L-PRF, termed PRF releasates (PRFR), could stimulate cell proliferation after 7 days [281]. Other studies instead focused on the effects over shorter time periods. Vahabi *et al.*, performed an MTT assay to examine fibroblast viability [282]. They showed that direct application of L-PRF membranes significantly increased the viability of fibroblasts at 24 hours however a reduction in viability was observed after 48 and 72 hours. In contrast, work by Fujioka-Kobayashi *et al.*, indicated that 20% L-PRF-derived conditioned medium did not affect the viability of human gingival fibroblasts through live-dead staining after 24 hours [283]. An increase in cell proliferation measured with the MTT assay was reported following 3 and 5 days of treatment. It should be noted that MTT assay is a measure of the metabolic activity of cells; therefore, it may not accurately determine the proliferative status of the cells. At 24 hours, Fujioka-Kobayashi *et al.*, also found a higher number of migratory cells in the L-PRF-treated group which was consistent with the results from Pitzurra *et al.*, who observed the ability of L-PRF to promote artificial wound healing [283], [284].

Drawbacks of L-PRF include that it should be utilised promptly due to the loss of its structural stability and elasticity over time [287]. Low tensile strength also makes L-PRF difficult for suturing [257], which may result in undesirable outcomes. In addition, the application of the gel formulation of L-PRF is limited for some clinical applications where combination with other biomaterials such as bone substitutes or scaffolds is required [285].

2.6.3.2 Advanced PRF (A-PRF)

Advanced PRF (A-PRF) is produced with a reduced RCF and increased centrifugation time compared to the standard L-PRF centrifugation protocol [288]. Researchers have also further developed an advanced PRF-plus (A-PRF+) by maintaining the centrifugation speed but lowering centrifugation time from the A-PRF preparation protocol [283]. These advanced PRF have been shown to contain significantly more growth factors and are capable of a more prolonged release compared to L-PRF [277], demonstrating a significant advantage for tissue regeneration. Figure 2.19 shows an example of an A-PRF gel clot prepared by spinning blood without anticoagulants at 200 g (1500 rpm) for 14 minutes.

In terms of the mechanical properties, the highest tensile strength and resistance to traction were obtained from A-PRF+ membrane followed by A-PRF and L-PRF, respectively [289]. Work by Ravi *et al.*, also found better properties of A-PRF as it demonstrated higher tensile strength and elastic modulus and lower degradation rate compared to L-PRF [290].

The biological function of A-PRF/A-PRF+ on oral mucosa cells has only been reported in work investigating fibroblasts. The previously mentioned work by Fujioka-Kobayashi *et al.*, indicated a more pronounced positive effect of A-PRF on cell migration and proliferation compared to L-PRF [283]. Pitzurra *et al.*, also observed faster wound closure in periodontal fibroblasts-treated with A-PRF-conditioned medium compared to L-PRF after 24 hours [284].

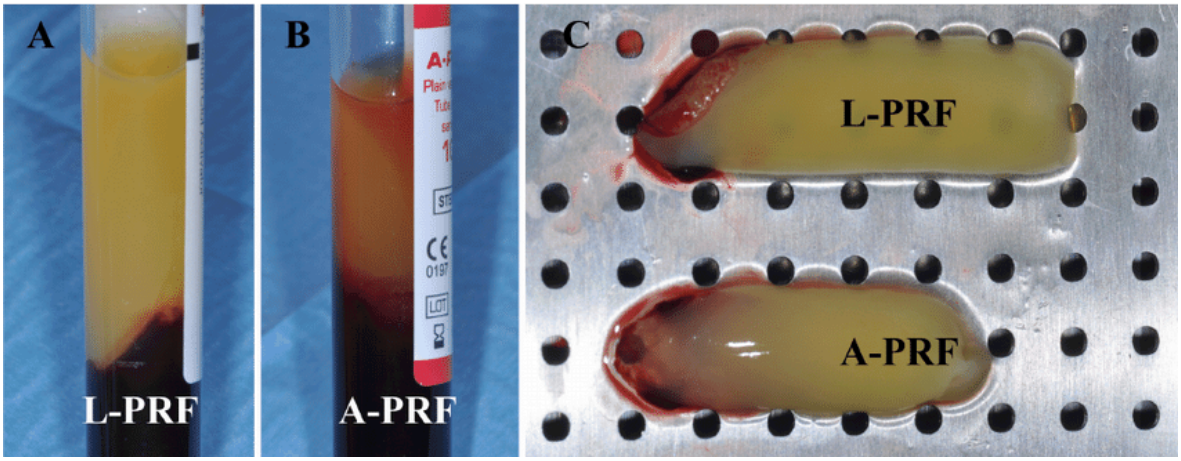

Figure 2.19 | ***Comparative macroscopic observations of L-PRF and A-PRF.*** *(A) shows L-PRF in a blood tube post-centrifugation at 400 g for 12 minutes, while (B) illustrates A-PRF after centrifugation at 200 g for 14 minutes. (C) displays L-PRF and A-PRF membranes after removal of red blood cell clots. Figure reproduced with permission from Ehrenfest et al.,* [280] *under Creative common License (CC BY-NC-ND 4.0).*

2.6.3.3 Injectable or Liquid PRF (I-PRF/Liquid-PRF)

I-PRF or liquid-PRF has been recently improved from the low-speed concept by using a lower centrifugation time and lower spinning speed, yielding higher concentrations of leukocytes, platelets and growth factors [274], [291].

Studies on how I-PRF influences the cellular activities of oral mucosa were examined in work investigating fibroblasts with 20% of I-PRF-derived conditioned medium used in all investigations. Miron *et al.*, showed that I-PRF increased the migration ability of gingival fibroblast at 24 hours [274]. Two studies conducted by Wang *et al.*, and Fujioka-Kobayashi *et al.*, also found a positive effect on cell migration at the same time point [278], [285]. These studies also used the transwell migration assay to evaluate cell migration. When investigating cell proliferation, higher cell numbers were observed from all studies after fibroblasts were treated with I-PRF for 5 days [274], [278], [285], [286]. However, the proliferative data should again be cautiously interpreted since the results were obtained from MTS, MTT, WST-1 and CellTiter-Glo® assays that do not directly measure cell proliferation, but rather cell metabolic activity.

Several studies looked at the gene expression of cells following I-PRF treatment and found an up-regulation of *PDGF, TGF-β* and *COL1A2* gene expression, indicating the role of I-PRF on wound healing and regeneration processes, especially in the connective tissues [274], [285]. With the effects of I-PRF on oral keratinocytes unknown, further investigation is needed to understand the bioactivity of I-PRF on oral mucosa cells.

I-PRF provides a significant advantage over L-PRF and A-PRF/A-PRF+ formulations as it contains a greater number of cells and growth factors as mentioned above. I-PRF is also versatile for many clinical applications as it can be used in an injectable formulation, mixed with bone substitutes or other biomaterials, or used as a coating on biological membranes to improve biological and physical properties [291]–[294]. These features make I-PRF an interesting candidate to be investigated further for use in oral soft tissue regeneration. Table 2.7 summarises the preparation protocol and properties of each type of platelet concentrates.

Table 2.7 | ***Summary of preparation protocols and properties of platelet concentrates***

Type	Spinning protocol		Estimated total amount of growth factor after 3 days (pg/mL)					Material properties	Advantages	Disadvantages	References
	Speed (g)	Time (minutes)	PDGF-BB	TGF-β1	VEGF	EGF	IGF				
PRP	*1st spin*: 100 – 900 *2nd spin*: 400 – 2000	*1st spin*: 5 – 10 *2nd spin*: 10 – 17	1,000 – 1,250	750 - 1,000	500 - 750	300 - 400	25 - 50	Gel (After activation)	- Present in a liquid form until activated - High release of growth factors during earlier time points	- Anticoagulants delay tissue healing - Multi-step centrifugation - Complexity and inconsistency of preparation protocols - Rapidly dissolve/unstable - Life-threatening complications - Short burst growth factor release	[261], [268], [269], [274], [277], [285], [295], [296]
L-PRF	280 400 400 700 708	10 (F) 12 (F) 15 (F) 12 (F) 12 (F)	500 - 750	1,000 - 1,250	500 - 750	400 - 500	150 - 175	Gel	- No additives (anticoagulants, $CaCl_2$ or bovine thrombin) - More steady and continual growth factors release than PRP	- Inconsistency of preparation protocols - Low tensile strength - Not injectable	[270], [272], [277], [280]–[284]
A-PRF **A-PRF+**	200 or 208 200 or 208	14 (F) 8 (F)	750 - 1,000	1,250 - 1,500	750 - 1,000	600 - 700	100 - 125	Gel	- No additives (anticoagulants, $CaCl_2$ or bovine thrombin) - More steady and continual growth factors release than PRP - Better mechanical properties than L-PRF	- Not injectable	[277], [283], [284], [288], [290]
I-PRF	44 60 200 300	8 (F) 3 (F) 8 (H) 5 (H)	500 – 2,000	5,000 – 7,500	100 - 500	500 - 800	2,000 - 2,500	Liquid	- No additives (anticoagulants, $CaCl_2$ or bovine thrombin) - Shortest preparation time - More steady and continual growth factors release than PRP - Injectable, more versatile	- Inconsistency of preparation protocols based on the type of centrifuge	[274], [278], [285], [286]

Abbreviations: F, Fixed-angled centrifuge; H, Horizontal swing centrifuge.

2.6.3.4 PRF in MRONJ research

While the above studies demonstrate PRF has a positive effect on oral fibroblast proliferation and migration, the results are more limited when looking specifically at PRF for MRONJ. This section will summarise the research which has been conducted to date *in vitro* and in clinical studies.

The previously mentioned study by Steller *et al.*, evaluated the effects of PRF in bisphosphonate-treated fibroblasts [252]. L-PRF was prepared by centrifugation at 400 g for 10 mins. They found that 5% L-PRF-derived conditioned medium enhanced fibroblast migration and proliferation in the presence of 80 μM ZA, demonstrating the regenerative properties of L-PRF on MRONJ *in vitro*.

Clinical applications of PRF in MRONJ have been documented extensively for both preventive and treatment purposes. It is worth noting that the majority of studies used PRF gel (either L-PRF or A-PRF) in combination with other existing treatments such as antibiotics, mouthwashes, debridement, or surgical necrotic tissue resection to examine the bioactivity of PRF. A summary of clinical studies examining PRF for MRONJ prevention is presented in Table 2.8. Asaka *et al.*, and Pispero *et al.*, investigated the effect of a PRF membrane on wound healing in patients receiving alendronate immediately after tooth extraction [240], [243]. They both found complete re-epithelialisation of oral mucosa which suggests the usefulness of PRF on MRONJ prevention. However, these findings should be cautiously interpreted as neither study had an appropriate control group to compare the efficacy of PRF.

Several papers reported the effect of PRF for the treatment of established MRONJ wounds, as shown in Table 2.9. The majority of articles were case reports with favourable outcomes observed in a small number of patients. Currently, there is one reported case on the use of I-PRF on MRONJ. Giudice *et al.*, applied A-PRF membrane with I-PRF to intraoral wounds and oro-cutaneous fistula in a patient diagnosed with stage III MRONJ who had alendronate therapy for the treatment of severe osteoporosis. They reported a complete wound healing of the necrotic area and closure of the fistula within 2 months. There was also no recurrence of bone exposure or wounds during a 5-year follow-up period [297]. Soydan *et al.*, reported mucosal coverage over an area of exposed bone after 2 weeks in a patient who received two layers of L-PRF membranes (Total case = 1) [247]. Both Gonen *et*

al., and Maluf *et al.,* observed a similar effect at the same time point (Total cases = 1 and 2, respectively) [239], [251]. Other studies that investigated the effects of PRF with a longer follow-up period ranged from 1 to 36 months and these studies also demonstrated good mucosal healing in most MRONJ patients [244], [248]–[250]. The type of bisphosphonate and severity of the disease may influence the success rate of PRF on MRONJ treatment. A study by Moura˜o *et al.*, observed excellent mucosal healing in all MRONJ patients (Total cases = 11) receiving oral alendronate to treat osteoporosis [244]. In contrast, a study by Kim *et al.*, reported that two patients, both diagnosed with stage III MRONJ and receiving ZA therapy to treat bone metastatic cancer, still had exposed necrotic bone 4 months after being treated with PRF a collagen sponge containing PRF and recombinant human bone morphogenic protein (rhBMP-2) impregnated collagen sponge [248]. This information indicates there may be limitations in the effectiveness of PRF for the treatment of more severe or advanced MRONJ cases.

Besides case reports, clinical trials have also been performed. Park *et al.*, assessed tissue healing after 1 and 4 months in established MRONJ patients who were given either L-PRF alone or in combination with rhBMP-2 impregnated collagen sponge [241]. Most patients in both groups (86% from L-PRF group and 96% from PRF with rhBMP-2 group) showed complete mucosal healing after 4 months. The number of patients with complete mucosal healing was higher in the combined treatment group than the L-PRF-treated group alone after 1 month. This correlated with results from Giudice *et al.*, who evaluated the effectiveness of surgical treatment with or without A-PRF in stage II and III MRONJ patients [242]. At 1 month postoperative, there were significantly more patients with favourable mucosal integrity, no necrotic bone exposure, and no signs of infection in the A-PRF-treated group compared to the group who received surgical treatment alone. These studies suggest that PRF may influence the early periods of wound healing.

To date, most of the existing evidence demonstrates beneficial effects of PRF and its potential to be used to treat MRONJ; however, stronger evidence is required to support changes in clinical practice and guidance for MRONJ treatment. Randomised controlled studies with adequately powered sample sizes are required to provide the strength of evidence required. Most of the studies described here were case reports which means there is a high risk of bias as positive results tend to be reported more readily.

Though previous studies have mentioned the therapeutic effect of PRF on tissue regeneration, the mechanism of how PRF facilitates wound healing, particularly in MRONJ, remains undefined. While a few studies have been conducted, experiments in 2D culture systems with just fibroblasts cannot fully represent the clinical scenario. To determine the mechanism through which PRF stimulates MRONJ wound healing and to understand its bioactivity, more comprehensive experiments with good quality *in vitro* and *in vivo* models are required.

Table 2.8 | ***Clinical studies on the effect PRF on preventing MRONJ***

Author (Year)	Type of study	No. of patients/ experimental sites	Type of medications	Interventions	Main outcomes	Key weaknesses	References
Asaka *et al.* (2017)	Clinical trial	102 - 73 control - 29 experimental	AL	- A PRF membrane was placed after tooth extraction	- Complete epithelium formation in 4 weeks was found in all patients received PRF - 9 patients (12%) in control group had delayed wound healing	- Different sample size in each group - Results from experimental group was collected prospectively while control data were done retrospectively - 75% of patients discontinued bisphosphonates treatment - Low risk of developing MRONJ since patients took oral bisphosphonates	[240]
Pispero *et al.* (2019)	Case report	1	AL	- Double layer of PRF membranes were applied in and above the alveolar socket	- Epithelialisation was completed after 2 weeks	- Single patient with no control - Low risk of developing MRONJ since patient took oral bisphosphonates	[243]

Abbreviations: AL, Alendronate.

Table 2.9 | A summary of studies on PRF applications for MRONJ treatment

Author (Year)	Type of study	No. of patients/ experimental sites	Type of medications	Interventions	Main outcomes	Key weaknesses	References
Soydan *et al.* (2014)	Case report	1	- ZA, PA	- Two layers of PRF membrane	- Complete mucosal coverage after 2 weeks post-operation - No gingival loss, inflammation, and bone exposure at 6-month postoperative follow-up	- Single patient with no control	[247]
Kim *et al*. (2014)	Case series	34	- AL, RS, ZA, PA	- PRF with rhBMP-2 impregnated collagen sponge	- 77% of patients had full cover mucosa after 1 month - 2 cases (both stage III MRONJ) had a failure from treatment	- Small sample size with no control - Heterogeneity in patient conditions (Drug types, indications, location of lesions)	[248]
Dinca *et al.* (2014)	Case report	10	- ZA, IB	- PRF membrane	- All patients showed sign of mucosal healing improvement with no exposed bone at 30 days	- Small sample size with no control - Heterogeneity in patient conditions (Age, location of lesions)	[249]
Nørholt *et al.* (2016)	Case series	15	- ZA, AL, IB, PA, Dmab	- Multiple PRF membrane coverage	- 93% of patients demonstrated complete mucosal healing with no symptoms	- Small sample size with no control - Different follow-up time point - Heterogeneity in patient conditions (Drug types, indications, location of lesions)	[250]
Park *et al.* (2016)	Clinical trials	55 - 25 controls - 30 experimental	- AL, ZA, RS, PA, IB, or combined	- Either a single L-PRF or rhBMP-2 soaked in collagen membrane with L-PRF	- At 4 weeks, higher proportion of patients (60%) treated with the combination regimen displayed complete mucosa healing with no signs of MRONJ compared to a group receiving L-PRF alone (36%)	- Outcomes may occur as a result of rhBMP-2 more than L-PRF - Heterogeneity in patient conditions (Drug types)	[241]

Abbreviations: ZA, Zoledronate; PA, Pamidronate; AL, Alendronate; RS, Risedronate; IB, Ibandronate; Dmab, Denosumab; rhBMP-2 = recombinant human bone morphogenic protein-2.

Table 2.9 (continued) | ***A summary of studies on PRF applications for MRONJ treatment***

Author (Year)	Type of study	No. of patients/ experimental sites	Type of medications	Interventions	Main outcomes	Key weaknesses	References
Gonen *et al.* (2017)	Case report	1	- ZA	- 2 layers of PRF membrane with local debridement and bone resection	- Epithelium healing was observed after 2 weeks - At 3 months, bone exposure was completely healed	- Single patient with no control	[251]
Maluf *et al.* (2017)	Case series	2	- ZA, Dmab	- PRF membrane	- Gingival healing with no bone exposure in both cases after 14 days	- Different follow-up period (7-20 months) - Very small sample size with no control	[239]
Giudice *et al.* (2018)	Clinical trials	47 - 23 controls - 24 experimental	- ZA, AL, IB, Dmab	- Either single surgical procedure or in combination with A-PRF	- Patients receiving a combination treatment demonstrated higher percentage of mucosal healing	- Heterogeneity in patient conditions (Drug types)	[242]
Moura˜o *et al.* (2020)	Case series	11	- AL	- Surgical bone debridement with PRF	- Excellent soft tissue healing was found in all patients	- Small sample size with no control - Different follow-up appointment (12-36 months) - Low risk of MRONJ recurrence since patients took oral bisphosphonates	[244]
Giudice *et al.* (2020)	Case report	1	- AL	- A-PRF membrane in combination with I-PRF injection	- Complete intraoral wound and oro-cutaneous fistula was completely healed after 50 days	- Single patient with no control	[297]
Law *et al.* (2021)	Case series	4	- IB, AL, ZA	- L-PRF membrane	- 3 out of 4 patients demonstrated a successful wound healing	- Very small sample size with no control - Heterogeneity in patient conditions (Drug types, indications, location, and size of lesions)	[298]

Abbreviations: ZA, Zoledronate; PA, Pamidronate; AL, Alendronate; RS, Risedronate; IB, Ibandronate; Dmab, Denosumab.

This literature review provides an overview of MRONJ, a condition which develops from the use of bisphosphonates to treat osteoporosis, bone cancer and other excessive bone resorption disorders. These medications cause detrimental effects on jaw bones and the overlying mucosa. To date, unresolved challenges around MRONJ persist as there is no effective therapeutic approach for patients. This highlights the research gap and emphasises the need to develop novel strategies that enhance the repair of overlying oral mucosa, which is considered to be key to resolve the disease.

Given the presented data in this section, there is a lack of comprehensive *in vitro* investigations on oral mucosa responses to either GGOH or I-PRF treatments in the presence of bisphosphonates. Furthermore, the mechanisms of these interventions on facilitating the soft tissue healing in MRONJ have yet to be conclusively elucidated. Explorations on the efficacy of both interventions will provide pivotal and useful information to improve the treatment approaches for MRONJ patients in the future.

CHAPTER 3

Aims and Objectives

3. Aims & Objectives

The primary aim of this study was to develop novel strategies for repairing soft tissue wounds which occur as a result of MRONJ. Two potential treatment approaches, Geranylgeraniol (GGOH) and injectable platelet-rich fibrin (I-PRF), were chosen and the response of the oral mucosa was examined using 2D and 3D *in vitro* assays. We hypothesised that these methods could prevent or reduce toxicity caused by bisphosphonates in the oral mucosa.

There are three experimental chapters in this thesis with the summary of objectives as follows:

1. To examine the effect of GGOH on the metabolic activity and behaviour of oral mucosa cells in the presence of bisphosphonates. (Chapter 4)

2. To develop a reproducible method to generate I-PRF and identify the components of I-PRF. (Chapter 5)

3. To investigate the responses of oral mucosa cells to I-PRF and the role of I-PRF on oral wound healing using 2D and 3D culture. (Chapter 5)

4. To evaluate the bioactivity of I-PRF on bisphosphonate-treated oral mucosa cells in 2D cell culture and 3D oral mucosa models. (Chapter 6)

CHAPTER 4

In vitro effect of geranylgeraniol (GGOH) on bisphosphonate-induced cytotoxicity of oral mucosa cells

4. *In vitro* effect of geranylgeraniol (GGOH) on bisphosphonate-induced cytotoxicity of oral mucosa cells

The work presented in this chapter has been published:
Rattanawonsakul K, Bullock G, Bolt R, Claeyssens F, Atkins S, Hearnden V. ***In vitro* Effect of Geranylgeraniol (GGOH) on Bisphosphonate-Induced Cytotoxicity of Oral Mucosa Cells.** Front Oral Health. 2022 Jun 20;3:892615. DOI: 10.3389/froh.2022.892615.

4.1 Introduction

Medication-related osteonecrosis of the jaw (MRONJ) is an adverse event caused by antiresorptive and antiangiogenic drugs, and is characterised by exposed, necrotic bone without mucosal healing after 8 weeks [114], [222]. The disease predominantly occurs in patients receiving intravenous nitrogen-containing bisphosphonates such as zoledronate (ZA) or pamidronate (PA) for the treatment of bone malignancies [9]. MRONJ can cause significant morbidity in terms of pain, discomfort, and dysfunctional oral habits which worsen the quality of life [149], [299].

Though the disease was first identified almost 20 years ago [300], the definitive pathophysiology of MRONJ has not yet been defined and is likely multifactorial [1]. Multiple contributing mechanisms have been proposed since the disease process was first characterised; including bone turnover impairment, angiogenesis inhibition, infection and inflammation and mucosal toxicity [1], [149]. A loss of mucosal covering leading to the exposure of bone is a clinical hallmark of MRONJ and an important target in the development of novel therapies [146]. Previous studies have demonstrated clinically relevant concentrations of both ZA and PA can induce significant toxicity in the cells and *in vitro* tissues of the oral mucosa [2], [123], [301] and that this interferes with the oral wound healing process [9], [116], highlighting the significance of soft tissue toxicity in the development and resolution of MRONJ.

The clinical management of MRONJ is challenging as there are limited data on its pathogenesis and there has been recent controversy over the current therapeutic strategies [1], [144]. The key factors in MRONJ management include (i) necrotic bone removal, (ii) soft

tissue restoration, and (iii) pain and infection control [190]. Currently, there is no standard treatment protocol for MRONJ [7]. Research is now required to develop alternative therapeutic measures to help manage the disease more effectively.

The action of nitrogen-containing bisphosphonates primarily inhibits the farsenyl pyrophosphate synthase (FPPS) enzyme of the mevalonate pathway causing disruption in the synthesis of isoprenoids including farsenyl pyrophosphate (FPP) and geranylgeranyl pyrophosphate (GGPP), as shown previously in Figure 2.10 [223]. The loss of these mevalonate intermediates negatively affects the prenylation of GTP-binding proteins such as Ras, Rho, Rac, Rap, and Cdc42 which are necessary for the growth, differentiation, and function of osteoclasts [107], [227] along with other cell types.

Geranylgeraniol (GGOH), an analogue molecule of GGPP, has previously been shown to play a pivotal role in the viability and proliferation of MSCs [302]. It has been demonstrated that GGOH counteracted bisphosphonate toxicity in several cell types including osteoclasts, osteoblasts, endothelial cells, keratinocytes, and fibroblasts [9], [10], [222]–[224]. However, previous studies of GGOH on cells of the oral mucosa have shown inconsistent and shown contradictory findings. Most studies were undertaken using a single GGOH concentration ranging between 0.5 µM to 50 µM to reverse the effect of bisphosphonates [9], [10], [114], [124], [133], [223] and very few studies have reported the cytotoxic effect of GGOH when exposed to cells in the absence of bisphosphonates [114]. Therefore, further studies are needed to define the *in vitro* function of GGOH on the oral mucosa and to determine an effective dose.

GGOH has also been tested in *in vivo* studies. MRONJ-induced rats exposed to GGOH demonstrated an improvement in oral wound healing [227]. Inflammatory tissues with favourable signs of tissue remodelling were observed in rats receiving 5 mM GGOH once daily in combination with ZA, when compared to a control group solely treated with ZA, suggesting the potential positive effect of GGOH on the healing of MRONJ wounds.

GGOH has not only attracted interest in the potential management of MRONJ, but also in further clinical applications in the management of cancer and drug complications as a result of its anti-inflammatory, antibacterial [230], [233] and anti-cancer properties [303]–[305]. GGOH has been found to be capable of inducing cellular apoptosis and reducing the viability of various cancer cells including: hepatoma, prostate carcinoma, or colon cancer

cells [303]–[305]. Other studies have shown that myotoxicity, the most common side effect of statins, can be prevented with GGOH [306].

4.2 Aim(s)

The aim of this chapter was to analyse the effect of GGOH on oral mucosa cells in both the presence and absence of clinically-relevant bisphosphonates, to determine the molecule's potential as a treatment for soft tissue damage in MRONJ. We hypothesised that GGOH could restore soft tissue damage caused by bisphosphonates by supplementing the depletion of geranylated proteins in cells of the oral mucosa (Figure 4.1).

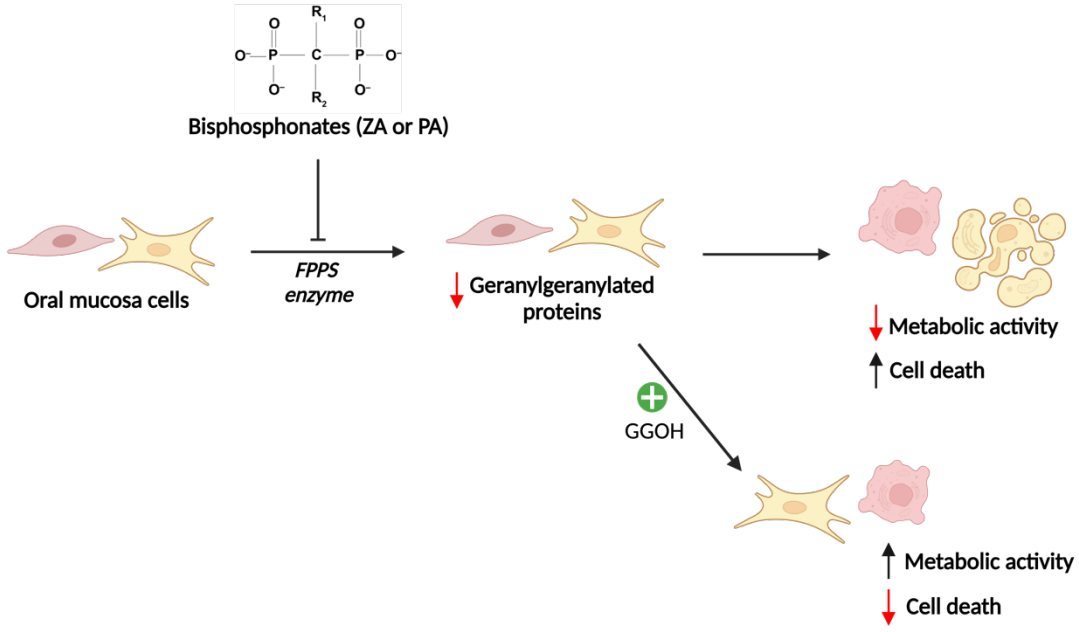

Figure 4.1 | A summary diagram of the hypothesis to support using GGOH to reduce bisphosphonate-induced oral mucosa toxicity. *Figure created using Biorender.com. Abbreviations: ZA, zoledronate; PA, pamidronate; FPPS, farsenylpyrophosphate synthase; GGOH, geranylgeraniol.*

4.3 Materials and Methods

4.3.1 Cells and culture medium

Three types of cells were used for the experiments. Human immortalised oral keratinocytes with human telomerase reverse transcriptase expression [74] (OKF6/TERT-2) between passage 4 to 25 were cultured in supplemented keratinocytes serum-free medium (KSFM, outlined in Table 4.1). Primary oral keratinocytes (NOKs) during passage 1 to 4 were cultured on a feeder layer of irradiated murine fibroblasts (i3T3) using supplemented Green's medium (Table 4.2). Primary oral fibroblasts (NOFs) between passage 2 to 10 were grown in DMEM with supplements (Table 4.3).

Table 4.1 | ***Composition of Keratinocyte Serum Free Medium (KSFM)***

Components	**Amount/ Volume**	**Final concentration**	**Supplier Name**
Keratinocyte serum free medium	495 mL	98 %	Life Technologies
Bovine pituitary extract	25 mg	0.05 mg/mL	
Recombinant human Epidermal growth factor (rh-EGF)	2.5 µg	0.005 µg/mL	
Penicillin/Streptomycin	5 mL	100 IU/mL / 100 µg/mL	Sigma-Aldrich

Table 4.2 | ***Composition of Green's Medium***

Components	Volume	Final concentration	Supplier Name
DMEM without Glutamine	330 mL	66 %	Sigma-Aldrich
Ham's Nutrient Mixture F12	108 mL	21.6 %	
Foetal bovine serum (FBS)	50 mL	10 %	Biosera
L-glutamine	5 mL	0.01 mg/mL	Sigma-Aldrich
Penicillin/Streptomycin	5 mL	100 IU/mL / 100 µg/mL	
Fungizone	1.25 mL	0.625 µg/mL	
Adenine	2 mL	0.025 µg/mL	
3,3,5-Tri-iodothyronine /Apo-Transferrin (T/T)	0.5 mL	1.36 ng/mL / 5 µg/mL	
Epidermal growth factor (EGF)	25 µL	5 ng/mL	
Insulin	2.5 mL	5 µg/mL	
Hydrocortisone	80 µL	4 µg/mL	
Cholera toxin	0.5 mL	8.47 ng/mL	

Table 4.3 | ***Composition of Dulbecco's Modified Eagle's Medium (DMEM)***

Components	Volume	Final concentration	Supplier Name
Dulbecco's Modified Eagle's Medium without glutamine	440 mL	88 %	Sigma-Aldrich
Foetal bovine serum (FBS)	50 mL	10 %	Biosera
L-glutamine	5 mL	0.01 mg/mL	Sigma-Aldrich
Penicillin/Streptomycin	5 mL	100 IU/mL / 100 µg/mL	

4.3.2 Buccal biopsies and primary cell isolation

Buccal mucosa tissues were biopsied from willing healthy volunteers following written informed consent under local anaesthetics by an oral surgeon to obtain primary oral keratinocytes and fibroblasts under the approval of the University of Sheffield Research Ethics Committee (No. 003463). All procedures were performed in accordance with the Declaration of Helsinki. After surgical procedures, specimens were preserved in phosphate buffered saline (PBS) (Sigma-Aldrich, UK) supplemented with 100 µg/mL penicillin/streptomycin (Sigma-Aldrich, UK) and 0.625 µg/mL fungizone (Sigma-Aldrich, UK) before oral keratinocytes and fibroblasts were isolated.

Tissue samples from the oral biopsies were then placed in 10 mL of 0.1% Difco™ Trypsin (BD Biosciences, UK) overnight to initiate cell detachment. On the following day, the specimen was poured into a petri dish and the epithelial cell layer was gently scraped off using a sterile scalpel and forceps in order to obtain keratinocytes while the remaining biopsy was placed back into PBS mixture and stored in a fridge. The epithelial cell suspension in Difco™ Trypsin was added into a universal tube, then 5 mL of Green's medium was added into the petri dish for washing, collecting the remaining keratinocytes and deactivating trypsin before transferring the mixture into the same tube. The mixture was centrifuged at 170 g (1000 rpm) for 5 minutes. The supernatant medium was gently discarded to prevent cell loss. The pellets were resuspended in Green's medium and added into T-75 tissue culture flasks containing 1 x 10^6 cells of i3T3 fibroblast feeder layer. The medium for primary oral keratinocytes (referred to subsequently as NOKs) was changed on the following day and the growth was monitored closely until cells were confluent.

The remaining biopsy was finely minced and soaked in 0.5 mg/mL collagenase A solution (Roche, UK) in a universal tube, and the tube was placed in the 5% carbon dioxide (CO_2) incubator at 37°C (LEEC Safe Touch190S, UK) overnight to detach the primary fibroblasts from the extracellular matrix. The next day, supplemented DMEM was added to the collagenase-containing specimen for collagenase deactivation and the suspension centrifuged at 608 g (2000 rpm) for 10 minutes. The supernatant was gently poured away and pellets resuspended with DMEM. Cell mixtures were added into T-25 flasks for fibroblast culture. Cell growth was also assessed and the medium was changed every 3-4 days until cells were confluent for passaging into T-75 flasks.

4.3.3 Cell growth and passaging

Cell culture experiments were performed in a biological safety cabinet class II (Walker, UK). Cells were incubated and maintained at 37°C in a 5% CO_2 atmosphere. Before the experiment, working surface area, equipment, and gloved hands were disinfected by 70% Industrial Methylated Spirit (IMS) (Thermo Fisher Scientific, UK).

All cells were grown in T-75 tissue culture flasks until reaching over 80% confluency. Cell passaging started by removing the old medium from flasks, then cells were washed with sterile PBS. Trypsin-EDTA solution (5 mg/mL trypsin and 2 mg/mL EDTA) (Sigma-Aldrich, UK) was added into tissue culture flasks and incubated for 5 minutes to detach cells. Serum-containing medium at a 1:1 ratio (v/v) was added to deactivate the trypsin enzyme. For primary keratinocyte (NOK) culture, 0.2 mg/mL ethylenediaminetetraacetic acid (EDTA) (Sigma-Aldrich, UK), was added into the flask after the PBS wash. EDTA was incubated for 5 minutes to remove the i3T3 feeder layer before adding trypsin-EDTA solution as described above. The cell suspension was centrifuged at 170 g (1,000 rpm) for 5 minutes. The supernatant was gently removed and cell pellets were resuspended in the specific medium for each cell type. The total cell number was counted using a haemocytometer (Hawksley, UK). Cells were then either seeded into well-plates for experiments or transferred to tissue culture flasks for continued culturing.

4.3.4 Bisphosphonates and geranylgeraniol (GGOH)

A stock solution of GGOH (20 mM) (Sigma-Aldrich, UK) was prepared in ethanol. It was aliquoted and stored at −20◦C. The solution was thawed and diluted with cell culture medium before each experiment. The working concentration of GGOH used in this study ranged from 0.5 to 100 µM (0.5, 1, 2.5, 5, 10, 25, 50 and 100 µM). Two nitrogen-containing bisphosphonates, PA and ZA (Sigma-Aldrich, UK), were used in this study. The concentrations of 100 µM PA and 10 µM ZA were chosen based on previously published work [78]. The maximum concentration of the ethanol vehicle did not exceed 0.5% (v/v) which did not cause significant toxicity in any of the cell types tested (data not shown).

4.3.5 Cell metabolic activity

Cells were seeded in culture plates at an optimum density (NOFs: 10,000 cells/cm^2, OKF6/TERT-2: 16,700 cells/cm^2, NOKs: 10,000 cells/cm^2 with i3T3: 5,000 cells/cm^2) and left to adhere for 24 hours. The following day, the medium was replaced with fresh medium containing different concentrations of GGOH or GGOH in combination with either 10 µM ZA or 100 µM PA. The viability was measured every 24 hours for 3 days. Cellular metabolic activity was measured using MTT assay (Sigma-Aldrich, UK) according to the manufacturer's instructions. Metabolically active (viable) cells convert a yellow tetrazolium salt to purple formazan. At each time point, cells were washed once with sterile PBS and incubated with 0.5 mg/mL MTT solution for 90 minutes. Acidified isopropanol was then added to solubilise the formazan crystals and absorbance was read at 540 nm with a reference reading at 630 nm. Results from each condition were normalised to the absorbance value of untreated cells cultured for 24 hours.

4.3.6 Morphological evaluation

Cell morphology was examined under a light inverted microscope (Motic AE2000). Images were captured using a digital camera (Moticam 2) and Motic image 2.0 Plus software.

4.3.7 Statistical analysis

Values were presented as mean with standard deviation (SD). Three independent experiments were conducted (N=3) and technical triplicates were used for each experiment (n=3), unless indicated otherwise. The Shapiro-Wilk test was used to test the normality of the data. All statistical analyses in this chapter were performed by using Prism 9 software (GraphPad, USA). The difference between each group was determined using a two-way analysis of variance (two-way ANOVA), unless indicated otherwise in the figure legend. Post-hoc multiple comparison (either Dunnett's or Dunn's test) was performed to compare between the experimental and control groups at each time point. Statistical significance was considered when the p-value was below 0.05.

4.4 Results

4.4.1 GGOH cytotoxicity on oral mucosa cells

The metabolic activity of oral mucosa cells in response to different GGOH concentrations after 72 hours were measured using the MTT assay (Section 4.3.5), and the results are illustrated in Figure 4.2. There were no changes in viability when NOFs were cultured with low GGOH doses (0.5 – 50 µM) while the highest GGOH concentration (100 µM) reduced the viability over the experimental period. The toxicity from 100 µM GGOH on NOFs was only statistically significant following 72-hour exposure ($p<0.05$) (Figure 4.2A), which is consistent with the changes to fibroblast morphology, as shown in Figure 4.3C. Cell rupture with an increase of intracellular components were observed.

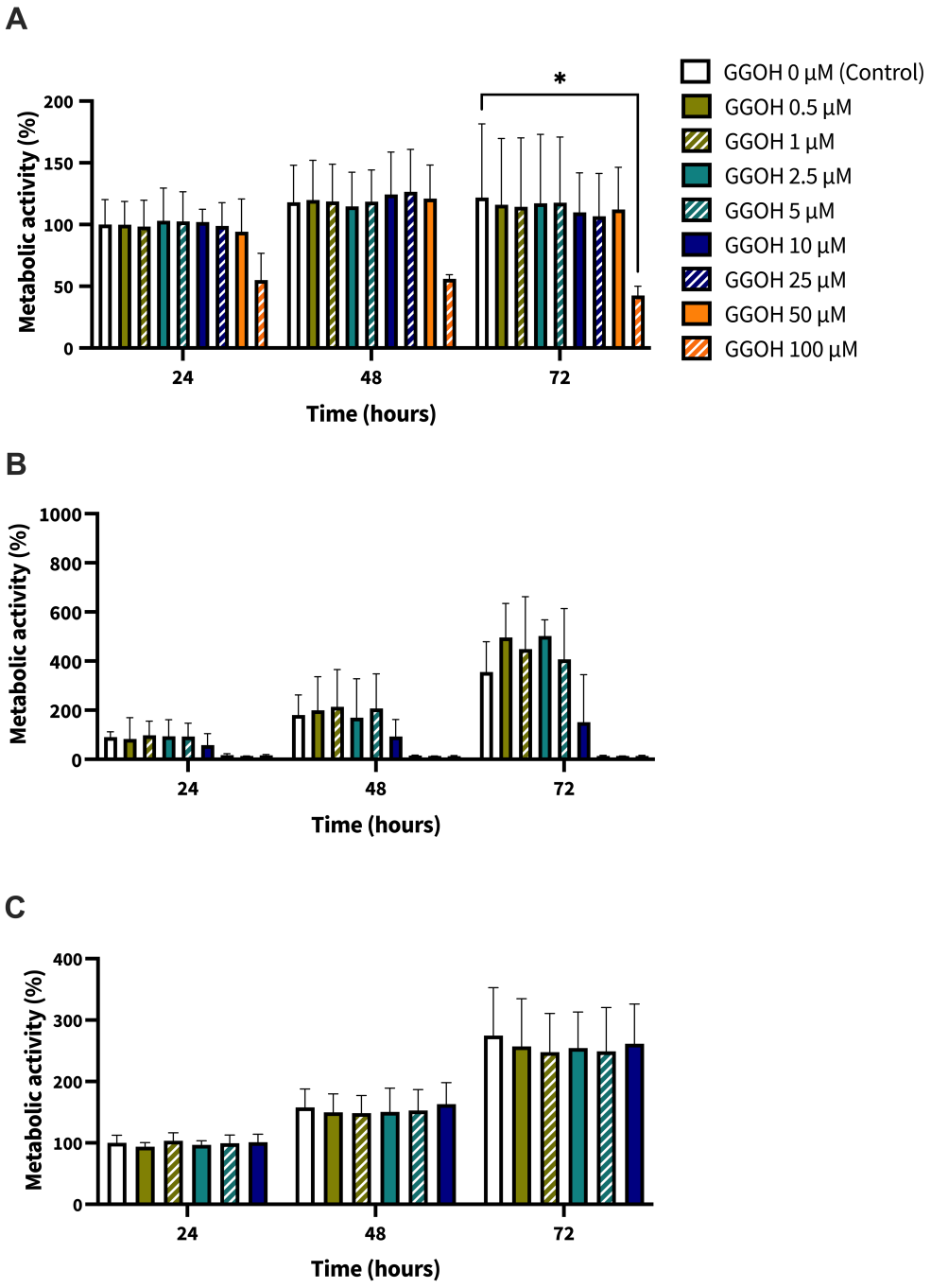

Figure 4.2 | ***Metabolic activity of oral mucosa cells in response to GGOH treatment***. *(A) Primary oral fibroblasts (NOFs), (B) immortalised oral keratinocytes (OKF6/TERT-2), and (C) primary oral keratinocytes (NOKs) were treated with varying concentrations of GGOH over a 72-hour period. Metabolic activity was assessed using the MTT assay at 24, 48, and 72-hour time points. Data for (A) and (C) are presented as the mean ± standard deviation, while (B) shows the median ± interquartile range. Results were obtained from three independent experiments with three technical replicates each (N=3, n=3) except for the control (GGOH 0 µM) and 10 µM in (B), which were derived from six experiments (N=6, n=3). Statistical analysis for (A) and (C) was performed using a two-way ANOVA followed by Dunnett's multiple comparison against the control (GGOH 0 µM) at each time point (* $p<0.05$), whereas (B) was analysed using a Kruskal-Wallis test followed by Dunn's test for comparison with the control. Abbreviations: GGOH, geranylgeraniol.*

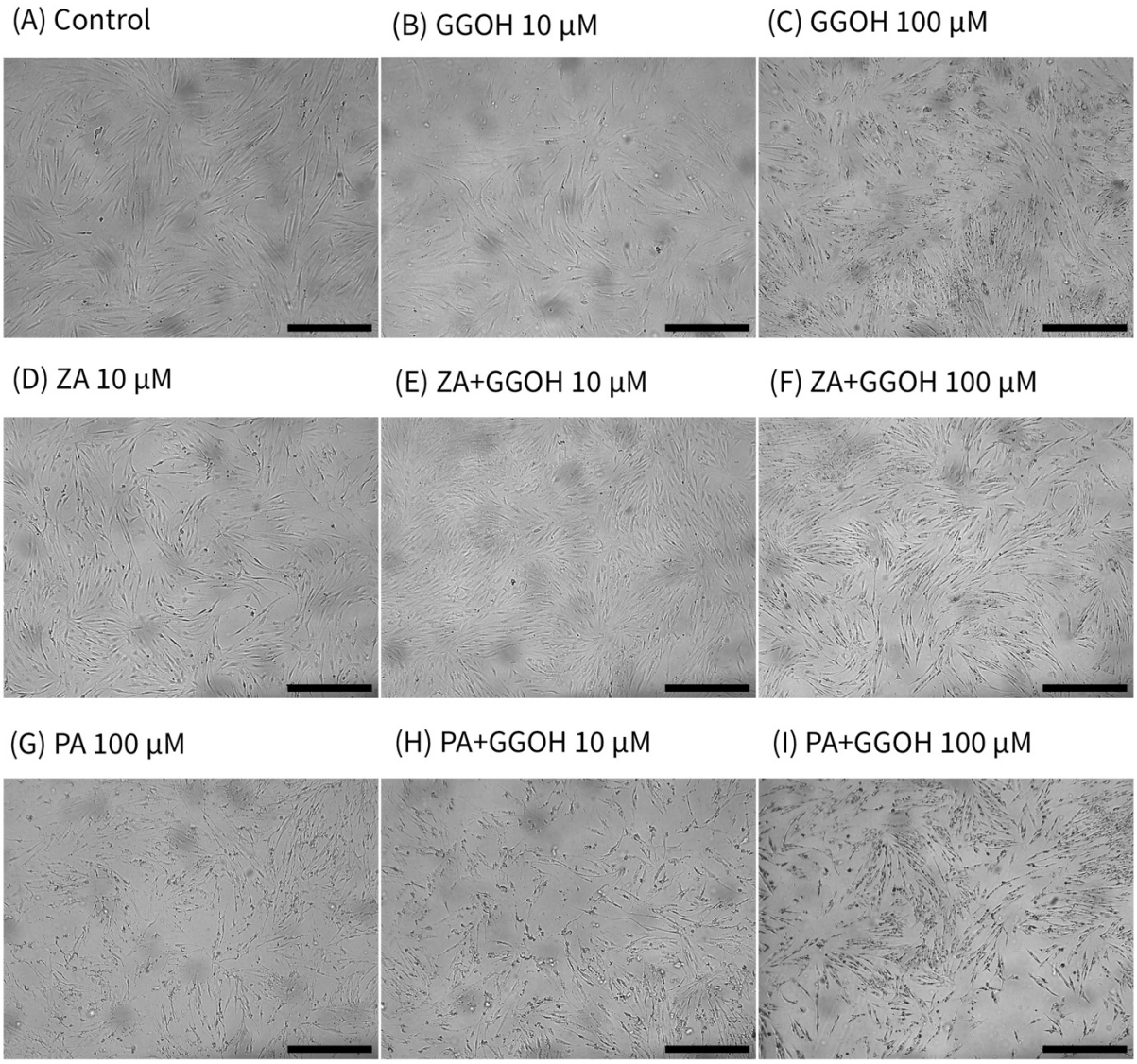

Figure 4.3 | ***The morphology of primary oral fibroblasts (NOFs) following 72 hours of treatment.*** *Each panel displays the morphology of NOFs in response to (A) untreated control (GGOH 0 µM), (B) GGOH 10 µM, (C) GGOH 100 µM, (D) ZA 10 µM, (E) ZA+GGOH 10 µM, (F) ZA+GGOH 100 µM, (G) PA 100 µM, (H) PA+GGOH 10 µM, (I) PA+GGOH 100 µM. Scale bar = 200 µm. Abbreviations: GGOH, geranylgeraniol; ZA, zoledronate; PA, pamidronate.*

The treatment of OKF6/TERT-2 with 0.5 – 5 μM GGOH did not affect the metabolic activity at any time point. However, concentrations of 10 μM and above of GGOH reduced the cellular metabolic activity at every time points (Figure 4.2B). There was no statistical significance observed from any conditions. A microscopic image (Figure 4.4B and C) demonstrated the unattached rounded cells, indicating dead cells.

Only GGOH doses from 0.5 to 10 μM were used to examine the effect of GGOH on NOKs because of the observed toxicity in OKF6/TERT-2. Figure 4.2C demonstrates the cellular viability of NOKs after incubation with GGOH for 72 hours. There were no significant changes in the viability from all GGOH concentrations at any time points.

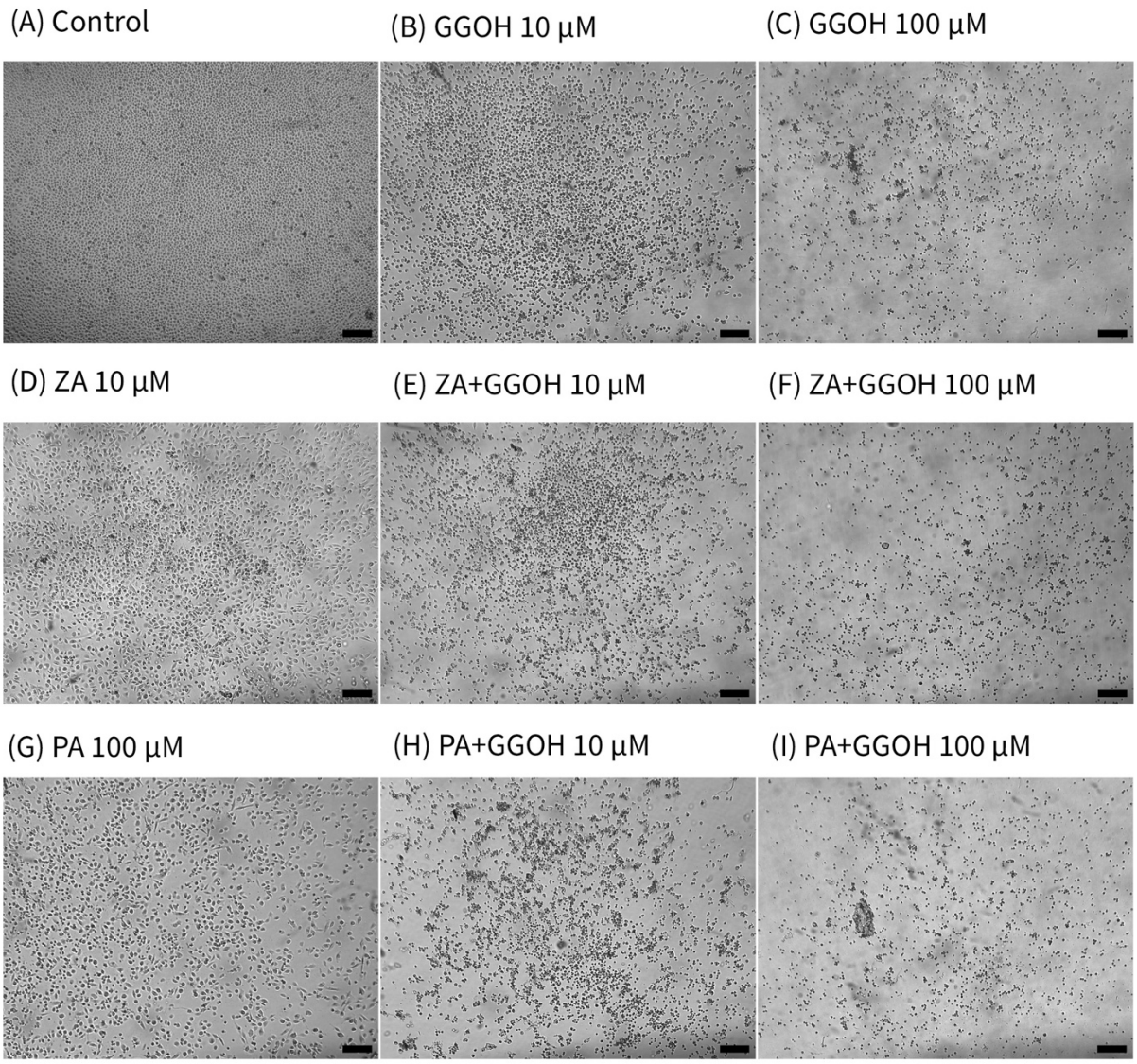

Figure 4.4 | ***The morphology of immortalised oral keratinocytes (OKF6/TERT-2) following 72 hours of treatment.*** *Each panel displays the morphology of OKF6/TERT2 cells in response to (A) untreated control (GGOH 0 µM), (B) GGOH 10 µM, (C) GGOH 100 µM, (D) ZA 10 µM, (E) ZA+GGOH 10 µM, (F) ZA+GGOH, 100 µM, (G) PA 100 µM, (H) PA+GGOH 10 µM, (I) PA+GGOH 100 µM. Scale bar = 200 µm. Abbreviations: GGOH, geranylgeraniol; ZA, zoledronate; PA, pamidronate.*

4.4.2 GGOH effect on ZA-induced toxicity of oral mucosa cells

To determine the ability of GGOH to reverse the toxicity of bisphosphonates, the cellular metabolic activity of oral mucosa cells in the presence of 10 μM ZA with different GGOH doses was assessed (Section 4.3.5). When NOFs were incubated with ZA-containing media without GGOH, the alteration of cell morphology was detected under the microscope (Figure 4.3D). Fibroblasts were observed to be thinner with more nuclear enlargement compared to the control (Figure 4.3A). The metabolic activity was negatively affected and significant toxicity was observed at the 72-hour time point ($p<0.05$). The combination treatment of 100 μM GGOH and 10 μM ZA caused a significant reduction of metabolic activity after 24 hours, indicating GGOH toxicity. At 48 and 72 hours, the addition of GGOH doses from 0.5 to 25 μM was able to increase the viability of ZA-treated NOFs compared to NOFs treated with ZA without GGOH. Three GGOH doses (5, 10, and 25 μM) significantly increased the metabolic activity of cells after 72 hours compared to ZA treatment alone ($p<0.05$) (Figure 4.5A). The increased confluence of NOFs in the presence of ZA and GGOH 10 μM is shown in Figure 4.3E.

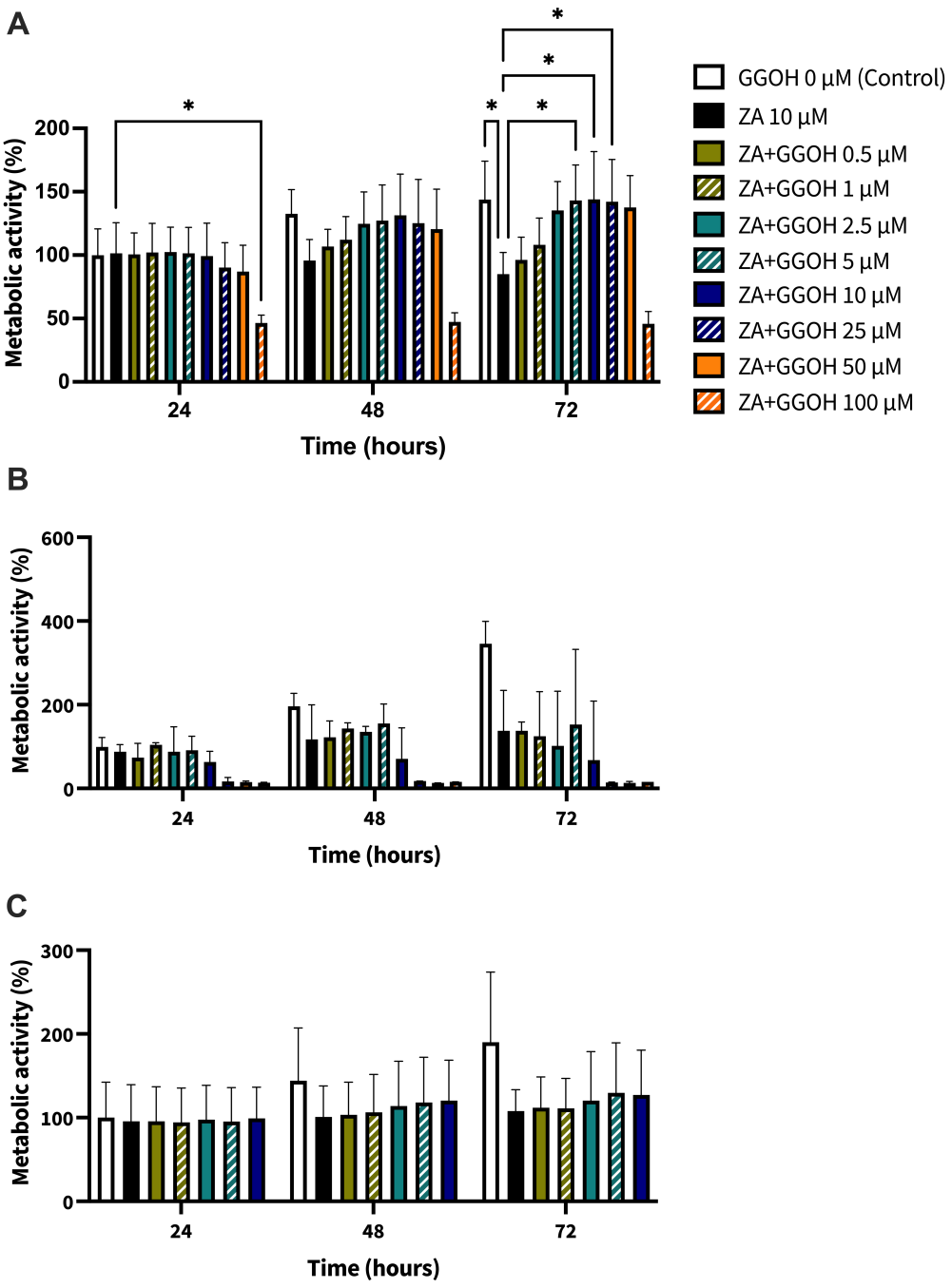

Figure 4.5* | *Metabolic activity of oral mucosa cells in response to GGOH treatment in the presence of ZA. *(A) Primary oral fibroblasts (NOFs), (B) immortalised oral keratinocytes (OKF6/TERT-2), and (C) primary oral keratinocytes (NOKs) were treated with varying concentrations of GGOH in combination with 10 µM ZA over a 72-hour period. The metabolic activity was assessed using the MTT assay at 24, 48, and 72-hour time points. Data are presented as the mean ± standard deviation for (A) and (C), while the median ± interquartile range are reported in (B). Results were obtained from three independent experiments with three technical replicates each (N=3, n=3) except for the GGOH 0 µM (control), ZA 10 µM and ZA+GGOH 10 µM of (B) which were derived from six experiments (N=6, n=3). Statistical analysis for (A) and (C) was conducted using a two-way ANOVA followed by Dunnett's multiple comparison against the 10 µM ZA at each time point (* $p<0.05$), whereas (B) was analysed using a Kruskal-Wallis test followed by Dunn's test for comparison with the 10 µM ZA. Abbreviations: GGOH, geranylgeraniol; ZA, zoledronate.*

Figure 4.5B demonstrates that 10 µM ZA was toxic to OKF6/TERT-2 with a reduction in the metabolic activity after 48 and 72 hours, which is correlated with the morphological changes shown in Figure 4.4D. GGOH did not increase the viability of ZA treated OKF6/TERT-2 at any time point or at any concentration tested. Instead, the combination of GGOH treatment (10 µM and above) with 10 µM ZA led to lower metabolic activity in OKF6/TERT-2 cells treated in combination. The morphological analysis in Figure 4.4E and D illustrates floating cells and cellular debris, confirming the toxic effect of ZA and GGOH on keratinocytes.

The reduction of metabolic activity was also observed in NOKs following culture with 10 µM zoledronate for 72 hours; however, a statistical significance was not found, as shown in Figure 4.5C. Treatment with GGOH (0.5 to 10 µM) had no effect on the metabolic activity of cells.

4.4.3 GGOH effect on PA-induced toxicity of oral mucosa cells

Since PA has lower potency than ZA, a higher dose of PA (100 μM) was used to induce the toxicity on oral mucosa cells. Figure 4.6A illustrates the response of PA-treated NOFs to different GGOH concentrations over 72 hours. PA produced a significant toxic effect at 48 and 72 hours, as shown by a reduction in the metabolic activity to approximately 90% and 40% of the 24-hour control, respectively (p<0.05). There were no differences in the metabolic activity from GGOH plus PA conditions at any time points, indicating that GGOH had no protective effect on PA-induced toxicity in NOFs. The alteration of fibroblast structure and morphology in the presence of PA and PA with GGOH (presented in Figure 4.3G, H and F) clearly demonstrates the toxicity.

When OKF6/TERT-2 cells were treated with PA, the viability was decreased after 48 and 72 hours. The addition of different GGOH doses again had no rescue effect on the viability of OKF6/TERT-2 in the presence of PA. Instead, the addition of 25 μM GGOH and above negatively affected the metabolic activities of OKF6/TERT-2 at all time points (Figure 4.6B). Morphological changes of OKF6/TERT-2 were seen in Figure 4.4H and 4.4I.

Figure 4.6C shows the metabolic activities of NOKs following incubation with PA and GGOH. PA alone reduced the viability at all time points. No rescue effect of GGOH was observed from any concentrations on PA-treated cells.

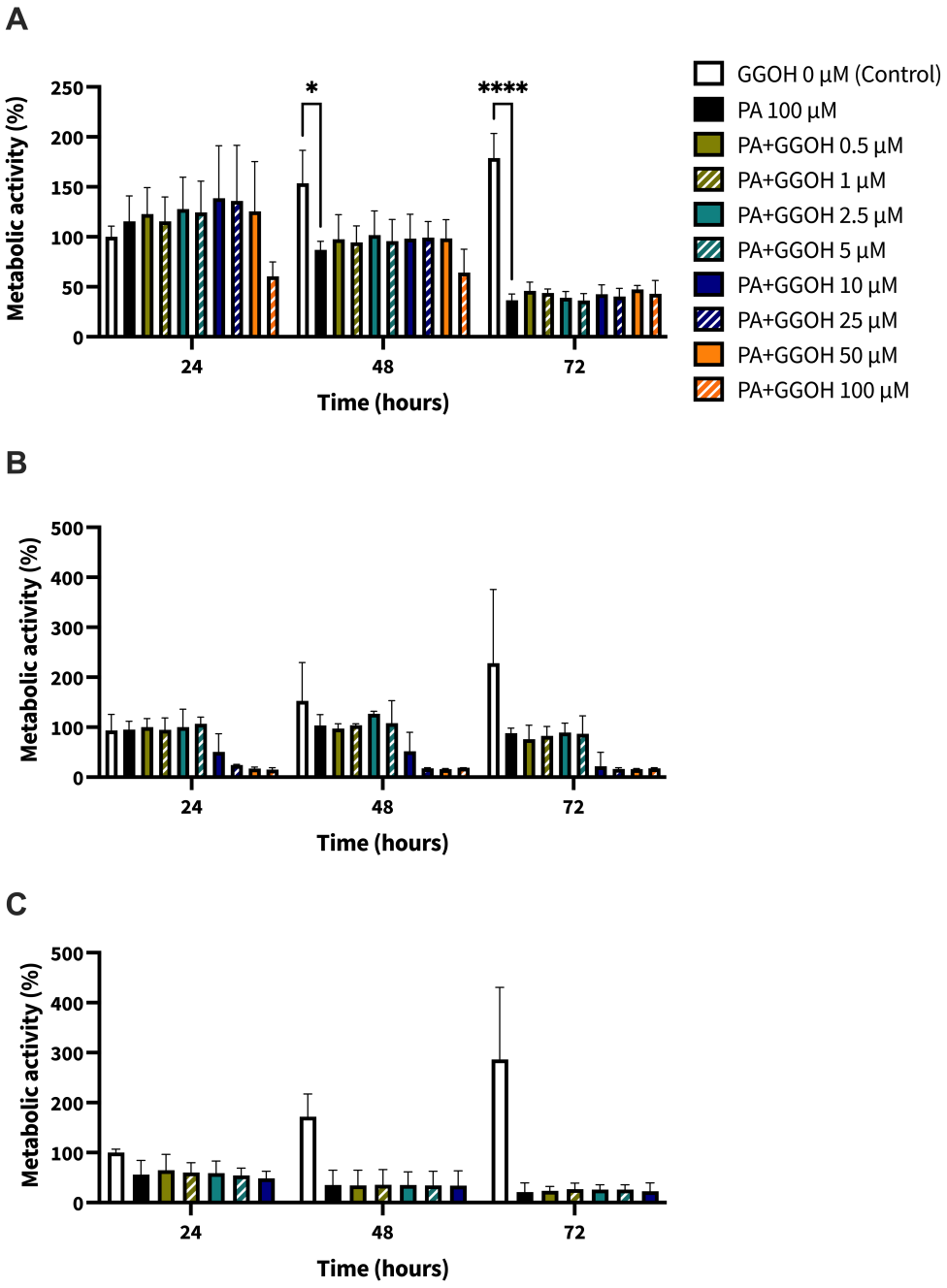

Figure 4.6* | *Metabolic activity of oral mucosa cells in response to GGOH treatment in the presence of PA. *(A) Primary oral fibroblasts (NOFs), (B) immortalised oral keratinocytes (OKF6/TERT-2), and (C) primary oral keratinocytes (NOKs) were treated with varying concentrations of GGOH in combination with 10 µM ZA over a 72-hour period. The metabolic activity was assessed using the MTT assay at 24, 48, and 72-hour time points. Data are presented as the mean ± standard deviation for (A) and (C), while the median ± interquartile range are reported in (B). All results in (A) and (B) were obtained from three independent experiments with three technical replicates each (N=3, n=3) except for the GGOH 0 µM (control), PA 100 µM and PA+GGOH µM of (B) which were derived from four experiments (N=4, n=3). All conditions of (C) were obtained from two independent experiments (N=2, n=3). Statistical analysis for (A) was conducted using a two-way ANOVA followed by Dunnett's multiple comparison against the 100 µM PA at each time point (* $p<0.05$, **** $p < 0.0001$), whereas (B) was analysed using a Kruskal-Wallis test followed by Dunn's test for comparison with the PA 100 µM. Abbreviations: GGOH, geranylgeraniol; PA, pamidronate.*

4.5 Discussion

The absence of effective treatment options has driven efforts to develop novel therapies for patients affected with MRONJ. Non-healing mucosal wounds resulting in the exposure of necrotic bone are the primary feature of MRONJ and are responsible for many of the symptoms including loss of function, infection and pain [146]. Therefore, the restoration of the soft tissue barrier is expected to support resolution of the disease and GGOH has been identified as a molecule of interest in MRONJ [10], [223].

GGOH, an isoprenoid molecule that can be converted to GGPP in the mevalonate pathway, has been proposed as a potential tool to overcome bisphosphonate toxicity by salvaging the loss of geranylated molecules to maintain normal cellular activities. GGOH's other biological activities including its restorative effects in nitrogen-containing bisphosphonates treated osteoclasts [222] and its anti-inflammatory and antimicrobial features [230], [233] led to our hypothesis that GGOH could improve mucosal integrity and wound healing in patients treated with nitrogen-containing bisphosphonates.

In this study, we evaluated the *in vitro* effects of GGOH on oral fibroblasts and keratinocytes, the cells responsible for oral wound healing and mucosal integrity [307], in combination with nitrogen-containing bisphosphonates to investigate the potential of GGOH to reduce soft tissue toxicity.

Prior to the evaluation of GGOH therapeutic effects on bisphosphonate-induced soft tissue toxicity, a cytotoxicity study of GGOH alone was necessary to verify its safety profile. We have demonstrated that low GGOH doses had no effect on the viability of keratinocytes and fibroblasts, in line with previous studies showing GGOH concentrations between 0.5 to 10 µM produced minimal toxicity to oral mucosa cells [10], [124], [224]. However, the metabolic activity of cells was negatively affected with GGOH doses of 10 µM and above in OKF6/TERT-2. To the best of our knowledge, the response of oral keratinocytes to this range of GGOH concentrations has not been reported before. This is the first study demonstrating the toxic effect of GGOH on oral keratinocytes which is important when considering GGOH based therapies for mucosal healing. Following these results, experiments using higher GGOH doses on primary keratinocytes were suspended.

Fibroblasts were less susceptible to GGOH toxicity than keratinocytes as the tolerated dose was higher (50 µM Vs 5 µM). Our findings on fibroblasts are consistent with

previous studies showing that 50 µM GGOH did not cause any adverse effect on fibroblast viability [9], [223]. However, the toxicity of GGOH at a similar concentration has also been reported [114]. Zafar *et al.*, demonstrated a significant reduction in the viability of gingival fibroblasts after treatment with a single dose of 50 µM GGOH [114]. It is worth noting that earlier studies did not fully evaluate the responses of oral mucosa cells to GGOH exposure, studying only a single GGOH concentration to examine the beneficial role of GGOH on counteracting bisphosphonate toxicity. Here, we provide results on the impact of different GGOH doses on oral mucosa cell toxicity which presents a more complete picture of the dose dependent effects of GGOH.

Though unwanted toxicity from individual GGOH treatment was found, the key aim of this study was to determine whether GGOH can protect cells from bisphosphonate induced toxicity. We used two nitrogen-containing bisphosphonates, ZA and PA, in this study since they are most associated with the risk of developing MRONJ [9]. The selected concentrations for both ZA and PA were clinically relevant and previously reported to be toxic to oral mucosa cells [9], [78]. In the present study, cells were cultured with different GGOH concentrations in combination with either ZA or PA simultaneously. We have shown that GGOH increased the viability of ZA-treated fibroblasts, but GGOH was unable to increase the viability in PA-treated cells. This was consistent with previous studies that showed GGOH successfully increased cellular viability in ZA treated cells [9], [114], [223], [224]. Interestingly, GGOH was able to restore the metabolic activity of fibroblasts to levels comparable with the untreated control group, indicating a cytoprotective effect in ZA treated cells. In terms of PA, the effects of GGOH were different between each study. Our findings support the work by Ziebart *et al.*, that showed GGOH had no effect on cell viability where even lower PA concentrations at 5 or 50 µM were used [224]. On the contrary, Cozin *et al.*, demonstrated that GGOH increased the metabolic activity of gingival fibroblasts if incubated with 30 µM PA, but saw no positive effect from 60 µM PA treatment [9], suggesting PA concentration influences the success of GGOH in preventing toxicity.

Meanwhile, GGOH failed to restore the metabolic activities of immortalised and primary oral keratinocytes from bisphosphonate toxicity and high doses of GGOH worsened the cellular viability of OKF6/TERT-2. Our findings are distinct from recent studies that reported the therapeutic effect of GGOH in keratinocytes. Kim *et al.*, demonstrated that 0.5

µM GGOH worked effectively against PA induced toxicity, while Pabst *et al.*, showed 10 µM GGOH had a positive effect on primary keratinocyte viability [10], [124]. Our results also showed that the combination treatment of PA and GGOH appear to be more toxic to primary keratinocytes compared to the immortalised cell line.

The different responses observed in fibroblasts and keratinocytes may be related to differences in mitochondrial activity between these cell types and their response to GGOH. Keratinocytes appear to be more sensitive to the toxicity of GGOH and bisphosphonates than fibroblasts, however, further exploration is required to confirm the mechanism. The observed differences between data shown here and those reported in the literature may be related to the variability in cell sources (particularly for primary cells isolated from different location of oral tissues such as gingiva, buccal mucosa or floor of mouth, and different patients where the variability are well known), incubation time, and evaluation methods.

The MTT assay, used in this study measured mitochondrial metabolic activity of cells as an indirect measure of cell viability. As with all viability assays there are limitations in this technique [308], however, the MTT assay is currently used as the gold standard assay to measure cytotoxicity [308] and has been previously used in GGOH studies [9], [10], [124], [223]

Based on our findings, GGOH appears to have a very narrow therapeutic window that makes it unsuitable for clinical use. The lowest dose of GGOH able to restore fibroblast viability in the presence of ZA was 5 µM however this same dose was unable to preserve the viability of keratinocytes and a small increase in dose (10 µM of GGOH) produced significant toxicity which could lead to further mucosal breakdown or other unwanted off-target effects.

Increasing GGOH levels could also produce a negative consequence in myeloma patients, which form a significant proportion of those suffering with MRONJ. A previous study has indicated that the loss of GGPP impaired the proliferative capacity of myeloma cells [309].Thus, the addition of GGOH could have the potential to stimulate the proliferation of cancer cells and worsen the disease, precluding the use of GGOH in patients with malignancies or at risk of malignancy.

Taken together, there are a few possible explanations for the failure of GGOH to protect oral soft tissues from bisphosphonate treatment. Here we have shown that GGOH

itself impairs the metabolic activity and therefore viability of oral mucosa cells and in some cases this impairment is compounded by the addition of bisphosphonates suggesting a synergistic effect in these cells. An alternative hypothesis is that the cytotoxic effect of bisphosphonates in cells of the oral mucosa may not occur through the mevalonate pathway (as is the case in osteoclasts); meaning GGOH is unable reverse the toxicity induced *via* this route to protect oral mucosa cells.

4.6 Summary

Although we have demonstrated that a narrow range of GGOH concentrations can reduce the toxicity caused by ZA in oral fibroblasts, the same restorative effect was not observed in keratinocytes. Marginally higher GGOH doses were shown to cause significant toxicity in oral keratinocytes and the combination of GGOH and nitrogen-containing bisphosphonates were in some cases synergistic. Therefore, the use of GGOH to treat bisphosphonate-induced soft tissue damage in MRONJ is not supported by the data presented here and its use in other applications should be carefully considered.

Chapter 5

The effect of injectable platelet-rich fibrin (I-PRF) on oral mucosa

5. The effect of injectable platelet-rich fibrin (I-PRF) on oral mucosa

5.1 Introduction

Platelet concentrates have been used for their regenerative potential in various applications, including skin rejuvenation, musculoskeletal injuries, and wound healing in the oral and maxillofacial region [235]. The first generation of platelet concentrates, known as PRP, was developed in 1990s with the goal of delivering supraphysiological concentrations of platelets and growth factors to enhance bone regeneration [236]. Despite its promising effect on tissue regeneration, PRP has been associated with several drawbacks, such as complex preparation methods, the use of anticoagulants that may delay the healing process and the risks of life-threatening coagulopathies from thrombin [261], [268], [269]. To overcome these challenges, the second-generation of platelet concentrates, known as PRF, was introduced which uses a simpler method (one-step centrifugation) and eliminates the use of additional substances [274], [275].

PRF is commonly prepared in a gel-like form, referred to as L-PRF, by centrifuging blood at 700 g for 12 minutes [310]. The fibrin clot structure of L-PRF provides a 3D network that entraps growth factors and various inflammatory cells [288]. Clinical studies have extensively shown the effectiveness of PRF on promoting soft tissue regeneration in many applications in dentistry such as socket management, gingival recessions, sinus elevation and MRONJ wounds [255]. Advancements in PRF development have led to new techniques including low-speed centrifugation. Using lower centrifugation speeds and times [274], resulted in different PRF derivatives, including liquid-PRF or I-PRF. I-PRF has been reported to contain a higher number of cellular contents and growth factors with prolonged growth factor release compared to PRP [274]. The liquid formulation of I-PRF makes it versatile and suitable for combining with a variety of materials such as bone grafts or biological scaffolds, thereby improving its properties and broadening its potential clinical applicability [291]–[294].

Various preparation protocols for I-PRF have been mentioned in the literature, but they predominantly use a specific prototype fixed-angle centrifuge [274], [275], [285], [291],

[294], [311] (Table 2.7). Recent evidence suggests that a horizontal centrifuge offers better cell separations [271] and is more practical for laboratory settings. However, a universal protocol for I-PRF preparation using a bench-top horizontal swing centrifuge has been studied with very limited evidence [271], [278]. Therefore, developing and characterising the I-PRF preparation protocol using a horizontal centrifuge system could provide benefits for both researchers and clinicians in utilising I-PRF.

Wound healing is a process involving a series of events aimed at restoring damaged tissues. Various type of cells including fibroblasts, keratinocytes, endothelial cells, and inflammatory cells work in a coordinated way under the regulation of various growth factors and cytokines, primarily derived from platelets, leukocytes, and surrounding tissues [37], [42]. As a result of its superior cellular contents, I-PRF is gaining attention as a potential approach for soft tissue repair. The evidence both *in vitro* and *in vivo* of the effectiveness of I-PRF on promoting wound healing has been increasing [312]; however, the mechanism of how I-PRF stimulates these processes remains unclear. In addition, limited *in vitro* research has been conducted on the impact of I-PRF on oral mucosa behaviour [274], [278], [285], [286]. Previous studies have particularly focused on fibroblasts, while keratinocytes are also crucial cells in the wound healing process (Table 2.6). Considering the mentioned benefits of using I-PRF, we hypothesised that I-PRF can facilitate wound healing through the release of secreted factors.

In this chapter, we evaluated the cellular characteristics of I-PRF prepared from a horizontal centrifugation system and identified its biological components using a cytokine antibody array. Subsequently, we investigated the effect of I-PRF on cell behaviour involved in the wound healing process using 2D culture assays. This included cell metabolic activity, migration, and proliferation. Furthermore, we conducted investigations on the response of 3D models of the oral mucosa to I-PRF to elucidate the bioactivity of I-PRF in a more representative model of native tissues.

5.2 Aim(s)

The aim of this chapter was to develop the preparation method to prepare I-PRF and characterise the cellular and biological properties of I-PRF. We also aimed to investigate the effect of secreted factors from I-PRF on oral mucosa cell and tissue function, particularly related to the wound healing process.

5.3 Materials and Methods

5.3.1 Two-dimensional (2D) cell culture

Immortalised oral keratinocyte cell line (FNB6/TERT) and human primary oral fibroblasts (NOFs) were used in this part of the study. FNB6/TERT [64], originally obtained from buccal mucosa biopsies, was kindly provided by Professor Craig Murdoch and Professor Keith Hunter from the School of Clinical Dentistry, The University of Sheffield. These cells were cultured in Green's medium. The composition of Green's medium is outlined in Table 4.2. Cells between passage 15 and 24 were used in the experiments.

NOFs were isolated from the minced lamina propria layer of the buccal biopsies as previously described in Section 4.3.2. The experimental protocols were ethically approved by the University of Sheffield Research Ethics Committee (Reference number 003463). All procedures were performed in accordance with the Declaration of Helsinki. NOFs were cultured in DMEM with supplements, as shown previously in Table 4.3. NOFs were used from passage 4 to 9.

Both cell types were cultured in a humidified 5% CO_2 incubator at 37°C. The cell culture procedures were performed as described previously in Section 4.3.3.

5.3.2 Collecting blood and harvesting I-PRF

Peripheral blood samples were collected from a vein in the arm of healthy volunteers by an appropriately trained individual (NHS healthcare professional or a trained phlebotomist). Written informed consent was obtained from all participants before undertaking the donation process. This project was ethically approved by the University of Sheffield Research Ethics Committee (Reference number 034492) and the National Health Service Ethics Committee (REC 22/NW/0034).

The collected blood was aliquoted into 9-mL non-coated tubes (Greiner Bio-One, UK) and immediately centrifuged at 300 g (1,310 rpm) for 5 minutes using a horizontal centrifuge (320R Universal, Hettich, Germany), as described elsewhere [278]. Following centrifugation, a liquid formulation of PRF (I-PRF) was harvested from the area above the yellow-red junction using a blunt fill needle 18G (BD Biosciences, UK), as illustrated in Figure 5.1.

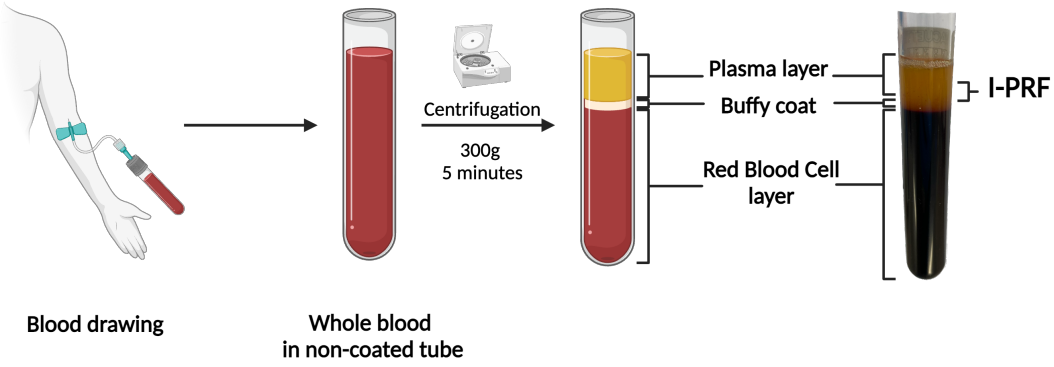

Figure 5.1 | ***Schematic diagram on the I-PRF preparation process.*** *Blood samples were collected from volunteers into tubes without anticoagulants and subsequently centrifuged at 300 g for 5 minutes. The I-PRF was collected from the interface between the yellow serum and the buffy coat layers as illustrated. Figure created using Biorender.com.*

5.3.3 Analysing platelets and white blood cell count

Blood samples were collected and aliquoted into K2-EDTA anti-coagulant coated tubes (Greiner Bio-One, UK). I-PRF was prepared as described in Section 5.3.2. Whole blood and prepared I-PRF samples were sent to the Sheffield Laboratory Medicine at the Royal Hallamshire hospital for a complete blood count to quantify platelet and white blood cell concentrations.

5.3.4 Preparing I-PRF-derived conditioned medium

To extract paracrine factors from PRF, 1 mL of I-PRF was transferred into a 6-well plate and incubated at 37°C in a humidified atmosphere with 5% CO_2 for 1 hour. Afterward, 5 mL DMEM with no supplements was added, and further incubated for 72 hours. This allowed growth factors and proteins to migrate from the I-PRF into the medium. This was termed "I-PRF-derived conditioned medium" and designated as 100% I-PRF concentration. The I-PRF-derived conditioned medium was collected, stored at -80°C, and thawed prior to each individual experiment.

5.3.5 Measuring total protein concentration using bicinchoninic (BCA) assay

The total protein concentration in I-PRF-derived conditioned medium was determined using a Pierce™ BCA protein assay kit (Thermo Fisher Scientific, UK). Prior to each experiment, a working solution of the BCA assay was prepared by mixing reagent A and reagent B at the 50:1 ratio according to the manufacturer's instruction. The I-PRF-derived conditioned medium was diluted with deionised water at a 1:10 ratio to eliminate the possible interference from phenol red in DMEM on the absorbance.

For each sample, 25 µL of diluted I-PRF-derived conditioned medium from three different donors and various concentrations of bovine serum albumin (BSA) standard solution ranging from 20 to 2000 µg/mL was added separately into a 96-well plate. Subsequently, 200 µL of the working reagent was added to each well. The plate was then incubated at 37°C for 30 minutes. All samples and standard protein solutions were performed in triplicate. The absorbance of each well was read at 562 nm using a Biotek ELX800 absorbance microplate reader spectrophotometer. A standard curve was generated using the absorbance values of the BSA standard solutions, as shown in Figure 5.2. The

diluted protein concentration of the I-PRF-derived conditioned medium was calculated using the equation generated from the standard curve. Finally, the calculated values were multiplied by 10 to obtain the actual total protein concentration.

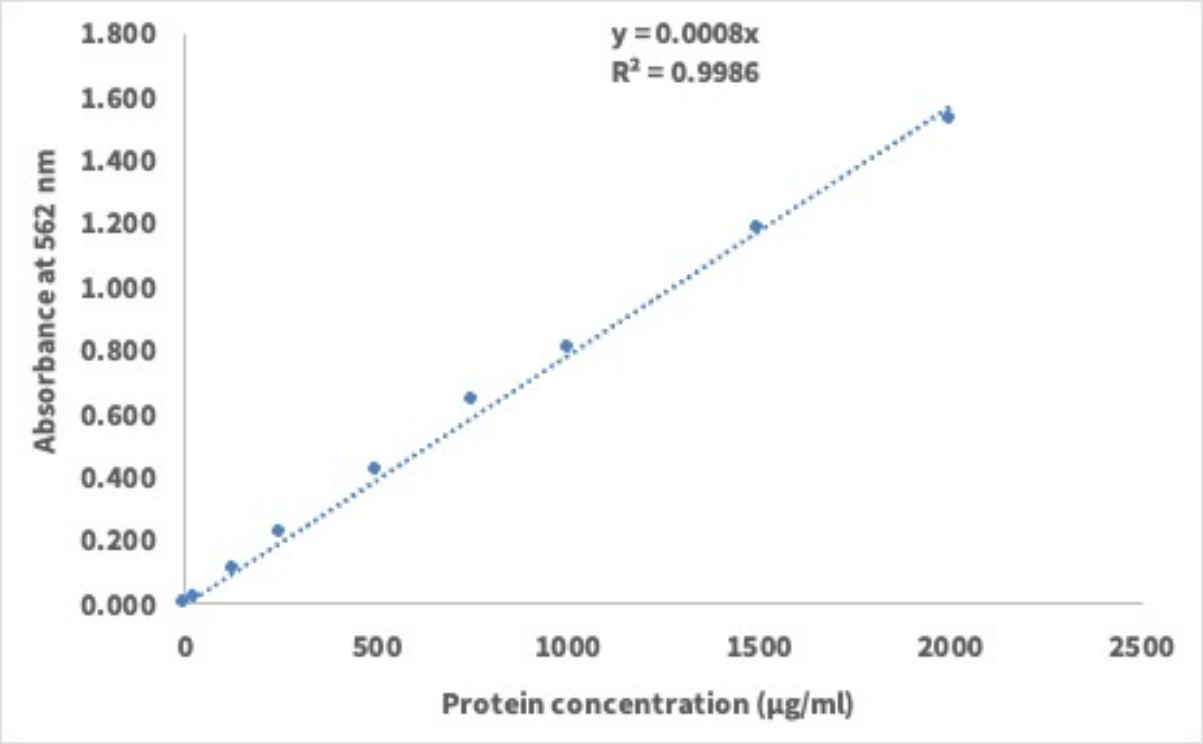

Figure 5.2 | ***Representative BSA protein standard curve.***

5.3.6 Investigating the expression of cytokines and mediators in I-PRF

A RayBio® C-Series human cytokine antibody array C1000 kit (Ray Biotech, USA) was used to investigate the presence of growth factors, cytokines, and mediators in the I-PRF-derived conditioned medium. The assay involved two membranes (C6 and C7 sheets), containing a total of 120 antibodies to human proteins printed in a circular shape. Each antibody was printed in duplicate vertically. The array map of antibodies on the C6 and C7 sheets can be found in Table 5.1 and 5.2, respectively.

I-PRF-derived conditioned medium samples from three different donors were used. Prior to the cytokine array assays, the total protein concentration was quantified using the BCA assay as described in Section 5.3.5. All samples were subjected to a 10-fold dilution with deionised water. The I-PRF-derived conditioned medium was further diluted with deionised water to obtain the lowest concentrations among the three samples, ensuring equal protein amounts across all samples.

Incubation procedures were conducted on a Stuart SSL4 see-saw rocker (Cole-Palmer, UK) at a speed of 30 cycles/second. Working solutions of all reagents were prepared following the manufacturer's instructions. Each membrane array was incubated with 2 mL blocking buffer for 30 minutes at room temperature to eliminate the non-specific binding of proteins. Subsequently, the blocking buffer was aspirated and replaced with 1 mL of diluted conditioned medium samples, and the membranes were incubated overnight at 4°C. The next day, the conditioned medium was removed, and each membrane was washed three times with 2 mL Wash Buffer 1 (1X) for 5 minutes at room temperature, followed by three washes with Wash Buffer 2 (1X) for 5 minutes each. Then, 1 mL of Biotinylated antibody cocktail prepared in blocking buffer was added to each membrane, and left overnight at 4°C. On the following day, the antibody cocktail was removed, and membranes were washed using Wash buffer 1 and Wash buffer 2 as previously mentioned. After the washing step, 2 mL of Horseradish-Peroxidase (HRP) conjugated with Streptavidin complex solution was added to each membrane, then left to incubate overnight at 4°C. The subsequent day, the HRP-streptavidin solution was aspirated, and membranes were washed again using similar procedures. Membranes were transferred onto paper towel and blotted to remove the excess wash buffer. Then, detection buffer (500 µL) was added to the membranes and incubated for 2 minutes. An image of each membrane was captured

(Figure 5.3A) using a high-sensitivity mode to visualise the chemiluminescence signal using a C-digit scanner (LI-COR Bioscience, UK).

To quantify the amount of protein, the dot blot analysis method was performed using ImageJ software, following the procedure provided on https://imagej.nih.gov/ij/docs/examples/dot-blot. The background was subtracted from each image using the rolling ball method in a 'Process/Subtract Background' command, shown in Figure 5.3B. Images were then inverted using an 'Edit/Invert' command, creating a black background with a white protein dot, without altering the image pixels (Figure 5.3C). The 'circle' tool was used to draw circles around each protein dot, ensuring equal sizes for all dots across the membrane (Figure 5.4). The integrated density of each dot was measured using the 'Analyse/Measure' command. The density represents the protein amount of each cytokine in the I-PRF-derived conditioned medium.

The relative expression of each cytokine in the I-PRF-derived conditioned medium was calculated by normalising with the positive control within the individual membrane and the control membrane (Basal DMEM without I-PRF-derived conditioned medium). The calculation equation is shown in Equation 5.1. The average intensity was calculated from values obtained from three different samples.

$$\textbf{Relative fold of cytokine A expression on membrane X} = \frac{D_X\left(\frac{P_X}{P_{Cont}}\right)}{D_{Cont}}$$

Equation 5.1* | *Relative fold of cytokine expression calculation

D_X = Average integrated density of cytokine A dots on membrane X
P_X = Average integrated density of positive control dots on membrane X
P_{Cont} = Average integrated density of positive control dots on control membrane
D_{Cont} = Average integrated density of cytokine A dots on the control membrane

Table 5.1 | Antibody map of C6 membrane

Column / Row	A	B	C	D	E	F	G	H	I	J	K	L	M	N
1	Positive control	Positive control	Negative control	Negative control	Blank	Angiogenin	BDNF	BLC (CXCL13)	BMP-4	BMP-6	Ck beta 8-1 (CCL23)	CNTF	EGF	Eotaxin-1 (CCL11)
2	Positive control	Positive control	Negative control	Negative control	Blank	Angiogenin	BDNF	BLC (CXCL13)	BMP-4	BMP-6	Ck beta 8-1 (CCL23)	CNTF	EGF	Eotaxin-1 (CCL11)
3	Eotaxin-2 (CCL24)	Eotaxin-3 (CCL26)	FGF-6	FGF-7 (KGF)	Flt-3 Ligand	Fractalkine (CX3CL1)	GCP-2 (CXCL6)	GDNF	GM-CSF	I-309 (CCL1)	IFN-gamma	IGFBP-1	IGFBP-2	IGFBP-4
4	Eotaxin-2 (CCL24)	Eotaxin-3 (CCL26)	FGF-6	FGF-7 (KGF)	Flt-3 Ligand	Fractalkine (CX3CL1)	GCP-2 (CXCL6)	GDNF	GM-CSF	I-309 (CCL1)	IFN-gamma	IGFBP-1	IGFBP-2	IGFBP-4
5	IGF-I	IL-10	IL-13	IL-15	IL-16	IL-1alpha	IL-1beta	IL-1ra	IL-2	IL-3	IL-4	IL-5	IL-6	IL-7
6	IGF-I	IL-10	IL-13	IL-15	IL-16	IL-1alpha	IL-1beta	IL-1ra	IL-2	IL-3	IL-4	IL-5	IL-6	IL-7
7	Leptin	LIGHT	MCP-1	MCP-2	MCP-3	MCP-4	M-CSF	MDC	MIG	MIP-1-delta	MIP-3-alpha	NAP-2	NT-3	PARC
8	Leptin	LIGHT	MCP-1	MCP-2	MCP-3	MCP-4	M-CSF	MDC	MIG	MIP-1-delta	MIP-3-alpha	NAP-2	NT-3	PARC
9	PDGF-BB	RANTES	SCF	SDF-1	TARC	TGF-beta 1	TGF-beta 3	TNF-alpha	TNF-beta	Blank	Blank	Blank	Blank	Positive control
10	PDGF-BB	RANTES	SCF	SDF-1	TARC	TGF-beta 1	TGF-beta 3	TNF-alpha	TNF-beta	Blank	Blank	Blank	Blank	Positive control

Table 5.2 | Antibody map of C7 membrane

Column / Row	A	B	C	D	E	F	G	H	I	J	K	L	M	N
1	Positive control	Positive control	Negative control	Negative control	Blank	Acrp30	AgRP	Angio poietin-2	Amphi regulin	axl	bFGF	Beta-NGF	BTC	CCL28
2	Positive control	Positive control	Negative control	Negative control	Blank	Acrp30	AgRP	Angio poietin-2	Amphi regulin	axl	bFGF	Beta-NGF	BTC	CCL28
3	CTACK	dtk	EGF-R	ENA-78	Fas/ TNFRSF6	FGF-4	FGF-9	G-CSF	GITR ligand	GITR	GRO	GRO-alpha	HCC-4	HGF
4	CTACK	dtk	EGF-R	ENA-78	Fas/ TNFRSF6	FGF-4	FGF-9	G-CSF	GITR ligand	GITR	GRO	GRO-alpha	HCC-4	HGF
5	ICAM-1	ICAM-3	IGF-BP-3	IGF-BP-6	IGF-I SR	IL-1 R4/ST2	IL-1 RI	IL11	IL12-p40	IL12-p70	IL17	IL-2 Ra	IL-6 R	IL8
6	ICAM-1	ICAM-3	IGF-BP-3	IGF-BP-6	IGF-I SR	IL-1 R4/ST2	IL-1 RI	IL11	IL12-p40	IL12-p70	IL17	IL-2 Ra	IL-6 R	IL8
7	I-TAC	Lympho tactin	MIF	MIP-1-alpha	MIP-1-beta	MIP-3-beta	MSP-a	NT-4	Osteo protegerin	Onco statin M	PlGF	sgp130	sTNF RII	sTNF-RI
8	I-TAC	Lympho tactin	MIF	MIP-1-alpha	MIP-1-beta	MIP-3-beta	MSP-a	NT-4	Osteo protegerin	Onco statin M	PlGF	sgp130	sTNF RII	sTNF-RI
9	TECK	TIMP-1	TIMP-2	TPO	TRAIL-R3	TRAIL-R4	uPAR	VEGF	VEGF-D	Blank	Blank	Blank	Blank	Positive control
10	TECK	TIMP-1	TIMP-2	TPO	TRAIL-R3	TRAIL-R4	uPAR	VEGF	VEGF-D	Blank	Blank	Blank	Blank	Positive control

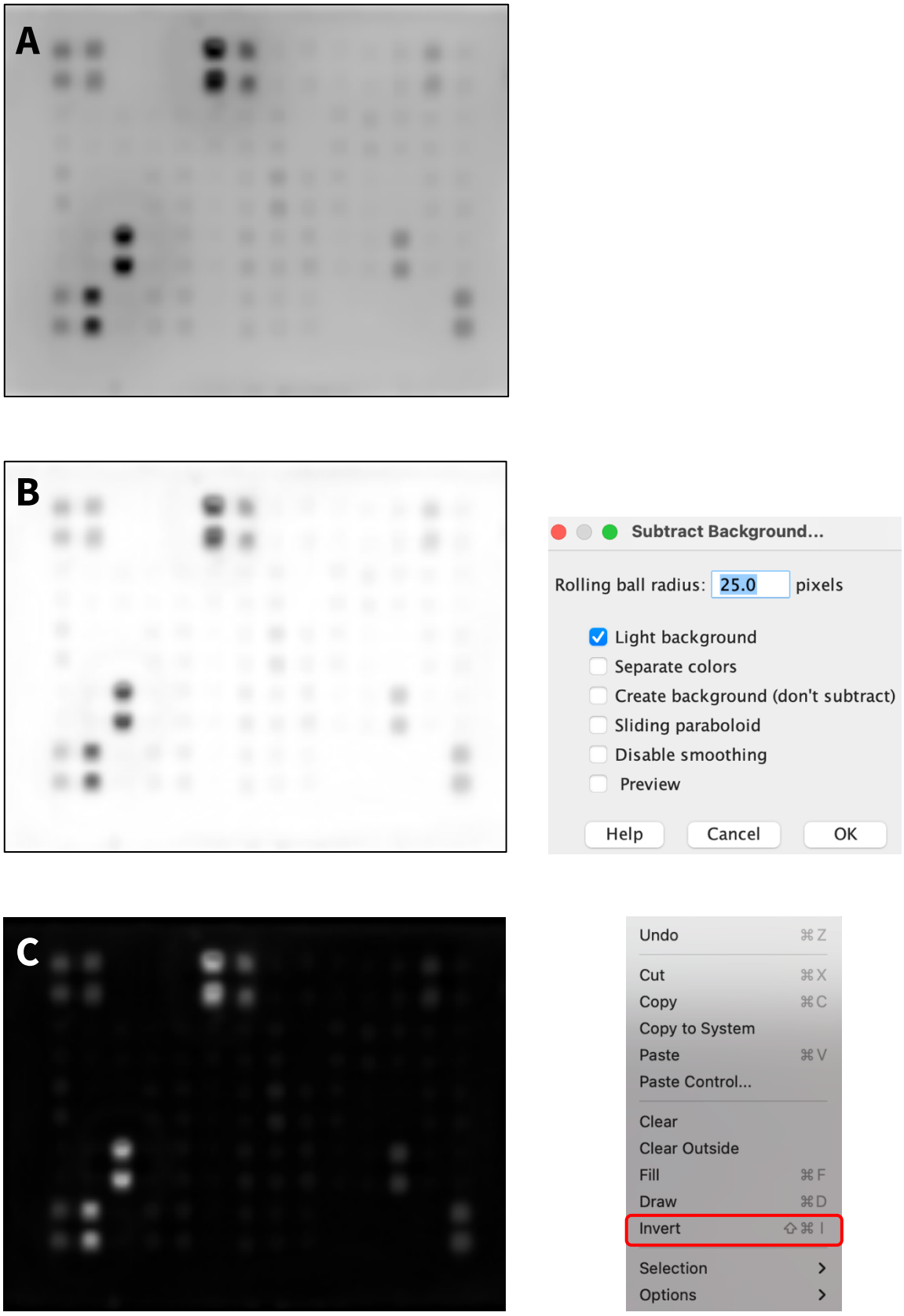

Figure 5.3 | ***Cytokine membrane images.*** *Panel (A) displays the raw cytokine membrane image, (B) shows the image after background subtraction using the rolling ball method, and (C) presents the image inverted to generate a black background with white protein dots.*

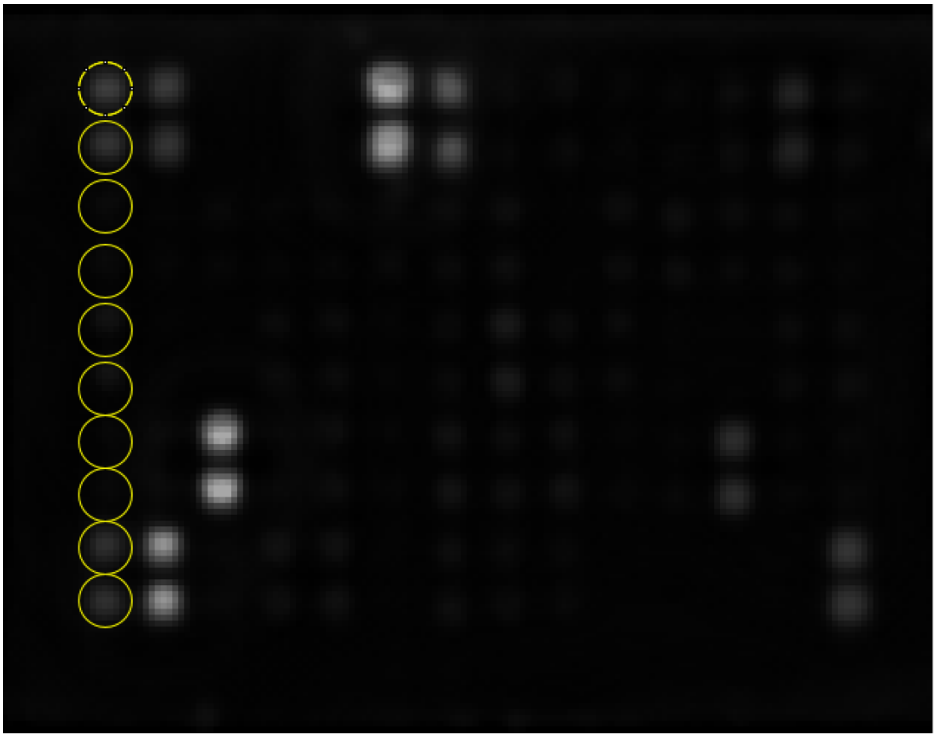

Figure 5.4 | ***Cytokine membrane images shown with circle tool being applied.*** *A circle tool was used to quantify the integrated density of each protein dot on the cytokine array membrane.*

5.3.7 Assessing metabolic activity in 2D cell culture

Serum and growth factor-free DMEM and Green's medium, designated as basal culture medium (PRF 0%), were used as a control for NOF and FNB6/TERT experiments, respectively. This was to eliminate the possible effect of any paracrine factors which may interfere with the effect of PRF. Prior to each experiment, a stock solution of I-PRF-derived conditioned medium (PRF 100%) was diluted with basal culture medium into various concentrations from 1 to 50%.

NOFs in supplemented DMEM were seeded at a density of 10,000 cells/cm^2 into 24-well plates. Separately, FNB6/TERT in Green's medium were seeded at a density of 16,700 cells/cm^2 into 48-well plates. After 24 hours, the medium was replaced with either basal culture medium (PRF 0%), I-PRF-conditioned medium (1, 2, 5, 10, 20, or 50%), or basal culture medium supplemented with 10% FBS (10% FBS with EGF for keratinocytes). Cells were incubated for a further 72 hours and the metabolic activity of both cell types were evaluated at 24 and 72 hours using an MTT assay as described in Section 4.3.5. Results were normalised to the 24-hour control (PRF 0%) value.

5.3.8 Assessing cell apoptosis and necrosis in 2D culture

NOFs and FNB6/TERT were seeded into a 6-well plate separately (NOFs: 5,500 cells/cm^2, FNB6/TERT: 16,700 cells/cm^2) and left to adhere for 24 hours. The next day, cells were treated with the I-PRF-derived conditioned medium (10, 20, or 50%).

After 72 hours of treatment, the supernatant was collected while cells were detached with 0.05% trypsin-EDTA. Both supernatant and detached cells were centrifuged separately at 6000 g for 5 minutes. Pellets from both compartments were resuspended in cold PBS and then centrifuged again at the same speed and time.

Annexin V-fluorescein isothiocyanate (FITC) with propidium iodide (PI) staining kit (RnD systems, UK) was used to determine apoptotic and necrotic cells. Each sample was stained with 100 µL staining solution containing components described in Table 5.3 for 15 minutes.

Stained cells were run through an LSRII flow cytometer (BD Biosciences, UK) to determine the cell status by using a 488 nm laser with a 530/30 nm filter for Annexin V-FITC dye and a 660/20 nm filter for PI dye. A minimum of 10,000 events per sample was measured

each time. Samples were analysed for 5 minutes at a medium speed in case they were unable to reach the minimum gate event (10,000). Cell status was defined as outlined Table 5.4.

Table 5.3 | ***The components of Annexin V-FITC staining kit per sample***

Components	Volume used (µL)
10x Binding buffer	10
10x Propidium iodide (PI)	10
Annexin V-FITC	1
Distilled water	79

Table 5.4 | ***Classification of each cell status based on Annexin V-FITC and PI staining***

Cell status	Annexin V-FITC staining	PI staining
Viable	Negative (-)	Negative (-)
Early apoptosis	Positive (+)	Negative (-)
Late apoptosis	Positive (+)	Positive (+)
Necrosis	Negative (-)	Positive (+)

5.3.9 Assessing cell proliferation in 2D culture

CellTrace™ Far Red carboxy-fluorescein diacetate N-succinimidyl diester (CFSE) cell proliferation staining kit (Thermo Fisher Scientific, UK) was used to evaluate oral mucosa cell proliferation. A stock solution (1 mM) of CFSE solution was prepared by adding 18 µL of dimethyl sulfoxide (DMSO) (Thermo Fisher Scientific, UK) to dissolve the supplied fluorescent dye. A working concentration of CFSE solution at 1 µM was prepared before each experiment by diluting the stock solution with 0.1% BSA in PBS. Cells were then stained at a concentration of $1x10^6$ cells per 1 mL of CFSE solution for 20 minutes at 37°C in the CO_2 incubator. Following this, cells were quenched with 10 mL cold DMEM and incubated on ice for 5 minutes. Cells were then washed with 0.1% BSA solution and centrifuged twice before seeding.

NOFs and FNB6/TERT were stained separately using CFSE, as outlined above. CFSE-stained NOFs and FNB6/TERT were seeded separately in a 6-well plate at 5,500 cells/cm^2 and 16,700 cells/cm^2 respectively. Unstained cells were also plated at the same density to act as a negative control. The next day, the medium from one of the wells containing stained cells, designated as a non-proliferative control, was replaced with the medium containing Mitomycin C at a concentration of 2 mg/mL for NOFs and 0.5 mg/mL for FNB6/TERT and treated for 4 hours [120]. Following this, the medium was removed, and cells were incubated with three different concentrations of PRF-conditioned medium (10, 20, or 50%) for 72 hours.

After 72 hours, cells were trypsinised using 0.05% trypsin-EDTA solution (Sigma-Aldrich, UK) and centrifuged (Hawk 15/05 Sanyo, UK) at 6000 g for 5 minutes. Cell pellets were resuspended with 10% formalin (Sigma-Aldrich, UK) and left at room temperature for fixation. After 30 minutes, cells were centrifuged and resuspended in PBS before flow cytometry analysis. Mean fluorescence intensity (MFI) was measured with a 488 nm laser and a 630/30 nm filter using an LSRII flow cytometer machine. Data was gated to remove debris. Each sample was analysed at a minimum of 10,000 events. If a sample did not contain enough cells and so was unable to reach the minimum gate event, samples were measured for 5 minutes at the medium speed settings.

The proliferation index was calculated by comparing the MFI of each experimental condition to the value of a mitomycin C-treated condition, as shown in Equation 5.2. Experiments were performed in three independent repeats.

$$\textbf{Proliferation index} = \frac{\textbf{MFI of Mitomycin C treated condition}}{\textbf{MFI of experimental condition}}$$

Equation 5.2 | ***Proliferation index calculation***

5.3.10 Assessing cell migration in 2D culture

Oris™ stoppers (Platypus Technologies, USA) were used to assess cell migration. NOFs at a density of 54,000 cells/cm^2 and FNB6/TERT at 132,000 cells/cm^2 were seeded separately into a 96-well plate containing the stoppers, thereby creating a cell-free gap zone as illustrated in Figure 5.5. The following day, medium containing mitomycin C at a concentration of 2 mg/mL and 0.5 mg/mL for NOFs and FNB6/TERT, respectively, was added to inhibit cell proliferation. After 4 hours, the stoppers were removed, and the medium was replaced with PRF-conditioned medium (10, 20, or 50%).

Cells were photographed using an inverted light microscope (Motic AE2000) with a digital camera (Moticam 2) at regular intervals for each cell type (every 24 hours up to 72 hours for NOFs and every 8 hours up to 24 hours for FNB6/TERT). A cell-free gap was measured by drawing a circular shape of the largest cell-free area using ImageJ software. (National Institute of Health). If the area was larger than one captured image, two images were captured and then combined using an automated merging tool in Adobe Photoshop 2023 software (Adobe). The area size was automatically calculated by the ImageJ software. The percentage of gap closure was obtained by comparing the measured value with the starting area size of each well.

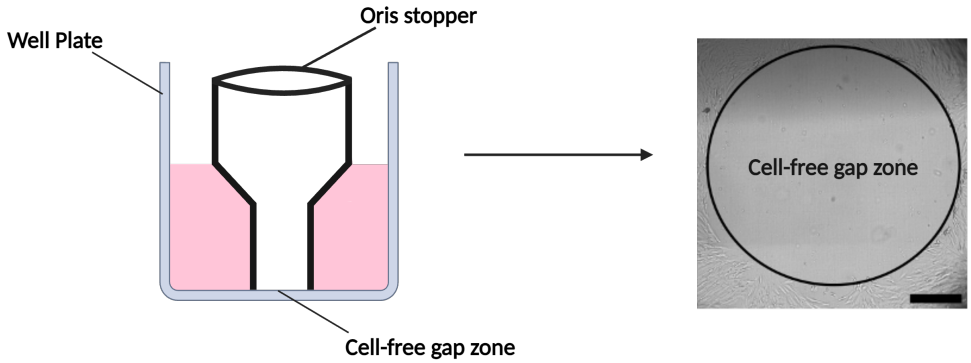

Figure 5.5 | ***Cell-free gap zone created by Oris™ Stoppers.*** *Scale bar = 0.5 mm.*

5.3.11 Constructing three-dimensional (3D) oral mucosa model

3D oral mucosa models were cultured as previously described [85] using acellular dermis seeded with oral fibroblasts and keratinocytes. A split-thickness skin graft was collected from human donors undergoing routine surgery. All volunteers provided their informed consent before participating in the study. The protocol was approved by the National Health Service Committee (15/YH/0177 and 21/NE/0115). The collected skin samples were placed in 1M NaCl solution and incubated at 37°C for a minimum of 24 hours to remove cells and detach the epithelium. In case of incomplete separation, the epithelial layer was peeled off using forceps. The de-epidermalised dermis (DED) was then washed three times in PBS, placed in DMEM containing 100 IU/mL Penicillin and 100 µg/mL Streptomycin and 0.0625 µg/mL Fungizone, and stored in a human tissue fridge at 4°C.

The DED was cut into approximately 1.5x1.5 cm squares and placed papillary placed uppermost into a 6-well plate. A stainless steel chamfered ring (produced in-house) with an inner diameter of 1 cm was placed on the DED. NOFs and FNB6/TERT were cultivated as previously described in Section 4.3.3. NOFs (250,000 cells in 0.25 mL DMEM) and FNB6/TERT ($1x10^6$ cells in 0.25 mL Green's medium) were seeded inside the ring of each model. Green's medium (3 mL) was added outside the ring to prevent leakage. The models were cultured at 37°C in a hydrated, 5% CO_2 atmosphere incubator.

After 24 hours, 0.25 mL of the medium inside the ring was removed and replaced with fresh complete Green's medium. The models were then returned to an incubator for 24 hours. The following day, 0.5 mL of medium inside the ring was removed and replaced with fresh complete Green's medium. After seeding cells for 72 hours, the ring was removed, and the surrounding DED outside the ring circumference was cut out using a scalpel to obtain a circular shape of the tissue-engineered oral mucosa (TEOM). The models were placed in 12 mm transwell inserts (THINCERT) with 0.4 µm pore diameter (Greiner Bio-One, UK). These inserts were then placed in 12-deep well plates (Greiner Bio-One, UK) to create an ALI for the TEOM, as shown in Figure 5.6.

The constructed TEOM was used to evaluate the effect of I-PRF on three scenarios of the oral epithelium: (i) epithelium formation, (ii) established epithelium, and (iii) wounded epithelium. TEOM were cultured at ALI for 14 days to assess the effect of I-PRF on epithelium formation and established epithelium while the wounded model experiments were

cultured at ALI for 17 days. A flowchart of the experimental procedures is presented in Figure 5.7.

The metabolic activity of TEOM in epithelium formation (See Section 5.3.13) and established epithelium (see Section 5.3.14) experiments were measured (See Section 5.3.12). TEOM from all three experiments (Section 5.3.13, 5.3.14, and 5.3.15) were washed twice in PBS and fixed in 10% formalin (Sigma, UK) for at least 24 hours for further analysis. Tissue sections were either stained with H&E solution (see Section 5.3.16) or subjected to an immunohistochemistry assay (see Section 5.3.18).

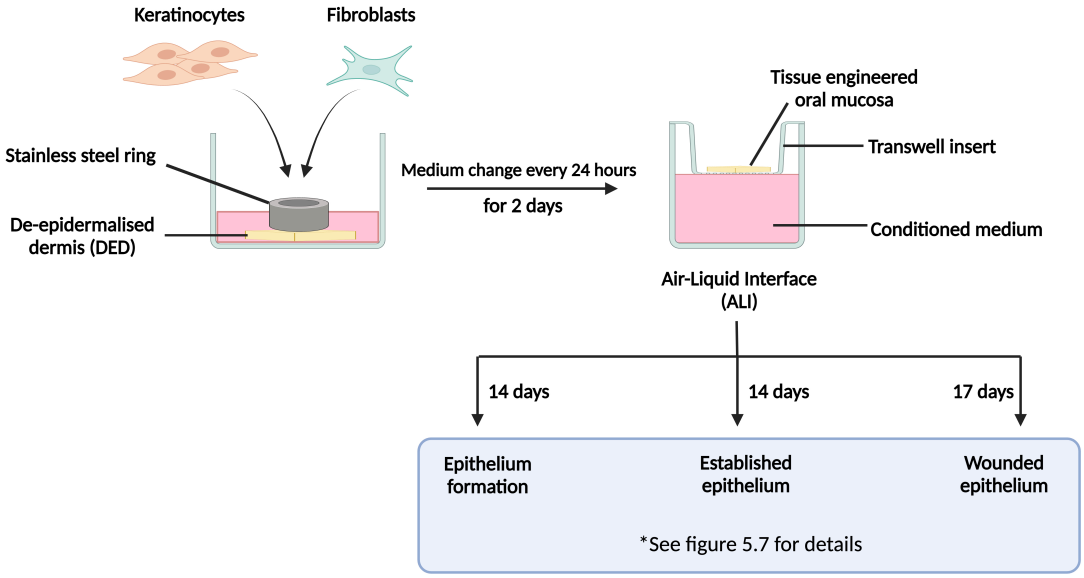

Figure 5.6* | *Schematic illustration of tissue-engineered oral mucosa (TEOM) construction. *Primary oral fibroblasts (NOFs) and immortalised oral keratinocytes (FNB6/TERT) were seeded onto a de-epidermalised dermis (DED) scaffold inside a stainless steel ring, and incubated for 72 hours. Following this period, the newly formed TEOM was transferred to a transwell insert to create an air-liquid interface (ALI). The TEOM was then cultured at an ALI for an additional 14 days for evaluation of epithelium formation and effects on the established epithelium. For experiments involving wounded epithelium, the TEOM was cultured for 17 days. Figure created using Biorender.com.*

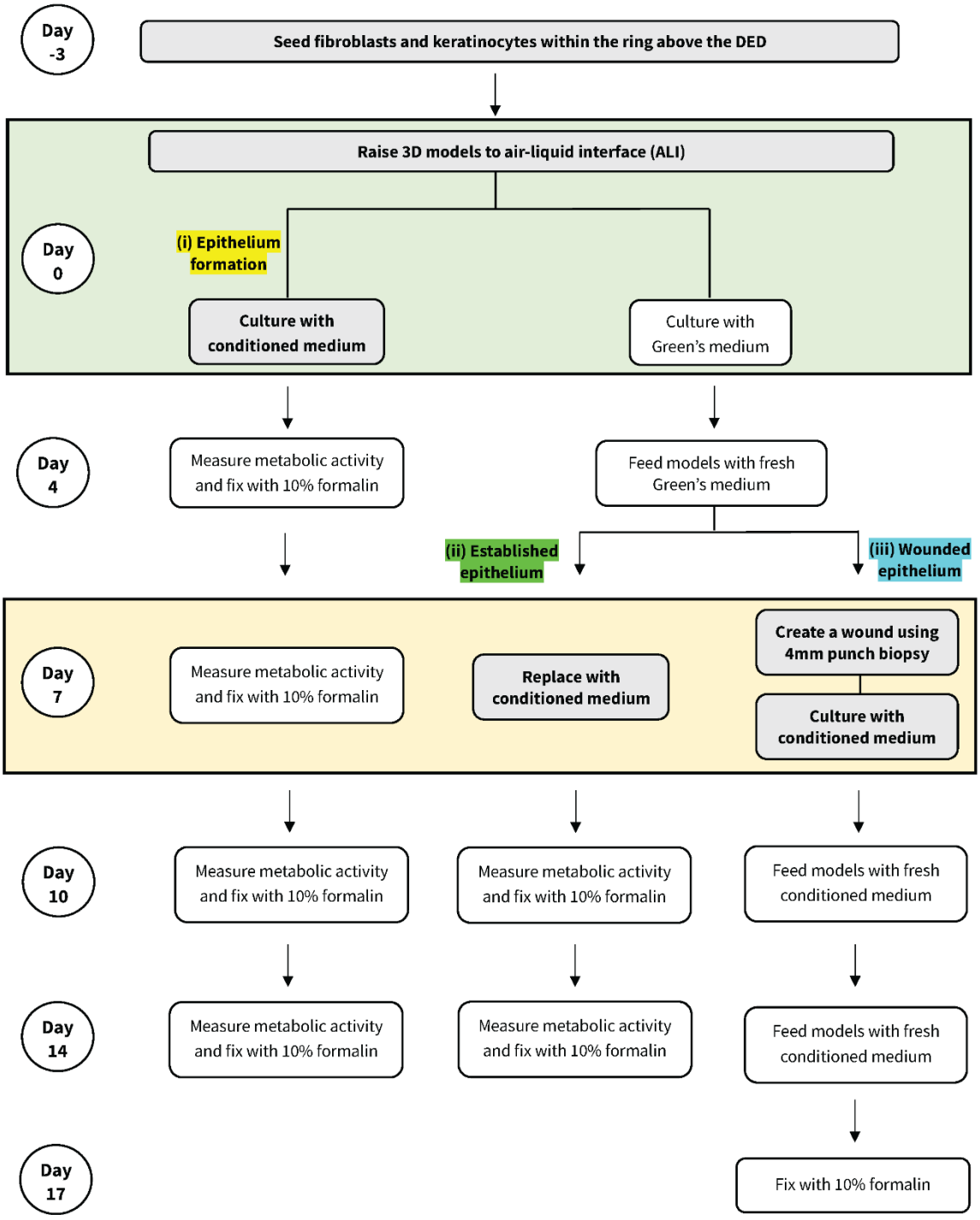

Figure 5.7 | Flow chart and timeline of the 3D culture experiments.

5.3.12 Assessing metabolic activity of TEOM

Resazurin was used to determine the metabolic activity of oral mucosa models. A stock solution (1 mM) was prepared by dissolving resazurin powder (STEMCELL™ Technologies, UK) in sterile PBS. Prior to each experiment, a working solution was prepared by diluting the stock solution with Green's medium at a 1:10 ratio. Each section of the TEOM was incubated in resazurin solution at 37°C. After 4 hours, 100 µL of the solution from each well was taken in triplicate into a 96-well assay plate. Readings were performed at 562/630 nm using an FLx800 fluorescence microplate reader (BioTek, UK). Values were normalised with the value obtained at the earliest time points measured for each experiment.

5.3.13 Assessing the effect of I-PRF on epithelium formation of TEOM

To evaluate the effect on epithelium formation, 3D oral mucosa models were cultured with different concentrations of I-PRF-derived conditioned medium (10, 20, or 50%) immediately after raising the models to an ALI. The preparation of I-PRF-derived conditioned media was described in Section 5.3.4. Models were quartered on days 4, 7, 10, and 14, and each section was used to examine the metabolic activity (as described in Section 5.3.12). The remaining parts of TEOM were placed back at ALI and continued culturing with fresh conditioned media. The metabolic activity results of each quarter were normalised with the values obtained on day 4 of the control model (PRF 0%).

5.3.14 Assessing the effect of I-PRF on established epithelium of TEOM

To investigate the effect of I-PRF on the existing epithelium, 3D models were cultured with Green's medium at an ALI for 7 days to allow the epithelium to stratify. The culture medium was then replaced with the I-PRF-derived conditioned medium (10, 20, or 50%). Models were cultured for a further 7 days. On days 10 and 14, models were bisected, and metabolic activity assay was measured (as described in Section 5.3.12) before being washed and fixed with 10% formalin for further analysis. Metabolic activity values were normalised with the day 7 value of the bisected control models (PRF 0%).

5.3.15 Assessing the effect of I-PRF on wounded epithelium of TEOM

To study the effect of I-PRF on the wounded epithelium, oral mucosa models were cultured with Green's medium at an ALI to create the established epithelium as described above (Section 5.3.14). On day 7, a 4 mm punch biopsy was used to create a wound at the centre of the models, as shown in Figure 5.8. The wounded models were then cultured with I-PRF-derived conditioned medium (PRF 0%, PRF20%, or FBS 10%) for a further 10 days.

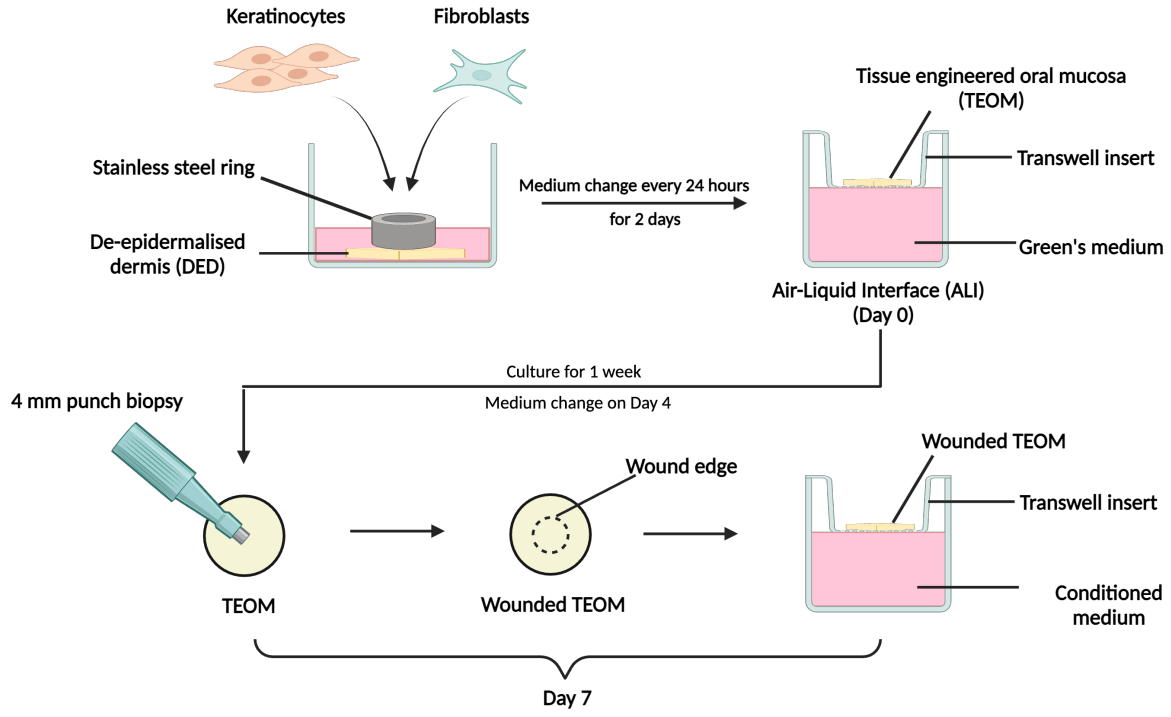

Figure 5.8 | ***Construction of wound models.*** *Tissue engineered oral mucosa (TEOM) were developed by seeding primary oral fibroblasts and immortalised oral keratinocytes (FNB6/TERT) for 72 hours, followed by lifting up to an air-liquid interface (ALI) using a transwell insert. The TEOM were cultured in Green's medium for one week. On day 7, the models were subjected to a 4 mm punch biopsy to simulate wounding and continued to be cultured at ALI for an additional 10 days in conditioned medium. Figure created using Biorender.com.*

5.3.16 Histological processing and Haematoxylin and Eosin (H&E) staining

Formalin-fixed TEOM was placed in a tissue cassette, then dehydrated, cleared, and infiltrated with wax using a Leica TP 1020 tissue processor (Leica Biosystems, UK). The procedures of tissue processing are shown in Table 5.5. After 18 hours, the processed samples were bisected and placed in a metal mould containing molten paraffin wax with an area of interest placed perpendicularly to the bottom surface. The models were embedded in a paraffin wax block using an Epredia™ HistoStar™ Embedding workstation (Epredia™, UK). Wax blocks were left on an ice plate for at least 1 hour to allow them to solidify before being taken out for sectioning. Wax blocks were first trimmed at a thickness of 30 µm using a Leica RM2145 microtome (Leica Biosystems, UK) until the TEOM samples were exposed. Models were sliced to obtain 5 µm thick sections. The tissue slices were immediately transferred to a water bath at 37°C to flatten the sections. Samples were picked up from the water bath and mounted onto SuperFrost™ Plus adhesion microscope slides (Epredia™, UK). Slides were placed in an oven at 60°C overnight to ensure good attachment of sections. The samples were stained with H&E stain using a protocol as outlined in Table 5.6. Stained slides were mounted with glass coverslips using DPX mounting medium (Merck, UK). Slides were left to dry before performing histological analysis. Images were taken using an inverted light microscope (Olympus CX43) with a Euromex camera (VC.3036 HD-Ultra). The backgrounds of the images were removed using Adobe Photoshop 2023 (Adobe) software. Brightness and contrast were adjusted using Image J software. A similar proportion of adjustment was applied to every single image. Scale bars were also added using ImageJ software.

Table 5.5 | ***Tissue processing procedure***

Solution	Time (hours)	Purpose (s)
70% IMS	1	To dehydrate the section
70% IMS	1	
80% IMS	1.5	
85% IMS	1.5	
90% IMS	1.5	
95% IMS	1.5	
100% IMS	1.5	
100% IMS	1.5	
Xylene	1.5	To clear and prepare the section for wax infiltration
Xylene	1.5	
Molten paraffin wax	2	To infiltrate wax into the section
Molten paraffin wax	2	

Table 5.6 | Haematoxylin and Eosin (H&E) staining procedure

Solution	Time	Purpose (s)
Xylene	3 minutes	To remove wax from the section
Xylene	3 minutes	
100% IMS	1 minutes	To gradually rehydrate the section
70% IMS	0.5 minutes	
Distilled water	1 minute	
Haematoxylin solution	1.5 minutes	To stain basophilic components of the section (e.g., nucleus)
Running tap water	4 minutes	To remove excess haematoxylin stain
Eosin solution	5 minutes	To stain acidophilic components of the section (e.g., collagen and cytoplasmic proteins)
Tap water	3 seconds	To gradually dehydrate the section
Tap water	3 seconds	
70% IMS	3 seconds	
100% IMS	30 seconds	
Xylene	Dunk (twice)	To clear the section before mounting

5.3.17 Measuring the epithelial thickness of TEOM

The analysis presented in this section were carried out by the integrated Master's student, Sarah Planchak, as a part of her dissertation. I have been involved in her training and supervision.

The Simple Interactive Object Extraction (SIOX) plugin in ImageJ/Fiji software was used to quantify the epithelium thickness. The epithelium was localised using a polygon tool, as shown in Figure 5.9. The selected area was segmented and labelled as a foreground segmentation using the 'segment' command and then refined to obtain the segmentation, shown in Figure 5.10. This preset segmentation was then applied to all images to generate a black-and-white image depicting the epithelium area, as shown in Figure 5.11. If there is a falsely selected region due to the differences in brightness, contrast, and colour intensity caused by staining procedures between images, an alternative segmentation can be applied.

The area and width of the epithelium were measured automatically using the 'Analyse/Measure' command provided by Image J/Fiji software. The epithelium thickness in micrometres (µm) was then calculated by dividing the area by the width. An area from a section of each biological repeat was measured. Epithelial thickness measurements were carried out in triplicate.

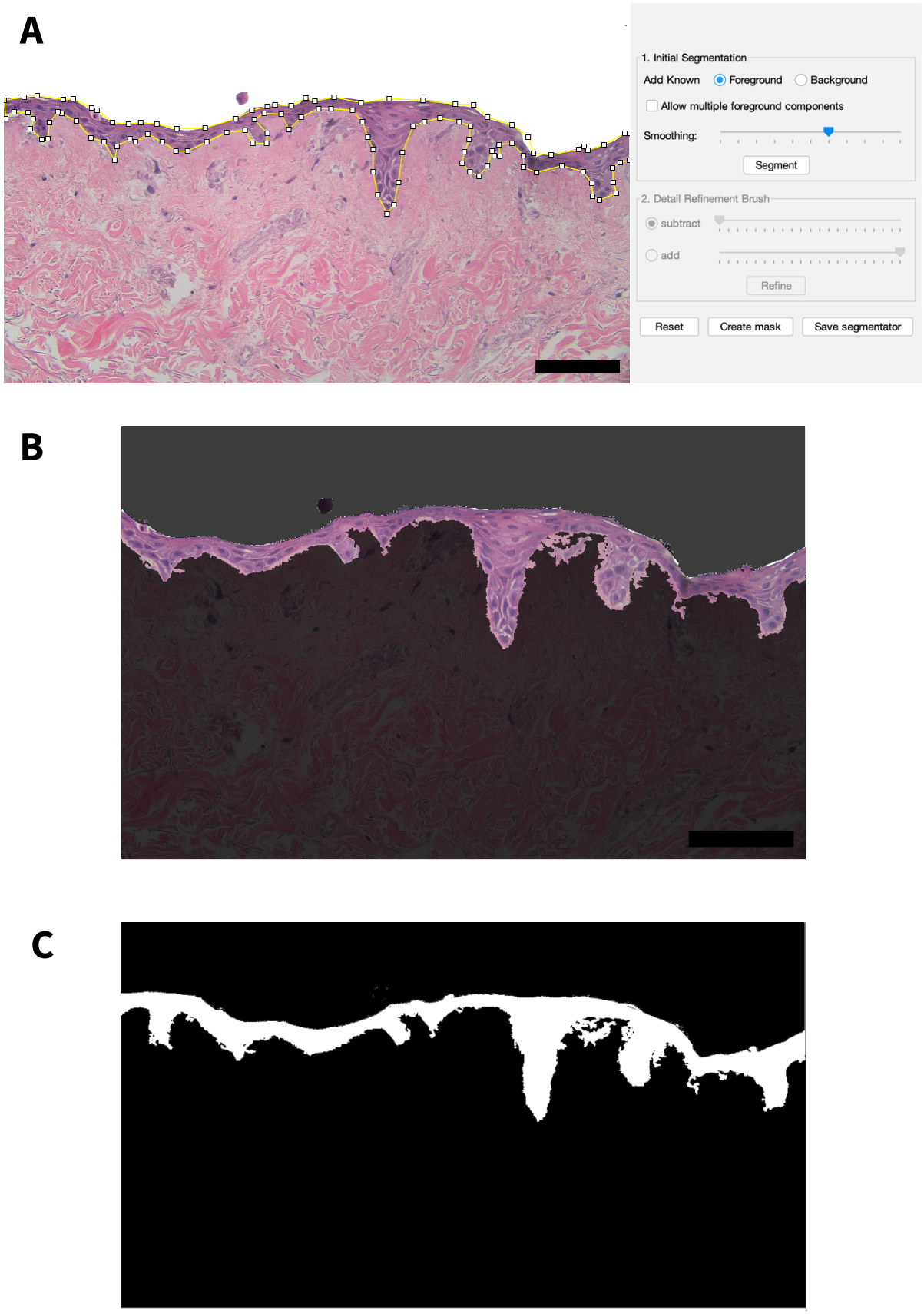

Figure 5.9 | ***Epithelium thickness measurement process.*** *(A) demonstrates the epithelium layer of TEOM outlined by the 'polygon' tool. (B) shows the segmentation of epithelium layer after refining. (C) shows a mask image in black and white which depicts the epithelium area. Scale bar = 100 µm.*

5.3.18 Immunohistochemistry staining for Ki-67 antibody of TEOM

To determine the effect of I-PRF on cell proliferation on TEOM, Ki-67 immunostaining was performed. Ki-67 is commonly used as a marker for cell proliferation as it is expressed in every phase during cell division except the resting stage (G0) [313], [314]. The Ki-67 antigen monoclonal primary antibody (MIB-1 clone, DAKO Omnis, UK) was used in combination with a mouse and rabbit specific horseradish peroxidase (HRP) with diaminobenzidine (DAB) detection kit (ab64264) (Abcam, UK) to detect the expression of Ki-67. The brown-stained nucleus resulting from the DAB stain indicates the expression of Ki-67. Most of reagents provided in the kit were ready-to-use, except the following solutions that needed to be prepared prior to each experiment

A) Sodium citrate buffer (10 mM) with 0.05% Tween-20 (pH 6.0)

Sodium citrate buffer was prepared by dissolving 2.94 g of tri-sodium citrate (dihydrate) in 1 L of distilled water. The pH of the solution was adjusted to 6.0 using 1N hydrochloric acid (HCl) (Thermo Fisher Scientific, UK). Tween-20 (0.5 mL) was added into the solution and stirred until homogenous.

B) 1X DAB solution

A 1X DAB solution was made by mixing 1 drop (approximately 30 µL) of 50X DAB chromogen with 50 drops (approximately 1.5 mL) of DAB substrate (Both solutions were provided in the kit).

Sections of TEOM (5 µm) were dewaxed using xylene and rehydrated with a serial concentration of alcohol, as shown in Table 5.7. Slides were incubated with hydrogen peroxide solution (provided in the kit) at room temperature for 30 minutes to neutralise the endogenous peroxidase activity. All incubation steps were performed in a humidified box to prevent the slides from drying. Slides were then rinsed with running tap water for 5 minutes. A heat-mediated antigen retrieval method was performed by submersing slides in a heated sodium citrate buffer solution (pH 6.0) in a rice cooker. After 2 hours, slides were washed with 1X PBS with 0.05% Tween-20 for 1 minute, followed by a wash for 5 minutes twice. Slides were gently blotted to remove the excess washing buffer. The section area was then localised using a PAP hydrophobic pen (Abcam, UK). A protein block solution (provided in the kit) was applied to the sections and incubated at room temperature for 30

minutes to block non-specific binding sites of protein. Slides were then blotted before adding 2-3 drops of mouse Ki-67 primary antibody. Slides were incubated at 4°C overnight.

The next day, slides were washed using a similar protocol as described above (1 minute once, then 5 minutes twice). Biotinylated goat anti-polyvalent was applied and incubated for 1 hour at room temperature. Slides were then washed again before incubating with Streptavidin peroxidase solution (provided in the kit) for 30 minutes at room temperature. Following this, slides were washed again. A 1X DAB solution was added onto each section and incubated for 5 minutes. Slides were washed with tap water for 5 minutes. Sections were then counterstained with a haematoxylin solution for 30 seconds before washing with tap water for 2 minutes to remove the excess stain. Slides were then dehydrated through increasing concentrations of IMS and finally cleaned with xylene, as shown in Table 5.8. Slides were then mounted with DPX mounting medium and covered with a coverslip. Slides were left overnight to dry. Images were captured using an inverted light microscope (Olympus CX43) with a Euromex camera (VC.3036 HD-Ultra).

Table 5.7 | Dewax and rehydration process for Ki-67 staining

Solution	Time
Xylene (1st)	10 minutes
Xylene (2nd)	5 minutes
100% IMS (1st)	5 minutes
100 % IMS (2nd)	3 minutes
95% IMS	3 minutes

Table 5.8 | Dehydration and clearing process for Ki-67 staining

Solution	Time
70% IMS	3 minutes
90% IMS	3 minutes
95% IMS	3 minutes
100% IMS (1st)	3 minutes
100 % IMS (2nd)	3 minutes
Xylene (1st)	3 minutes
Xylene (2nd)	3 minutes

5.3.19 Statistical analysis

Mean with a standard deviation (SD) was used to present the data. "N" represents number of biological replicates, where "n" indicates number of technical replicates in each biological repeat. GraphPad Prism 9 software was used to analyse the data. The Shapiro-Wilk test was used to test the normality of the data. All results except the blood cell counts in Section 5.4.1 were analysed using one-way ANOVA followed by a Dunnett's post-hoc comparison test. Platelet and white blood cell concentrations between the whole blood and PRF were compared using an unpaired T-test. Statistical significance was indicated when the p-value < 0.05.

5.4 Results

5.4.1 Platelet count was higher in I-PRF compared to the whole blood

To validate the method used to prepare I-PRF (as described in Section 5.3.2), whole blood and I-PRF samples were collected from healthy volunteers and sent for complete blood count analysis (Section 5.3.3). Data shows that I-PRF had significantly higher platelet concentrations with approximately $6.80x10^{11}$ platelets/L while the whole blood had approximately $2.45x10^{11}$ platelets/L (Figure 5.10A). In terms of white blood cells, there was no significant difference between the two groups (Figure 5.10B).

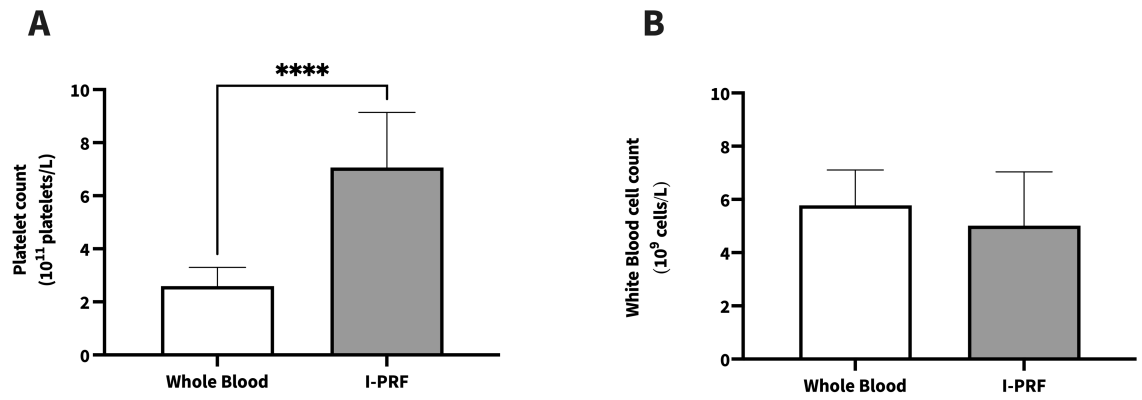

Figure 5.10 | Platelet and white blood cell count. *(A) Platelet and (B) white blood cell count obtained from whole blood or I-PRF from healthy volunteers. Data are shown from nine volunteers (N=9). Data are presented as the mean ± standard deviation. An unpaired t-test was carried out to test the statistical significance (**** p<0.0001). Abbreviations; I-PRF, injectable platelet-rich fibrin.*

5.4.2 PDGF-BB, TGF- β1, and EGF were the most abundant growth factors found in I-PRF

To characterise the components released from I-PRF into the conditioned medium, an antibody array (C1000 kit) containing 120 different cytokines was used (described in Section 5.3.6). The I-PRF-derived conditioned medium collected from three different volunteers was used. Values are presented as relative expression in comparison to basal DMEM (Equation 5.1).

Firstly, we analysed the growth factors which have been reported in the literature to be present in PRF [274], [278], [311]. Our results showed high quantities of PDGF-BB, TGF-β1, and EGF, with relative expression of 9.95, 2.66, and 2.83 times, respectively, compared to basal DMEM (Figure 5.11A). VEGF-A, IGF-1 and bFGF were found to be present at similar levels relative to basal DMEM.

We next evaluated the interleukins, as they play a role in mediating inflammatory responses during the healing process. In general, all interleukins were found at higher levels in the I-PRF-derived conditioned medium than basal DMEM, with notably high expression observed for IL-8, IL-10, and IL-13, as shown in Figure 5.11B. IL-8 in I-PRF-derived conditioned medium was 8.75 times higher than the baseline level, while IL-10 and IL-13 were present at 3.49 and 3.43 times the amount in basal DMEM, respectively.

The remaining cytokines were analysed and categorised into three groups (High, Medium, or Low expression) based on the quantities relative to the levels in basal DMEM. Figure 5.11C shows a group of highly expressed cytokines, with relative expressions over 5. Among these, adiponectin, angiogenin, MCP-1 (or CCL2), and RANTES (or CCL5) were present in the I-PRF-derived conditioned medium with amounts over 10 times higher than basal DMEM. Angiogenin demonstrated the highest relative expression of all cytokines, with 21.95 times the amount found in basal DMEM. Cytokines with relative expressions between 2.5 to 5 in relative to the baseline levels were classified as the ‘medium expression’ group (Figure 5.11D). This group included AgRP, BDNF, EGF-R, ENA-78, Eotaxin-3, GM-CSF, G/R/O-alpha, IGFBP-1, I-TAC, MCP-2, MCP-3, and TIMP-2. All other cytokines with their relative expression value are listed in alphabetical order in Table 5.9.

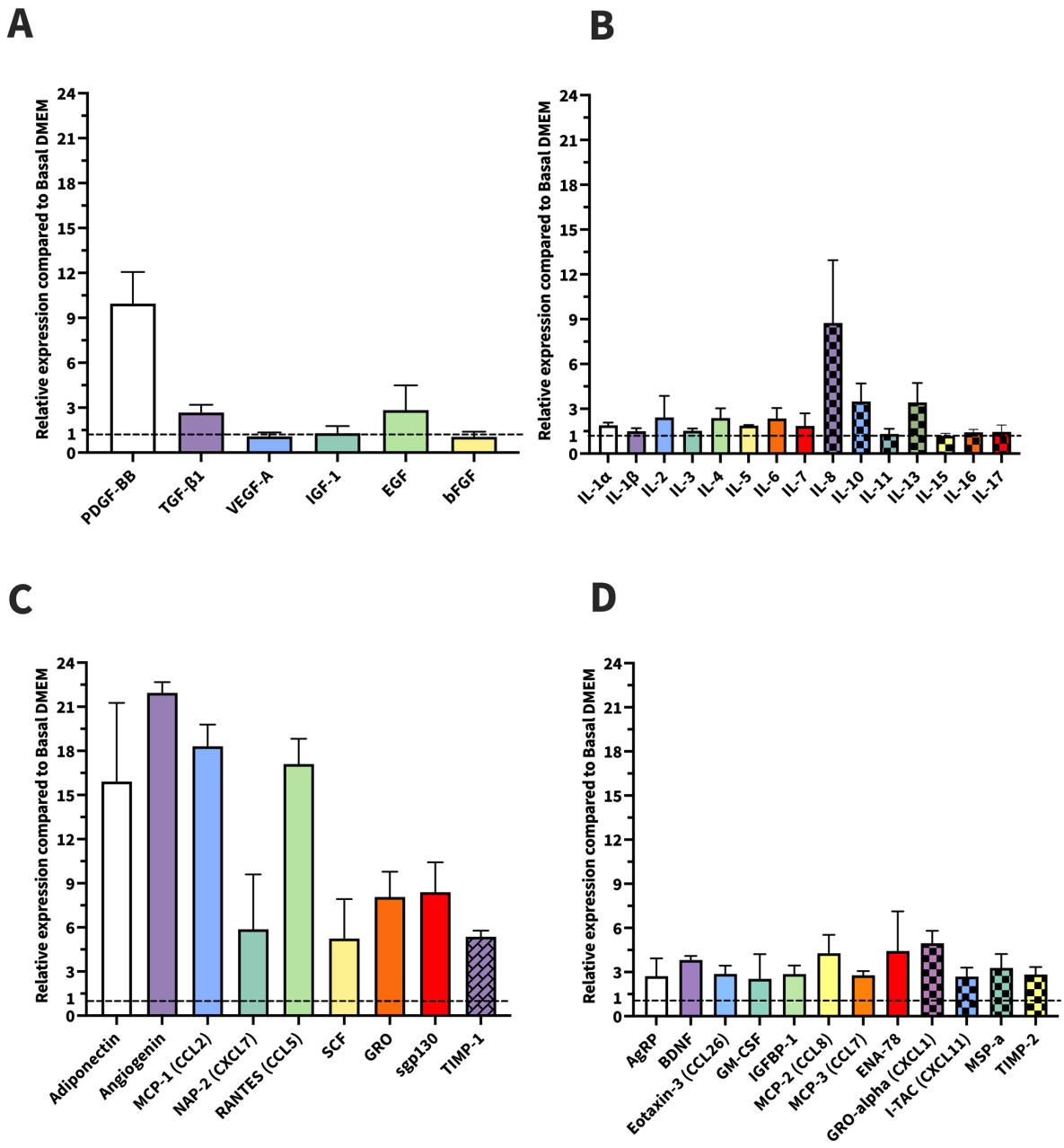

Figure 5.11 | ***Relative expression of growth factors, interleukins and cytokines in I-PRF.*** *Panel (A) displays growth factors, (B) interleukins, (C) cytokines with values higher than 5, and (D) cytokines with values between 2.5 – 5, in I-PRF-derived conditioned medium compared to basal DMEM. Data are shown from three volunteers (N=3). Data are presented as the mean ± standard deviation. The dotted line indicates the concentration of cytokine in basal DMEM.*

Table 5.9 | Relative expression of the remaining cytokine proteins on the antibody membrane array compared to basal DMEM (alphabetical ordered)

Cytokines	Relative expression	Cytokines	Relative expression	Cytokines	Relative expression
Amphiregulin	1.07	**GITR**	0.89	**MIF**	0.97
Angiopoietin-2	1.24	**GITR ligand**	1.02	**MIG**	1.26
Axl	0.99	**HCC-4**	1.14	**MIP-1-alpha**	0.80
Beta-NGF	1.26	**HGF**	2.12	**MIP-1-beta**	2.17
BLC	1.90	**I-309**	1.96	**MIP-1-delta**	2.30
BMP-4	1.17	**ICAM-1**	2.34	**MIP-3-alpha**	2.09
BMP-6	2.09	**ICAM-3**	1.14	**MIP-3-beta**	1.85
BTC	1.13	**IFN-gamma**	1.84	**NT-3**	1.49
CCL28	1.60	**IGF-BP-3**	1.27	**NT-4**	1.17
CK beta 8-1	1.44	**IGF-BP-6**	1.96	**Oncostatin M**	0.70
CNTF	1.21	**IGF-I SR**	1.25	**Osteoprotegerin**	1.34
CTACK	1.50	**IGFBP-2**	2.13	**PARC**	1.74
Dtk	1.39	**IGFBP-4**	1.72	**PlGF**	1.64
Eotaxin	0.92	**IL-1 R4/ST2**	1.06	**SDF-1**	1.18
Eotaxin-2	2.17	**IL-1 RI**	1.23	**sTNF RII**	2.42
EGF-R	3.12	**IL-1ra**	1.25	**sTNF-RI**	1.47
Fas/TNFRSF6	2.32	**IL-2 Ra**	1.32	**TARC**	1.95
FGF-4	1.58	**IL-6 R**	7.23	**TGF-beta 3**	1.62
FGF-6	1.45	**IL12-p40**	1.17	**TNF-alpha**	1.89
FGF-7	1.32	**IL12-p70**	0.87	**TNF-beta**	1.65
FGF-9	1.04	**Leptin**	2.00	**TPO**	1.60
Flt-3 Ligand	1.59	**Lymphotactin**	2.15	**TRAIL-R3**	1.31
Fractalkine	2.15	**M-CSF**	1.69	**TRAIL-R4**	1.02
G-CSF	1.43	**MCP-4**	1.91	**uPAR**	2.05
GCP-2	1.91	**M-CSF**	1.69	**VEGF-D**	1.18
GDNF	1.32	**MDC**	1.69		

5.4.3 I-PRF increased the metabolic activity of oral mucosa cells

MTT was used to determine the metabolic activity of oral mucosa cells (Section 4.3.5). Figure 5.12 demonstrates the response of NOFs to different concentrations of PRF-conditioned medium over 72 hours. All results were normalised to the 24-hour value of the control (PRF 0%). The metabolic activity of the control was increased by approximately 25% over the experimental period. There was no significant change in the NOF metabolic activity after 24-hours of culture. After 72 hours, the metabolic activity of I-PRF-treated NOFs increased in a dose-dependent fashion with statistical significance compared to the control (PRF 0%) observed from NOFs incubated with 50% I-PRF-derived conditioned medium.

In terms of FNB6/TERT, the metabolic activity of the negative control was increased around 200% between 24 and 72 hours, as shown in Figure 5.13, indicating a higher metabolic rate compared to NOFs. At 24 hours, no concentrations of I-PRF-derived conditioned medium used affected FNB6/TERT metabolic activity. A slight increase in metabolic activity was seen after treating cells with the I-PRF-derived conditioned medium for 72 hours; however, no statistical significance was observed from any conditions. Based on this data, three concentrations of I-PRF-derived conditioned medium (10%, 20%, and 50%) were chosen for future experiments as these doses produced the most increase in the metabolic activity across both cell types.

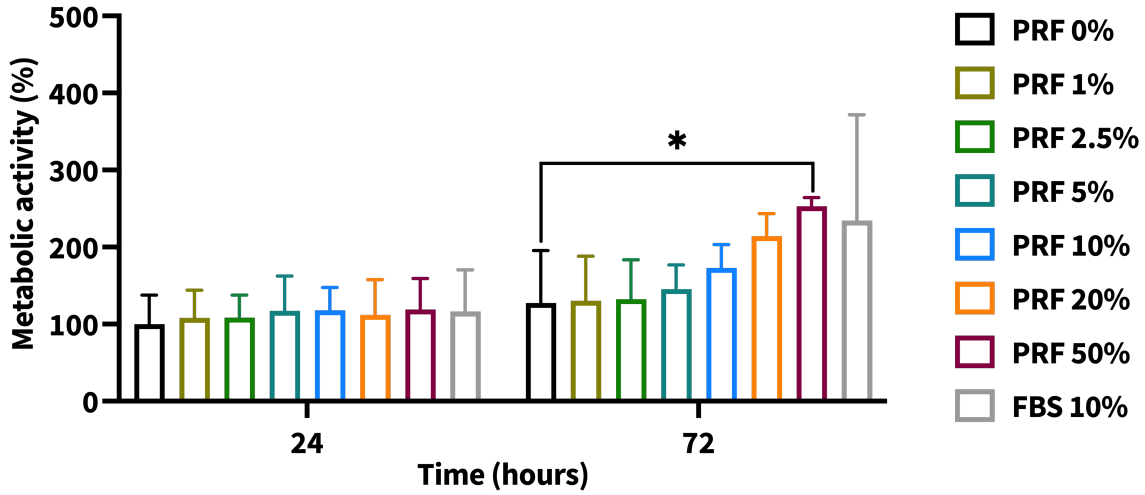

Figure 5.12 | ***Metabolic activity of primary oral fibroblasts (NOFs) in response to I-PRF-derived conditioned medium***. *NOFs were treated with different concentrations of I-PRF-derived conditioned medium or Green's medium (containing FBS 10%) for 24 and 72 hours. Metabolic activity was assessed using the MTT assay. Data are presented as the mean ± standard deviation from four independent experiments with three technical replicates each (N=4, n=3) except PRF 0% and FBS 10%, which were derived from three experiments (N=3, n=3). Statistical significance was determined using a one-way ANOVA, followed by Dunnett's multiple comparison against the control (PRF 0%) at each time point (*p<0.05). Abbreviations: PRF, platelet-rich fibrin; FBS, foetal bovine serum; ANOVA, analysis of variance.*

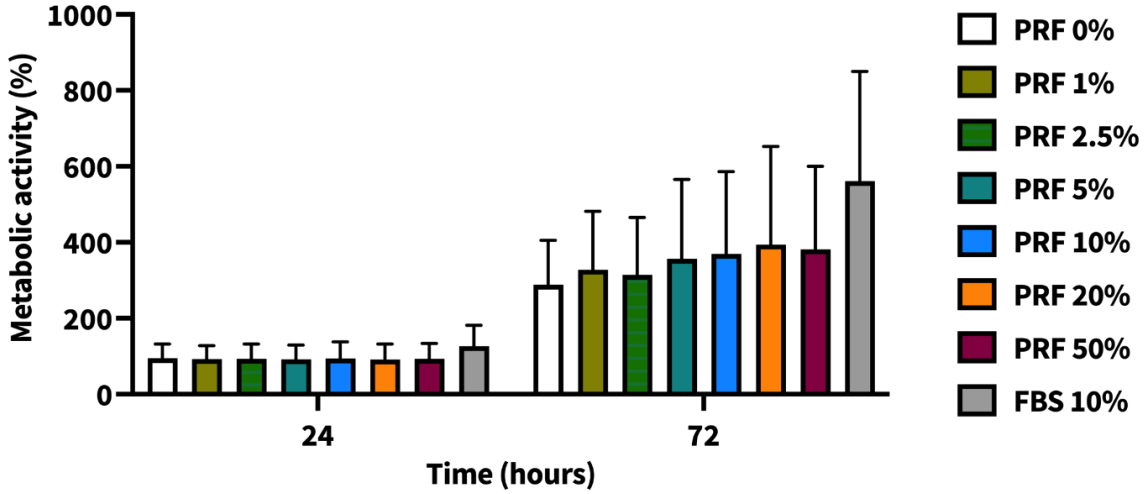

Figure 5.13 | ***Metabolic activity of immortalised oral keratinocytes (FNB6/TERT) in response to I-PRF-derived conditioned medium***. *FNB6/TERT were treated with different concentrations of I-PRF-derived conditioned medium or Green's medium (containing FBS 10%) for 24 and 72 hours. Metabolic activity was measured using the MTT assay. Data are presented as the mean ± standard deviation from five independent experiments with three technical replicates each (N=5, n=3) except PRF 0% and FBS 10%, which were derived from four experiments (N=4, n=3). Statistical significance was determined using a one-way ANOVA, followed by Dunnett's multiple comparison against the control (PRF 0%) at each time point. Abbreviations: PRF, platelet-rich fibrin; FBS, foetal bovine serum; ANOVA, analysis of variance.*

5.4.4 I-PRF did not induce apoptosis or necrosis of oral mucosa cells

Following the investigations on the metabolic activity, we next tested the biocompatibility of I-PRF on both oral fibroblasts and keratinocytes. Oral mucosa cells were stained with Annexin V-conjugated with FITC and propidium iodide to determine cell status after having a single treatment of different concentrations of I-PRF-derived conditioned medium (10, 20 or 50%) for 72 hours as outlined in Section 5.3.8.

Figure 5.14 shows the percentage of NOFs in each stage after 72-hour treatment with I-PRF-derived conditioned medium. In the untreated (control) fibroblast samples, the majority of cells (93%) were viable (Annexin V- PI-) after 72 hours. Approximately 1%, 4%, and 2% of cells were found in early apoptotic (Annexin V+ PI-), late apoptotic (Annexin V+ PI+), and necrotic (Annexin V- PI+) stages, respectively. I-PRF-derived conditioned medium produced no significant differences in the cell status. A reduction of viable cell proportion was observed from fibroblasts treated with DMEM containing FBS 10%, with only 75% viable, but 14% of cells were positively stained with both Annexin V and PI, indicating late apoptotic cells. However, no statistical significance was observed between any conditions.

The proportion of FNB6/TERT at each stage in the presence of I-PRF-derived conditioned medium for 72 hours was shown in Figure 5.15. There was no significant difference between any groups at each stage. All conditions had approximately 90% viable cells, 1% early apoptotic cells, 6% late apoptotic cells, and 3% necrotic cells.

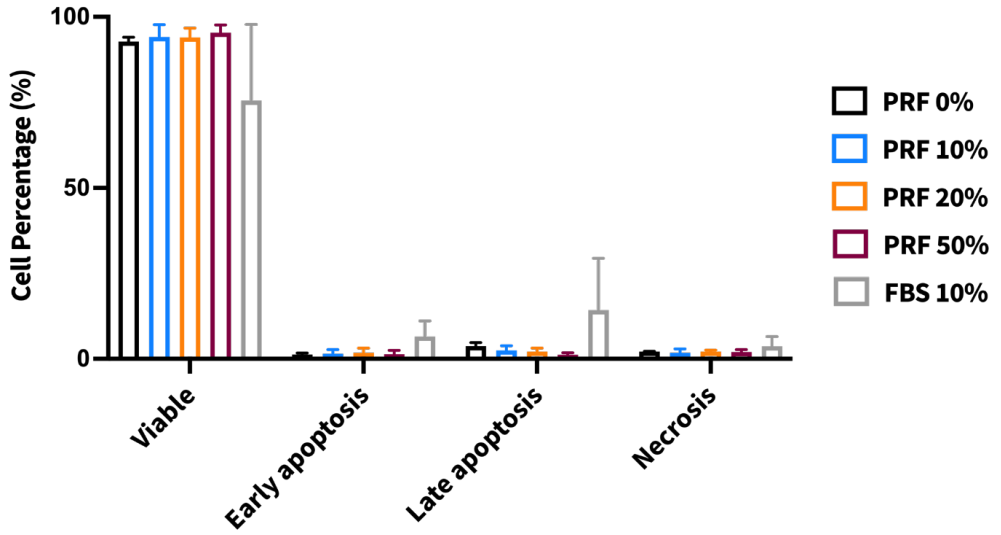

Figure 5.14 | ***Apoptotic status following annexin V-FITC and propidium iodide (PI) staining of primary oral fibroblasts (NOFs) treated with I-PRF-derived conditioned medium.*** *NOFs were treated with different concentrations of I-PRF-derived conditioned medium or Green's medium (containing FBS 10%) for 72 hours. Cell status was assessed using annexin V-FITC and PI staining. Data are presented as the mean ± standard deviation from three independent experiments (N=3, n=1). Statistical significance was determined using a one-way ANOVA followed by Dunnett's multiple comparison against the control (PRF 0%) of each group. Abbreviations: PRF, platelet-rich fibrin; FBS, foetal bovine serum; ANOVA, analysis of variance.*

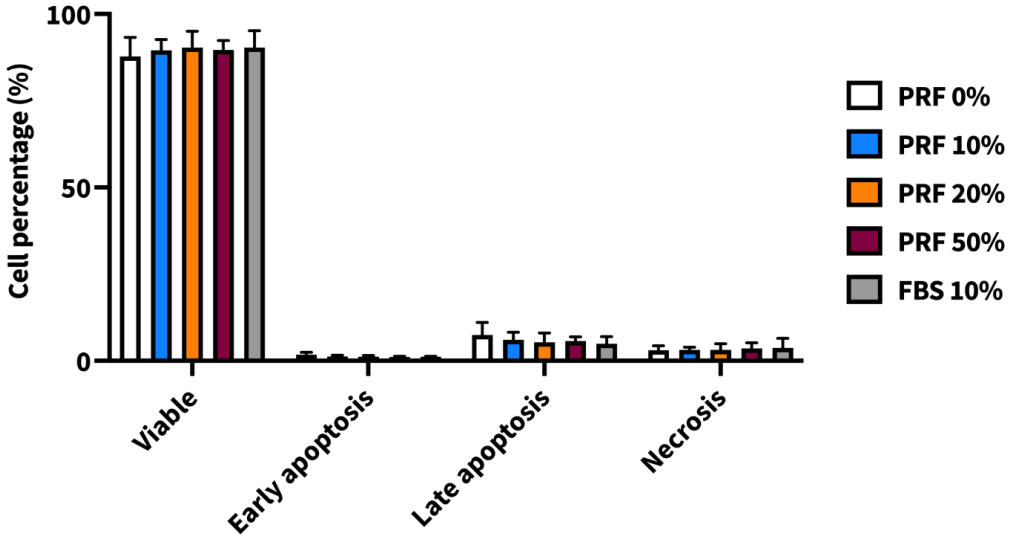

Figure 5.15 | ***Apoptotic status following annexin V-FITC and propidium iodide (PI) staining of immortalised oral keratinocytes (FNB6/TERT) treated with I-PRF-derived conditioned medium.*** *FNB6/TERT were treated with different concentrations of I-PRF-derived conditioned medium or Green's medium (containing FBS 10%) for 72 hours. Cell status was assessed using annexin V-FITC and PI staining. Data are presented as the mean ± standard deviation from three independent experiments (N=3, n=1). Statistical significance was determined using a one-way ANOVA, followed by Dunnett's multiple comparison against the control (PRF 0%) of each group. Abbreviations: PRF, platelet-rich fibrin; FBS, foetal bovine serum; ANOVA, analysis of variance.*

5.4.5 I-PRF induced proliferation of oral mucosa cells

Another important mechanism involved in the healing process is cell proliferation, which was assessed using Cell trace CFSE fluorescence dye (Section 5.3.9). Mean fluorescence intensity (MFI) was obtained from CFSE-stained cells by the flow cytometry method. Data were normalised to the value obtained with mitomycin C treated cells, designated as a non-proliferative control, to obtain the proliferation index. The proliferation index represents the proliferative capacity of cells. A higher value indicates higher cell proliferation.

Figure 5.16 shows the proliferation index of NOFs in response to I-PRF-conditioned medium after 24 and 72 hours. At 24 hours, the proliferative index of NOFs treated with all concentrations of I-PRF-derived conditioned medium and FBS 10% was significantly increased compared to the control, which was complete DMEM without FBS as described in Section 5.3.7. We also observed a similar trend at the 72-hour time point. The addition of I-PRF-conditioned medium significantly increased NOF proliferation. The proliferative index of all I-PRF-treated conditions was higher than the DMEM supplemented with FBS 10%, suggesting a more pronounced effect of PRF compared to FBS.

There was no significant change in FNB6/TERT proliferation in the presence of I-PRF-conditioned medium at a 24-hour time point, as shown in Figure 5.17. At 72 hours, I-PRF increased FNB6/TERT proliferation in comparison to the PRF 0% control; however, no statistical significance was observed.

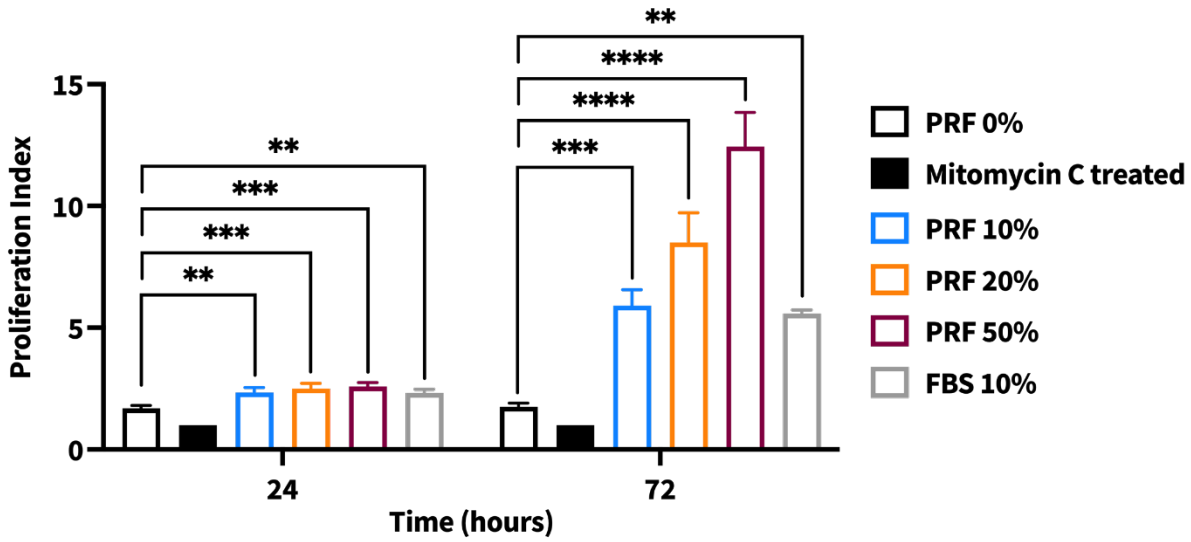

Figure 5.16 | ***Proliferation index of primary oral fibroblasts (NOFs) in response to I-PRF-derived conditioned medium***. *NOFs were cultured in three concentrations of I-PRF derived conditioned medium or Green's medium (containing FBS 10%) for 24 or 72 hours. Proliferation index was calculated using mean fluorescence intensity from flow cytometry results. Data are presented as the mean ± standard deviation from three independent experiments (N=3, n=1). Statistical significance was determined using a one-way ANOVA followed by Dunnett's multiple comparison against the control (PRF 0%) of each group (** p<0.01, *** p<0.001, and **** p<0.0001). PRF, platelet-rich fibrin; FBS, foetal bovine serum; ANOVA, analysis of variance.*

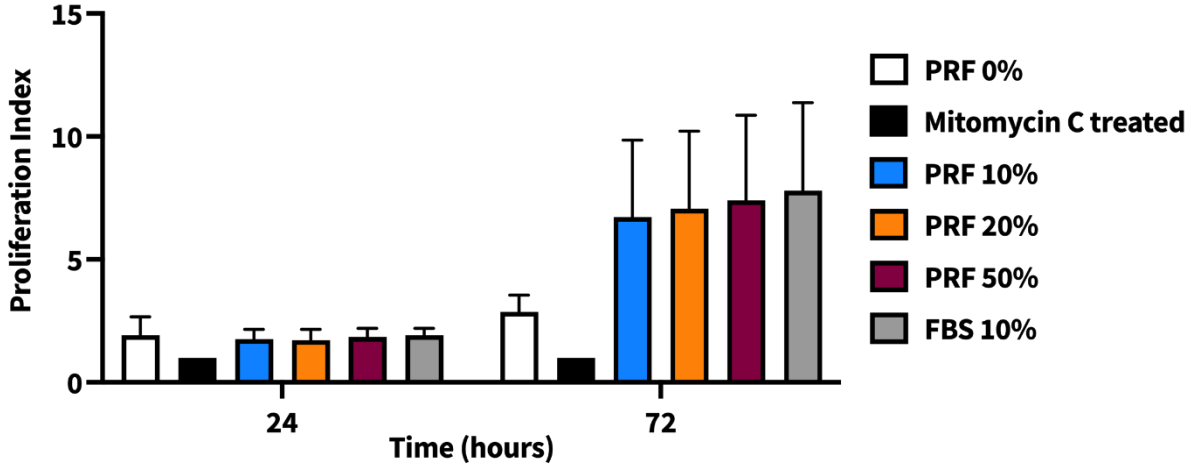

Figure 5.17 | ***Proliferation index of immortalised oral keratinocyte (FNB6/TERT) in response to I-PRF-derived conditioned medium***. *FNB6/TERT were treated with three concentrations of I-PRF-derived conditioned medium or Green's medium (containing FBS 10%) for 24 or 72 hours. Proliferation index was calculated using mean fluorescence intensity from flow cytometry results. Data are presented as the mean ± standard deviation from three independent experiments (N=3, n=1). Statistical significance was determined using a one-way ANOVA followed by Dunnett's multiple comparison against the control (PRF 0%) of each group. PRF, platelet-rich fibrin; FBS, foetal bovine serum; ANOVA, analysis of variance.*

5.4.6 I-PRF affected the migration rate of both oral fibroblasts and keratinocytes

Cell migration plays a vital role in the healing process as cells migrate across the wound bed to close the wound [33]. Here, we aimed to investigate whether I-PRF affects the migration of oral mucosa cells. The migration rate of cells was examined by creating a gap in the cell layer using Oris™ stoppers and then measuring the decrease in gap size over time (Section 5.3.10). The *in vitro* gap in the cell layer was used to represent a clinical wound. Prior to incubation with I-PRF-conditioned medium, oral mucosa cells were treated with mitomycin C for 4 hours in order to rule out possible interference from cell proliferation.

Figure 5.18 demonstrates the migration of NOFs over 72 hours. At 24 hours, a higher percentage of gap closure was observed from cells treated with 50% I-PRF-derived conditioned medium compared to the controls (PRF 0%). A similar trend was also seen after 48-hours. All concentrations of I-PRF-derived conditioned medium and FBS-containing medium produced a higher percentage of gap closure (over approximately 97%) after 72 hours of treatment. Around 90% of the gap was closed in the control wells, indicating cells were unable to migrate far enough to close the gap. Representative images of each condition are shown in Figure 5.19.

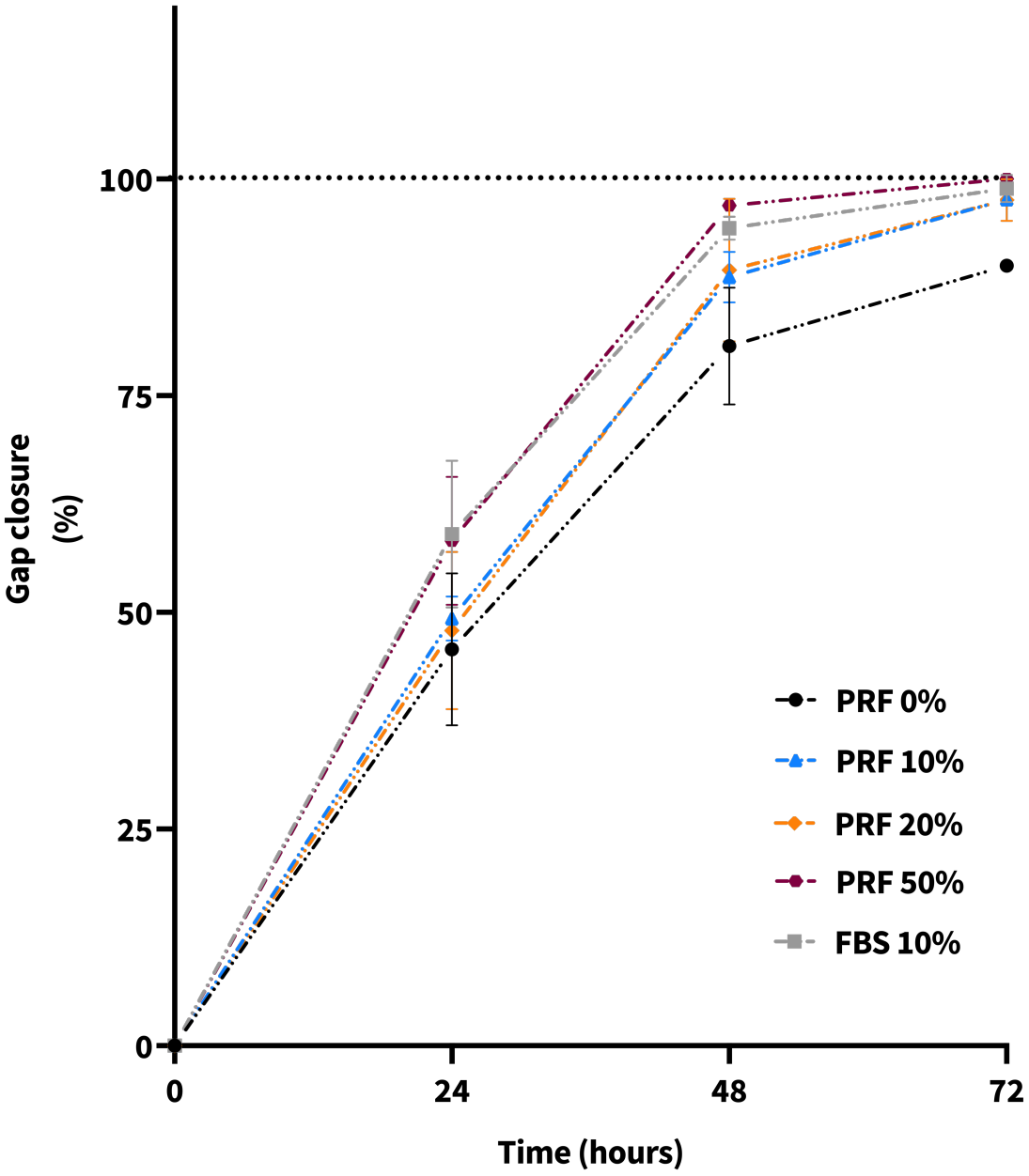

Figure 5.18 | ***Migration analysis of primary oral fibroblasts (NOFs) in response to I-PRF-derived conditioned medium.*** *NOFs were cultured with three concentrations of I-PRF-derived conditioned medium or Green's medium (containing FBS 10%) for 72 hours. The migration, assessed by measuring gap closure of each well, was quantitatively analysed at 24-hour intervals (24, 48, and 72 hours). Data are presented as the mean ± standard deviation from two independent experiments with six technical replicates each (N=2, n=6).*

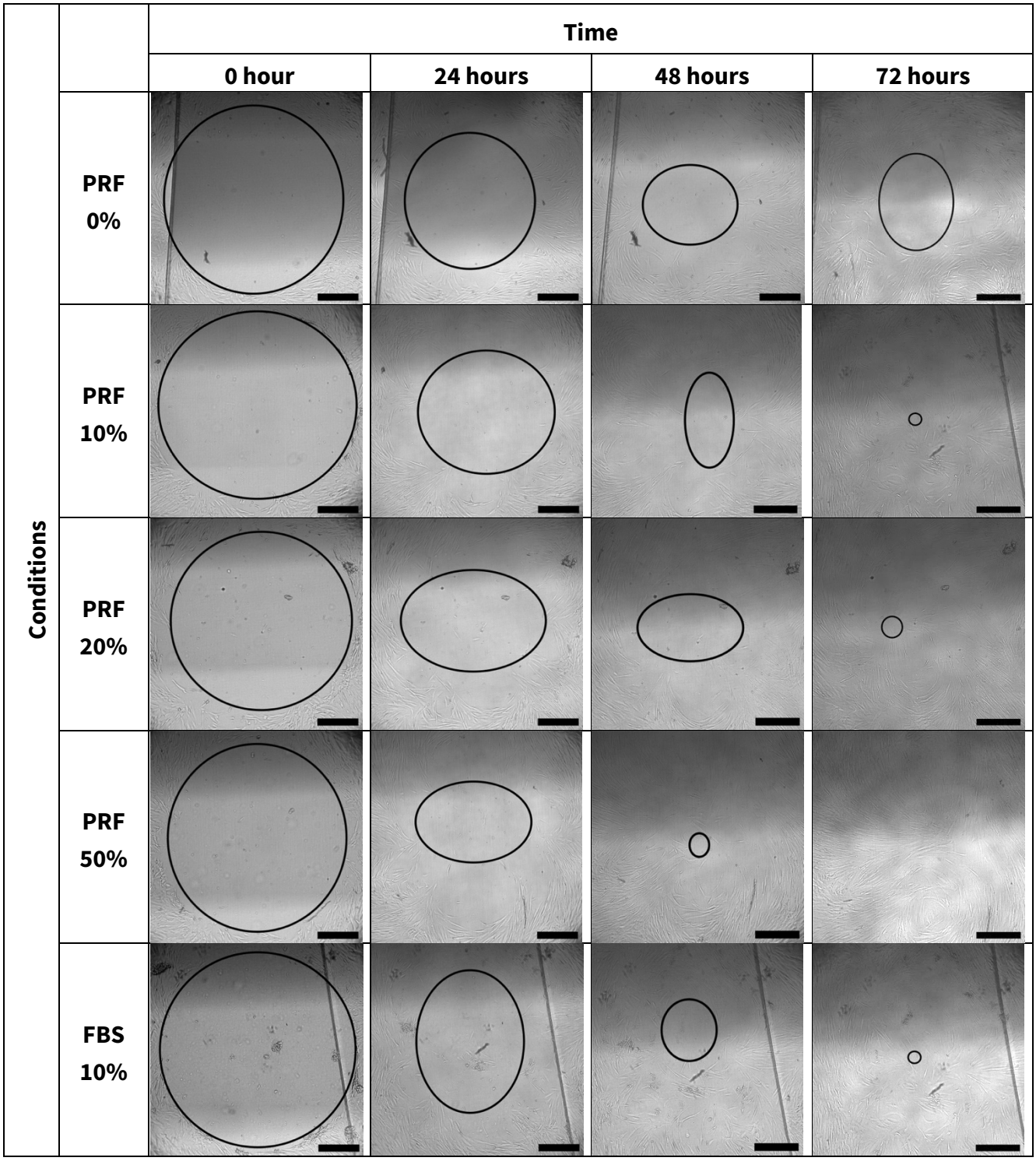

Figure 5.19 | ***Representative images of primary oral fibroblast (NOF) migration over 72 hours in the presence of I-PRF-derived conditioned medium****. NOFs were treated with varying concentrations of I-PRF-derived conditioned medium or complete DMEM (containing FBS 10%), and incubated for 72 hours. Images show the migration pattern of NOFs, captured using an inverted microscope at 4x magnification. Circles have been added to each image to illustrate the remaining gap. Scale bars = 0.5 mm.*

Figure 5.20 demonstrates the migration of FNB6/TERT over 24 hours with representative images from each condition in Figure 5.21. The migration of FNB6/TERT was faster than NOFs, leading to a shorter experimental time-course. When treated with I-PRF-derived conditioned medium, the migration rate of FNB6/TERT after 8-hours of culture was higher in all conditions compared to the negative control. At 16 hours, the gap had closed faster in all tested conditions compared to the negative control. An increase was observed with the conditioned medium containing FBS 10%, PRF 20% and PRF 50%.

All conditions produced a gap closure over 98% after 24 hours, while the controls only had approximately 65% of a filled gap, indicating an increase in cell migration in all conditions compared to the control during a 24-hour time point.

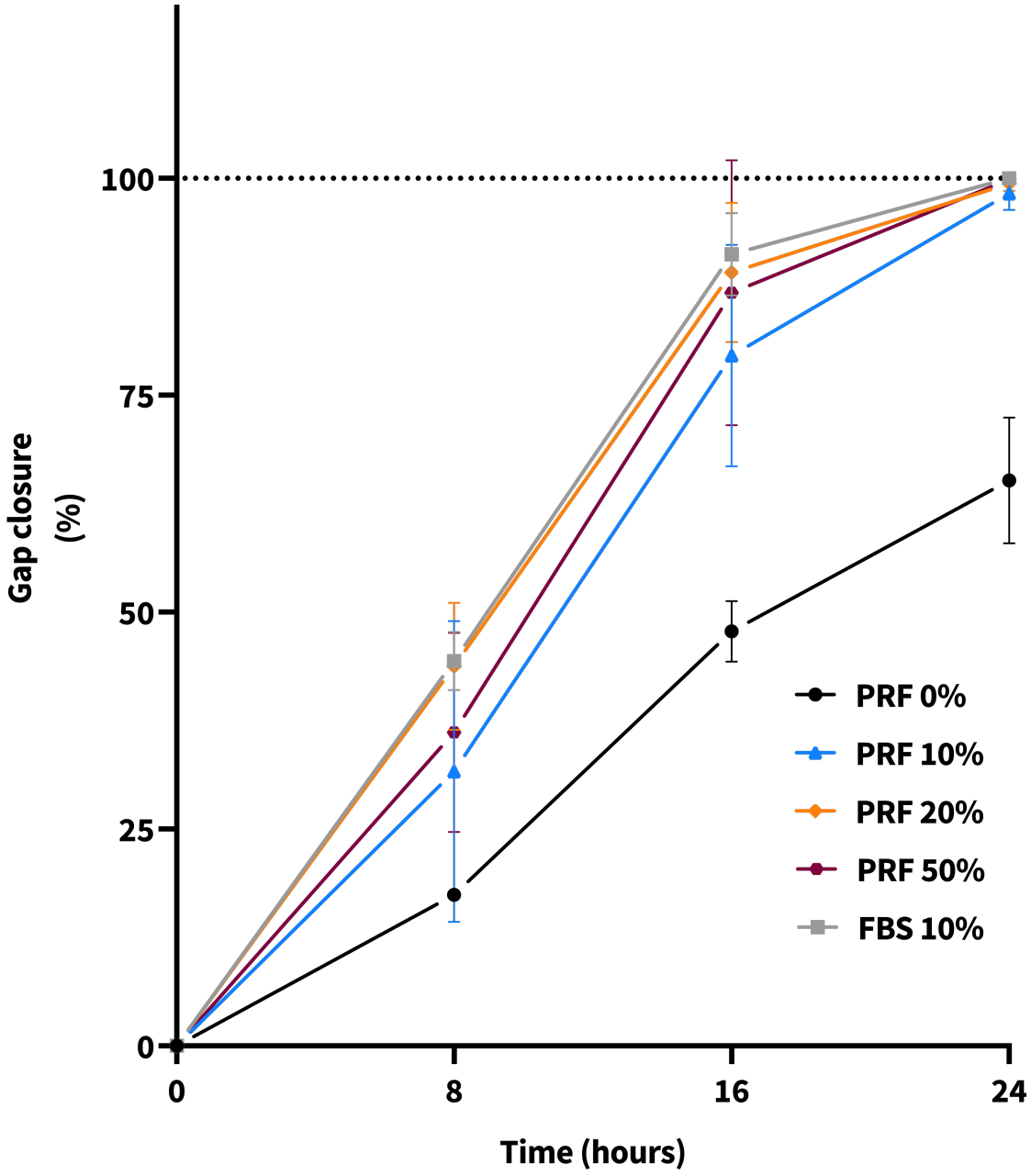

Figure 5.20 | Migration analysis of immortalised oral keratinocytes (FNB6/TERT) in response to I-PRF-derived conditioned medium. *FNB6/TERT were cultured with three concentrations of I-PRF-derived conditioned medium or Green's medium (containing FBS 10%) for 24 hours. The migration, assessed by measuring gap closure of each well, was quantitatively analysed at 8-hour intervals (8, 16, and 24 hours). Data are presented as the mean ± standard deviation from two independent experiments with six technical replicates each (N=2, n=6).*

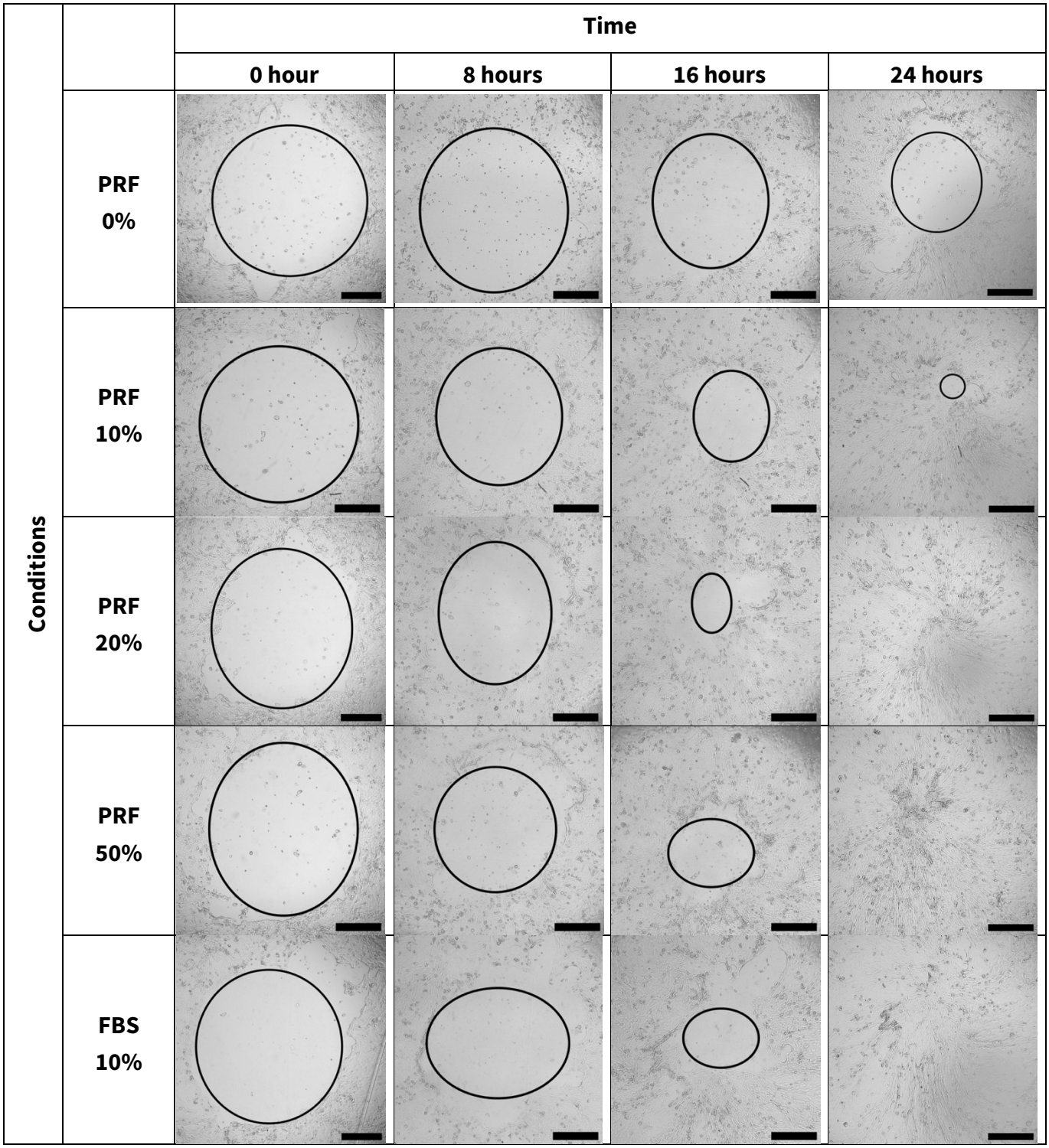

Figure 5.21 | ***Representative images of immortalised oral keratinocyte (FNB6/TERT) migration over 24 hours in the presence of different I-PRF-derived conditioned medium****. FNB6/TERT were treated with varying concentrations of I-PRF-derived conditioned medium or Green's medium (containing FBS 10%), and incubated for 72 hours. Images show the migration pattern of FNB6/TERT cells, captured using an inverted microscope at 4x magnification. Circles have been added to each image to illustrate the remaining gap. Scale bars = 0.5 mm.*

5.4.7 I-PRF did not affect the metabolic activity of TEOM during the process of epithelium formation

To examine the bioactivity of I-PRF in a scenario closer to the clinical settings, TEOM constructed with oral fibroblasts and keratinocytes on DED, was used as a study model in this thesis. TEOM were cultured in different concentrations of I-PRF-derived conditioned medium at ALI for 14 days to evaluate the effect of I-PRF on the epithelium formation process, as described in Section 5.3.13. The metabolic activity of TEOM was determined using resazurin (Section 5.3.12). Our results demonstrated that I-PRF had no significant effect on the metabolic activity of TEOM at any time points during the experimental period (Figure 5.22).

Epithelium morphology and thickness were investigated (Section 5.3.16 and 5.3.17) to evaluate the effect of I-PRF. Figure 5.23A - E illustrates the formation of the epithelial layer of TEOM after being cultured with I-PRF-derived conditioned medium for 4 days. All conditions demonstrated a multi-layered epithelium of TEOM with densely packed cuboidal keratinocytes observed in the basal layer. At the superficial layer, only one or two layers of keratinocytes had a flattened shape at this time point. A slight increase in epithelial thickness was observed in all I-PRF-treated concentrations in comparison to the control (PRF 0%), as shown in Figure 5.23F. However, no statistical significance was observed. The epithelial thickness of the control TEOM was around 35 µm while the thickest epithelium was approximately 60 µm observed from the 20% I-PRF-derived conditioned medium condition.

Following H&E staining, immunohistochemical staining of Ki-67 was performed to detect proliferative cells in the epithelium layer, which could affect the thickness of the oral epithelium. Brown-stained nuclei indicate the immune-positive-staining of Ki-67. Our results showed positive staining of Ki-67 at the basal region of the epithelium of TEOM across all conditions (Figure 5.24A - E). Additionally, Ki-67 positive cells were found at the suprabasal layer of TEOM-treated with PRF 50% and FBS 10% (Figure 5.24D and 5.24E) compared to the control which were only found at the basal layer, indicating the possibility of a proliferative effect from I-PRF on basal keratinocytes during the formation of the epithelium.

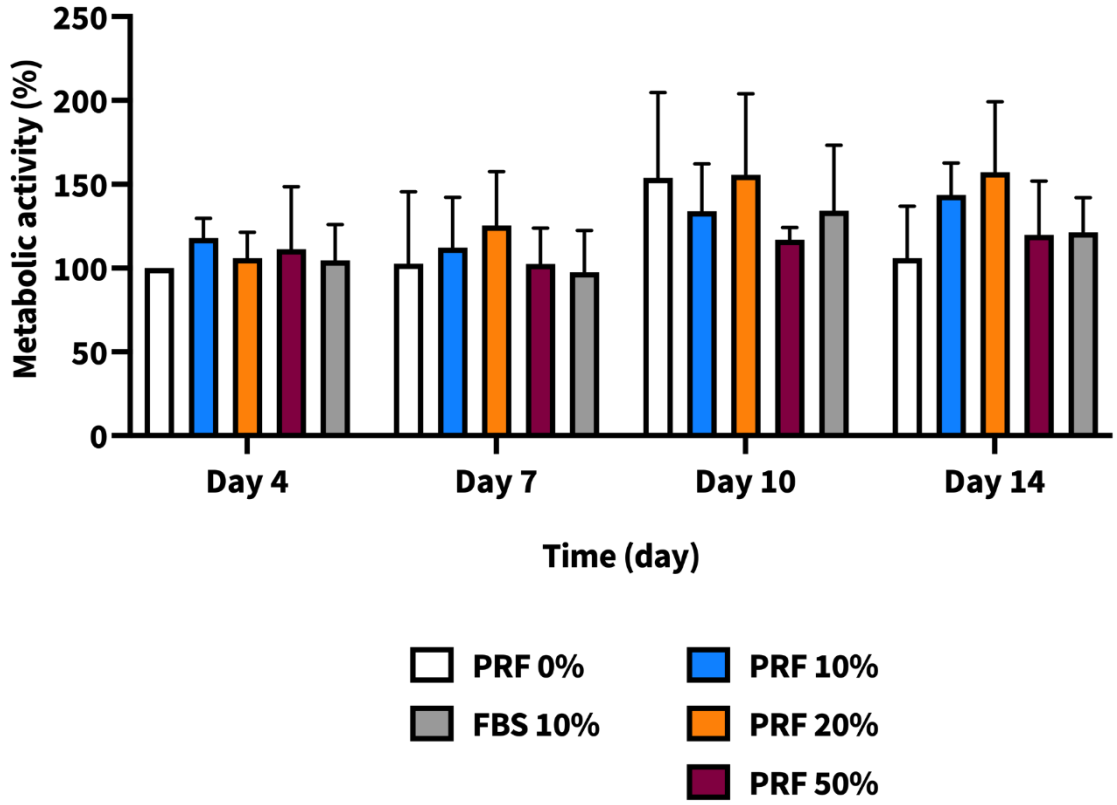

Figure 5.22 | ***Metabolic activity of tissue-engineered oral mucosa (TEOM) in the presence of I-PRF-derived conditioned medium over 14 days***. *TEOM was incubated at an air-liquid interface with different concentrations of I-PRF-derived condition medium for 14 days. Metabolic activity was assessed on days 4, 7, 10, and 14 using the resazurin assay. Data are presented as the mean ± standard deviation from three independent experiments (N=3, n=1). Statistical significance was determined using a one-way ANOVA followed by Dunnett's multiple comparison against the control (PRF 0%) at each time point. Abbreviations: PRF, platelet-rich fibrin; FBS, foetal bovine serum; ANOVA, analysis of variance.*

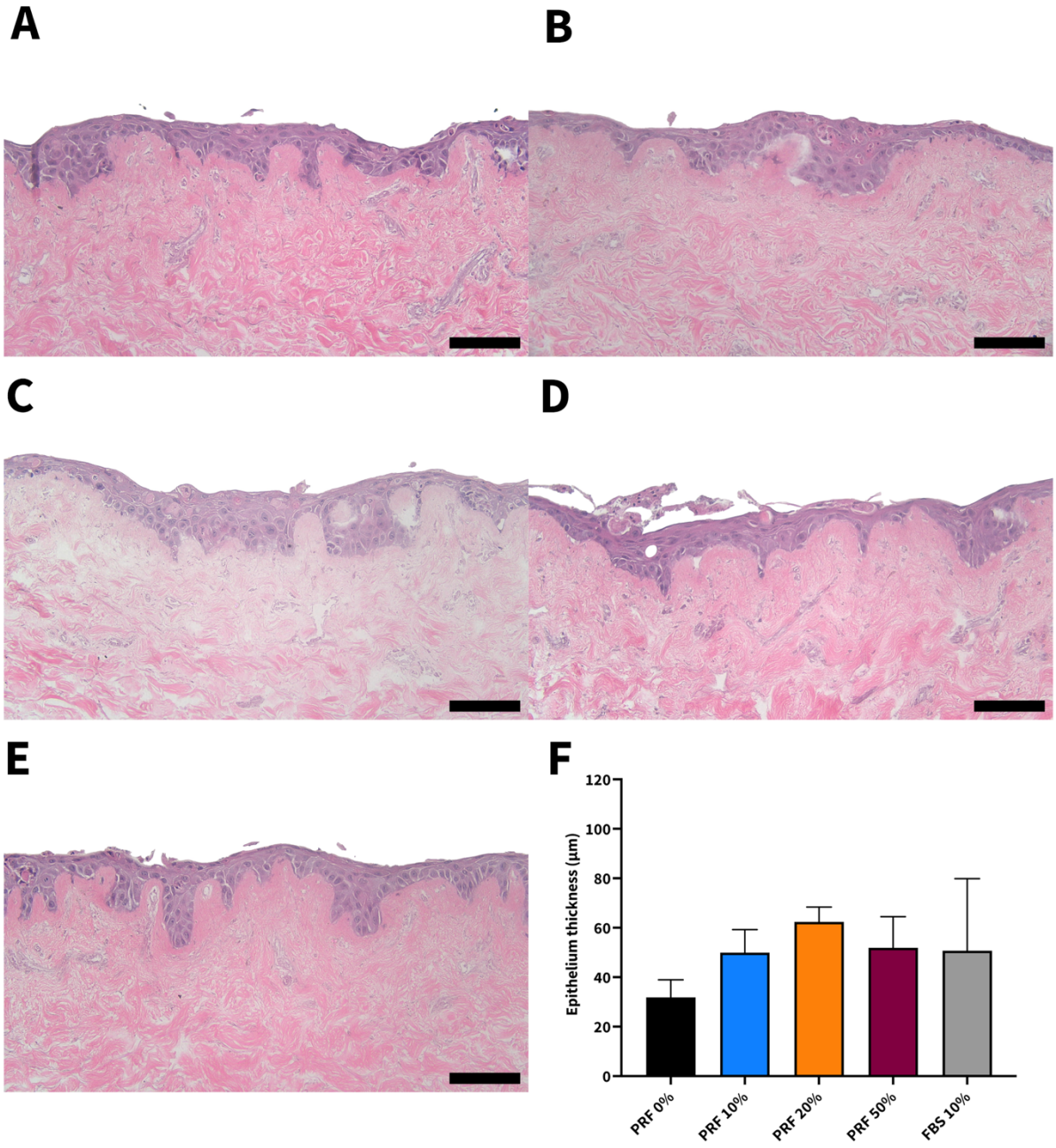

Figure 5.23 | ***H&E-stained sections of tissue-engineered oral mucosa (TEOM) treated with conditioned medium for 4 days.*** *Panels display TEOM sections cultured in conditioned medium containing (A) PRF 0%, (B) PRF 10%, (C) PRF 20%, (D) PRF 50% and (E) FBS 10% for 4 days. (F) demonstrates the epithelium thickness of TEOM after 4 days of culture. Representative images from three independent experiments (N=3, n=1) were used. Scale bar = 100 µm (20x magnification). A one-way ANOVA, followed by Dunnett's multiple comparison was carried out on the data in (F) to test the statistical significance against the control (PRF 0%). Abbreviations: H&E, haematoxylin and eosin; TEOM, tissue-engineered oral mucosa; PRF, platelet-rich fibrin; FBS, foetal bovine serum; ANOVA, analysis of variance.*

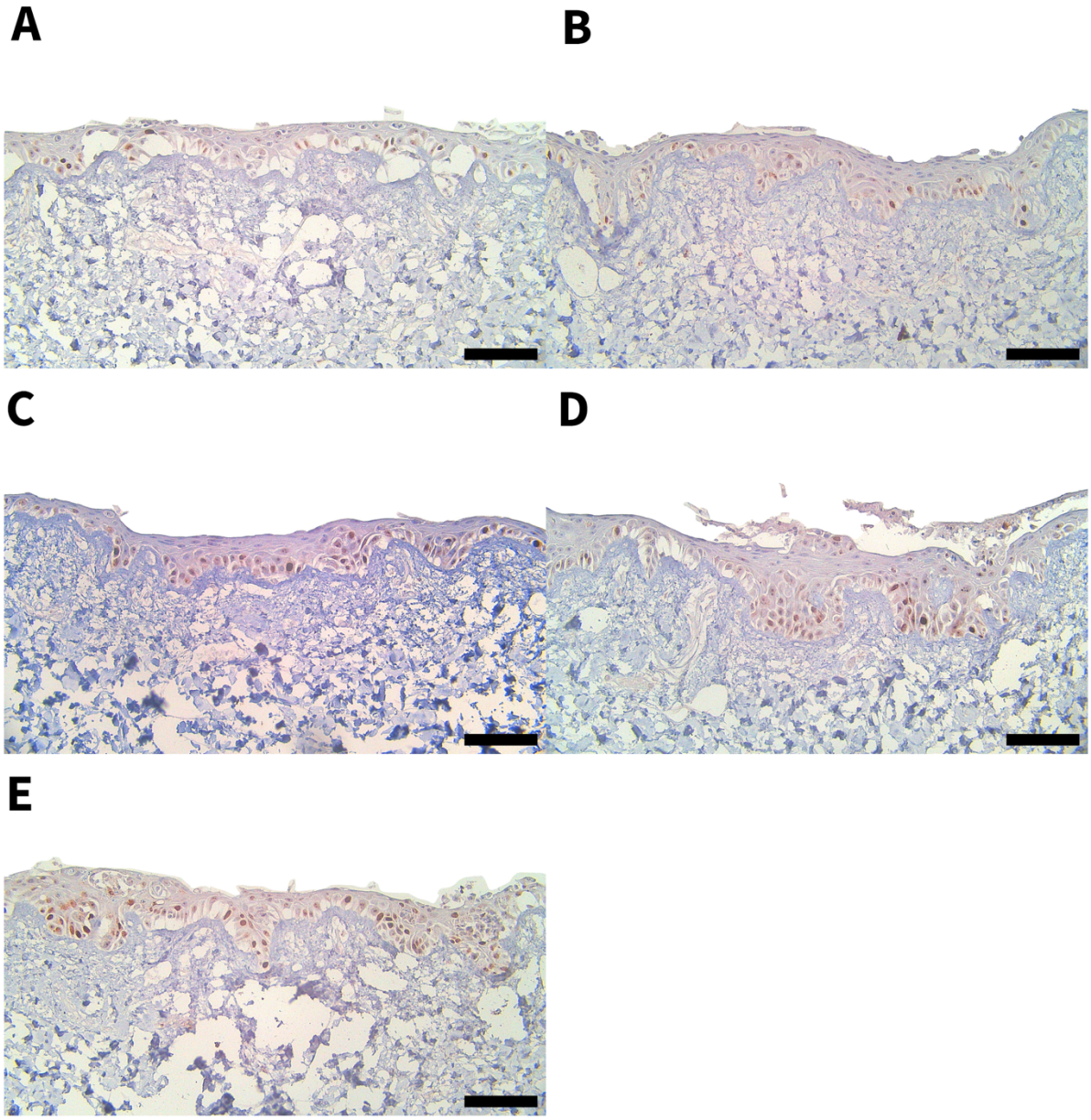

Figure 5.24 | ***Immunohistochemistry staining for Ki-67 in tissue-engineered oral mucosa (TEOM) treated with conditioned medium for 4 days.*** *Panels display TEOM sections cultured in conditioned medium containing (A) PRF 0%, (B) PRF 10%, (C) PRF 20%, (D) PRF 50% and (E) FBS 10% for 4 days, followed by staining with a Ki-67 antibody and DAB. Representative images from three independent experiments (N=3, n=1) were used. Scale bar = 100 µm (20x magnification). Abbreviations: TEOM, tissue-engineered oral mucosa; PRF, platelet-rich fibrin; FBS, foetal bovine serum; DAB, diaminobenzidine.*

Figure 5.25A – E shows the H&E-stained sections of TEOM after 7 days of culture with different concentrations of I-PRF-derived conditioned medium. Again, histological analysis revealed a similar morphology of the epithelium across all conditions. A healthy and well-formed epithelium with multiple layers of keratinocytes was observed. Some notable changes were detected in the PRF 50%- and FBS 10%-treated TEOM, as there were more flattened keratinocytes at the suprabasal and superficial layers of the epithelium compared to day 4 results. PRF 50% and FBS 10% conditions demonstrated the thickest epithelium among all conditions on day 7 of culture, as shown in Figure 5.25F. However, there was no significant difference in epithelial thickness between the I-PRF-treated conditions and the control.

In Figure 5.26, Ki-67-stained sections are presented. Our results showed the Ki-67 positive cells were strictly observed at the basal region of the epithelium in both control and all I-PRF-treated conditions. However, Ki-67 positive cells were also found at the lower suprabasal layer in some areas of the FBS 10%-treated TEOM. No notable difference was observed in Ki-67 expression between conditions.

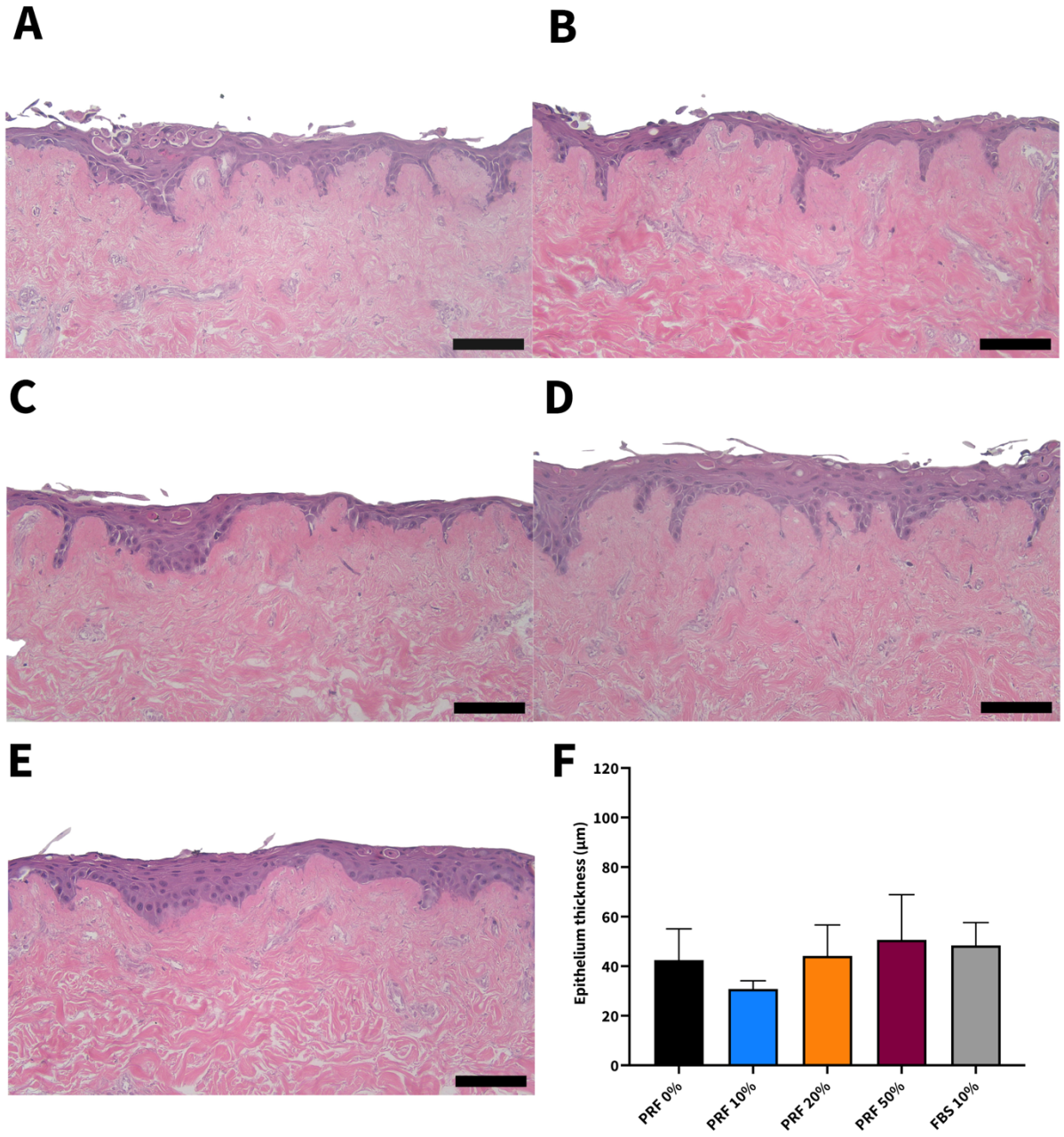

Figure 5.25 | ***H&E-stained sections of tissue-engineered oral mucosa (TEOM) treated with conditioned medium for 7 days.*** *Panels display TEOM sections cultured in conditioned medium containing (A) PRF 0%, (B) PRF 10%, (C) PRF 20%, (D) PRF 50% and (E) FBS 10% for 7 days. (F) demonstrates the epithelium thickness of TEOM after 4 days of culture. Representative images from three independent experiments (N=3, n=1) were used. Scale bar = 100 µm (20x magnification). A one-way ANOVA followed by Dunnett's multiple comparison was carried out on the data in (F) to test the statistical significance against the control (PRF 0%). Abbreviations: H&E, haematoxylin and eosin; TEOM, tissue-engineered oral mucosa; PRF, platelet-rich fibrin; FBS, foetal bovine serum; ANOVA, analysis of variance.*

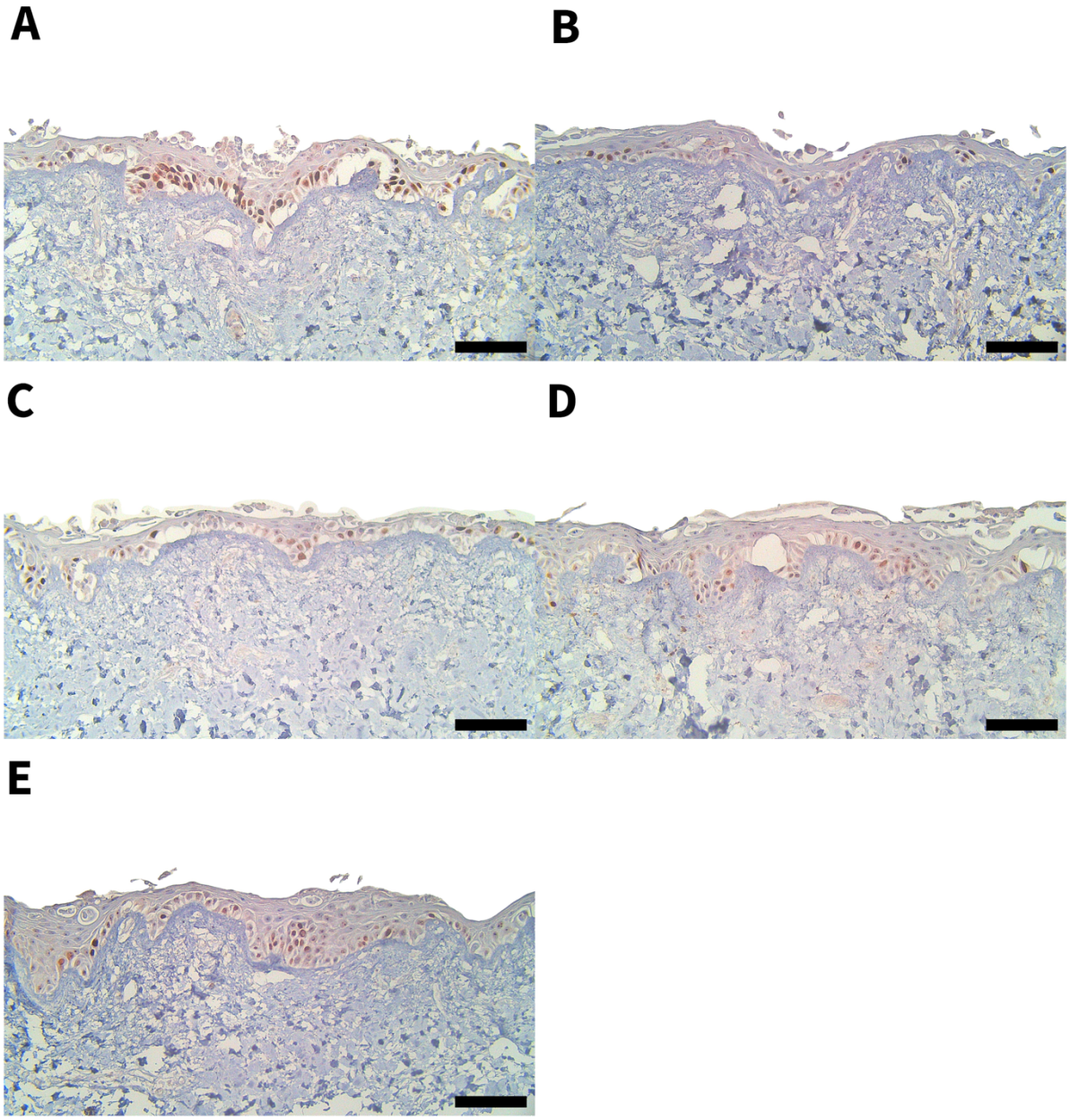

Figure 5.26 | ***Immunohistochemistry staining for Ki-67 in tissue-engineered oral mucosa (TEOM) treated with conditioned medium for 7 days.*** *Panels display TEOM sections cultured in conditioned medium containing (A) PRF 0%, (B) PRF 10%, (C) PRF 20%, (D) PRF 50% and (E) FBS 10% for 7 days, followed by staining with a Ki-67 antibody and DAB. Representative images from three independent experiments (N=3, n=1) were used. Scale bar = 100 µm (20x magnification). Abbreviations: TEOM, tissue-engineered oral mucosa; PRF, platelet-rich fibrin; FBS, foetal bovine serum; DAB, diaminobenzidine.*

Figure 5.27A demonstrates the stratified squamous epithelium of the control TEOM after 10 days in culture. A slightly thinner epithelium was observed in TEOM treated with 10%, 20% or 50% I-PRF-derived conditioned medium when compared to the control (Figure 5.29B – 5.29D), while the epithelium morphology of TEOM treated with FBS 10% was similar to the control (PRF 0%). This observation correlates with the thickness measurement shown in Figure 5.27F. A dose-dependent increase in thickness was observed in TEOM treated with I-PRF-derived conditioned medium. However, only TEOM treated with FBS 10% and PRF 50% showed comparable thickness to the control model.

The immunostaining of Ki67 was similar across all conditions, as shown in Figure 5.28. All Ki-67 positive cells were located at the basal layer of the epithelium. No remarkable difference was observed between any conditions.

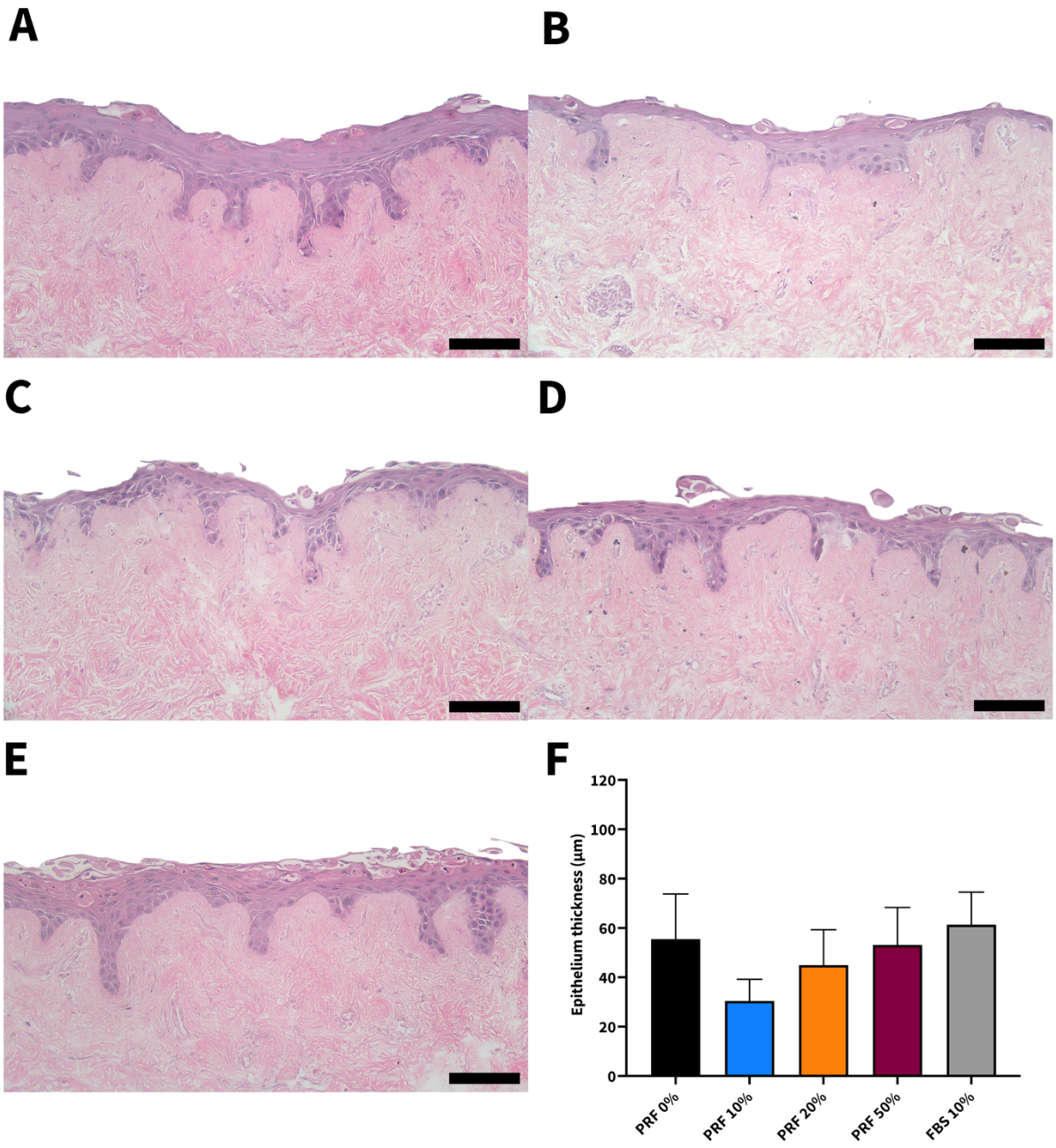

Figure 5.27 | ***H&E-stained sections of tissue-engineered oral mucosa (TEOM) treated with conditioned medium for 10 days.*** *Panels display TEOM sections cultured in conditioned medium containing (A) PRF 0%, (B) PRF 10%, (C) PRF 20%, (D) PRF 50% and (E) FBS 10% for 10 days. (F) demonstrates the epithelium thickness of TEOM after 4 days of culture. Representative images from three independent experiments (N=3, n=1) were used. Scale bar = 100 µm (20x magnification). A one-way ANOVA followed by Dunnett's multiple comparison was carried out on the data in (F) to test the statistical significance against the control (PRF 0%). Abbreviations: H&E, haematoxylin and eosin; TEOM, tissue-engineered oral mucosa; PRF, platelet-rich fibrin; FBS, foetal bovine serum; ANOVA, analysis of variance.*

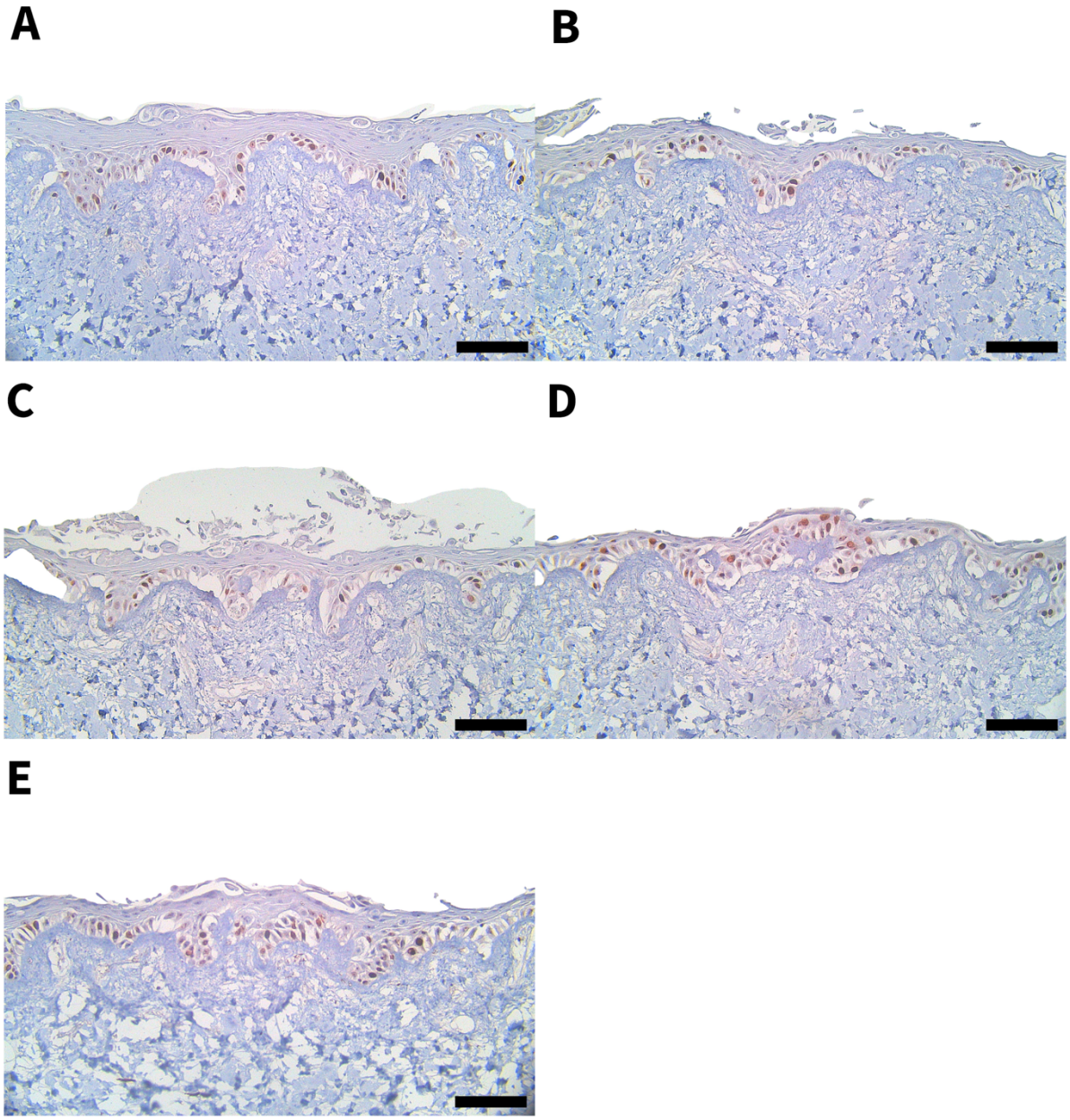

Figure 5.28 | ***Immunohistochemistry staining for Ki-67 in tissue-engineered oral mucosa (TEOM) treated with conditioned medium for 10 days.*** *Panels display TEOM sections cultured in conditioned medium containing (A) PRF 0%, (B) PRF 10%, (C) PRF 20%, (D) PRF 50%, and (E) FBS 10% for 10 days followed by staining with a Ki-67 antibody and DAB. Representative images from three independent experiments (N=3, n=1) were used. Scale bar = 100 µm (20x magnification). Abbreviations: TEOM, tissue-engineered oral mucosa; PRF, platelet-rich fibrin; FBS, foetal bovine serum; DAB, diaminobenzidine.*

On day 14, the epithelium morphology was quite similar across all conditions. The control TEOM showed a multi-layer of stratified squamous keratinocytes (Figure 5.29A). The basal cells retained their cuboidal shape, as observed during earlier time points. TEOM treated with any concentrations of I-PRF-derived conditioned medium or FBS 10% still presented with cuboidal keratinocyte at the basal layer of the epithelium (Figure 5.29B – E). Figure 5.29F demonstrates the epithelium thickness of TEOM treated with different conditioned medium for 14 days. The control TEOM demonstrated the thickest epithelium with a large variability observed. There was no statistical significance between any I-PRF-treated conditions compared to the control.

Again, all conditions demonstrated Ki-67 positive cells were limited to the keratinocytes above the basement membrane of TEOM, as shown in Figure 5.30.

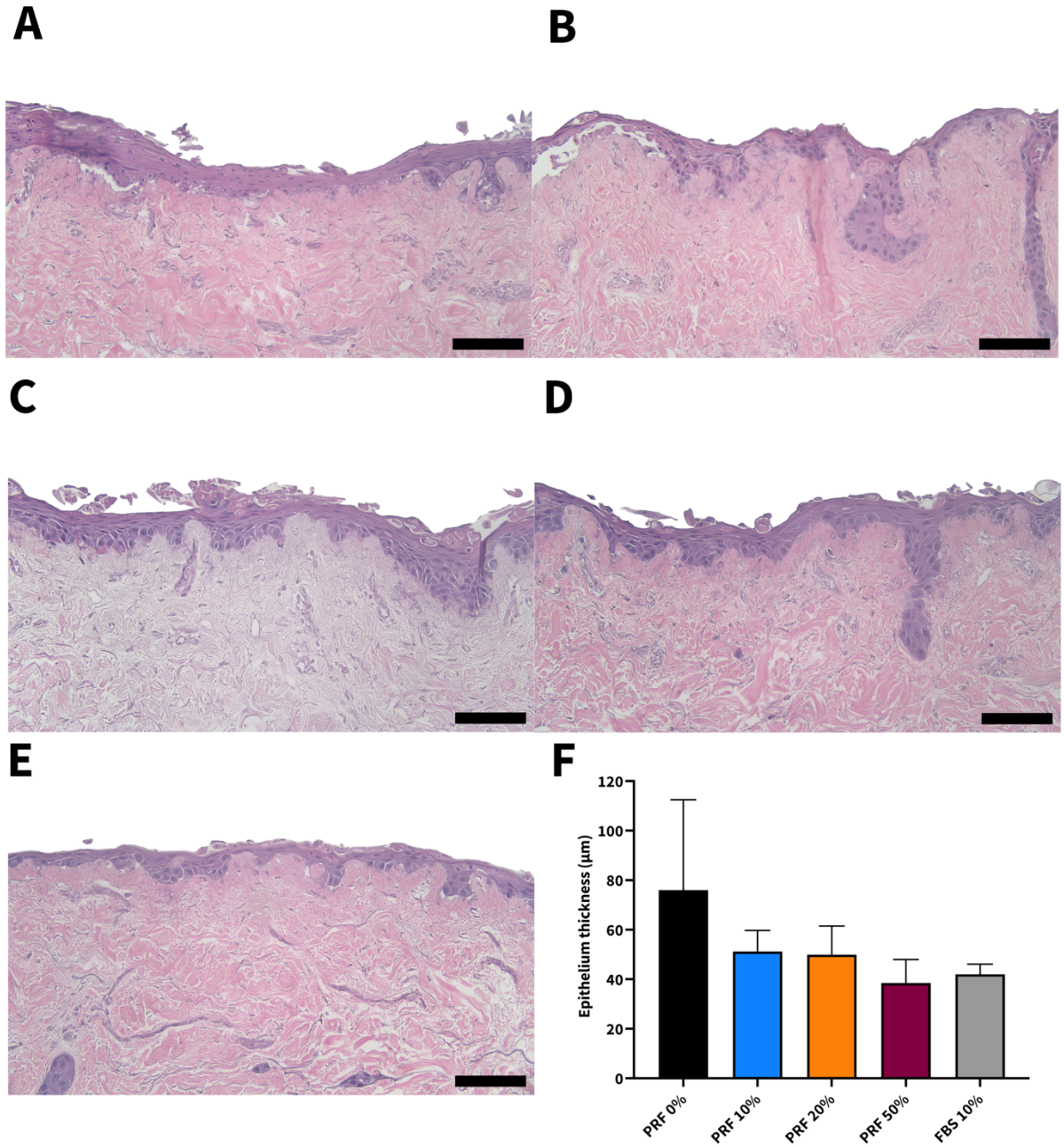

Figure 5.29 | ***H&E-stained sections of tissue-engineered oral mucosa (TEOM) treated with conditioned medium for 14 days.*** *Panels display TEOM sections cultured in conditioned medium containing (A) PRF 0%, (B) PRF 10%, (C) PRF 20%, (D) PRF 50% and (E) FBS 10% for 14 days. (F) demonstrates the epithelium thickness of TEOM after 4 days of culture. Representative images from three independent experiments (N=3, n=1) were used. Scale bar = 100 µm (20x magnification). A one-way ANOVA followed by Dunnett's multiple comparison was carried out on the data in (F) to test the statistical significance against the control (PRF 0%). Abbreviations: H&E, haematoxylin and eosin; TEOM, tissue-engineered oral mucosa; PRF, platelet-rich fibrin; FBS, foetal bovine serum; ANOVA, analysis of variance.*

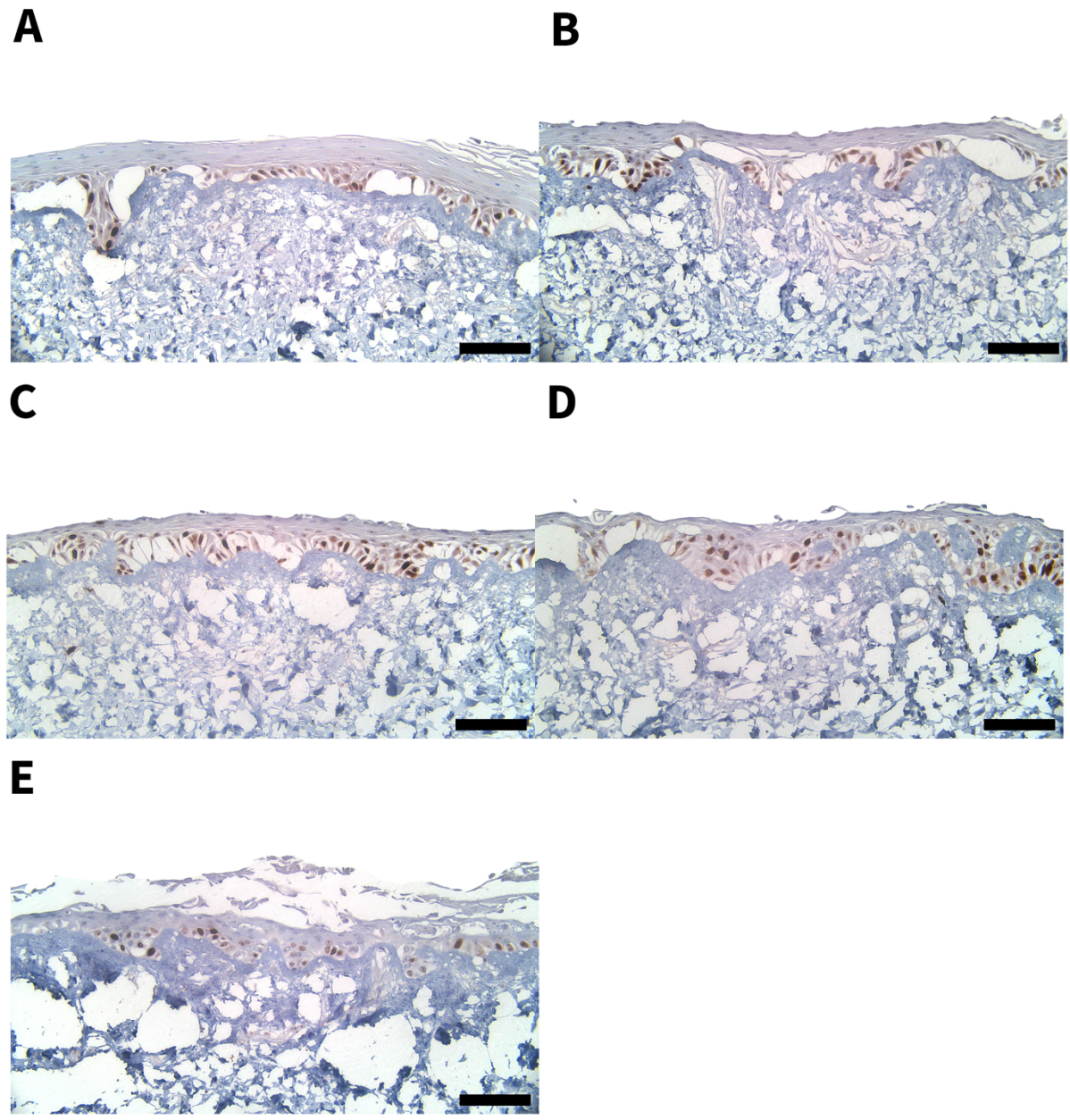

Figure 5.30 | ***Immunohistochemistry staining for Ki-67 in tissue-engineered oral mucosa (TEOM) treated with conditioned medium for 14 days.*** *Panels display TEOM sections cultured in conditioned medium containing (A) PRF 0%, (B) PRF 10%, (C) PRF 20%, (D) PRF 50% and (E) FBS 10% for 14 days followed by staining with a Ki-67 antibody and DAB. Representative images from three independent experiments (N=3, n=1) were used. Scale bar = 100 µm (20x magnification). Abbreviations: TEOM, tissue-engineered oral mucosa; PRF, platelet-rich fibrin; FBS, foetal bovine serum; DAB, diaminobenzidine.*

5.4.8 I-PRF maintained the integrity and thickness of established epithelium of TEOM

To evaluate whether I-PRF could maintain the integrity of oral epithelium, TEOM was constructed and cultured in Green's medium at ALI for 7 days to allow the epithelium to stratify. After 1 week, the medium was replaced by different concentrations of I-PRF-derived conditioned medium and the models were cultured for a further 7 days (Section 5.3.14). Figure 5.31 illustrates the metabolic activity of TEOM after incubating with I-PRF-derived conditioned medium. We found that I-PRF had no effect on the metabolic activity of TEOM on day 10 or day 14.

Histological analysis revealed that the epithelium morphology remained unaffected by I-PRF treatment. A multi-layered stratified squamous epithelium was shown in all tested conditions (Figure 5.32A – E). Although there was a slight increase in epithelium thickness with all concentrations of I-PRF-derived conditioned medium (Figure 5.32F), no statistical significance was detected when comparing any PRF-treated conditions with the control.

Similar trends in outcomes were observed on day 14. All tested conditions produced multi-layered keratinocytes with cuboidal-shaped cells located at the basal layer, with more superficial cells starting to differentiate and flatten (Figure 5.33A – E). There was an increase in epithelial thickness from all conditions, indicating the growth of epithelium, shown in Figure 5.33F. No significant difference was observed between any conditions.

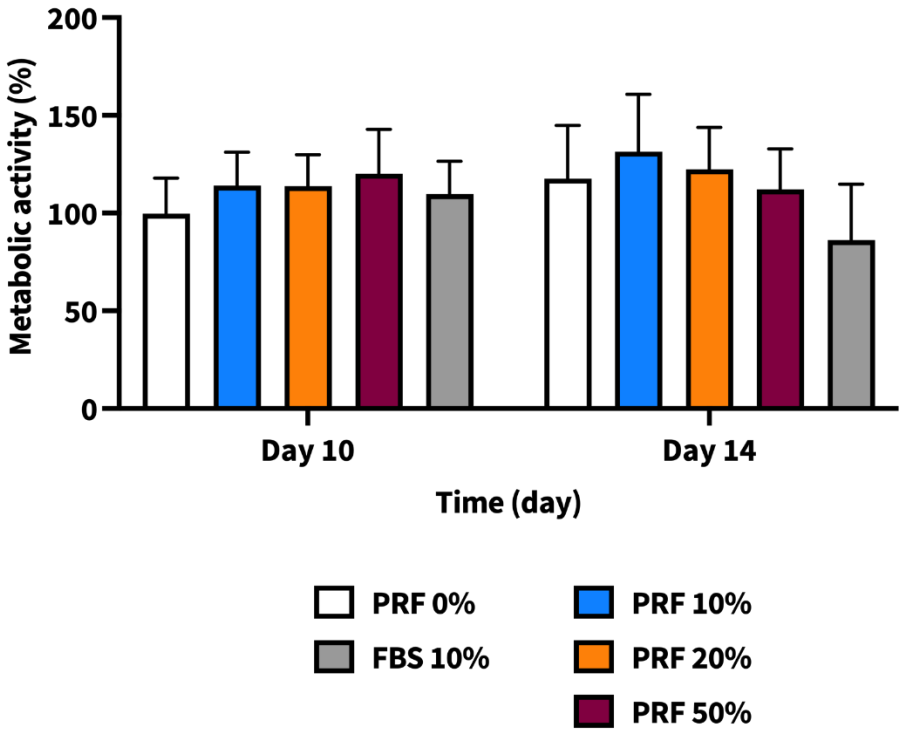

Figure 5.31 | ***Metabolic activity of tissue-engineered oral mucosa (TEOM) when treated with Green's medium for 7 days, followed by I-PRF-derived conditioned medium for a further 7 days.*** *TEOM was incubated with Green's medium at an air-liquid interface for 7 days, then cultured with varying concentrations of I-PRF-derived condition medium for an additional 7 days (total of 14 days). Metabolic activity was assessed on days 10, and 14 using the resazurin assay. Data are presented as the mean ± standard deviation from three independent experiments (N=3, n=1). Statistical significance was determined using a one-way ANOVA followed by Dunnett's multiple comparison against the control (PRF 0%) at each time point. Abbreviations: TEOM, tissue-engineered oral mucosa; PRF, platelet-rich fibrin; FBS, foetal bovine serum; ANOVA, analysis of variance.*

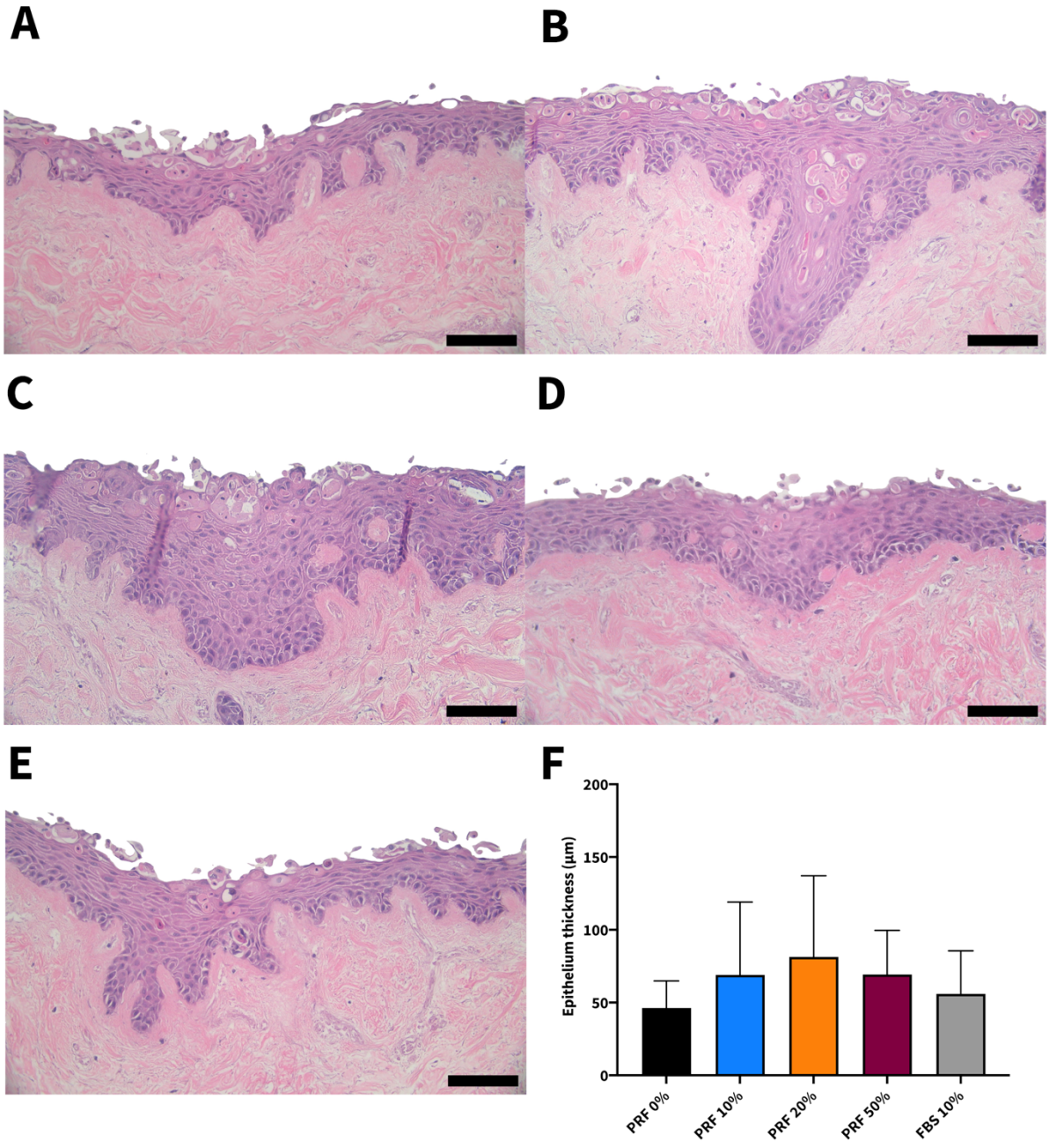

***Figure 5.32* | H&E-stained sections of tissue-engineered oral mucosa (TEOM) treated with Green's medium for 7 days, followed by I-PRF-derived conditioned medium for a further 3 days.** *Panels display TEOM sections cultured in Green's medium at an air-liquid interface for 7 days, then cultured with I-PRF-derived condition medium containing (A) PRF 0%, (B) PRF 10%, (C) PRF 20%, (D) PRF 50% and (E) FBS 10% for an additional 3 days (total of 10 days). (F) demonstrates the epithelium thickness of TEOM after 10 days of culture. Representative images from three independent experiments (N=3, n=1) were used. Scale bar = 100 µm (20x magnification). A one-way ANOVA followed by Dunnett's multiple comparison was carried out on the data in (F) to test the statistical significance against the control (PRF 0%). Abbreviations: H&E, haematoxylin and eosin; TEOM, tissue-engineered oral mucosa; PRF, platelet-rich fibrin; FBS, foetal bovine serum; ANOVA- analysis of variance.*

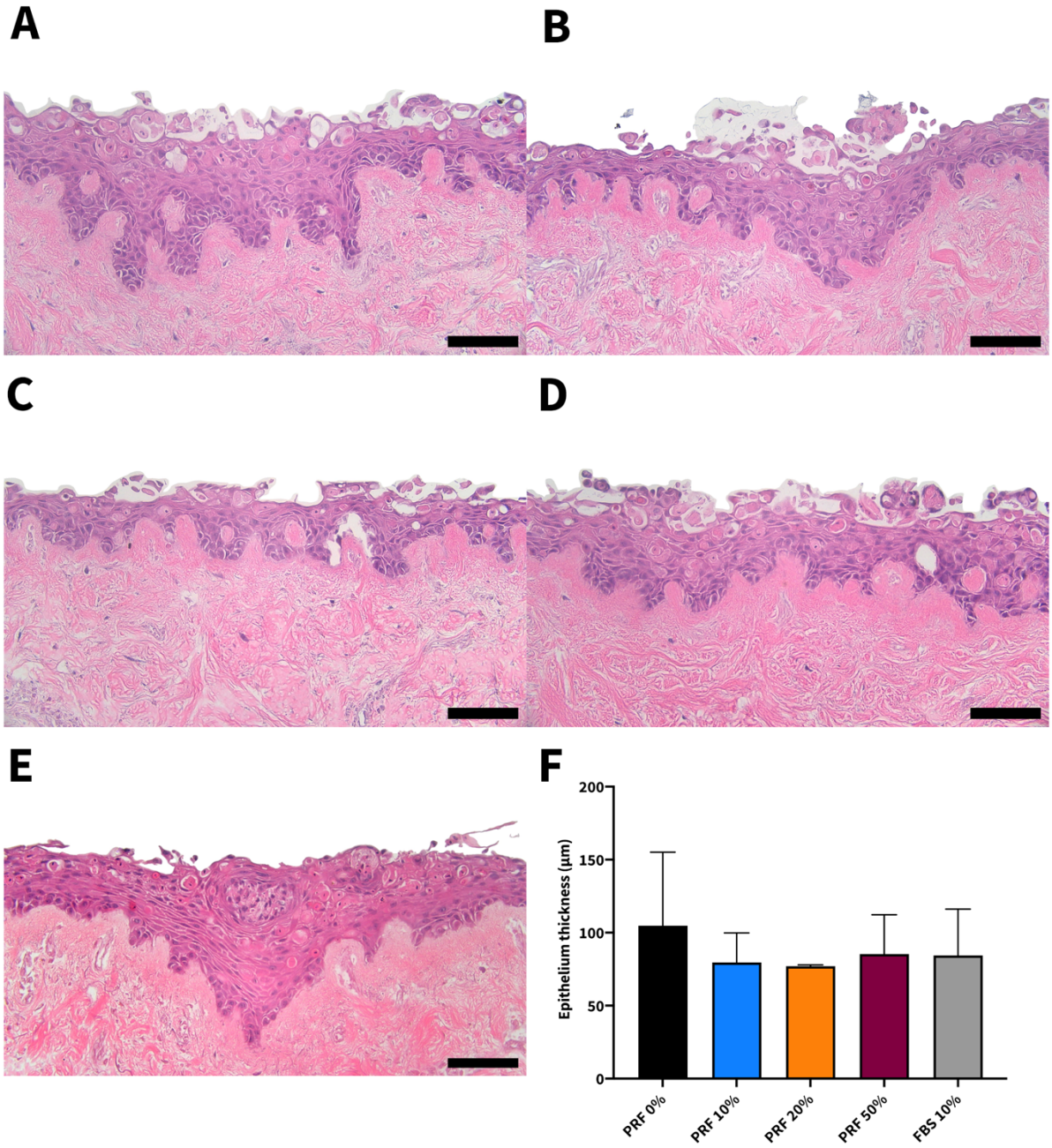

Figure 5.33 | H&E-stained sections of tissue-engineered oral mucosa (TEOM) treated with Green's medium for 7 days, followed by I-PRF-derived conditioned medium for a further 7 days. *Panels display TEOM sections cultured in Green's medium at an air-liquid interface for 7 days, then cultured with I-PRF-derived condition medium containing (A) PRF 0%, (B) PRF 10%, (C) PRF 20%, (D) PRF 50% and (E) FBS 10% for an additional 7 days (total of 14 days). (F) demonstrates the epithelium thickness of TEOM after 10 days of culture. Representative images from three independent experiments (N=3, n=1) were used. Scale bar = 100 µm (20x magnification). A one-way ANOVA followed by Dunnett's multiple comparison was carried out on the data in (F) to test the statistical significance against the control (PRF 0%). Abbreviations: H&E, haematoxylin and eosin; TEOM, tissue-engineered oral mucosa; PRF, platelet-rich fibrin; FBS, foetal bovine serum; ANOVA, analysis of variance.*

5.4.9 I-PRF enhanced the migration and infiltration into a wounded area of TEOM

To investigate the potential of I-PRF in improving wound healing, TEOM with established epithelium were constructed and wounded using a 4mm punch biopsy (Section 5.3.15). Wounded TEOM was then cultured in I-PRF-derived conditioned medium at ALI for a further 10 days.

Figure 5.34A illustrates the histological morphology of TEOM immediately after wounding. Both the epithelium and connective tissue layer were damaged. By day 10, an ingrowth of the epithelium was observed in all conditions including the control (Figure 5.34B). TEOM-treated with the conditioned medium containing either FBS 10% or PRF 20% showed an increase in cell infiltration into the wounded region, as shown in Figure 5.34C and 5.34D.

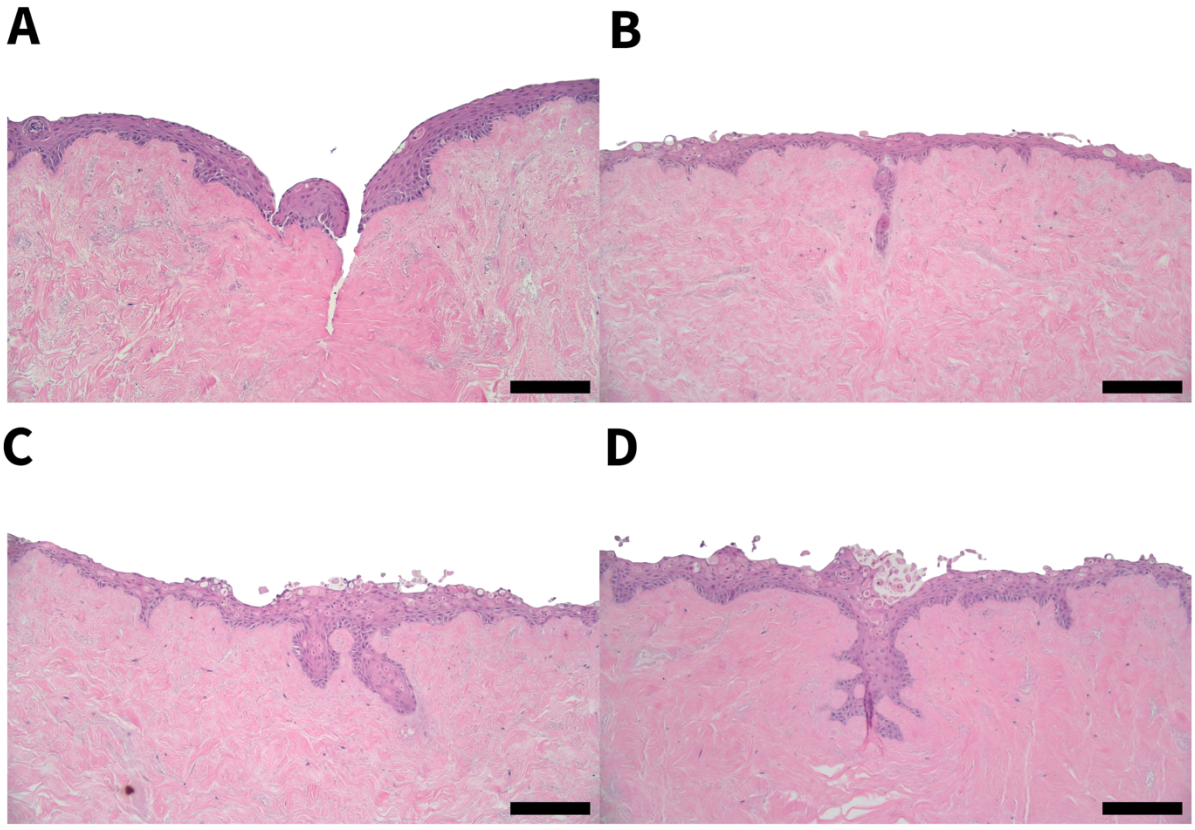

Figure 5.34 | ***H&E-stained sections of wounded tissue-engineered oral mucosa (TEOM).*** *Panel (A) displays H&E-stained sections of TEOM-treated with Green's medium for 7 days and being wounded with a 4 mm punch biopsy. Wounded models were treated with conditioned medium containing (B) PRF 0%, (C) FBS 10% and (D) PRF 20%, and cultured for a further 10 days (total of 17 days) at an air-liquid interface. Representative images were used. Scale bar = 200 µm (10x magnification). Abbreviations: H&E, haematoxylin and eosin; TEOM, tissue-engineered oral mucosa; PRF, platelet-rich fibrin; FBS, foetal bovine serum.*

5.5 Discussion

This part of the study investigated the biological composition of I-PRF and how I-PRF affects the behaviour of oral mucosa cells and TEOM. Currently, there is a growing number of clinical studies with promising outcomes utilising I-PRF for both hard and soft tissue regeneration [294]. However, there is limited *in vitro* evidence to describe the mechanistic regulation of I-PRF on oral soft tissue repair. Here, we successfully prepared I-PRF and demonstrated the expression of cytokines released from I-PRF. Our *in vitro* data demonstrated some improvements in oral wound healing through a combination of both 2D and 3D cell assays. Our results suggest that I-PRF can enhance oral mucosa cell proliferation and migration through its paracrine effects of platelet-derived mediators.

The biological impacts of I-PRF on oral keratinocytes and fibroblasts were examined, given their pivotal roles as two key cellular components of the oral mucosa during the healing process. To the best of our knowledge, this is the first demonstration of how I-PRF affects the behaviour of oral keratinocytes. Our results showed that I-PRF did not produce any toxicity on either cell type, as confirmed by cellular metabolism and viability assays. These findings are in line with previous studies that reported no significant effect on fibroblast viability with I-PRF treatment. [274], [275], [278], [285].

Our approach in assessing cell viability differs from other studies. While previous studies used Calcein-AM with propidium iodide (PI), known as live-dead staining assay, we used Annexin V-FITC with PI, which allows apoptosis and necrosis detection. Both techniques provide essential information and can differentiate between viable and dead cells, thereby indicating the biocompatibility of I-PRF on oral mucosa cells.

We observed a slight increase of the metabolic activity of both oral fibroblasts and keratinocytes when treated with higher concentrations of I-PRF. It is also worth noting that all previous studies have only examined one concentration (20%) of conditioned medium derived from I-PRF. Here, we have examined a wider range of concentrations from 1% to 50%. While we aimed to include 100% I-PRF concentration to mimic clinical scenarios, the limited supply of I-PRF available prevented us from performing these experiments. Based on our results, we decided to choose three concentrations of I-PRF-derived conditioned medium (10%, 20% and 50%) for further experiments.

The migration and proliferation of oral keratinocytes and fibroblasts play pivotal roles in the wound healing process [38]. Both cell types are required to migrate across the wounded area before proliferating to facilitate the repair of the oral mucosa. Wound healing is a complex process controlled by a mixture of cytokines and growth factors [37], making it challenging to pinpoint which factors take the primary control. Delayed healing in chronic wounds has been linked to an insufficient amount of growth factors such as PDGF, EGF, TGF-β, VEGF, and bFGF [37]. I-PRF comprises a mixture of cytokines and bioactive factors at a supraphysiological level [274], therefore, we hypothesised that I-PRF might enhance cell proliferation by supplementing these bioactive factors that are depleted in wounds.

Here, we found that I-PRF markedly increased the proliferation of both cell types, with a statistical significance observed on I-PRF-treated fibroblasts. Our findings are consistent with earlier studies that also reported an increase of fibroblast proliferation after I-PRF treatment compared to the non-PRF treatment [274], [278], [285], [286]. It is also worth noting that different centrifugation systems (i.e., speed, time, and type of centrifuge) were used in each study. This suggests that the impact of I-PRF on oral mucosa cell proliferation remains unaffected by the preparation protocol.

Interestingly, a variety of assays such as MTS, MTT, WST-1 and CellTiter-Glo® have been used in PRF studies to determine the cell proliferation. It is important to emphasise that these methods, all in fact, assessed the metabolic activity rather than directly measuring cell proliferation. They rely on enzyme activity to convert the substrate into coloured formazan products, or quantify the amount of ATP molecules, which represent metabolically active cells [315]. These assays may not accurately reflect an increase in cell number or cell proliferation. The metabolic activity can be altered by various factors such as stress, stimuli, injury, or chemical toxicity, thereby producing false-positive outcomes. Our study used the CFSE staining method which distinguishes between undivided and divided cell populations based on changes in fluorescence intensity. A decrease in fluorescence intensity indicates cellular expansion or proliferation [316]. This method provides a more direct and representative measurement of cell proliferation. Thereby, our data suggest a promising positive effect of I-PRF on cell proliferation.

We proceeded to explore how I-PRF affected cell migration as part of wound closure. A variety of techniques to determine cell migration have been used in various PRF studies,

with the transwell assay being the most commonly used method. This assay assesses the migration ability of cells in response to a chemoattractant through the pores of transwell inserts [317]. It, however, has some challenges in obtaining precise outcomes because only a limited number of cells can cross a filter membrane. Using this method, it is also difficult to continuously monitor the cells throughout the experiment since the migrated cells have to be fixed before being observed under the microscope [317]. In our study, we used the cell exclusion zone method using an Oris™ stopper. This stopper generates a physical barrier that creates a well-defined circular cell-free area, mimicking the clinical wound. This approach offers more informative and real-time data in terms of cell morphology and migration behaviours, which is suitable for demonstrating the effect of I-PRF on oral mucosa migration.

Another interesting point to be addressed is that previous studies have not controlled for proliferation, which can occur simultaneously with migration during the healing process. To ensure that only the effects of cell migration were measured, we used Mitomycin C to inhibit cell proliferation. Mitomycin C has been shown to have an inhibitory effect on cell growth and has been used as a chemotherapeutic agent for breast cancers [318]. Use of this chemical allows us to obtain more accurate data on the migratory responses of oral mucosa cells since the proliferation was controlled.

Our results demonstrated that all concentrations of I-PRF, as well as the FBS control, resulted in a higher percentage of gap closure, indicative of increased migration of oral keratinocytes and fibroblasts compared to PRF 0%. This indicates the importance of serum (including growth factors) on cell migration. These findings are consistent with previous studies that have shown the beneficial effects of PRF treatments, not only I-PRF but also other formulations, on the migration of fibroblasts [252], [274], [278], [283], [284] , suggesting the potential role of PRF on enhancing cell migration.

Although our results in 2D culture have already demonstrated the potential therapeutic effects of I-PRF on oral mucosa cells, it is crucial to further evaluate the bioactivity in a more clinically representative model. This is because the behaviour and responses of cells in the 3D *in vitro* system may differ from those observed from the 2D culture.

Newly formed epithelium and established epithelium were evaluated since both types of epithelia are involved in the healing of wounds. To the best of our knowledge, this is the first investigation of the effect of I-PRF on 3D models of the oral mucosa. We demonstrated that I-PRF treatment had no significant effect on the metabolic activity of the TEOM on the appearance of either of these epithelia. The finding is correlated with our previously shown 2D results, where oral mucosa cells were examined separately. Different methods were used to measure the metabolic activity between two experiments. For the 3D culture, resazurin was chosen as it allows further testing to be carried out in contrast to MTT, which is an end-point assay [315], thus making subsequent histological analysis of the 3D models possible.

We further investigated whether PRF affects the histological appearance of TEOM. Surprisingly, our observations revealed that the morphology of the epithelium was quite similar across all conditions, including the control TEOM (PRF 0%), at every time point. This outcome was unexpected, as we hypothesised that the absence of supplemented serum in the media would limit epithelial growth. However, our findings align with a study conducted by Izumi *et al.*, who successfully constructed TEOM models using serum-free culture medium without a feeder layer. They suggested that the removal of serum components might lead to an increase the number of undifferentiated keratinocytes which allow cells to continue proliferating [80]. This could explain why the control TEOM still produced the multi-layered structure of epithelium as in other conditions.

Interestingly, the behaviour of oral mucosa in both 2D and 3D cultures displayed similarities when treated with the conditioned medium containing either I-PRF or FBS 10%. FBS is a well-known supplement used for *in vitro* cell cultivation [319]. Both I-PRF and FBS are produced from blood by-products and offer comparable characteristics by supplying essential elements for cell growth and maintenance such as serum proteins, growth factors and cytokines [319]. Contrarily to our findings, previous studies conducted by Kawase *et al.*, and Grawish *et al.*, suggested that PRF offered superior benefits over FBS on the growth of periosteal sheets and human dental pulp stem cells, respectively [320], [321]. The differences between our work and the existing literature may be affected by variations in the sources, batches, or preparations of PRF and FBS used across studies. Additionally, intrinsic cellular responses between each type of cells to either I-PRF or FBS could

contribute to the different outcomes. While it remains unclear which is more effective, I-PRF appears to be a more suitable option for human applications. This is because the use of FBS raises concerns about the potential for contaminants such as viruses, endotoxins, fungi or bacteria [319]. Furthermore, FBS is derived from a xenogeneic source which could have risks from immunogenic reactions [321] compared to the autologous origin of I-PRF.

To gain more understanding of the influence of PRF on epithelium integrity, we performed a quantitative assessment of the epithelial layer thickness. This analysis also allowed us to observe any potential differences in the growth pattern during the formation process. Our results showed no statistically significant differences in the epithelium thickness between any conditions. We observed a slight increase of epithelium thickness of TEOM treated with I-PRF compared to the control model on day 4. In contrast, a slightly thicker epithelium was found the control TEOM compared to the I-PRF-treated conditions at later time points.

Correspondingly to our *in vitro* data, a randomised controlled study was conducted by Albatal *et al.*, who investigated the healing of palatal wound after the subepithelial connective tissue graft was harvested. They observed that patients receiving I-PRF exhibited thicker palatal tissues compared to the groups without I-PRF during the first and second months after surgery while no difference was found during a 3-month follow up [322]. Multiple studies in the literature also reported significant enhancement with L-PRF in soft tissue healing after tooth extraction within the first week in comparison to the spontaneous healing of the non-PRF group [323]–[325].

Based on our findings and evidence shown here, it appears that the addition of I-PRF, which contains containing high quantities of cytokines, might enhance epithelium formation during the initial days of the healing process. This finding suggests potential clinical implications, as a rapidly established intact epithelial barrier could better protect the healing wounds from infection or inflammation which could disrupt the healing process.

Considering the increased epithelium thickness observed at the early time point, we hypothesised that the thicker epithelium may be a result of the stimulation of both migration and proliferation of oral mucosa cells as demonstrated in our 2D results. Unlike the healing in a clinical situation, our models lack the presence of a wound edge, which

makes it challenging to examine the effect of I-PRF on the migration of keratinocytes during the formation process. However, investigations on cell proliferation and stratification following lifting of models to ALI are still possible. Therefore, we decided to investigate whether I-PRF enhances the proliferation of epithelial cells by performing immunohistochemistry staining of Ki-67, a marker of actively proliferating cells.

Our results showed that there were more Ki-67 positive cells present in TEOM treated with the medium conditioned with I-PRF compared to the control during an early stage of epithelium formation (day 4), however this effect was not observed at the later time points. In addition, we also observed that the Ki-67 positive cells were also found at the suprabasal layer. Ki-67 is predominantly found in basal keratinocytes of native oral mucosa as these are the most proliferative keratinocytes in the epithelium [314], observing suprabasal Ki-67 positive cells could indicate that I-PRF induces an increase of proliferating keratinocytes during the development of the epithelium, which could accelerate the healing process.

To enable us to study the effect of I-PRF on wound healing and epithelial migration in our TEOM model, an *in vitro* wound model was constructed using a punch biopsy. We observed cellular ingrowth into the wound area of the TEOM treated with 20% I-PRF-derived conditioned medium, indicating the ability of I-PRF to induce the keratinocyte migration and proliferation in wound healing. Our findings are supported by Nicoletti *et al.*, who investigated the effect of PRP on the healing of wounds in *ex vivo* skin explants. They demonstrated complete epithelialisation of punch biopsy wounds after 10 days of culture in medium conditioned with 2.5% PRP [326]. However, we observed differences in the healing appearance. Our models demonstrated migrating epithelium into the wounded area, while Nicoletti *et al.*, showed the wound edge of the epithelium migrating across the connective tissue layer without any ingrowth. It appears that the wounds created in our work (Figure 5.34A) were deeper into the connective tissue layer (approximately 250 µm from the basal layer of the epithelium) compared to their work (approximately 100 µm). This suggests that the depth of the generated wounds could affect the appearance of wound healing in *in vitro* models.

Following the proliferative phase, wound healing progresses to the remodelling phase, where the epithelium and connective tissue undergo a reorganisation process to achieve complete wound closure. This stage normally occurs a few weeks after the injury and can extend over several months [44]. Thereby, longer culture periods would provide additional insights into how I-PRF affects the final healing stage. However, our *in vitro* model has limitations regarding the culture duration. The experimental protocol requires at least 7 days for the epithelium to stratify. The previous unpublished findings from our group have shown a reduction in metabolic activity and decreased epithelium thickness of the models after 18 days of culture. As a result, the maximum duration we could perform the wounding experiments was limited to 10 days, as we did in this study.

We encountered challenges when identifying trends in the impact of different I-PRF concentrations on the metabolic activity and epithelium thickness in our models, mainly due to variability. This variability may have originated from several factors including the limited quantity of I-PRF and cells available for each experimental setup. We were only able to perform one technical repeat for each experiment, which hindered us from detecting any changes within each replicate. In addition, three biological repeats were carried out from different sources of DED, I-PRF, and cells for construction the oral mucosa models, which also produced a larger variability.

While I-PRF displays some promising effects on the oral wound healing *in vitro*, the overall findings demonstrate a mix of outcomes, not all of which align with previous literature. In particular, the varying preparation protocols could influence the cellular composition and potentially affect the biological effects of I-PRF on oral wound healing. Considering these limitations and the data collected, our results provide some encouraging data to support the use of I-PRF to stimulate the healing process of the oral mucosa but further research is needed.

The method for preparing I-PRF in this work was originally developed by Fujioka-Kobayashi *et al.*, who spun blood at 300 g for 5 minutes using a horizontal centrifuge [278]. While the majority of previous studies used a fixed-angle centrifuge to prepare I-PRF (Table 2.7), Miron *et al.*, showed that a horizontal swing centrifuge produce a higher yield of platelets and leukocytes compared to a fixed-angle system [271]. The horizontal centrifugation method also improves the quality of cell separation and reduces the shear

stress on cells [310]. Given this evidence and the availability of a horizontal swing centrifuge in our laboratory led us to use this preparation method for our I-PRF work.

The cellular characteristics of I-PRF were examined by measuring the amount of platelets and leukocytes, as they play a major role in wound healing and tissue regeneration [44]. Our study revealed that the platelet count in I-PRF was approximately 2.72-fold higher than that in whole blood. This aligned with the definition of platelet concentrates as "autologous blood fractions containing supraphysiological concentrations of platelets" (with an average range for adults is between 150 – 450 x 10^9 platelets/L) [255]. The findings were consistent with a study by Miron *et al.*, which also reported a 2.49-fold increase of platelets in I-PRF compared to whole blood [271].

In terms of leukocytes, our results showed a comparable amount between I-PRF and whole blood, with a slight decrease observed in I-PRF samples. This differs from Miron *et al.*, who reported an increase of around 1.78-fold of leukocytes in I-PRF compared to whole blood [271]. It is worth noting that both studies used the horizontal centrifuge method for preparing I-PRF, but the centrifugation protocols differed. Miron *et al.*, used a lower RCF but longer spinning time (200 g for 8 minutes) compared to our work (300 g for 5 minutes). Previous studies by Wend *et al.*, and Miron *et al.*, compared the effect of RCF on the platelet and leukocyte number, with both showing that I-PRF prepared with lower RCF contained higher numbers of platelets and leukocytes than higher RCF [292], [310]. The results presented here, along with findings from other studies, support that I-PRF preparation using lower RCF results in higher cellular content, which may potentially increase the amount of growth factors and its ability to stimulate the healing of wounds and tissue regeneration.

However, it is important to note that insufficient RCF during the preparation of I-PRF could also lead to inadequate separation of cells, which may result in a lower yield of platelets. This was supported by a slight decrease in platelet count reported in a study by Miron *et al.*, compared to our own results. They suggested that a spinning force of 200 g or lower failed to obtain a suitable number of leukocytes and platelets [310]. Therefore, it is crucial to carefully select the RCF for I-PRF preparation. The RCF should be strong enough to ensure proper cell separation without causing the platelets and leukocytes to segregate out from the area where I-PRF is collected.

The location for harvesting I-PRF is another critical factor that significantly affects the differences in cell numbers. In the literature, two main fractions of I-PRF have been discussed: (i) yellow I-PRF, collected from the upper yellow layer above the buffy coat, and (ii) red I-PRF, which retains the components from the buffy coat layer [327]. It is challenging to determine the exact location that I-PRF is collected in each study. Some studies stated that I-PRF was collected from the upper liquid layer of centrifuged blood [274], [275], [285], [292], assuming it to be the yellow fraction, while others clearly stated that I-PRF used in their work was harvested from the buffy coat layer, or the red fraction [278], [327]. To date, the choice of the better fraction to utilise is still debatable.

Thanasrisuebwong *et al.*, investigated the morphological structure and cellular contents of these two fractions using a scanning electron microscope (SEM). They found that the fibrin structure of yellow I-PRF is more dense and organised than the red I-PRF, but higher cellular component, including platelets and leukocytes, was observed in red I-PRF [327]. They suggested that the yellow fraction might be preferable in terms of the physical properties, while the red I-PRF is probably better in terms of the biological properties [327]. Leukocytes are known to be a rich source of growth factor production and play a significant role in modulating not only immune cells but also other cell types such as fibroblasts, keratinocytes, and endothelial cells during the process of wound healing [274]. Having a greater number of leukocytes in red I-PRF could provide therapeutic benefits in promoting wound healing. However, it is important to consider that leukocytes and other inflammatory cells in I-PRF could potentially increase pro-inflammatory cytokines, causing delayed and ineffective wound healing [328]. In addition, collecting I-PRF too close to the red layer may result in the inclusion of red blood cell components including haemoglobin, haem and iron molecules, which may produce cytotoxic effects and tissue injury [329]. Based on the evidence, we decided to collect I-PRF in this study from the area above the yellow-red junction, assuming this to be yellow I-PRF, to avoid contamination from red blood cells.

In this study, the collection of demographical data from volunteers was not permitted; thus, we cannot rule out the possibility that the heterogeneity of volunteers in terms of age, sex or genetics could also influence the variations in cellular number in I-PRF.

Once we had determined our preparation methods, the expression of paracrine factors released from I-PRF was analysed to identify the biological characteristics of I-PRF. To date, only a few studies have provided an overview of cytokines released by PRF, particularly for I-PRF. We found that PDGF-BB, TGF-β1, and EGF were the only growth factors found in high quantities in I-PRF-derived conditioned medium when compared to the basal DMEM or serum-free medium. We anticipated this since these growth factors are produced and released after the degranulation of platelets [37]. Previous studies showed a peak release of PDGF-BB, TGF-β1, and EGF within the first 72 hours after platelets were artificially degranulated *in vitro* [274], [327], [330]. This is in line with the incubation period used whilst preparing I-PRF-derived conditioned medium in our work and possibly explains the high expression of these growth factors in the conditioned medium. Our findings are supported by Hermida-Nogeuira *et al.*, who reported that TGF-β1 and EGF were the most abundant molecules found in the conditioned medium prepared from L-PRF [331].

Surprisingly, we did not detect VEGF and IGF-1 in I-PRF, contrary to our expectations, considering that they have been present in other PRF formulations [283]. VEGF is well-known for its potent role in regulating angiogenesis [44], while IGF-1 plays a role in cell proliferation and migration of oral mucosa cells [332]. Both are important growth factors in the wound healing process. Our results contradict several previous studies that reported the presence of these factors in I-PRF with peak release within 3 days [274], [278], [327], [333], [334]. Differences in centrifugation methods and the area where I-PRF were collected could possibly contribute to these contradictory results.

Furthermore, variability between donors could be another possible factor affecting the presence of growth factors in I-PRF. The previously mentioned study by Hermida-Nogueira *et al.*, demonstrated differences in VEGF expression, measured by cytokine array between four volunteers [331], indicating variations in cytokine expression among individuals. Further investigations with larger sample sizes are required to confirm the presence of these factors in I-PRF across wider populations.

Our results from the cytokine analysis showed that all subtypes of interleukins were found to be present in I-PRF-derived conditioned medium in relation to the basal DMEM. Interleukins, which are a subset of cytokines, are produced and released by various cell types including lymphocytes, macrophages, neutrophils, endothelial cells, fibroblasts, and

also keratinocytes [335]. Each interleukin has a distinct role in regulating immune response and inflammation. For example, IL-1 and IL-8 are primarily recognised as pro-inflammatory cytokines, while IL-10 is typically known as an anti-inflammatory cytokine [336]–[338]. Besides, the direct effects of these interleukins on fibroblasts and keratinocytes have also been discussed, as cytokine receptors are found in these cells [339].

According to our findings, IL-8 (or CXCL8), IL-10 and IL-13 demonstrated the highest levels. Monocytes and fibroblasts serve as predominant sources for the secretion of IL-8 [337]. It has been suggested that IL-8 is a chemotactic factor for neutrophils during the inflammatory phase of wound healing [335]. A study by Steude *et al.*, showed that IL-8 enhanced keratinocyte proliferation in an organotypic skin culture [340] by binding to the CXCR1 or CXCR2 receptors which have been reported to be expressed on oral keratinocytes [341]. Kroeze *et al.*, also showed that IL-8 could induce keratinocyte migration *in vitro* [339]. IL-10 is mainly produced from monocytes, macrophages and helper T-lymphocytes [336]. IL-10 has been reported to control the function of TGF-β in the remodelling phase of wound healing [342]. IL-13, found in most types of leukocytes [338], was also demonstrated to stimulate fibroblast proliferation and differentiation directly [343]. In addition, cytokines present in substantial amounts in I-PRF, including adiponectin [344], BDNF [345], GM-CSF [346], SCF [347], CXCL1 [339], and CXCL11 [348], have also been demonstrated to modulate the proliferation and migration of either fibroblasts or keratinocytes.

We also observed that angiogenin was highly present in our cytokine array. While the role of angiogenin in regulating fibroblast or keratinocytes has not been mentioned commonly in the literature, it has been shown to have prominent effects in inducing endothelial cell proliferation and migration for angiogenesis [349], which is another crucial mechanism in the healing process. However, we cannot conclude whether I-PRF indeed promotes blood vessel formation which may facilitate oral mucosa healing since our work focused solely on fibroblasts and keratinocytes.

Although the combination of cytokines present in I-PRF most likely contributes to the overall effect, our primary focus was on PDGF-BB, EGF and TGF-β1 which are the most abundant growth factors found in I-PRF derived conditioned medium. Evidence has indicated that PDGF exerts a potent stimulatory effect on fibroblast proliferation and differentiation in oral mucosa tissues by binding with its specific tyrosine kinase receptors,

thereby promoting cell mitosis and increasing the production and secretion of ECM [350]. EGF plays a crucial role in the epithelialisation process of wound healing by stimulating the proliferation of keratinocytes. This effect is mediated through the activation of the epidermal growth factor receptor (EGFR) which is predominantly expressed in the basal layer of the epithelium [37]. The role of TGF-β1 in cell proliferation appears to be paradoxical, as it has shown to have mitogenic properties on fibroblasts but appears to counteract the effect of EGF induced keratinocyte proliferation [351]. Based on our results and the published literature, we suggest that I-PRF potentially accelerates oral mucosa healing by increasing cell proliferation through the combined effect of cytokines and growth factors.

The improvement in cell migration also correlates with the cytokine data, where we observed high levels of PDGF, TGF-β1, and EGF. During the proliferative phase of the healing process, EGF primarily regulates keratinocyte migration at the wound edge by activating EGFR, while TGF-β1 serves as a chemoattractant for fibroblasts to migrate to the wounded area [37]. TGF-β1 has also been reported to promote keratinocyte migration by increasing the affinity of α3β1 integrin to ECM proteins [352] and altering cellular polarity to a more migratory phenotype [351]. In addition, the effect of I-PRF on oral mucosa cell migration could also occur as a result of cytokine activities found in I-PRF. Besides the role of IL-8 which has been mentioned previously, Kroeze *et al.*, also reported that CXCL1 (G/R/O-α) was able to induce keratinocyte migration [339]. Totelli *et al.*, also found that fibrin matrices containing CXCL-11, known as I-TAC, stimulated keratinocyte migration *in vitro* and induced wound closure of a full-thickness skin wound in diabetic mice [348]. These findings all suggest that these growth factors and cytokines could partly influence an increase in keratinocyte migration. These studies support the possible role of I-PRF on enhancing cell migration which importantly contributes to wound healing.

However, we are not able to conclude at this point that these cytokines found at high levels are responsible the observed cellular responses. Similarly, we cannot confirm that low-intensity cytokines are not present in I-PRF. A limitation of the cytokine antibody array is that the data only represents the relative fold change of cytokines found in the I-PRF-derived conditioned medium compared to the control. This semi-quantitative data does not truly represent the exact cytokine amounts in the samples and *in vivo*. The intensity is

also linked to the sensitivity of each antibody on the array. Other methods such as enzyme-linked immunosorbent assay (ELISA) which reference the amount using a standard curve with known concentrations of each cytokine, should be performed to obtain precise measurements. In addition, testing the effect of each individual cytokine in isolation would provide stronger evidence of the mechanism through which molecules exert these effects.

Taken together, I-PRF offers promising advantages as it is biocompatible, simple to prepare and obtained from an autologous source. Our findings and evidence presented here show some promising effects of I-PRF on wound healing, primarily on cell proliferation. We suggest that these observed effects could occur as a result of paracrine signals released from I-PRF. To confirm the full mechanism, more investigations on specific groups of cytokines is needed. We also observed varied responses of the oral mucosa following I-PRF treatment, which are possibly related to the variability in the preparation protocols (such as speeds, times, or location for harvesting I-PRF) or inherent variability in our TEOM model. There is a need to develop an agrees standardised preparation protocol for I-PRF.

Although the therapeutic effect of I-PRF on oral mucosa has been evaluated, assessing its effectiveness in disease treatment remains a significant challenge. Responses and associated factors of normal healing may vary *in vivo* and become even more complex in specific diseases. The changes and disruptions to homeostasis while having the diseases could potentially alter the responses of cells and tissues to I-PRF during the healing process. Therefore, it is crucial to investigate the effects of I-PRF on wound healing in specific *in vitro* models that mimic each oral disease condition. These investigations are essential to gain more understanding of the mechanistic regulation specific to each disease.

5.6 Summary

In summary, our work in this chapter showed some therapeutic potential of I-PRF on oral wound healing using 2D and 3D *in vitro* models. We successfully developed a protocol for harvesting PRF in a liquid formulation, known as I-PRF, and identified its secretome profile. The role of I-PRF in accelerating the wound healing process of oral mucosa is likely from the combined effect of paracrine factors released from I-PRF observed here as an increase of cell proliferation and migration.

Chapter 6

The effect of injectable-platelet-rich fibrin (I-PRF) on bisphosphonate-induced oral mucosa toxicity

6. The effect of injectable-platelet-rich fibrin (I-PRF) on bisphosphonate-induced oral mucosa toxicity

6.1 Introduction

Difficulties in management and unpredictable outcomes from existing MRONJ therapies have led to the development of complementary strategies to improve patient's quality of life [8], [237], [299]. In Chapter 4, we selected GGOH as a possible treatment choice for MRONJ based on its counteracting mechanism against bisphosphonates through the mevalonate pathway. However, we have discovered that GGOH is toxic to oral fibroblasts and keratinocytes and unable to prevent oral soft tissue wound healing in the presence of bisphosphonates. Other potential approaches have been reviewed, which include stem cell therapies, laser technologies, growth factors, hydroxyapatite crystals, or antimicrobial agents [78], [197], [208], [210], [216]. Platelet concentrates have also been investigated since they have been used to enhance tissue regeneration in many applications in dentistry, such as periodontal surgery, gingival recessions, and MRONJ [255].

Clinical applications of PRF to promote and restore soft tissue wounds in MRONJ patients have been studied [8], [353]. However, the strength of evidence is still low, and the majority of the literature are case reports with only a few randomised controlled trials, meaning the effectiveness of PRF, particularly I-PRF, remains poorly understood. There are also a limited number of *in vitro* studies on how I-PRF facilitates the healing process of wounds affected by bisphosphonates [252], even though the cytotoxicity of bisphosphonates on oral soft tissues is well-documented [2]. Therefore, it is crucial to investigate the effects of I-PRF on oral mucosa and gain more understanding of how I-PRF plays a part in the wound healing process.

In Chapter 5, we examined the cellular effects of I-PRF on oral mucosa cells and TEOM. We showed some therapeutic activity of PRF on the wound healing process of the oral mucosa using the wound models of TEOM.

In this chapter, we will assess the therapeutic role of I-PRF against bisphosphonate toxicity on oral mucosa cellular activities involved in the wound healing process using 2D cell assays and 3D *in vitro* oral mucosa models. The cell processes investigated included

metabolic activity, proliferation, and migration of oral mucosa cells. In addition, we also investigated whether PRF could prevent oral mucosa cell death caused by bisphosphonates using cell apoptosis and necrosis assays. Following the 2D experiments, the metabolic activity, epithelium morphology, and thickness of TEOM were also evaluated to determine the effect of PRF on protecting oral mucosa from bisphosphonate toxicity in a more clinically relevant situation.

6.2 Aim(s)

To investigate the cellular response of oral mucosa to I-PRF in the presence of bisphosphonates and to determine whether I-PRF can support oral mucosa healing and tissue integrity in MRONJ-like conditions using 2D and 3D *in vitro* models.

6.3 Materials and Methods

6.3.1 2D Cell culture

Primary oral fibroblasts (NOFs) and immortalised oral keratinocytes (FNB6/TERT) were used in this part of the study. In brief, NOFs were grown in DMEM with supplements (composition can be found in Table 4.2), and FNB6/TERT cells were grown in Green's medium (composition can be found in Table 4.3). All general cell culture procedures were performed as described in Section 4.3.3.

6.3.2 Assessing metabolic activity in 2D culture

MTT assay was carried out to determine the metabolic activity of oral mucosa cells in the presence of I-PRF-derived conditioned medium and bisphosphonates. NOFs (10,000 cells/cm^2) and FNB6/TERT (16,700 cells/cm^2) were seeded separately into 24- and 48-well plates, respectively. After 24 hours, cells were then incubated with I-PRF-derived conditioned medium at different concentrations (10, 20, or 50%) in combination with either ZA or PA for 72 hours. Different concentrations of ZA and PA were chosen based on the previous study [78]. Table 6.1 summarises the concentrations of ZA and PA used on each type of cells. Culture medium without serum and growth factors, or basal culture medium (PRF 0%), were used as controls. The metabolic activity of both cell types was evaluated at 24 and 72 hours. Procedures for performing MTT assay were used as described previously in Section 4.3.5. Results were normalised to the 24-hour control value.

Table 6.1 | ***ZA and PA concentration used for metabolic activity experiments***

	Fibroblasts (NOFs)	**Keratinocytes (FNB6/TERT)**
ZA (µM)	10	10
PA (µM)	100	30

6.3.3 Assessing cell proliferation in 2D culture

To evaluate whether I-PRF could restore the proliferative capacity of oral mucosa cells affected by bisphosphonate toxicity, CFSE staining followed by flow cytometry analysis was used. A working solution of CFSE was made as described previously in Section 5.3.9. Both fibroblasts and keratinocytes were labelled with 1 µM CFSE before seeding into well plates. CFSE-labelled cells were separately seeded into 6-well plates at a density of 5,500 cells/cm^2 for NOFs and 16,700 cells/cm^2 for FNB6/TERT. Non-labelled control and non-proliferative control were also prepared as mentioned before (Section 5.3.9).

For this part of work, cells were incubated with three different concentrations of I-PRF-derived conditioned medium (10, 20, or 50%) in combination with either 10 µM ZA or 100 µM PA for 72 hours. Serum-free medium (PRF 0%) was also used as a control. Cells were collected, washed, and fixed with 10% formalin after 3 days. These fixed cells were analysed using a flow cytometry, and the mean fluorescence intensity (MFI) was measured using procedures as explained in Section 5.3.9. The proliferation index was calculated using Equation 5.2.

6.3.4 Assessing cell migration in 2D culture

To examine how I-PRF affects the migration ability of bisphosphonate-treated oral mucosa cells, a cell-free gap zone created with Oris™ stoppers was measured. Procedures as previously described in Section 5.3.10 were used. NOFs (54,000 cells/cm^2) and FNB6/TERT (132,000 cells/cm^2) were seeded separately into a 96-well plate with stoppers in place and incubated for 24 hours. The following day, cells were treated with Mitomycin C for 4 hours to inhibit cell proliferation. The stoppers were removed and the media were then replaced with the conditioned medium containing different concentrations of I-PRF-conditioned medium (10, 20, or 50%) in combination with either ZA or PA. Table 6.2 illustrates the bisphosphonate dose used in each type of cell. These sub-toxic concentrations, used to limit the possible cellular toxicity, were chosen based on our previous data [120]. Images were captured and analysed as previously described (Section 5.3.10).

Table 6.2** | **ZA and PA concentration used for migration assay

	Fibroblasts (NOFs)	**Keratinocytes (FNB6/TERT)**
ZA (µM)	5	10
PA (µM)	30	10

6.3.5 Assessing cell apoptosis and necrosis in 2D culture

The Annexin V-FITC with PI staining assay were carried out to determine whether I-PRF can reduce apoptosis or necrosis in oral mucosa cells treated with bisphosphonates. The experimental procedures were performed as described previously in Section 5.3.8.

In brief, NOFs at the density of 5,500 cells/cm^2 and FNB6/TERT at the density of 16,700 cells/cm^2 were seeded in to a 6-well plate separately and incubated for 24 hours. The following day, the old medium was removed and replaced with the I-PRF-derived conditioned medium (10, 20, or 50%) in combination with either ZA or PA (described in Table 6.1).

After 3 days, both supernatant and cells were collected and centrifuged separately at 6000 g for 5 minutes. Then, pellets were resuspended in chilled PBS and centrifuged again. The pellets were stained with 100 µL with Annexin V-FITC with PI staining solution for 15 minutes. Preparation of the staining solution was previously shown in Table 5.3.

After 15 minutes, cells were analysed through an LSRII flow cytometer using conditions previously described in Section 5.3.8. Stained cells were categorised into four groups based on the positivity stained which can be viable, early apoptosis, late apoptosis, and necrosis. Positive staining of each dye was used to determine the cell status which were previously defined in Table 5.4. A minimum of 10,000 events per sample was measured each time. Samples were analysed for 5 minutes at a medium speed in cases where they were unable to reach the minimum gate event (10,000).

6.3.6 Constructing of TEOM

The production of TEOM was previously described in Section 5.3.11. Briefly, co-culture of NOFs and FNB6/TERT with a density of 1:4 were seeded inside the stainless steel chamfered ring on top of a 1.5 cm^2 of de-epidermalised dermis (DED). Models were submerged in Green's medium (composition shown in Table 4.2) for two days before lifting up to an air-liquid interface using a transwell insert, as shown in Figure 5.6.

In this chapter, constructed TEOM were used to evaluate the effect of I-PRF on either the epithelium formation or the established epithelium of bisphosphonate-treated TEOM. The experimental timeline is as previously shown in Figure 5.7.

6.3.7 Investigating I-PRF effects on epithelium formation of bisphosphonate-treated TEOM

The effect of I-PRF on epithelial stratification of bisphosphonate-treated TEOM was investigated. Immediately after lifting the TEOM up to an ALI, TEOM was treated with conditioned media containing different concentrations of I-PRF-derived conditioned medium (10, 20, or 50%) with either 10 µM ZA or 50 µM PA for 14 days. The concentrations of ZA and PA were chosen based on the previous results from our group [120].

Metabolic activity of the TEOM was evaluated using resazurin (as described in Section 5.3.12). Values were normalised with the value obtained at the earliest time points. After measuring metabolic activity, models were washed with PBS twice before being immersed in 10% formalin for at least 24 hours for fixation. TEOM underwent histological processing as described in Section 5.3.16. Sections were either stained with H&E solution (Section 5.3.16) or used for immunolabelling (Section 6.3.9). The measurement of epithelium thickness was also performed using the protocol described in Section 5.3.17.

6.3.8 Investigating I-PRF effects on established epithelium of bisphosphonate-treated TEOM

The experimental procedures were previously described in Section 5.3.14. In brief, TEOM was cultured in Green's medium (composition shown in Table 4.2) at ALI for 7 days before the medium was replaced with the conditioned media and continued culturing for a week further. The difference between the experiments performed in this chapter and those

in the previous chapter was the composition of the conditioned medium. In this chapter, the conditioned medium contained either ZA 30 µM alone or in combination with three concentrations of I-PRF-derived conditioned medium (10, 20, and 50%). The metabolic activity of bisected TEOM from each condition was assessed on days 10 and 14. Models were histologically processed as described previously (Section 5.3.16). The epithelium morphology and thickness were also observed (Section 5.3.17).

6.3.9 Investigating the apoptotic status of TEOM

To determine whether I-PRF could reduce bisphosphonate-induced cell apoptosis in TEOM, the terminal deoxynucleotidyl transferase-mediated dUTP nick end labelling (TUNEL) assay was carried out. The transferase enzyme catalyses the deoxynucleotides at the free 3' ends of fragmented DNA, which are found in apoptotic cells [354]. The signal is detected by using either chromogenic or fluorescence methods.

In this work, the chromogenic TUNEL assay kit (Abcam, UK) with streptavidin-conjugated with horseradish peroxidase (HRP) and diaminobenzidine (DAB) was used. The reaction between HRP and DAB produces a brown stain which indicates cell apoptosis.

Prior to the experiment, a working solution of chemicals was prepared as follows:

A) 10X Tris-Buffered Saline (TBS)

A stock solution of TBS (10x) was prepared by dissolving 24 g of Tris-base and 44 g of NaCl with 1 L of deionised water. The pH of the solution was adjusted to 7.6 using 1N Sodium hydroxide (NaOH). A 10-fold dilution of 10X TBS with deionised water was made to obtain a working solution of TBS (1X) for the experiments.

B) 1X Proteinase K solution

A Proteinase K solution (1X) was made from a stock solution (100X) (provided in the kit) by adding 1 µL to 99 µL deionised water.

C) 3% Hydrogen peroxide (H_2O_2) solution

A 3% H_2O_2 solution was made from a stock solution (30%) (Sigma-Aldrich, UK) by diluting 1 in 10 in methanol.

D) Terminal deoxynucleotidyl transferase (TdT) solution

A TdT solution was made by adding 1 µL of TdT enzyme to 39 µL TdT labelling reaction mix solution (provided in the kit).

E) 1X Conjugate solution

A 1X conjugate solution was made by adding 4 µL of a stock solution (25X) to 96 µL blocking buffer (provided in the kit).

F) 1X DAB solution

A 1X DAB solution was made by diluting DAB solution 1 with DAB solution 2 at 1:30 (both solutions provided in the kit)

All other solutions were used as provided in the kit. Formalin-fixed TEOM models were processed and embedded in paraffin wax as described in Section 5.3.16. A 5 µm thick section mounted on a Superfrost Plus slide was used for this assay. Sections were de-paraffinised in xylene and rehydrated in gradually decreased concentrations of alcohol at room temperature, as shown in Table 6.3. Slides were then immersed in 1X TBS for 5 minutes. The area surrounding the specimens was dried, and the sections were localised with PAP hydrophobic pen (Abcam, UK). A Proteinase K solution (1X) was added to the specimen and incubated at room temperature for 20 minutes. Slides were then washed in 1X TBS for 5 minutes.

Following this, the endogenous peroxidases were inactivated with 3% hydrogen peroxide for 5 minutes at room temperature. Specimens were covered with TdT equilibration buffer for 30 minutes. Slides were carefully blotted with absorbent paper towel. A TdT solution containing TdT enzyme, prepared as mentioned above, was immediately applied to the slides. A coverslip was placed to ensure an equal distribution of the solution across the section and also to prevent evaporation. Slides were then placed in a humidified chamber inside an incubator at 37°C. After 1.5 hours, the coverslip was removed, and slides were rinsed gently with 1X TBS for 5 minutes. Then, stop buffer was added and incubated for 5 minutes. Slides were washed again in 1X TBS for 5 minutes before incubating with blocking buffer at room temperature for 10 minutes. Slides were blotted, and 1X conjugate buffer was applied to the sections. Slides were incubated in a humidified chamber at room temperature for 30 minutes.

Colour development was performed by adding 1X DAB solution to the specimens and incubating at room temperature. After 15 minutes, slides were rinsed with deionised water. Sections were counterstained with Methyl Green solution (provided in the kit) for 3

minutes. Slides were carefully blotted to remove the counterstain solution. Slides were then dipped in the 100% ethanol twice, followed by a dip in 100% xylene twice. Slides were then mounted with a DPX mounting medium and covered with a coverslip. Images were captured using an inverted light microscope (Olympus CX43) with a Euromex camera (VC.3036 HD-Ultra).

Table 6.3 | ***Deparaffinisation and rehydration process of TEOM sections for TUNEL assay***

Solution	Time (minutes)
Xylene	5
Xylene	5
100% IMS	5
100% IMS	5
90% IMS	3
80% IMS	3
70% IMS	3

6.3.10 Statistical analysis

Statistical analysis was performed using GraphPad Prism 9 software. Data was shown as mean with standard deviation (SD). “N” indicates the number of biological repeats, where “n” represents the number of technical replicates in each biological repeat. The Shapiro-Wilk test was used to test the normality of the data. All results were analysed using one-way ANOVA followed by a Dunnett’s post-hoc comparison test, unless otherwise stated in the figure legends. Statistical significance was indicated when the p-value < 0.05.

6.4 Results

6.4.1 I-PRF increased the metabolic activity of ZA-treated fibroblasts but not keratinocytes

To determine the effect of I-PRF on bisphosphonate-induced oral mucosa toxicity, 10 μM ZA was added in combination with selected concentrations of I-PRF-derived conditioned medium (10, 20, and 50%) (Section 6.3.2). Figure 6.1 shows the metabolic activity of NOFs after treating with ZA and I-PRF-derived conditioned medium for 72 hours. At 24 hours, ZA caused a slight, non-statistically significant reduction of fibroblast metabolic activity. The addition of I-PRF-derived conditioned medium as well as ZA to fibroblasts led to an increase of metabolic activity dose-dependently; however no statistical significance was observed from any conditions.

The metabolic activity of NOFs was significantly decreased compared to the control (PRF 0%) following 72 hours of ZA treatment. A dose-dependent increase of fibroblast metabolic activity was seen from the addition of I-PRF-derived conditioned medium in comparison to the ZA-treated condition; however, no statistical significance was found.

Figure 6.2 illustrates the response of FNB6/TERT to I-PRF-derived conditioned medium in the presence of ZA. When FNB6/TERT were treated with ZA or additional I-PRF-derived conditioned media, no difference was found at a 24-hour time point among any conditions compared to the control. At 72 hours, ZA slightly decreased the cellular metabolic activity with no significant effect of I-PRF-derived conditioned medium observed.

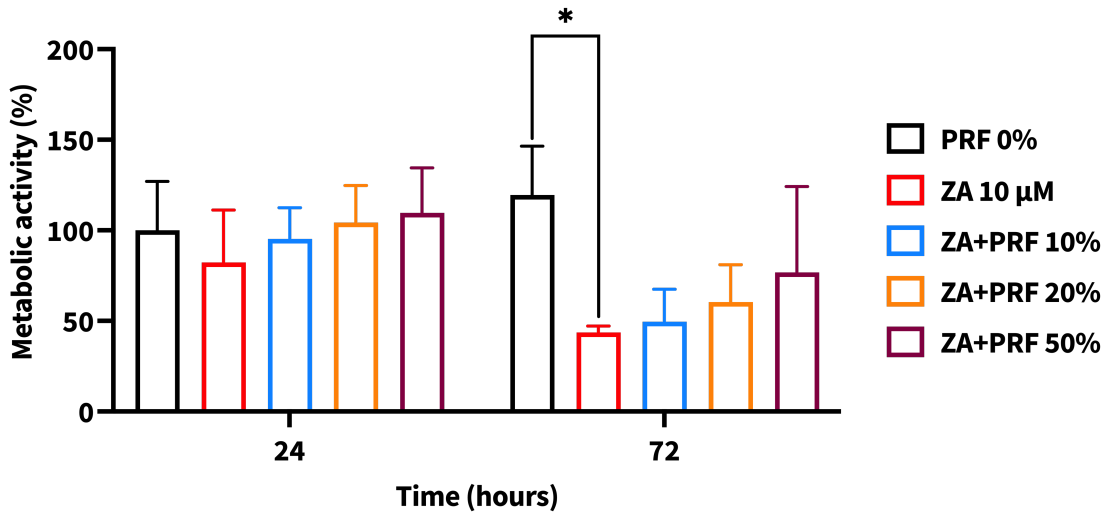

***Figure 6.1 | Metabolic activity of primary oral fibroblasts (NOFs) in the presence of ZA 10 µM in combination with I-PRF-derived conditioned medium**. NOFs were treated with different concentrations of I-PRF-derived conditioned medium in combination with 10 µM ZA for 72 hours. Metabolic activity was assessed at 24 and 72 hours using the MTT assay. Data are presented as the mean ± standard deviation from four independent experiments with three technical replicates each (N=4, n=3) except PRF 0% and ZA 10 µM which were derived from three experiments (N=3, n=3). A one-way ANOVA followed by Dunnett's multiple comparison were carried out to test the statistical significance against ZA 10 µM at each time point (*p<0.05). Abbreviations: ZA, zoledronate; PRF, platelet-rich fibrin; ANOVA, analysis of variance.*

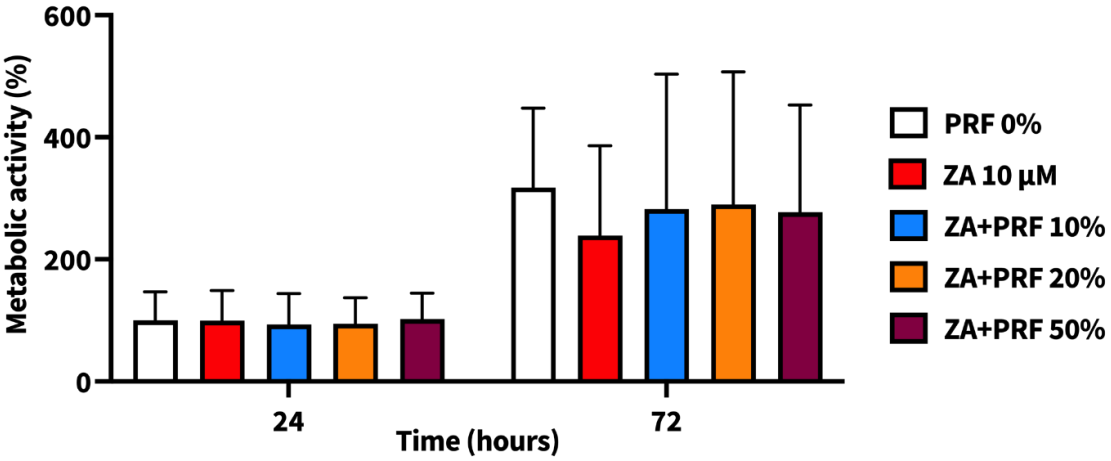

***Figure 6.2 | Metabolic activity of immortalised oral keratinocytes (FNB6/TERT) in the presence of ZA 10 µM in combination with I-PRF-derived conditioned medium**. FNB6/TERT cells were treated with different concentrations of I-PRF-derived conditioned medium in combination with 10 µM ZA for 72 hours. Metabolic activity was assessed at 24 and 72 hours using the MTT assay. Data are presented as the mean ± standard deviation from five independent experiments with three technical replicates each (N=5, n=3) except PRF 0% and ZA 10 µM which were derived from four experiments (N=4, n=3). A one-way ANOVA followed by Dunnett's multiple comparison were carried out to test the statistical significance against ZA 10 µM at each time point. Abbreviations: ZA, zoledronate; PRF, platelet-rich fibrin; ANOVA, analysis of variance.*

6.4.2 I-PRF successfully reduced the toxicity of PA in oral fibroblasts but not in keratinocytes

A higher concentration of PA (100 µM) was chosen to induce toxicity on NOFs because of its lower potency in comparison to ZA. Figure 6.3 shows the response of NOFs in the presence of different concentrations of I-PRF-conditioned medium in combination with PA. At 24 hours, PA lowered the metabolic activity of NOFs. Adding I-PRF-derived conditioned medium to PA-treated cells increased cell metabolic activity for all concentrations; however, no statistical significance was observed from any conditions. The overall trend was similar at a 72-hour time point. Fibroblast metabolic activity was significantly reduced after treating with PA. Cells incubated with all doses of I-PRF-derived conditioned medium in the presence of PA had a higher level of metabolic activity than PA-treated cells alone with a statistical significance observed from PRF 20% and 50% conditions, indicating the positive effect of I-PRF in this instance.

Figure 6.4 demonstrates the metabolic activity of FNB6/TERT over 72 hours in the presence of PA and I-PRF-derived conditioned medium. A lower concentration of PA (30 µM) was used to induce toxicity than that used for NOFs, indicating lower susceptibility of keratinocytes to PA compared to fibroblasts. At 24 hours, there was no significant difference between any groups compared to the untreated controls. PA led to a slight reduction of the metabolic activity after 72 hours. When treated with I-PRF-derived conditioned medium, there was no change in the metabolic activity of FNB6/TERT.

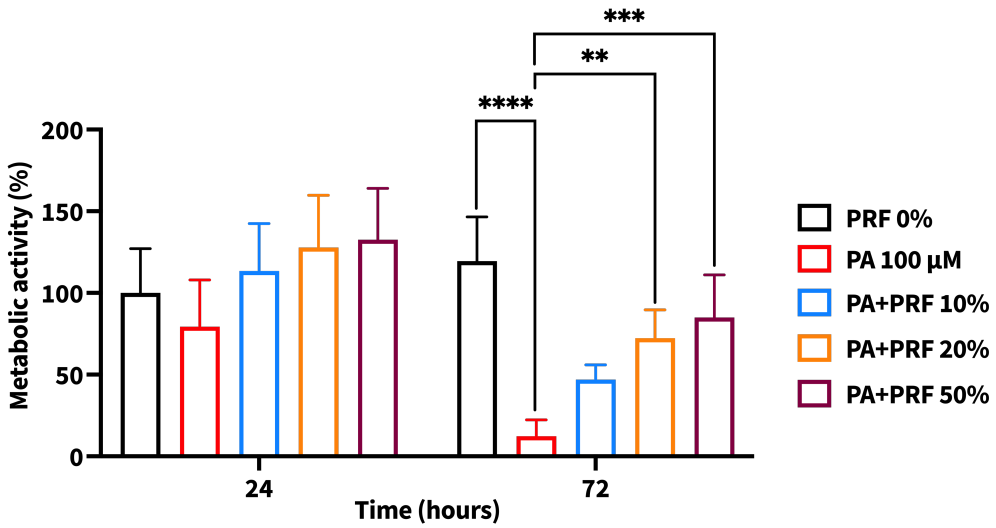

Figure 6.3 | ***Metabolic activity of primary oral fibroblasts (NOFs) in response to 100 µM PA in combination with I-PRF-derived conditioned medium***. *NOFs were treated with different concentrations of I-PRF-derived conditioned medium in combination with 100 µM PA for 72 hours. Metabolic activity was assessed at 24 and 72 hours using the MTT assay. Data are presented as the mean ± standard deviation from four independent experiments with three technical replicates each (N=4, n=3) except PRF 0% and PA 100 µM which were derived from three experiments (N=3, n=3). A one-way ANOVA followed by Dunnett's multiple comparison were carried out to test the statistical significance against 100 µM PA at each time point (**p<0.01, ***p<0.001, ****p<0.0001). Abbreviations: PA, pamidronate; PRF, platelet-rich fibrin; ANOVA, analysis of variance.*

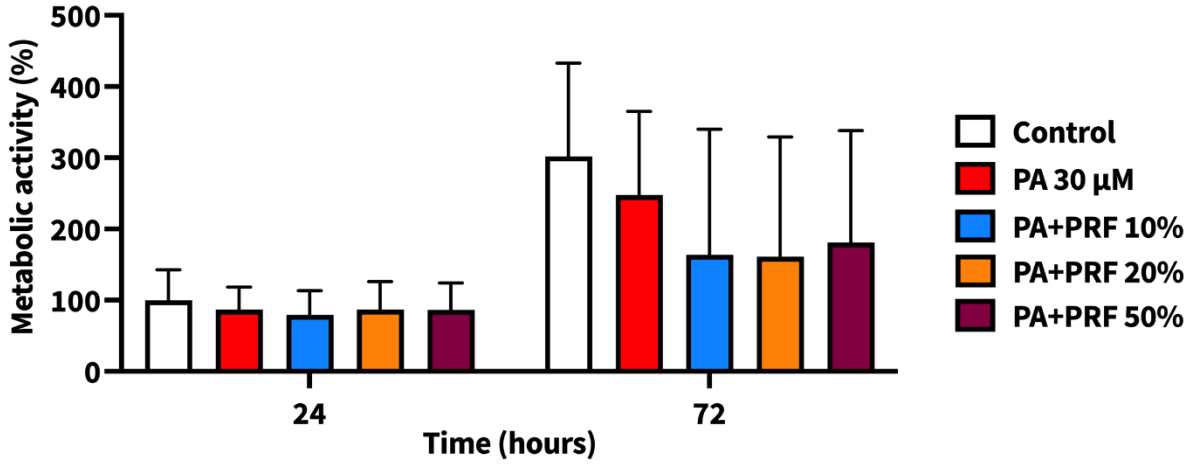

Figure 6.4 | ***Metabolic activity of immortalised oral keratinocytes (FNB6/TERT) in response to 30 µM PA in combination with I-PRF-derived conditioned medium***. *FNB6/TERT cells were treated with different concentrations of I-PRF-derived conditioned medium in combination with 30 µM PA for 72 hours. Metabolic activity was assessed at 24 and 72 hours using the MTT assay. Data are presented as the mean ± standard deviation from four independent experiments with three technical replicates each (N=4, n=3) except PRF 0% and 30 µM PA which were derived from three experiments (N=3, n=3). A one-way ANOVA followed by Dunnett's multiple comparison were carried out to test the statistical significance against 30 µM PA at each time point. Abbreviations: PA, pamidronate; PRF, platelet-rich fibrin; ANOVA, analysis of variance.*

6.4.3 I-PRF increased cell proliferation of both fibroblasts and keratinocytes when treated with ZA

The literature has shown that bisphosphonates reduce cell proliferation [2], which plays a role in the tissue healing process [38]. We hypothesised that the addition of I-PRF would restore the proliferation of oral mucosa cells and improve wound healing affected by bisphosphonates. Cells were stained with CFSE fluorescence dye, and cell proliferation was evaluated in the form of the mean fluorescence intensity (MFI) using a flow cytometer as described in Section 6.3.3. The MFI value was calculated using Equation 5.2.

Figure 6.5 shows the NOF proliferation over 72 hours of the I-PRF-derived conditioned medium treatment with 10 µM ZA. At 24 hours, ZA produced a slight reduction in the proliferation index in comparison to the untreated control (PRF 0%). The proliferation index increased in a dose-dependent fashion after adding I-PRF-derived conditioned medium to ZA-treated NOFs with a statistical significance observed compared to the PRF 50% condition. When treated with ZA, the proliferation index was lower than the control after 72 hours. The addition of I-PRF-derived conditioned medium produced a higher value of proliferation index, with a statistically significant increase observed when cells were cultured with 50% I-PRF-derived conditioned media.

The proliferation index of FNB6/TERT was also reduced when incubated with 10 µM ZA after 24 hours, as shown in Figure 6.6. A higher proliferation index was observed from all I-PRF-treated conditions in the presence of ZA. However, there was no statistical significance. At 72 hours, the trend was similar to the 24-hour results, with a statistically significant increase found when cells were incubated with 50% of I-PRF-derived conditioned media from a ZA+PRF 50% condition.

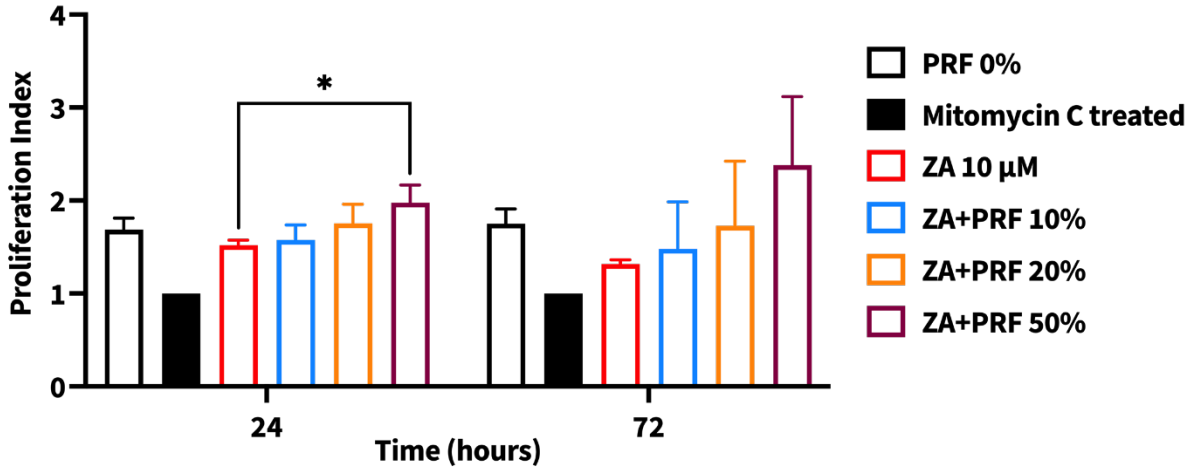

Figure 6.5 | ***Proliferation index of primary oral fibroblasts (NOFs) in response to 10 µM ZA in combination with I-PRF-derived conditioned medium***. *NOFs were cultured with three concentrations of I-PRF derived conditioned medium in combination with 10 µM ZA for 72 hours. Proliferation index was calculated using mean fluorescence intensity from flow cytometry results. Data are presented as the mean ± standard deviation from three independent experiments (N=3, n=1). Statistical significance was determined using a one-way ANOVA followed by Dunnett's multiple comparison against the ZA 10 µM at each time point (*p<0.05). Abbreviations: ZA, zoledronate; PRF, platelet-rich fibrin; ANOVA, analysis of variance.*

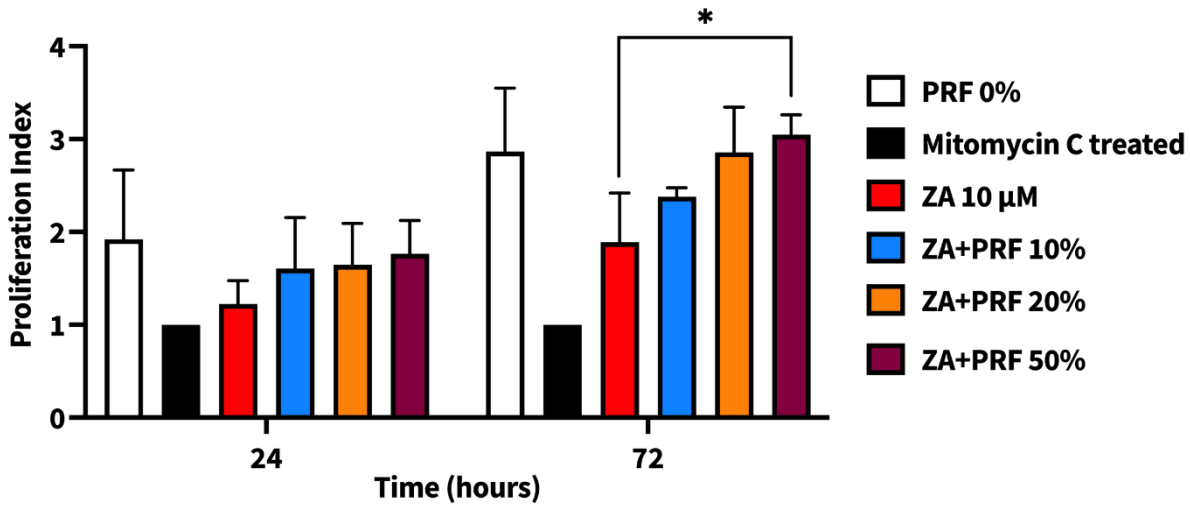

Figure 6.6 | ***Proliferation index of immortalised oral keratinocytes (FNB6/TERT) in response to 10 µM ZA in combination with I-PRF-derived conditioned medium.*** *FNB6/TERT cells were cultured with three concentrations of I-PRF derived conditioned medium in combination with 10 µM ZA for 72 hours. Proliferation index was calculated using mean fluorescence intensity from flow cytometry results. Data are presented as the mean ± standard deviation from three independent experiments (N=3, n=1). Statistical significance was determined using a one-way ANOVA followed by Dunnett's multiple comparison against the ZA 10 µM at each time point (*p<0.05). Abbreviations: ZA, zoledronate; PRF, platelet-rich fibrin; ANOVA, analysis of variance.*

6.4.4 I-PRF did not affect the proliferation of PA-treated cells

A lower proliferative index was observed in both PA-treated NOFs (Figure 6.7) and FNB6/TERT (Figure 6.8) after 24 hours, indicating the negative effect of PA on oral mucosa cell proliferation. There was no significant change after adding I-PRF-derived conditioned medium from both cell types in the presence of PA. At 72 hours, PA caused a statistically significant reduction of the proliferative index of both NOFs and FNB6/TERT; however, the addition of I-PRF-derived conditioned medium produced no significant effect on the proliferation at a 72-hour time point.

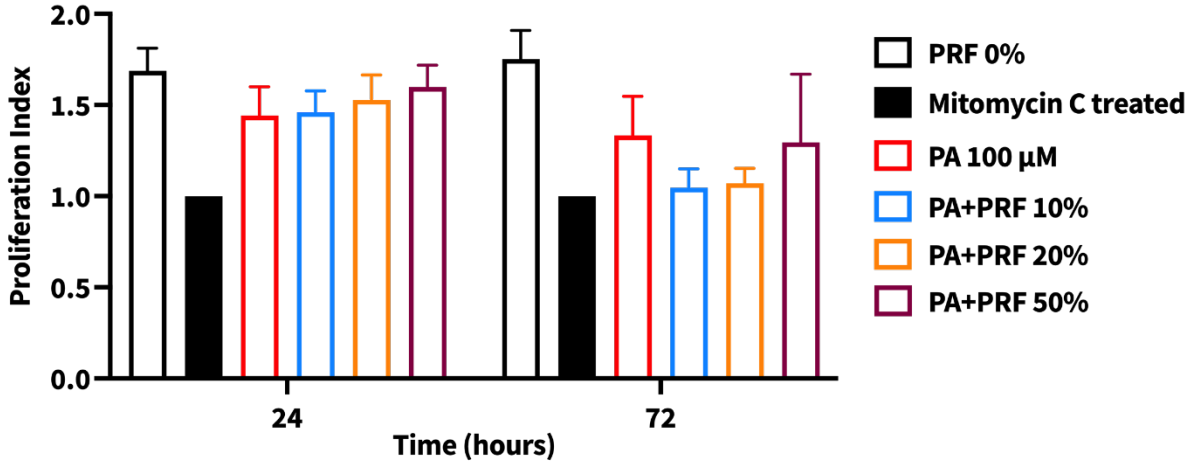

Figure 6.7 | ***Proliferation index of primary oral fibroblasts (NOFs) in response to 100 µM PA in combination with I-PRF-derived conditioned medium***. *NOFs were cultured with three concentrations of I-PRF derived conditioned medium in combination with 100 µM PA for 72 hours. Proliferation index was calculated using mean fluorescence intensity from flow cytometry results at 24- and 72-hour time point. Data are presented as the mean ± standard deviation from three independent experiments (N=3, n=1). Statistical significance was determined using a one-way ANOVA followed by Dunnett's multiple comparison against the PA 100 µM at each time point. Abbreviations: PA, pamidronate; PRF, platelet-rich fibrin; ANOVA, analysis of variance.*

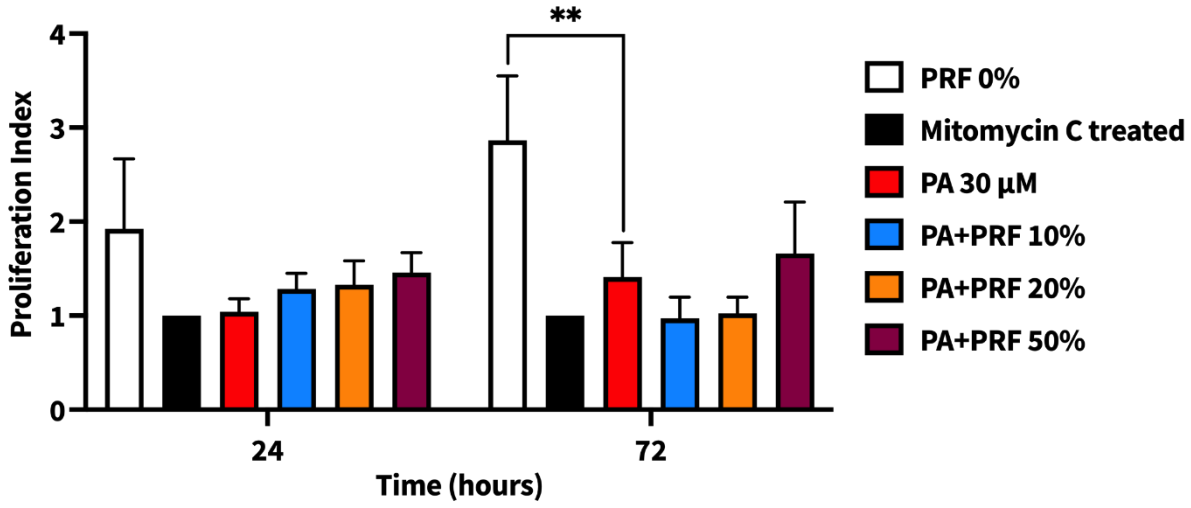

Figure 6.8 | ***Proliferation index of immortalised oral keratinocytes (FNB6/TERT) in response to 30 µM PA in combination with I-PRF-derived conditioned medium.*** *FNB6/TERT cells were cultured with three concentrations of I-PRF derived conditioned medium in combination with 30 µM PA for 72 hours. Proliferation index was calculated using mean fluorescence intensity from flow cytometry results at 24- and 72-hour time point. Data are presented as the mean ± standard deviation from three independent experiments (N=3, n=1). Statistical significance was determined using a one-way ANOVA followed by Dunnett's multiple comparison against the PA 30 µM at each time point (**p<0.01). Abbreviations: PA, pamidronate; PRF, platelet-rich fibrin; ANOVA, analysis of variance.*

6.4.5 I-PRF increased gap closure of keratinocytes but not fibroblasts in the presence of ZA

ZA was added simultaneously with I-PRF-derived conditioned medium to either NOFs or FNB6/TERT. The amount of gap closure, representing the migration ability of oral mucosa cells across the wound in the clinical scenario, was measured from captured images (Section 6.3.4). The concentrations of bisphosphonates were chosen based on previous work [120] and were different between each cell type (Table 6.2). These concentrations were sub-toxic, unlike the previously used doses in the metabolic activity and proliferation assay, as shown in Table 6.1. This was to rule out possible toxicity affecting the migration ability of oral mucosa cells.

NOFs were treated with 5 µM ZA and the gap closure of ZA (87%) was slightly lower than the control (PRF 0%) (90%), as shown in Figure 6.9. When I-PRF-derived conditioned medium was added, a slightly higher percentage of gap closure was observed from all doses compared to the ZA treatment alone after 24 hours. At 48 hours, 20% and 50% I-PRF-derived conditioned medium produced a higher percentage of gap closure than the ZA treatment alone, indicating a faster rate of cell migration. These data were in line with the images shown in Figure 6.10, which show a smaller gap remaining when compared to the ZA treatment.

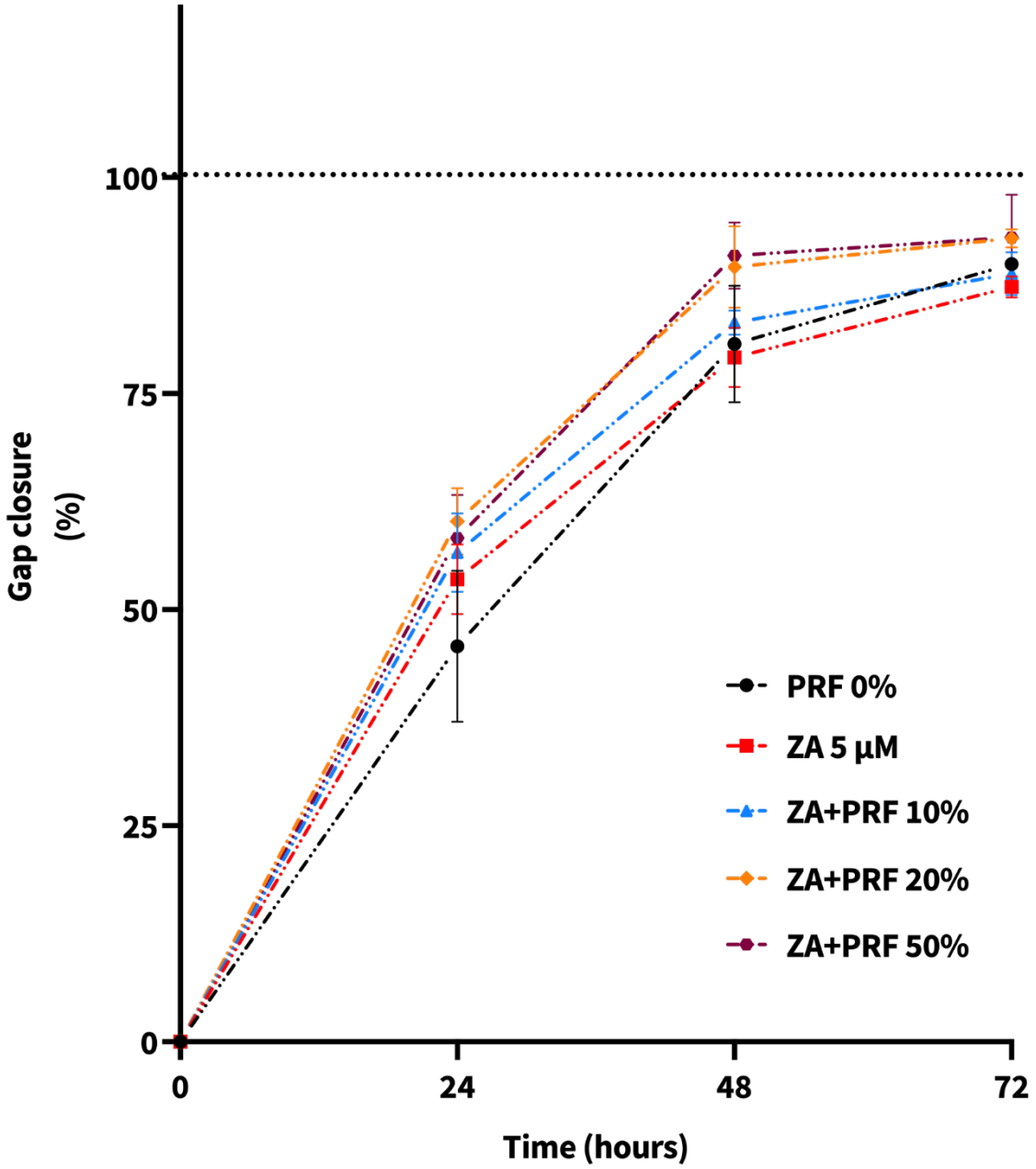

Figure 6.9 | Migration analysis of primary oral fibroblasts (NOFs) in response to 5 µM ZA in combination with I-PRF-derived conditioned medium. *NOFs were treated with different concentrations of I-PRF-derived conditioned medium in combination with 5 µM ZA for 72 hours. The migration, assessed by measuring gap closure of each well, was quantitatively analysed at 24-hour intervals (24, 48, and 72 hours). Data are presented as the mean ± standard deviation from two independent experiments with six technical replicates each (N=2, n=6). Abbreviations: ZA, zoledronate; PRF, platelet-rich fibrin.*

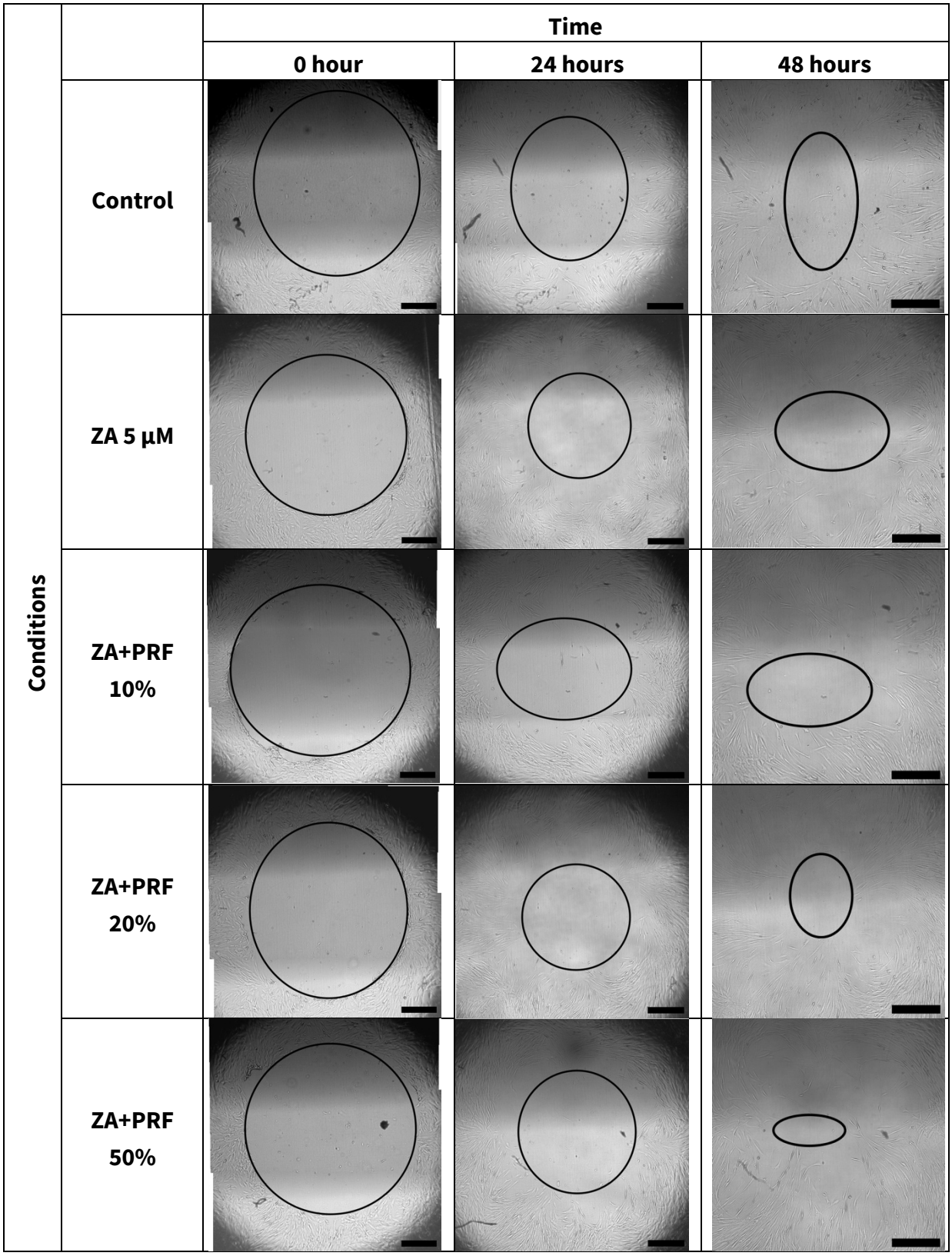

Figure 6.10 | ***Representative images of primary oral fibroblast (NOF) migration over 72 hours in the presence of different I-PRF-derived conditioned medium in combination with ZA****. NOFs were treated with 5 µM ZA alone or in combination with I-PRF-derived conditioned medium, and incubated for 72 hours. Images show the migration pattern of NOFs, captured using an inverted microscope at 4x magnification. Circles have been added to each image to illustrate the remaining gap. Scale bars = 0.5 mm. Abbreviations: ZA, zoledronate; PRF, platelet-rich fibrin.*

Figure 6.11 demonstrates the migration of FNB6/TERT when treated with 10 μM ZA alone or in combination with different doses of I-PRF-derived conditioned medium over 24 hours. In contrast to data obtained from fibroblasts (Figure 6.9), approximately 65% of the gap was closed over the experimental period in keratinocytes treated with serum-free medium (PRF 0%). A higher percentage of gap closure was observed after treating FNB6/TERT with 10% and 20% of I-PRF-derived conditioned medium after 8 hours. At 16 hours, all I-PRF-derived conditioned medium produced improved gap closure compared to ZA treatment alone. A similar trend was observed during the 24-hour time point. Adding PRF produced an increase in the migration rate of ZA-treated FNB6/TERT. Gaps were closed entirely in all I-PRF-treated groups. Representative images of FNB6/TERT migration over 24 hours in the presence of ZA and I-PRF-derived conditioned medium are shown in Figure 6.12.

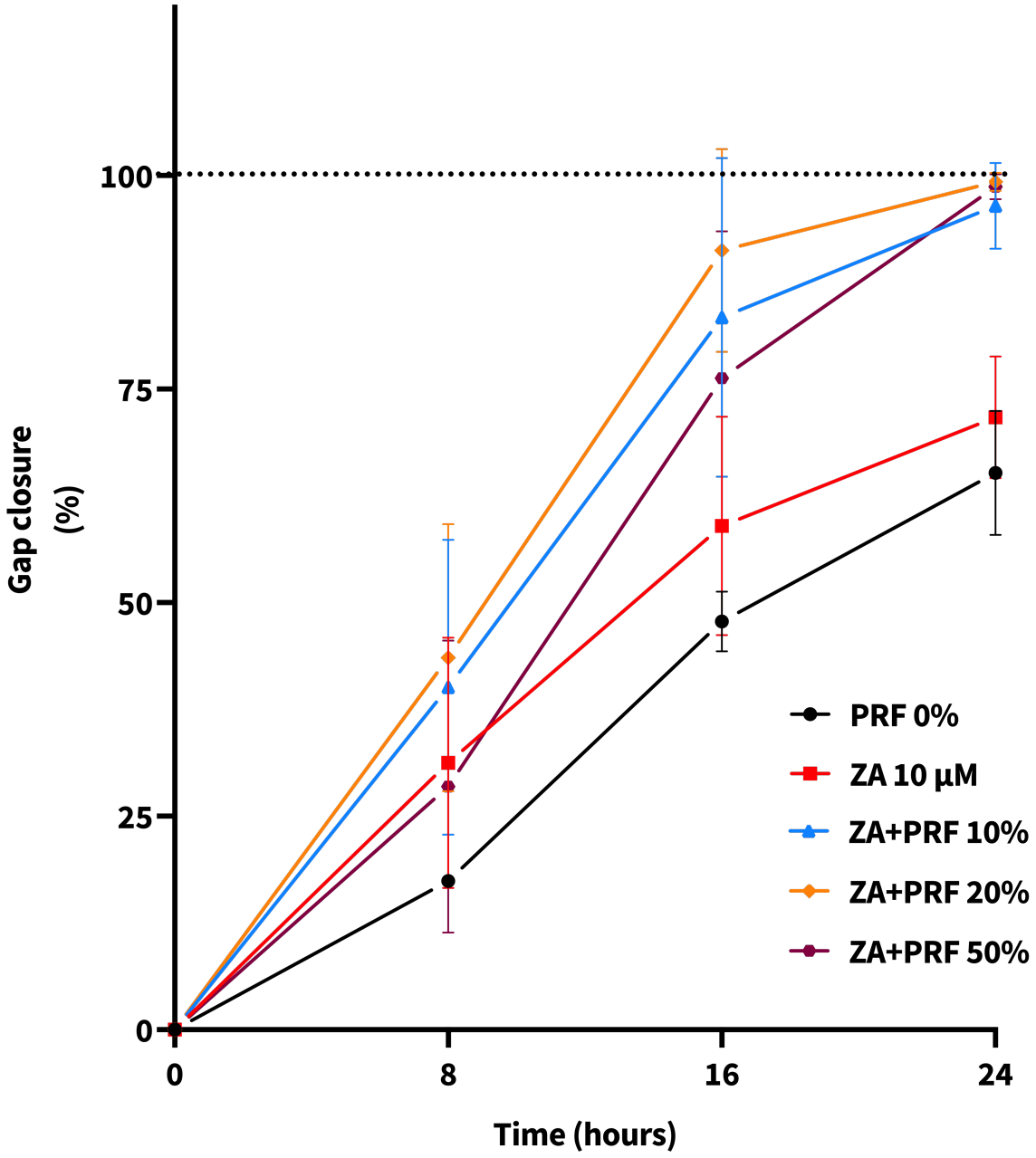

Figure 6.11 | ***Migration analysis of immortalised oral keratinocytes (FNB6/TERT) in response to 10 µM ZA in combination with I-PRF-derived conditioned medium.*** *FNB6/TERT cells were treated with different concentrations of I-PRF-derived conditioned medium in combination with 10 µM ZA for 72 hours. The migration, assessed by measuring gap closure of each well, was quantitatively analysed at 24-hour intervals (24, 48, and 72 hours). Data are presented as the mean ± standard deviation from two independent experiments with six technical replicates each (N=2, n=6). Abbreviations: ZA, zoledronate; PRF, platelet-rich fibrin.*

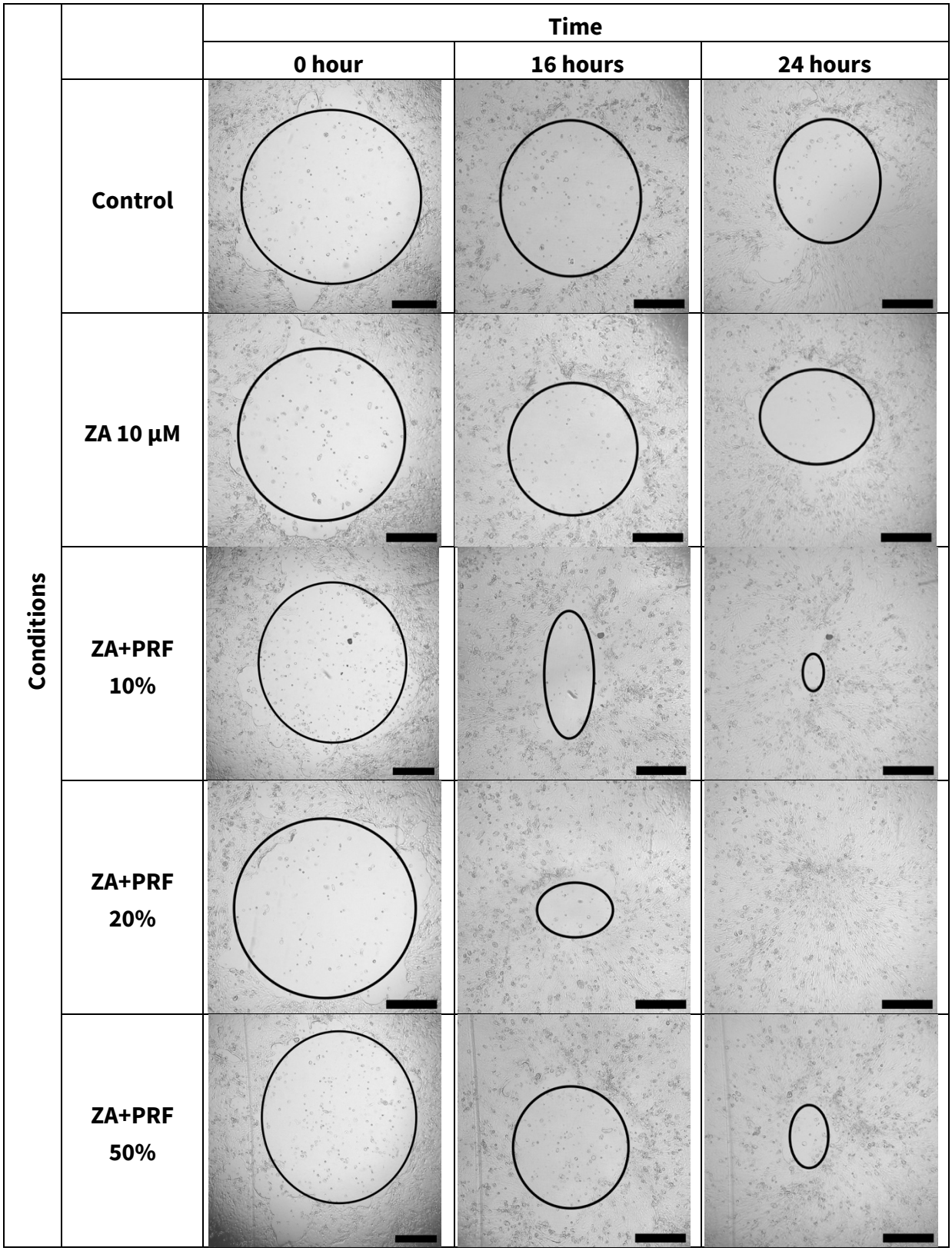

Figure 6.12 | Representative images of immortalised oral keratinocyte (FNB6/TERT) migration over 24 hours in the presence of different I-PRF-derived conditioned medium in combination with ZA. *FNB6/TERT cells were treated with 10 µM ZA alone or in combination with I-PRF-derived conditioned medium, and incubated for 72 hours. Images show the migration pattern of FNB6/TERT, captured using an inverted microscope at 4x magnification. Circles have been added to each image to illustrate the remaining gap. Scale bars = 0.5 mm. Abbreviations: ZA, zoledronate; PRF, platelet-rich fibrin.*

6.4.6 I-PRF increased gap closure of oral mucosa cells in the presence of PA

A sub-toxic concentration of PA (30 µM) was added to NOFs in combination with different doses of I-PRF-derived conditioned medium to determine whether the I-PRF would be able to improve cell migration (Section 6.3.4). After 48 hours, NOFs treated with 30 µM PA exhibited a gap closure of approximately 73%, which was lower than that of the untreated controls (PRF 0%) at around 81%, as shown in Figure 6.13. Addition of I-PRF-derived conditioned medium resulted in increased gap closure across all concentrations, ranging approximately from 86 to 93%. A similar tread was observed at a 72-hour time point where all I-PRF-treated conditions, as well as the untreated control, showed greater gap closure compared to the PA treatment alone. Figure 6.14 shows representative images from each condition.

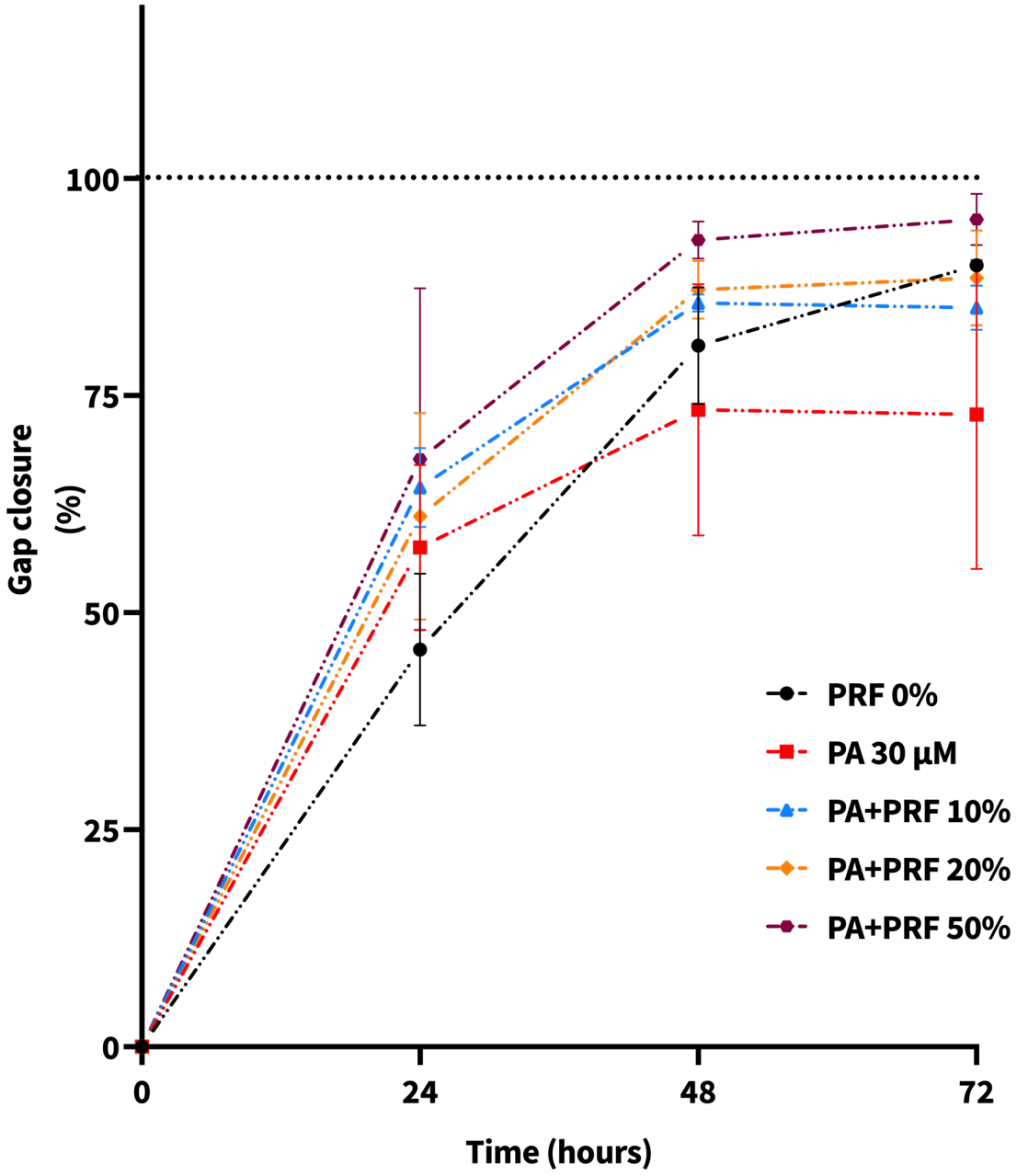

Figure 6.13 | Migration analysis of primary oral fibroblasts (NOFs) in response to 30 µM PA in combination with I-PRF-derived conditioned medium. *NOFs were treated with different concentrations of I-PRF-derived conditioned medium in combination with 30 µM PA for 72 hours. The migration, assessed by measuring gap closure of each well, was quantitatively analysed at 24-hour intervals (24, 48, and 72 hours). Data are presented as the mean ± standard deviation from two independent experiments with six technical replicates each (N=2, n=6). Abbreviations: PA, pamidronate; PRF, platelet-rich fibrin.*

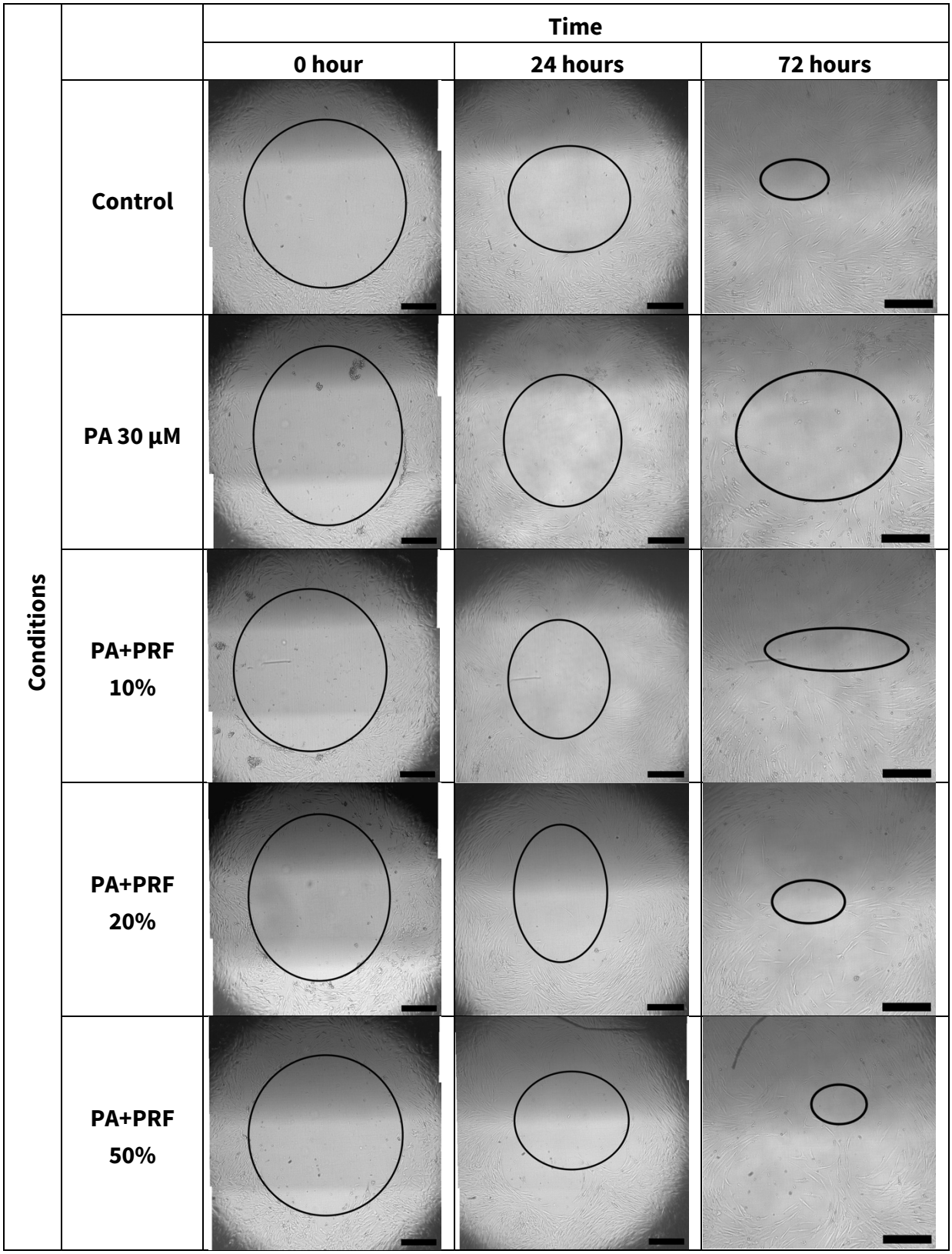

Figure 6.14 | ***Representative images of primary oral fibroblast (NOF) migration over 72 hours in the presence of different I-PRF-derived conditioned medium in combination with PA****. NOFs were treated with 30 µM PA alone or in combination with I-PRF-derived conditioned medium, and incubated for 72 hours. Images show the migration pattern of NOFs, captured using an inverted microscope at 4x magnification. Circles have been added to each image to illustrate the remaining gap. Scale bars = 0.5 mm. Abbreviations: PA, pamidronate; PRF, platelet-rich fibrin.*

With FNB6/TERT treated with 10 μM PA, the addition of I-PRF-derived conditioned medium at any concentrations did not affect cell migration after 8 hours. A positive effect of PRF was observed during 16 hours, as shown in Figure 6.15. All I-PRF+PA conditions produced higher gap closure than the PA-treated cells. At 24 hours, fewer FNB6/TERT in the presence of PA alone were able to migrate into the gap, with around 65% of the gap being filled, while the addition of I-PRF treatment produced complete gap closure. Figure 6.16 shows representative images of FNB6/TERT migration in the presence of PA and I-PRF-derived conditioned medium over 24 hours.

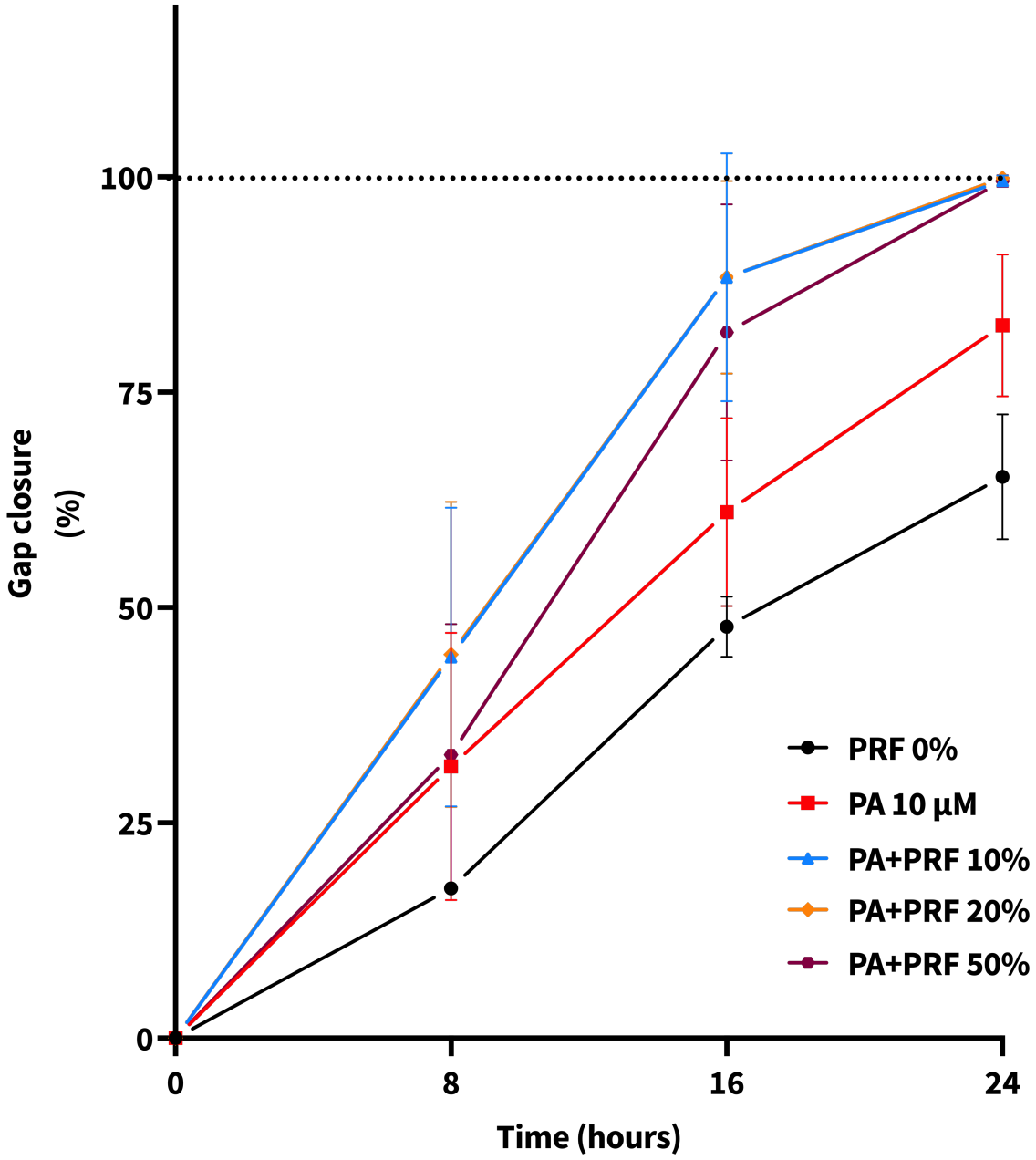

Figure 6.15 | Migration analysis of immortalised oral keratinocytes (FNB6/TERT) in response to 10 µM PA in combination with I-PRF-derived conditioned medium. *FNB6/TERT cells were treated with different concentrations of I-PRF-derived conditioned medium in combination with 10 µM PA for 24 hours. The migration, assessed by measuring gap closure of each well, was quantitatively analysed at 8-hour intervals (8, 16, and 24 hours). Data are presented as the mean ± standard deviation from two independent experiments with six technical replicates each (N=2, n=6). Abbreviations: PA, pamidronate; PRF, platelet-rich fibrin.*

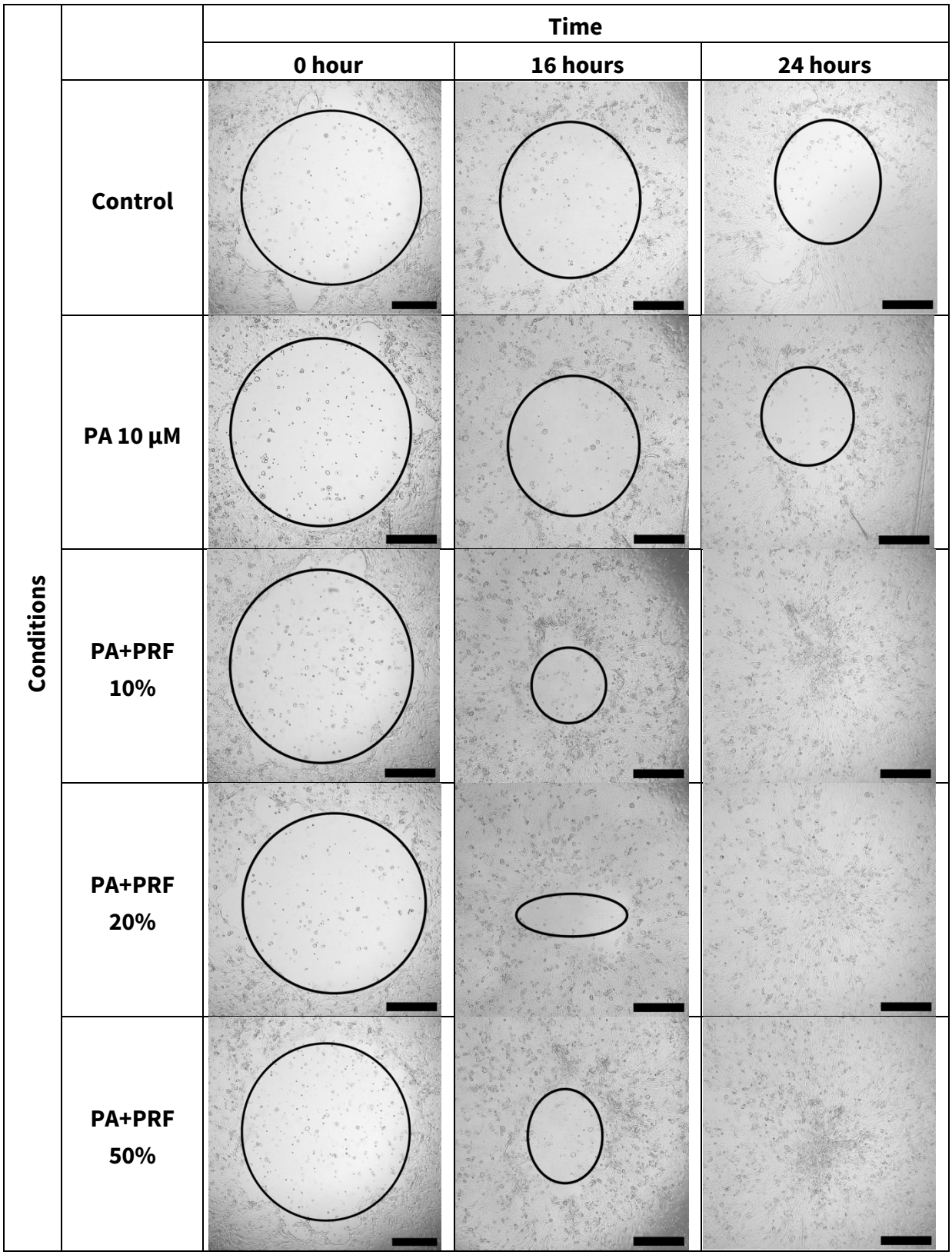

Figure 6.16 | ***Representative images of immortalised oral keratinocyte (FNB6/TERT) migration over 24 hours in the presence of different I-PRF-derived conditioned medium in combination with PA***. *FNB6/TERT cells were treated with 10 µM PA alone or in combination with I-PRF-derived conditioned medium, and incubated for 72 hours. Images show the migration pattern of FNB6/TERT, captured using an inverted microscope at 4x magnification. Circles have been added to each image to illustrate the remaining gap. Scale bars = 0.5 mm. Abbreviations: PA, pamidronate; PRF, platelet-rich fibrin.*

6.4.7 I-PRF reduced PA-induced fibroblast apoptosis but increased cell necrosis

Since bisphosphonates have been demonstrated to have cytotoxic effects on oral mucosa cells *via* the apoptosis pathway [2], this section aimed to study whether I-PRF could prevent bisphosphonate-induced cell death. Oral mucosa cells were stained with Annexin V-conjugated with FITC and propidium iodide (PI) to determine cell status after having a single treatment of I-PRF-derived conditioned medium in combination with either ZA or PA for 72 hours (Section 6.3.5).

After being treated with 10 µM ZA for 72 hours, fibroblasts had approximately 83% viable cells, as shown in Figure 6.17, which was lower than the untreated control (92%). However, this was not statistically significant. The addition of I-PRF-derived conditioned medium caused no change in comparison to the ZA-treated group.

In terms of keratinocytes, 10 µM ZA decreased the percentage of viable cells with an increase of late-apoptotic cells after 72 hours. Figure 6.18 shows the proportion of keratinocytes in each stage after treating with ZA in combination with I-PRF-derived conditioned medium. Similar to fibroblasts, I-PRF produced no effect on ZA-induced apoptosis on keratinocytes.

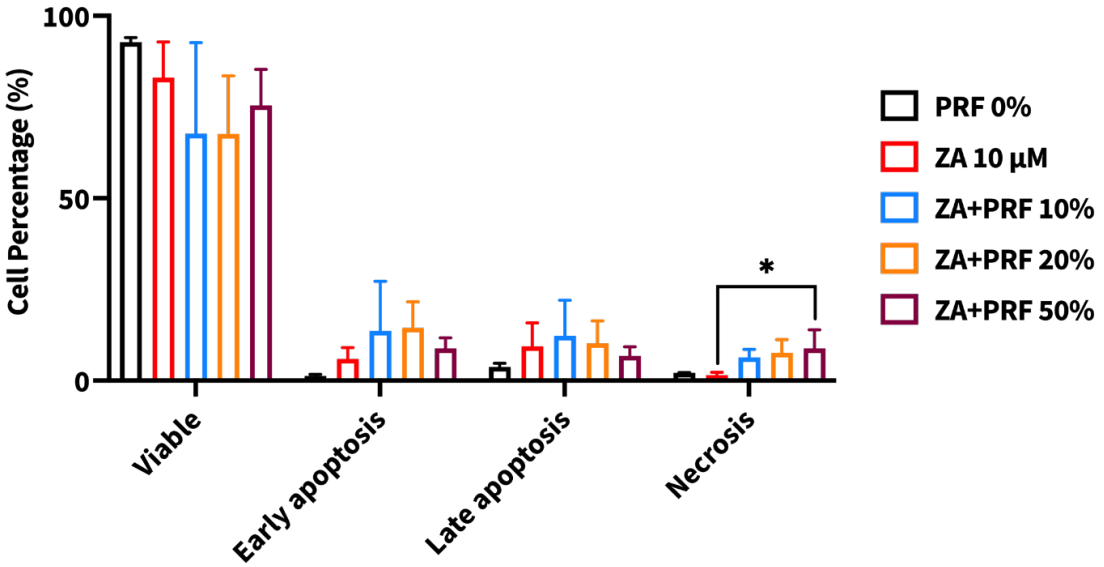

Figure 6.17 | Apoptotic status following annexin V-FITC and propidium iodide (PI) staining of primary oral fibroblasts (NOFs) treated with 10 µM ZA with I-PRF-derived conditioned medium. *NOFs were treated with different concentrations of I-PRF-derived conditioned medium in combination with 10 µM ZA for 72 hours. Cell status was assessed using annexin V-FITC and PI staining. Data are presented as the mean ± standard deviation from three independent experiments (N=3, n=1). Statistical significance was determined using a one-way ANOVA followed by Dunnett's multiple comparison against the 10 µM ZA of each group (* p<0.05). Abbreviations: ZA, zoledronate; PRF, platelet-rich fibrin; ANOVA, analysis of variance.*

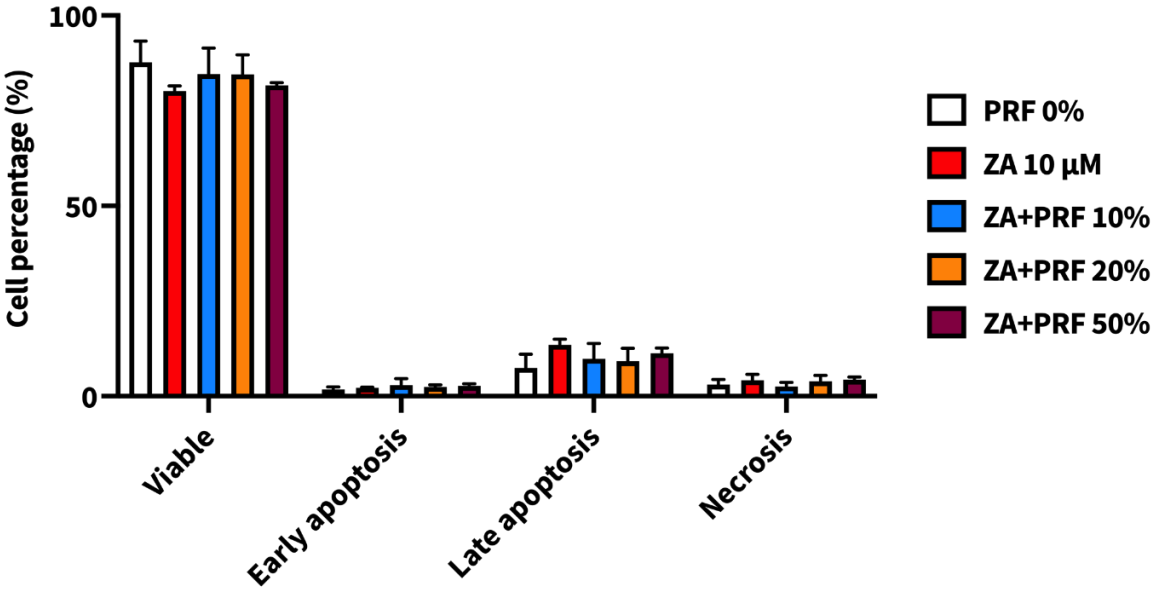

Figure 6.18 | Apoptotic status following annexin V-FITC and propidium iodide (PI) staining of immortalised oral keratinocytes (FNB6/TERT) treated with 10 µM ZA with I-PRF-derived conditioned medium. *FNB6/TERT were treated with different concentrations of I-PRF-derived conditioned medium in combination with 10 µM ZA for 72 hours. Cell status was assessed using Annexin V-FITC and PI staining. Data are presented as the mean ± standard deviation from three independent experiments (N=3, n=1). Statistical significance was determined using a one-way ANOVA followed by Dunnett's multiple comparison against the 10 µM ZA of each group. Abbreviations: ZA, zoledronate; PRF, platelet-rich fibrin; ANOVA, analysis of variance.*

A higher dose of PA than ZA was used to induce cell death. When 100 μM PA was added to NOFs, the number of unstained cells decreased, with only approximately 15% of cells still viable compared to over 90% of the untreated control. The amount of non-viable cells instead increased, with approximately 6% early apoptotic, over 75% late apoptotic, and 8% necrotic cells, as shown in Figure 6.19.

With the addition of I-PRF-derived conditioned medium, all concentrations produced higher viable cells than the PA-treated group; however, this was not significant. The number of cells in late apoptotic stages decreased dose-dependently, inversely proportional to the number of necrotic cells.

Figure 6.20 demonstrates the percentage of FNB6/TERT in each stage after treating with 30 μM PA with I-PRF-derived conditioned medium for 72 hours. The number of viable cells from the PA-treated condition was lower than the control; however, this was not significant. All doses of I-PRF-derived conditioned medium did not affect PA-induced cell death.

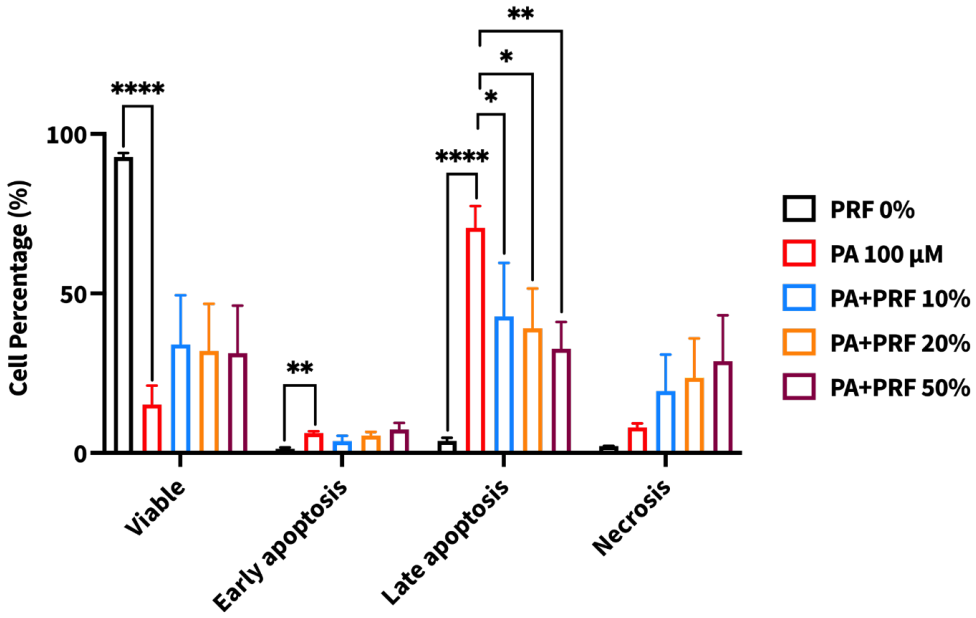

Figure 6.19 | Apoptotic status following annexin V-FITC and propidium iodide (PI) staining of primary oral fibroblasts (NOFs) treated with 100 µM PA with I-PRF-derived conditioned medium. *NOFs were treated with different concentrations of I-PRF-derived conditioned medium in combination with 100 µM PA for 72 hours. Cell status was assessed using annexin V-FITC and PI staining. Data are presented as the mean ± standard deviation from three independent experiments (N=3, n=1). Statistical significance was determined using a one-way ANOVA followed by Dunnett's multiple comparison against the 100 µM PA of each group (* p<0.05, ** p<0.01, ****p<0.0001). Abbreviations: PA, pamidronate; PRF, platelet-rich fibrin; ANOVA, analysis of variance.*

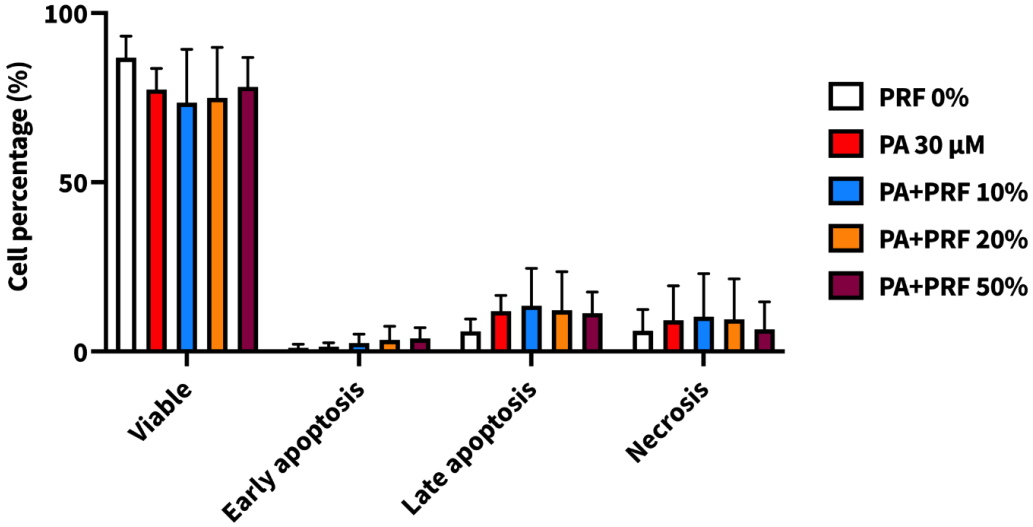

Figure 6.20 | Apoptotic status following annexin V-FITC and propidium iodide (PI) staining of immortalised oral keratinocytes (FNB6/TERT) treated with 30 µM PA with I-PRF-derived conditioned medium. *FNB6/TERT were treated with different concentrations of I-PRF-derived conditioned medium in combination with 30 µM PA for 72 hours. Cell status was assessed using Annexin V-FITC and PI staining. Data are presented as the mean ± standard deviation from three independent experiments (N=3, n=1). Statistical significance was determined using a one-way ANOVA, followed by Dunnett's multiple comparison against the 30 µM PA of each group. Abbreviations: PA, pamidronate; PRF, platelet-rich fibrin; ANOVA, analysis of variance.*

6.4.8 I-PRF increased the metabolic activity of ZA-treated TEOM

Though we obtained promising results from the 2D culture experiments, it is essential to study the biological effect of I-PRF in a setting that more closely resembles native oral tissues. TEOM containing both NOFs and FNB6/TERT has been used to produce *in vitro* models for bisphosphonate-induced soft tissue toxicity and examine whether I-PRF could reduce the toxicity.

To study the effect of the epithelium formation process, TEOM was constructed (Section 5.3.11) and immediately cultured with the conditioned medium containing both ZA and I-PRF after raising the models to ALI (Section 6.3.7). The metabolic activity was assessed as described previously (Section 5.3.12).

Figure 6.21 shows the metabolic activity of the TEOM after being treated with the conditioned medium containing ZA 10 µM with different concentrations of I-PRF for 14 days. Our results demonstrated the reduction of the metabolic activity of ZA-treated TEOM without I-PRF over 14 days, with a statistical significance observed on day 14. This indicates the toxicity of ZA on the oral mucosa. When I-PRF was added, the metabolic activity of the models increased in a dose-dependent fashion on days 7, 10, and 14. However, no statistical significance was observed from any conditions at any time point when compared to ZA treatment alone.

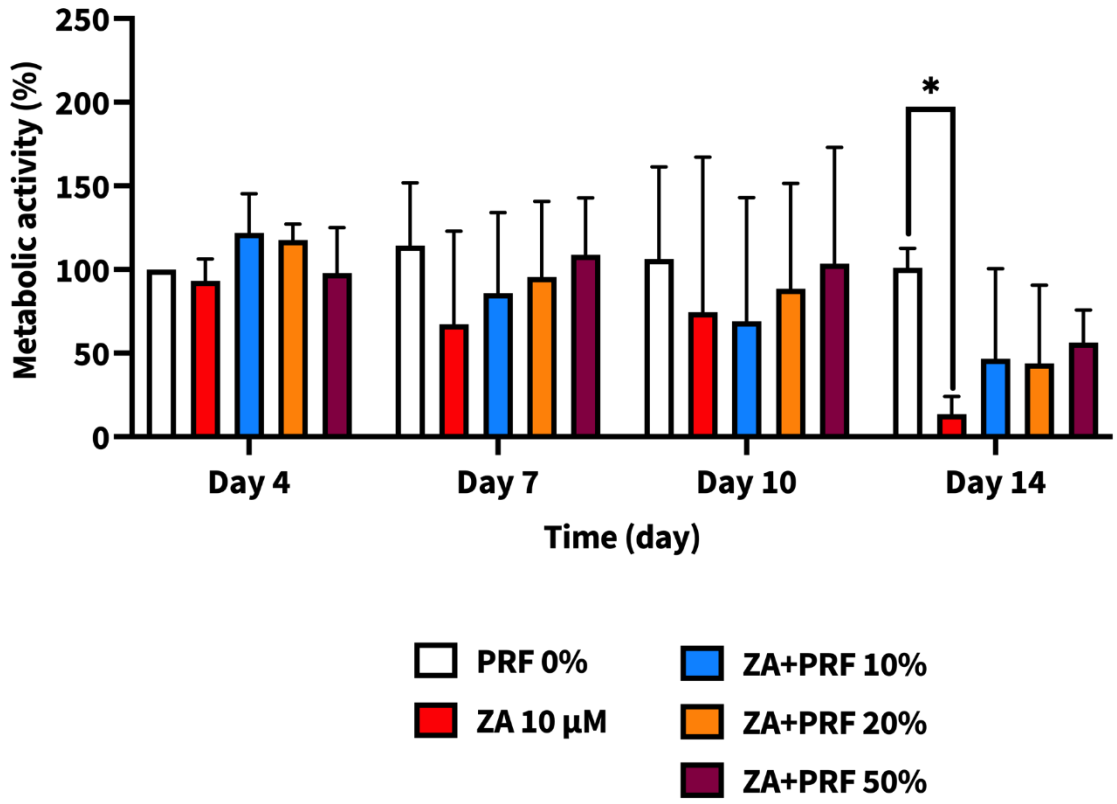

Figure 6.21 | ***Metabolic activity of tissue-engineered oral mucosa (TEOM) treated with 10 µM ZA and I-PRF-derived conditioned medium over 14 days****. TEOM was incubated at an air-liquid interface with different concentrations of I-PRF-derived condition medium in combination with 10 µM ZA for 14 days. Metabolic activity was assessed on days 4, 7, 10, and 14 using the resazurin assay. Data are presented as the mean ± standard deviation from three independent experiments (N=3, n=1). Statistical significance was determined using a one-way ANOVA, followed by Dunnett's multiple comparison against the 10 µM ZA at each time point (* p< 0.05). Abbreviations: ZA, zoledronate; PRF, platelet-rich fibrin; ANOVA, analysis of variance.*

Figure 6.22A demonstrates a thin layer of epithelium with some differentiated keratinocytes at the top layer obtained from the control TEOM after 4 days. When treated with 10 µM ZA, the epithelium was still present with a slight reduction in epithelial thickness, as shown in Figure 6.22B and 6.22F, respectively. However, this was not statistically significant. Figure 6.22C, D, and E shows the epithelial morphology of the TEOM following 4 days of treatment with the conditioned medium containing different I-PRF concentrations and 10 µM ZA. The histological analysis revealed that the epithelium morphology was quite similar across all conditions, with the epithelium two or three-cells thick. The thickness increased with increasing doses of I-PRF in a dose-dependent fashion, demonstrated in Figure 6.22F, without any statistical significance.

Figure 6.23 shows the epithelial morphology and thickness of TEOM after incubating with ZA and the conditioned medium for 7 days. A stratified epithelium was again seen from all conditions (Figure 6.23A, B, C, D, and E). However, a slightly thinner epithelium layer was observed from ZA-treated TEOM without I-PRF, as shown in Figure 6.23B. This was correlated with the thickness measurement demonstrated in Figure 6.23F, as the epithelial thickness was lower in comparison to the control. The addition of I-PRF produced a slightly thicker epithelium when compared to the ZA-treated TEOM alone. However, no statistical significance was found.

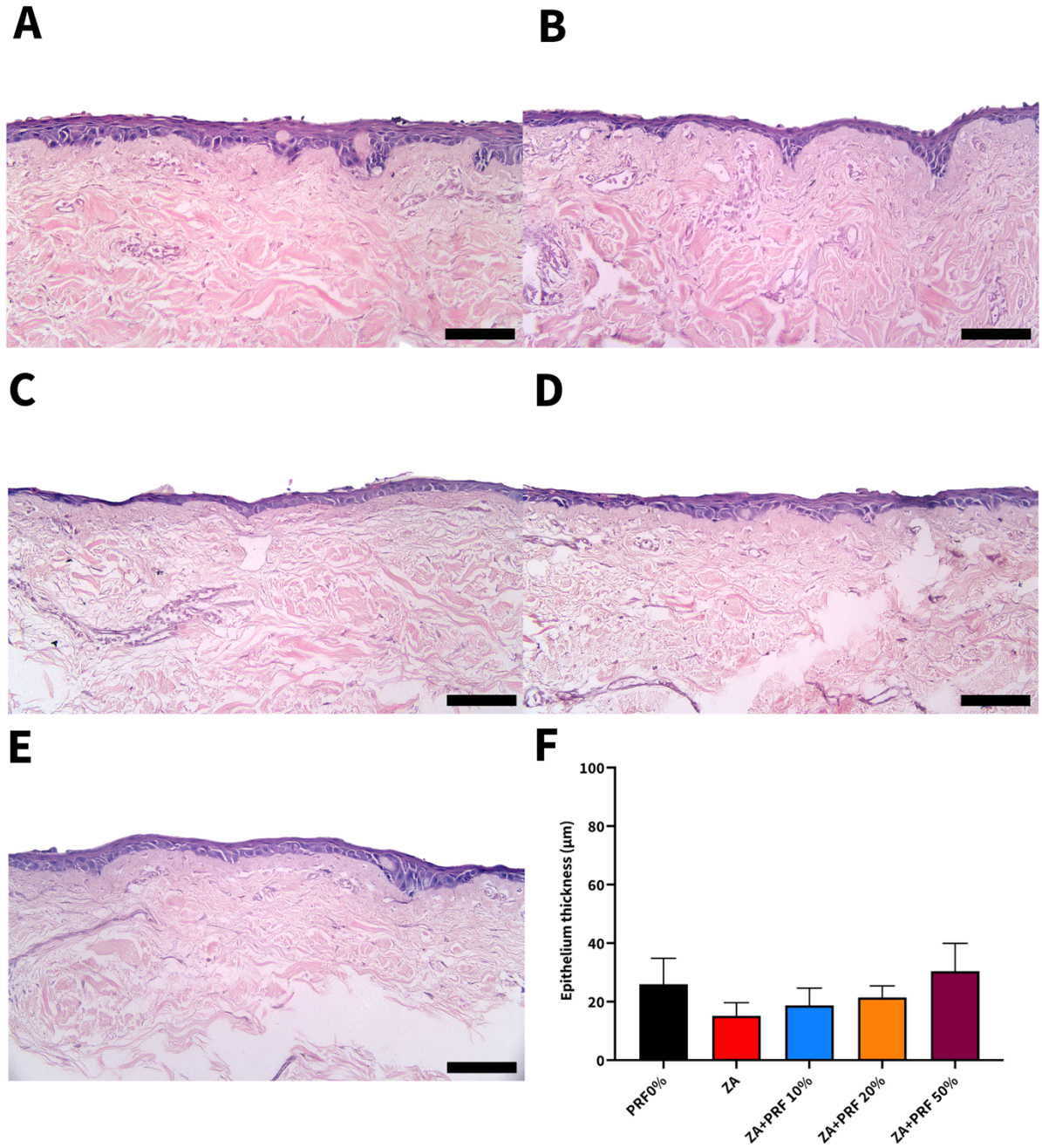

Figure 6.22 | H&E-stained sections of tissue-engineered oral mucosa (TEOM) treated with 10 µM ZA and I-PRF-derived conditioned medium for 4 days. *Panels display TEOM sections cultured in conditioned medium containing (A) PRF 0%, (B) ZA 10 µM, (C) ZA+PRF 10%, (D) ZA+PRF 20% and (E) ZA+PRF 50% for 4 days. (F) demonstrates the epithelium thickness of TEOM after 4 days of culture. Representative images from three independent experiments (N=3, n=1) were used. Scale bar = 100 µm (20x magnification). A one-way ANOVA followed by Dunnett's multiple comparison was carried out on the data in (F) to test the statistical significance against the control (PRF 0%). Abbreviations: H&E, haematoxylin and eosin; TEOM, tissue-engineered oral mucosa; PRF, platelet-rich fibrin; ZA, zoledronate; ANOVA, analysis of variance.*

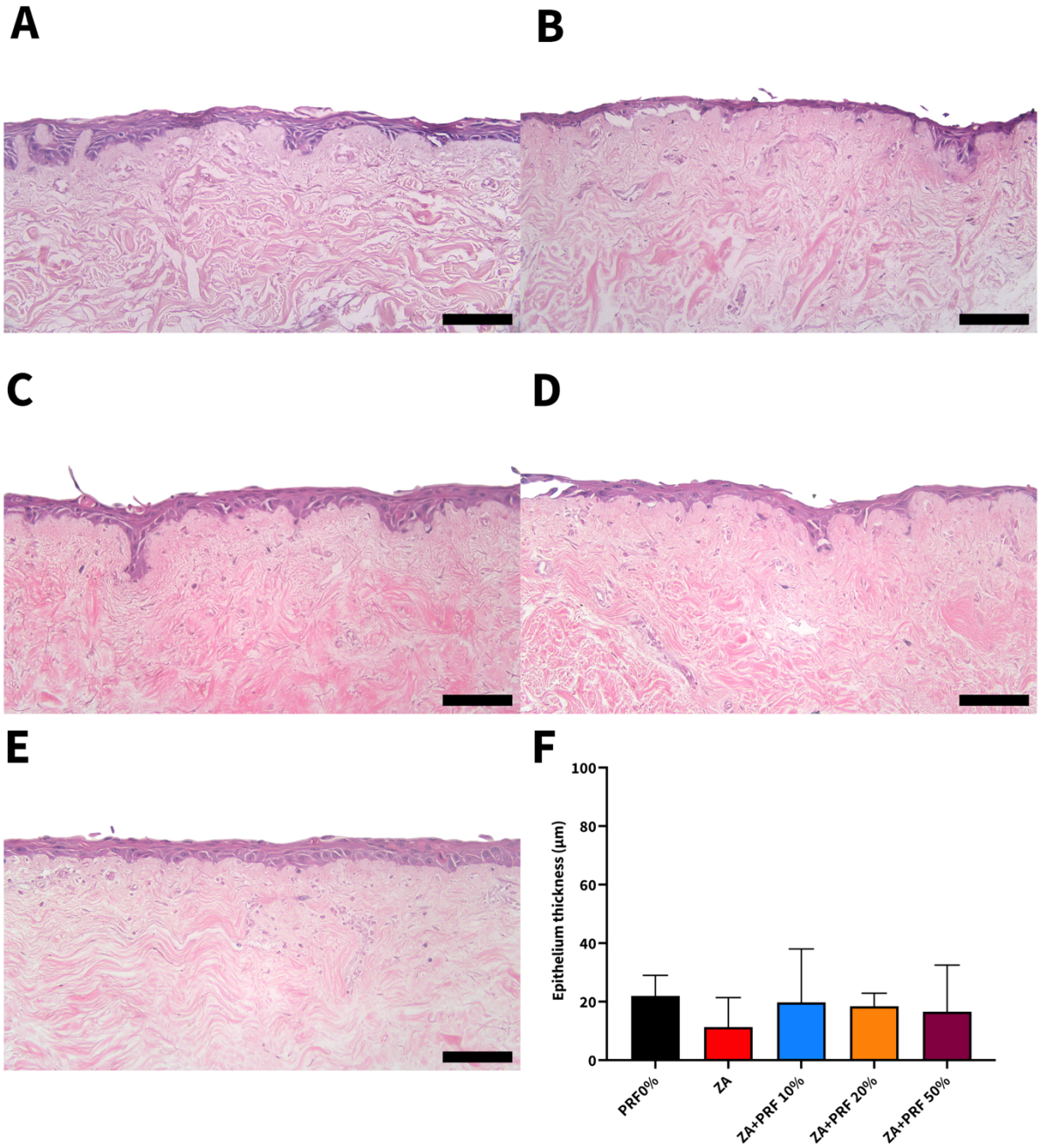

Figure 6.23 | H&E-stained sections of tissue-engineered oral mucosa (TEOM) treated with 10 µM ZA and I-PRF-derived conditioned medium for 7 days. *Panels display TEOM sections cultured in conditioned medium containing (A) PRF 0%, (B) ZA 10 µM, (C) ZA+PRF 10%, (D) ZA+PRF 20% and (E) ZA+PRF 50% for 4 days. (F) demonstrates the epithelium thickness of TEOM after 7 days of culture. Representative images from three independent experiments (N=3, n=1) were used. Scale bar = 100 µm (20x magnification). A one-way ANOVA followed by Dunnett's multiple comparison was carried out on the data in (F) to test the statistical significance against the control (PRF 0%). Abbreviations: H&E, haematoxylin and eosin; TEOM, tissue-engineered oral mucosa; PRF, platelet-rich fibrin; ZA, zoledronate; ANOVA, analysis of variance.*

After 10 days in culture, a multi-layered stratified squamous epithelium of the control TEOM was demonstrated, as shown in Figure 6.24A. Cuboidal keratinocytes were seen in the basal cell layer, above which were squamous keratinocytes and superficially differentiated flattened keratinocytes could be observed.

A complete loss of epithelial layer was seen after 10 days of culture in the conditioned medium containing ZA 10 µM alone (Figure 6.24B). When I-PRF was added, the epithelium remained visible in all I-PRF-treated conditions after 10 days (Figure 6.24C, D, and E). The thickness measurements supported the histological appearance, shown in Figure 6.24F, with ZA significantly reducing the thickness of TEOM. The addition of I-PRF produced a thicker epithelium layer than the ZA treatment alone. However, there was no statistical significance.

TUNEL assay is used to detect DNA breaks which can be found in cells undergoing apoptosis. This assay was used to evaluate whether I-PRF could reduce bisphosphonate-induced cell apoptosis in 3D models of the oral mucosa (Section 6.3.9). Green stained nuclei indicate viable cells, while apoptotic cells are indicated when nuclei stain brown. Figure 6.25B shows the brown stained cells across the epithelium layer of ZA-treated TEOM after 10 days. The addition of all I-PRF doses produced less visible brown-stained epithelial cells and more green-stained cells, as shown in Figures 6.25C, D, and E, indicating a possibly lower number of apoptotic cells compared to TEOM with ZA treatment alone.

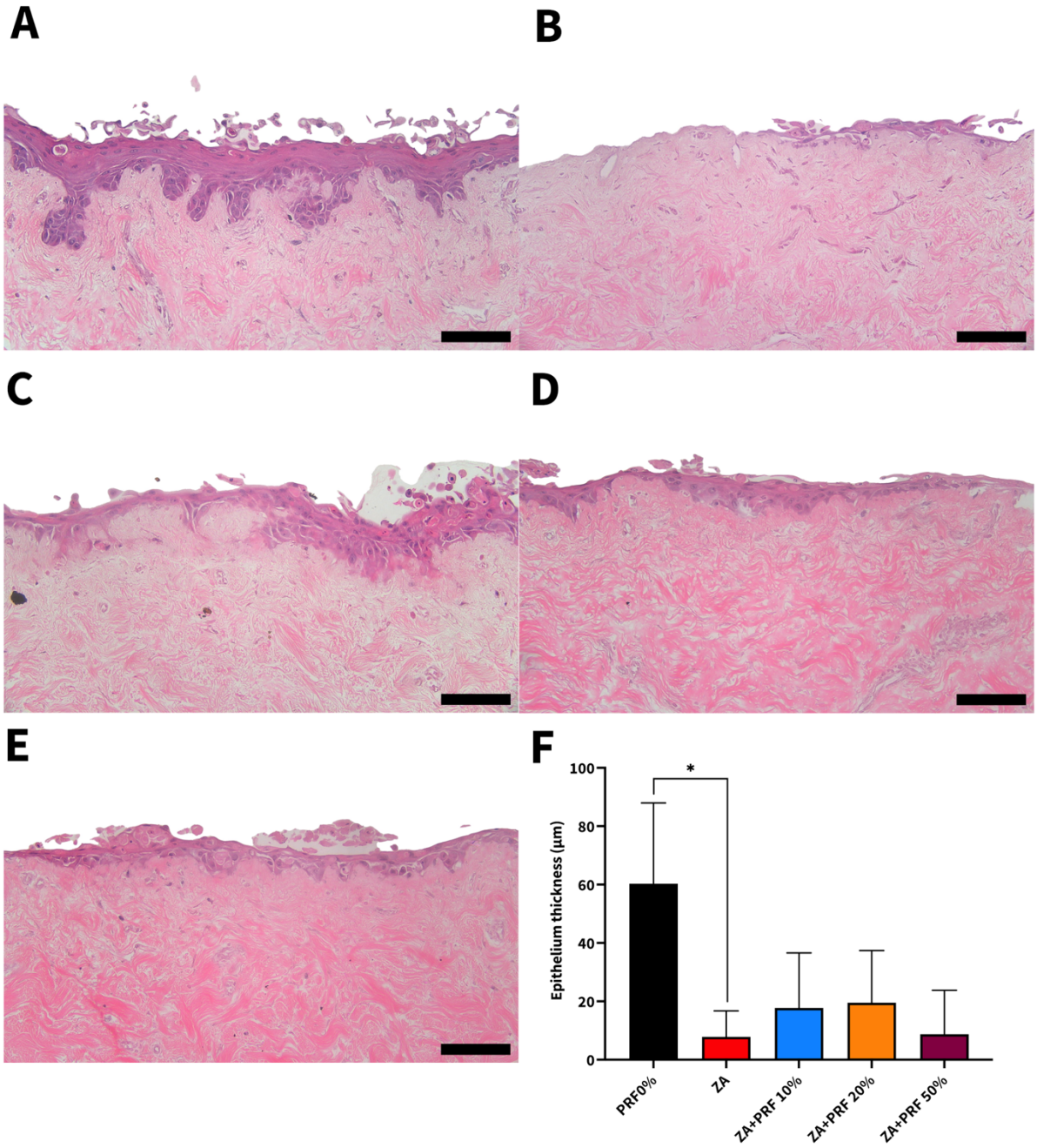

Figure 6.24 | ***H&E-stained sections of tissue-engineered oral mucosa (TEOM) treated with 10 µM ZA and I-PRF-derived conditioned medium for 10 days.*** *Panels display TEOM sections cultured in conditioned medium containing (A) PRF 0%, (B) ZA 10 µM, (C) ZA+PRF 10%, (D) ZA+PRF 20% and (E) ZA+PRF 50% for 10 days. (F) demonstrates the epithelium thickness of TEOM after 10 days of culture. Representative images from three independent experiments (N=3, n=1) were used. Scale bar = 100 µm (20x magnification). A one-way ANOVA followed by Dunnett's multiple comparison was carried out on the data in (F) to test the statistical significance against the ZA 10 µM (* $p<0.05$). Abbreviations: H&E, haematoxylin and eosin; TEOM, tissue-engineered oral mucosa; PRF, platelet-rich fibrin; ZA, zoledronate; ANOVA, analysis of variance.*

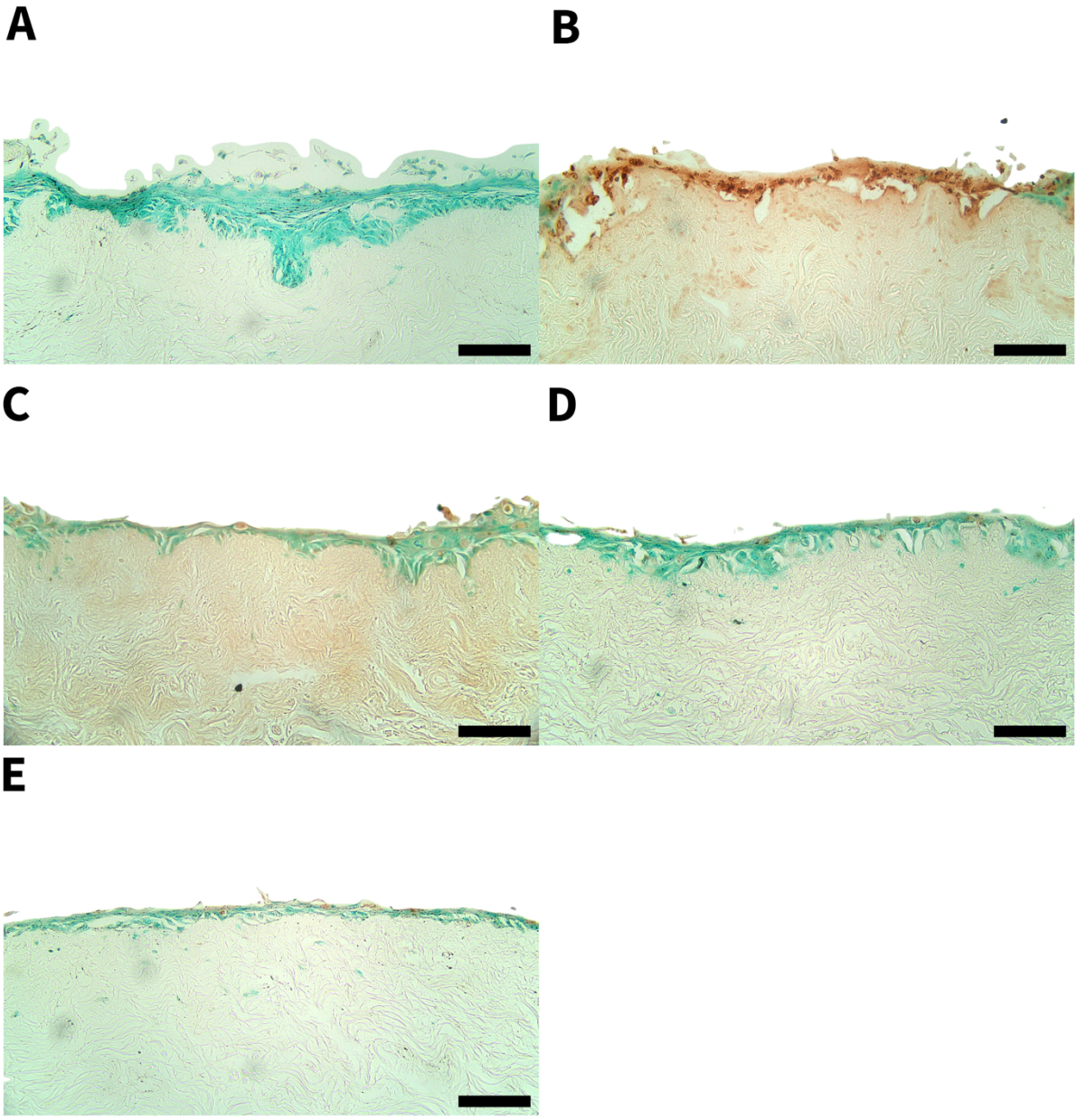

Figure 6.25* | *TUNEL-stained sections of tissue-engineered oral mucosa (TEOM) treated with 10 µM ZA and I-PRF-derived conditioned medium for 10 days. *TEOM sections were cultured in conditioned medium containing (A) PRF 0%, (B) ZA 10 µM, (C) ZA+PRF 10%, (D) ZA+PRF 20% and (E) ZA+PRF 50% for 10 days, and TUNEL assay was carried out. Green stained nuclei indicate viable cells, while apoptotic cells are indicated when nuclei stain brown. Representative images were used. Scale bar = 100 µm (20x magnification). Abbreviations: TUNEL, terminal deoxynucleotidyl transferase-mediated dUTP nick end labelling; TEOM, tissue-engineered oral mucosa; PRF, platelet-rich fibrin; ZA, zoledronate.*

Figure 6.26 shows the histological sections of TEOM after culturing for 14 days. A histological section of control TEOM, shown in Figure 6.26A, demonstrated a multi-layered epithelium of viable cells, confirmed by TUNEL assay (Figure 6.27A), as seen previously during earlier time points. Similar to day 10, a complete loss of epithelium layer was observed from TEOM treated with ZA alone without I-PRF. TEOM sections obtained on day 14, shown in Figure 6.26C, D, and E, demonstrated that TEOM cultured with ZA and all concentrations of I-PRF were only able to produce a single epithelial layer which was disrupted and damaged. A mix of cells with TUNEL-positive (brown-stained) and -negative (green-stained) nuclei were observed from all concentrations of PRF (Figure 6.27C, D, and E). The thickness measurement data, demonstrated in Figure 6.26F, showed no difference between all conditions of I-PRF treatment to the ZA-treated TEOM alone.

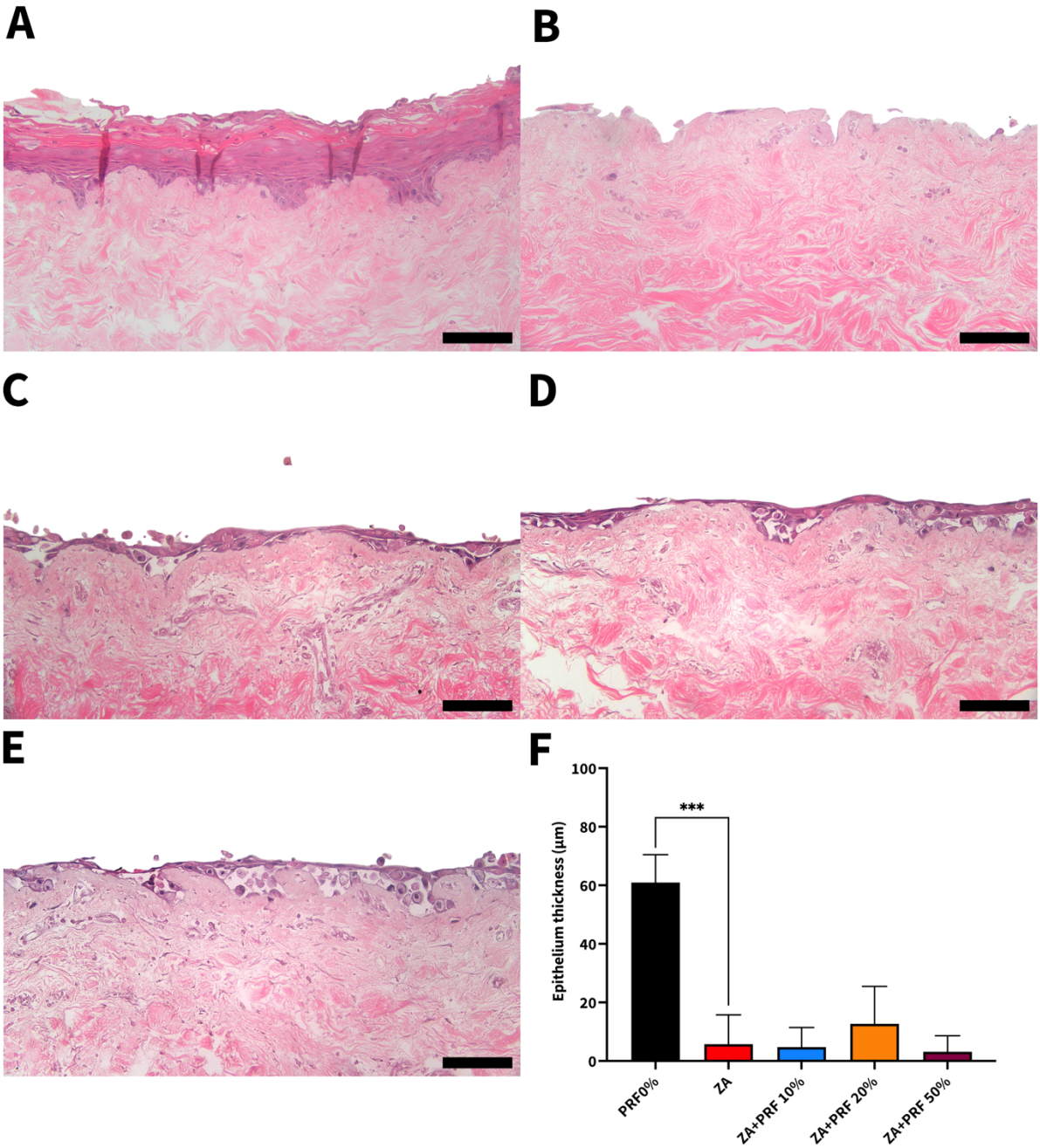

Figure 6.26 | H&E-stained sections of tissue-engineered oral mucosa (TEOM) treated with 10 µM ZA and I-PRF-derived conditioned medium for 14 days. *Panels display TEOM sections cultured in conditioned medium containing (A) PRF 0%, (B) ZA 10 µM, (C) ZA+PRF 10%, (D) ZA+PRF 20% and (E) ZA+PRF 50% for 14 days. (F) demonstrates the epithelium thickness of TEOM after 14 days of culture. Representative images from three independent experiments (N=3, n=1) were used. Scale bar = 100 µm (20x magnification). A one-way ANOVA followed by Dunnett's multiple comparison was carried out on the data in (F) to test the statistical significance against the ZA 10 µM (*** p<0.001). Abbreviations: H&E, haematoxylin and eosin; TEOM, tissue-engineered oral mucosa; PRF, platelet-rich fibrin; ZA, zoledronate; ANOVA, analysis of variance.*

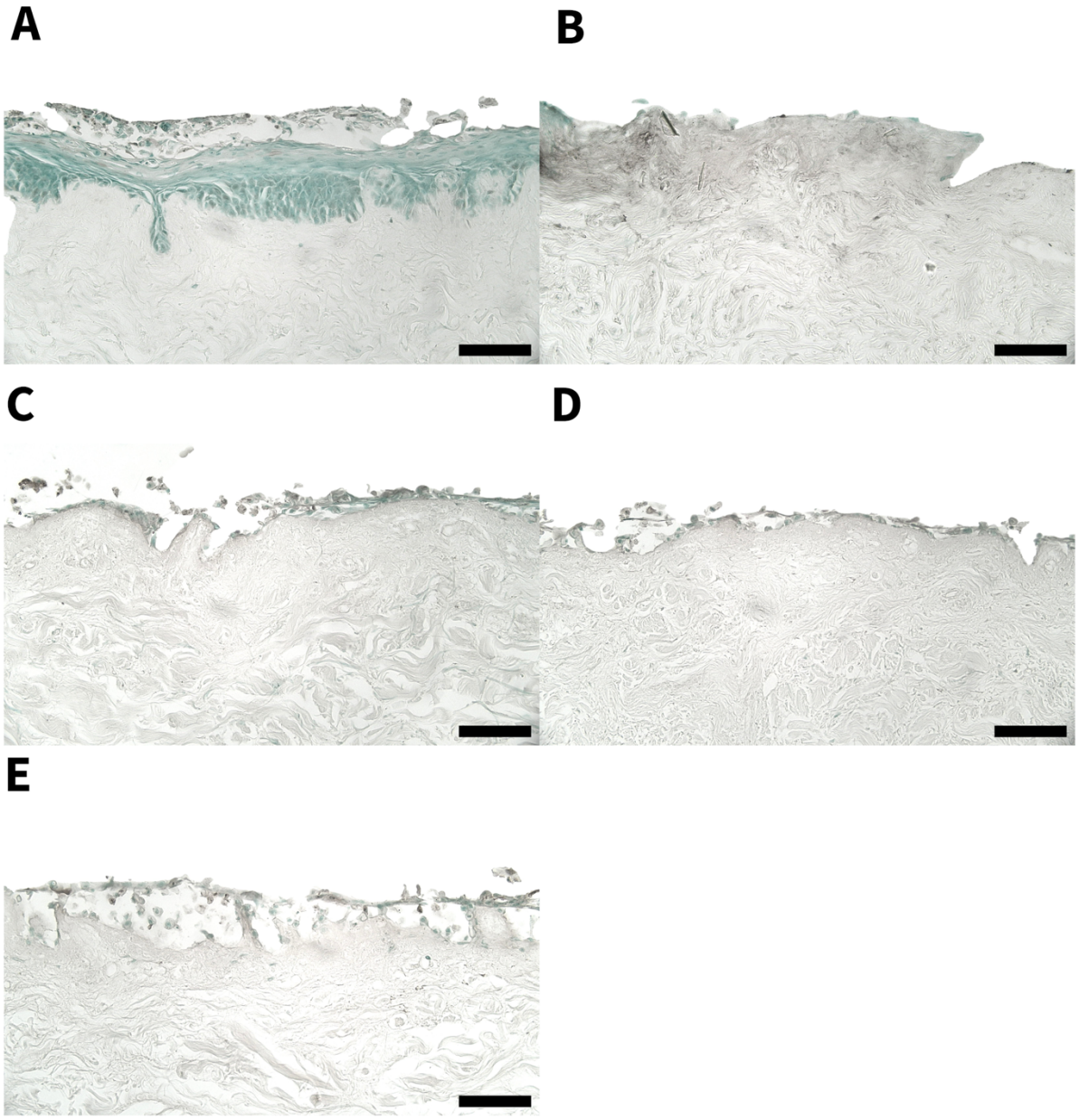

Figure 6.27 | TUNEL-stained sections of tissue-engineered oral mucosa (TEOM) treated with 10 µM ZA and I-PRF-derived conditioned medium for 14 days. *TEOM sections were cultured in conditioned medium containing (A) PRF 0%, (B) ZA 10 µM, (C) ZA+PRF 10%, (D) ZA+PRF 20% and (E) ZA+PRF 50% for 14 days, and TUNEL assay was carried out. Green stained nuclei indicate viable cells, while apoptotic cells are indicated when nuclei stain brown. Representative images were used. Scale bar = 100 µm (20x magnification). Abbreviations: TUNEL, terminal deoxynucleotidyl transferase-mediated dUTP nick end labelling; TEOM, tissue-engineered oral mucosa; PRF, platelet-rich fibrin; ZA, zoledronate.*

6.4.9 I-PRF did not affect the metabolic activity, epithelium morphology and thickness of PA-treated TEOM

Following the experiments on how I-PRF affects the epithelium stratification of TEOM in the presence of ZA, we replaced ZA with PA since PA has also been reported to be associated with the development of MRONJ in patients [9]. The concentration of PA (50 µM) was selected based on the previous work in our group, which is the minimum concentration to produce toxicity [120]. Figure 6.28 shows that the metabolic activity of the control (PRF 0%) was increased over the experimental course. When treated with PA alone, the metabolism of TEOM was not affected at any time points. Interestingly, a slight increase of the metabolic activity value compared to the control was observed on days 10 and 14. The addition of I-PRF-derived conditioned medium also did not produce any significant effect on the TEOM metabolism at any time point. This was in line with the histological analysis, shown in Figure 6.29 – 6.32 (A - E), with the multi-layered epithelium of TEOM remaining visible after the treatment with either PA alone or I-PRF combined with PA. The measurement of epithelium thickness was performed, and only a slight reduction was observed from PA-treated TEOM without I-PRF from day 7, shown in Figure 6.30F. The addition of I-PRF in the conditioned medium did not affect the epithelium thickness. A similar trend was observed on days 10 and 14, shown in Figure 6.31F and 6.32F, respectively. No statistical difference between any conditions was found at any time point.

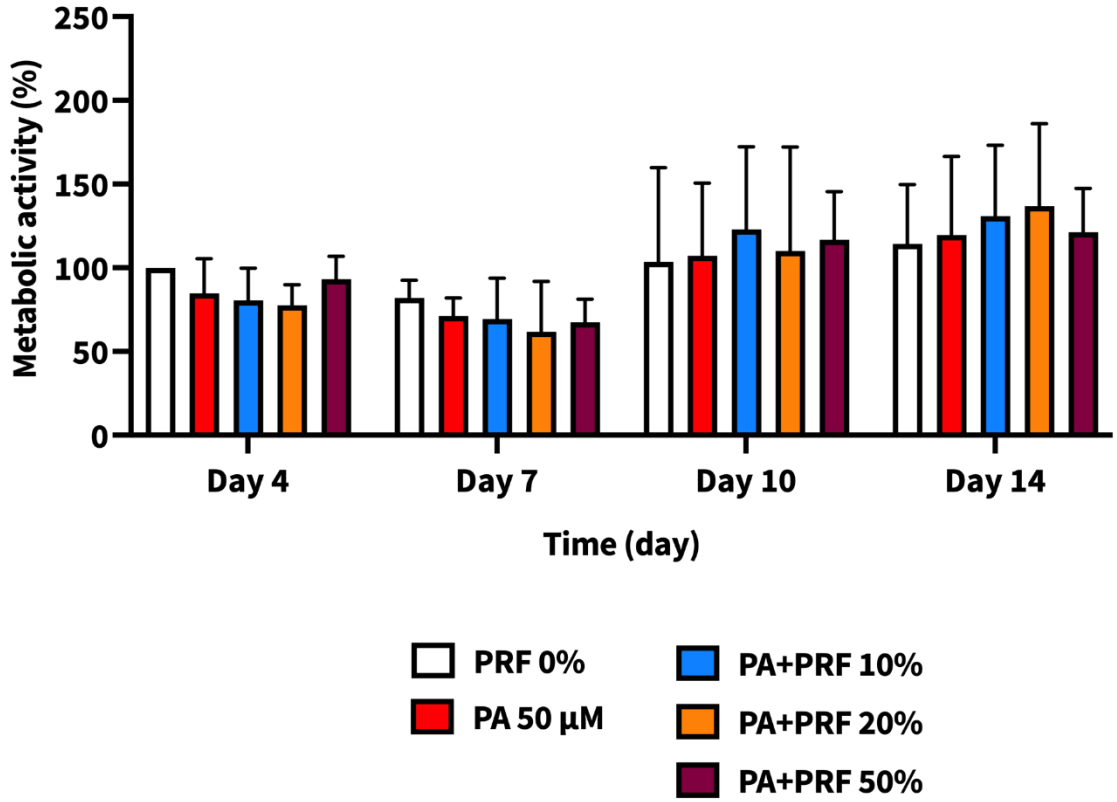

Figure 6.28 | ***Metabolic activity of tissue-engineered oral mucosa (TEOM) treated with 50 µM PA and I-PRF-derived conditioned medium over 14 days****. TEOM was incubated at an air-liquid interface with different concentrations of I-PRF-derived condition medium in combination with 50 µM PA for 14 days. Metabolic activity was assessed on days 4, 7, 10, and 14 using the resazurin assay. Data are presented as the mean ± standard deviation from three independent experiments (N=3, n=1). Statistical significance was determined using a one-way ANOVA, followed by Dunnett's multiple comparison against the 10 µM ZA at each time point. Abbreviations: PA, pamidronate; PRF, platelet-rich fibrin; ANOVA, analysis of variance.*

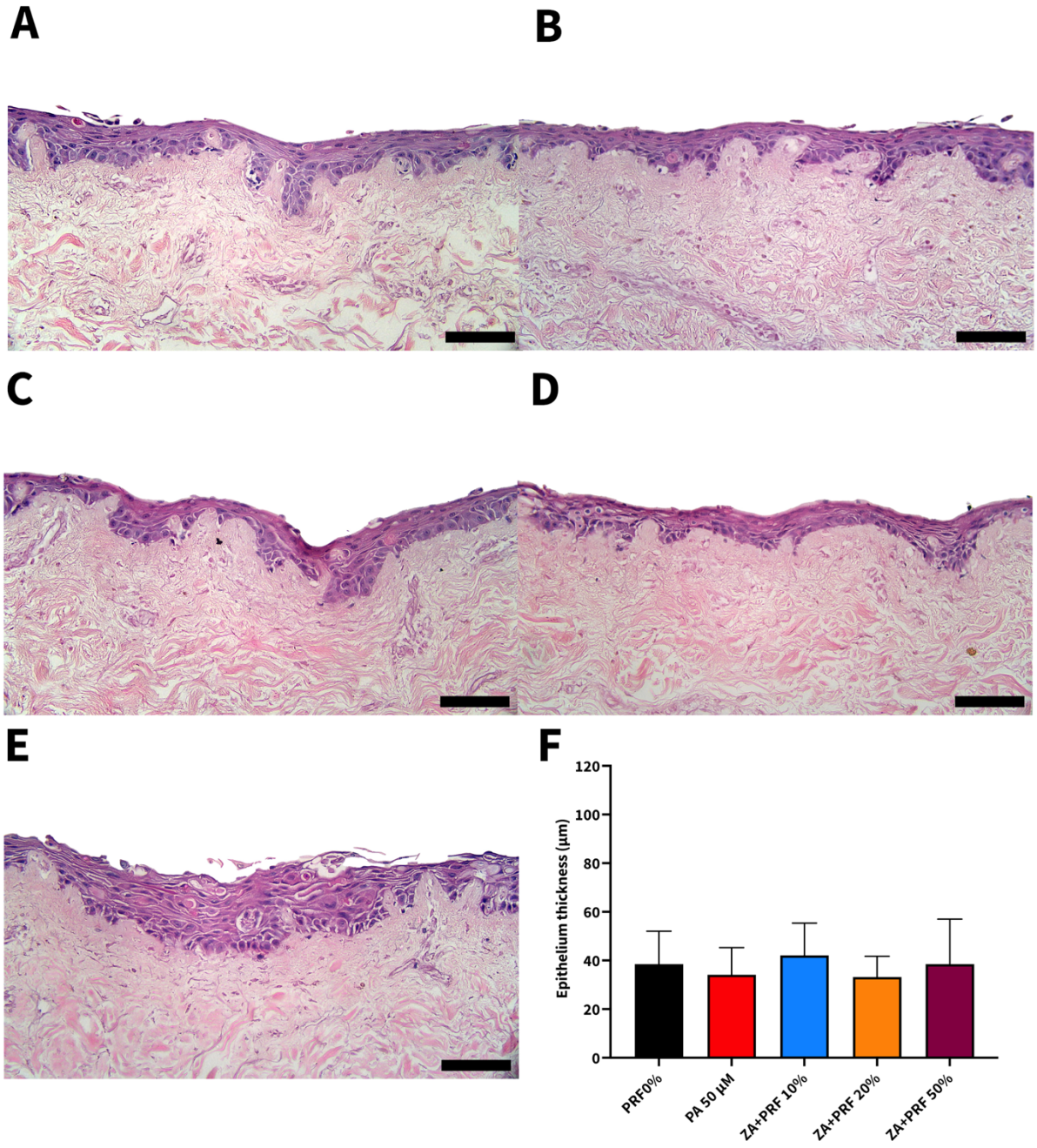

Figure 6.29 | H&E-stained sections of tissue-engineered oral mucosa (TEOM) treated with 50 µM PA and I-PRF-derived conditioned medium for 4 days. *Panels display TEOM sections cultured in conditioned medium containing (A) PRF 0%, (B) PA 50 µM, (C) PA+PRF 10%, (D) PA+PRF 20% and (E) PA+PRF 50% for 10 days. (F) demonstrates the epithelium thickness of TEOM after 4 days of culture. Representative images from three independent experiments (N=3, n=1) were used. Scale bar = 100 µm (20x magnification). A one-way ANOVA followed by Dunnett's multiple comparison was carried out on the data in (F) to test the statistical significance against the PA 50 µM. Abbreviations: H&E, haematoxylin and eosin; TEOM, tissue-engineered oral mucosa; PRF, platelet-rich fibrin; PA, pamidronate; ANOVA, analysis of variance.*

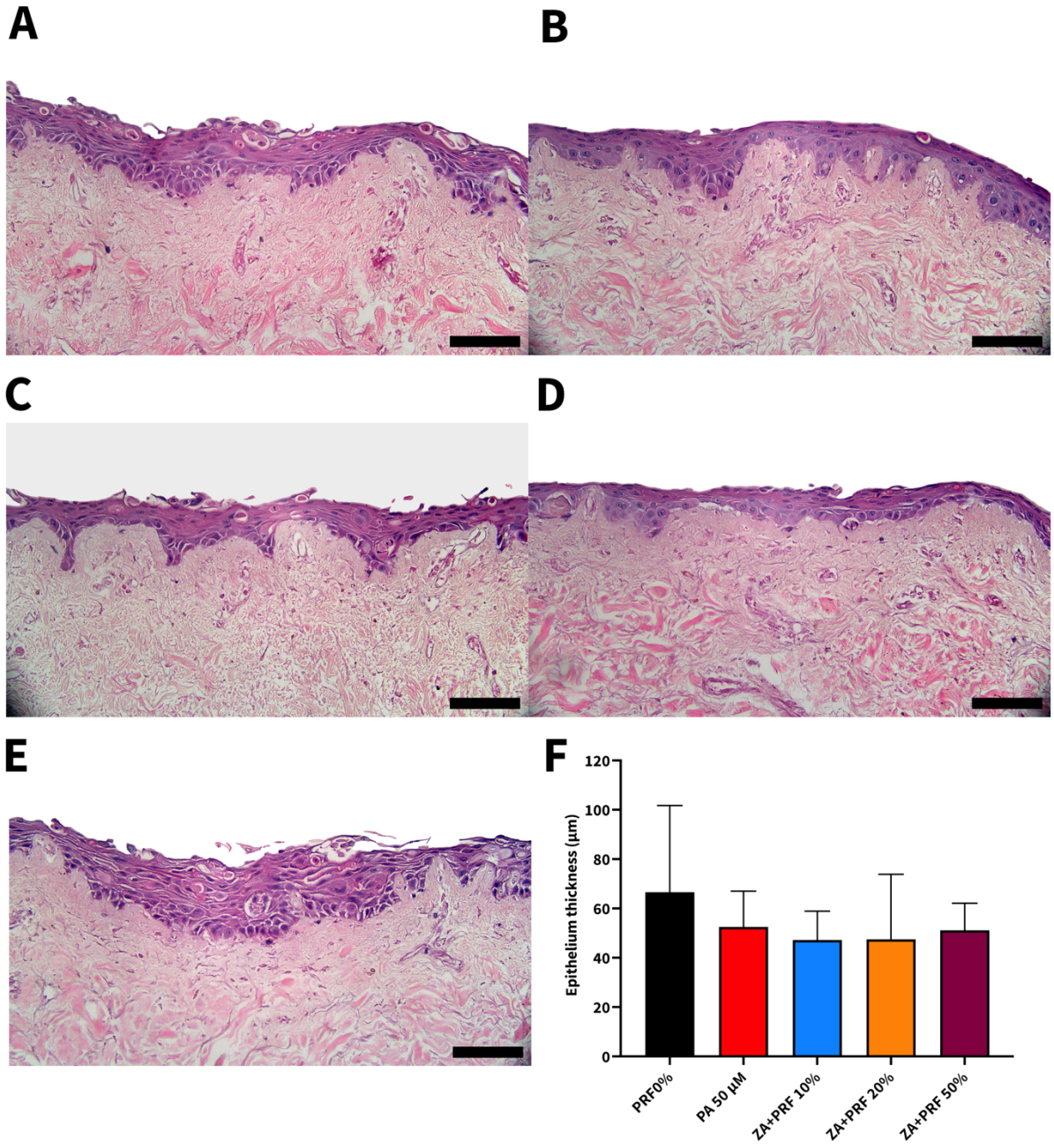

Figure 6.30 | H&E-stained sections of tissue-engineered oral mucosa (TEOM) treated with 50 µM PA and I-PRF-derived conditioned medium for 7 days. *Panels display TEOM sections cultured in conditioned medium containing (A) PRF 0%, (B) PA 50 µM, (C) PA+PRF 10%, (D) PA+PRF 20% and (E) PA+PRF 50% for 7 days. (F) demonstrates the epithelium thickness of TEOM after 7 days of culture. Representative images from three independent experiments (N=3, n=1) were used. Scale bar = 100 µm (20x magnification). A one-way ANOVA followed by Dunnett's multiple comparison was carried out on the data in (F) to test the statistical significance against the PA 50 µM. Abbreviations: H&E, haematoxylin and eosin; TEOM, tissue-engineered oral mucosa; PRF, platelet-rich fibrin; PA, pamidronate; ANOVA, analysis of variance.*

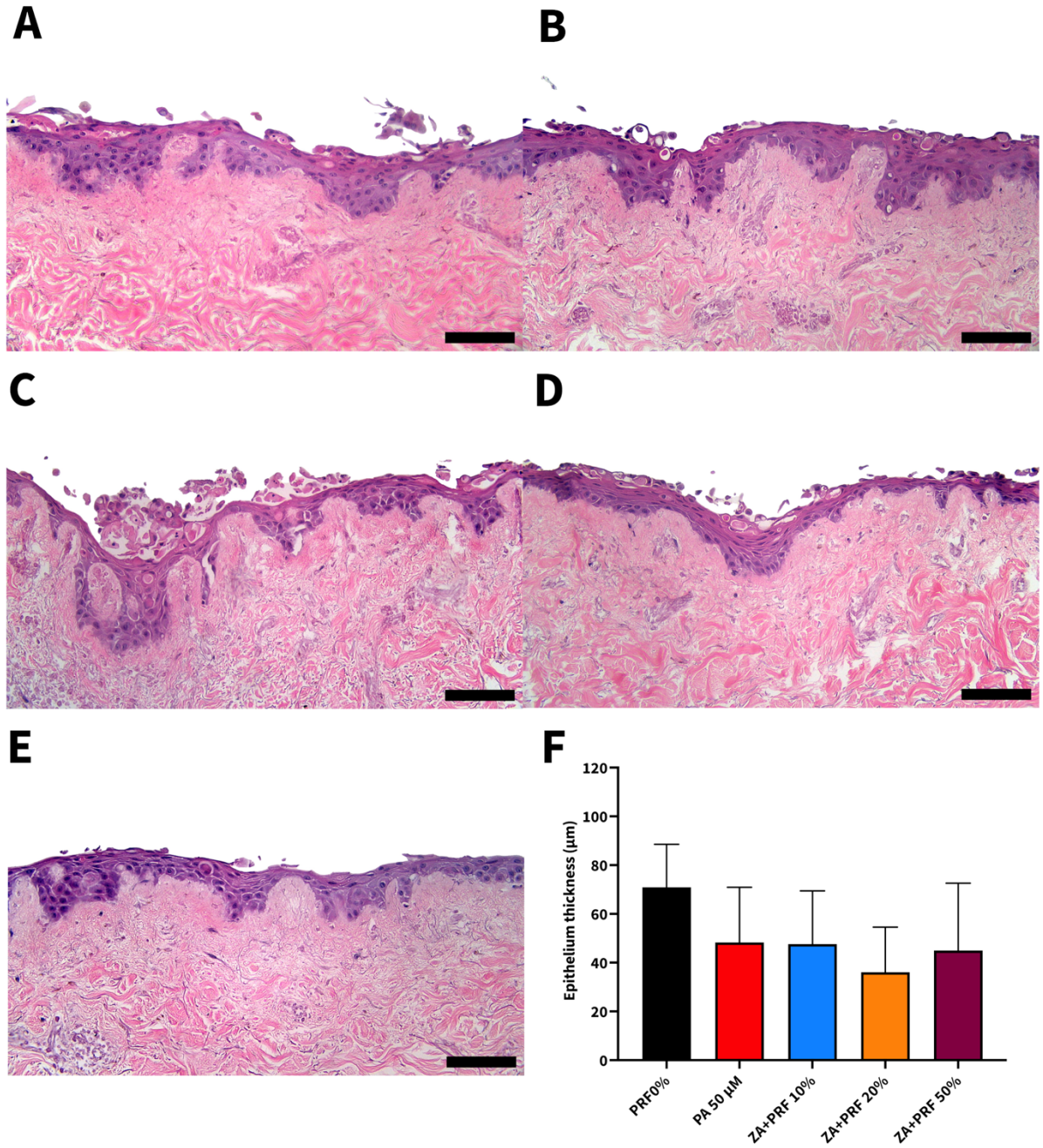

Figure 6.31 | ***H&E-stained sections of tissue-engineered oral mucosa (TEOM) treated with 50 µM PA and I-PRF-derived conditioned medium for 10 days.*** *Panels display TEOM sections cultured in conditioned medium containing (A) PRF 0%, (B) PA 50 µM, (C) PA+PRF 10%, (D) PA+PRF 20% and (E) PA+PRF 50% for 10 days. (F) demonstrates the epithelium thickness of TEOM after 10 days of culture. Representative images from three independent experiments (N=3, n=1) were used. Scale bar = 100 µm (20x magnification). A one-way ANOVA followed by Dunnett's multiple comparison was carried out on the data in (F) to test the statistical significance against the PA 50 µM. Abbreviations: H&E, haematoxylin and eosin; TEOM, tissue-engineered oral mucosa; PRF, platelet-rich fibrin; PA, pamidronate; ANOVA, analysis of variance.*

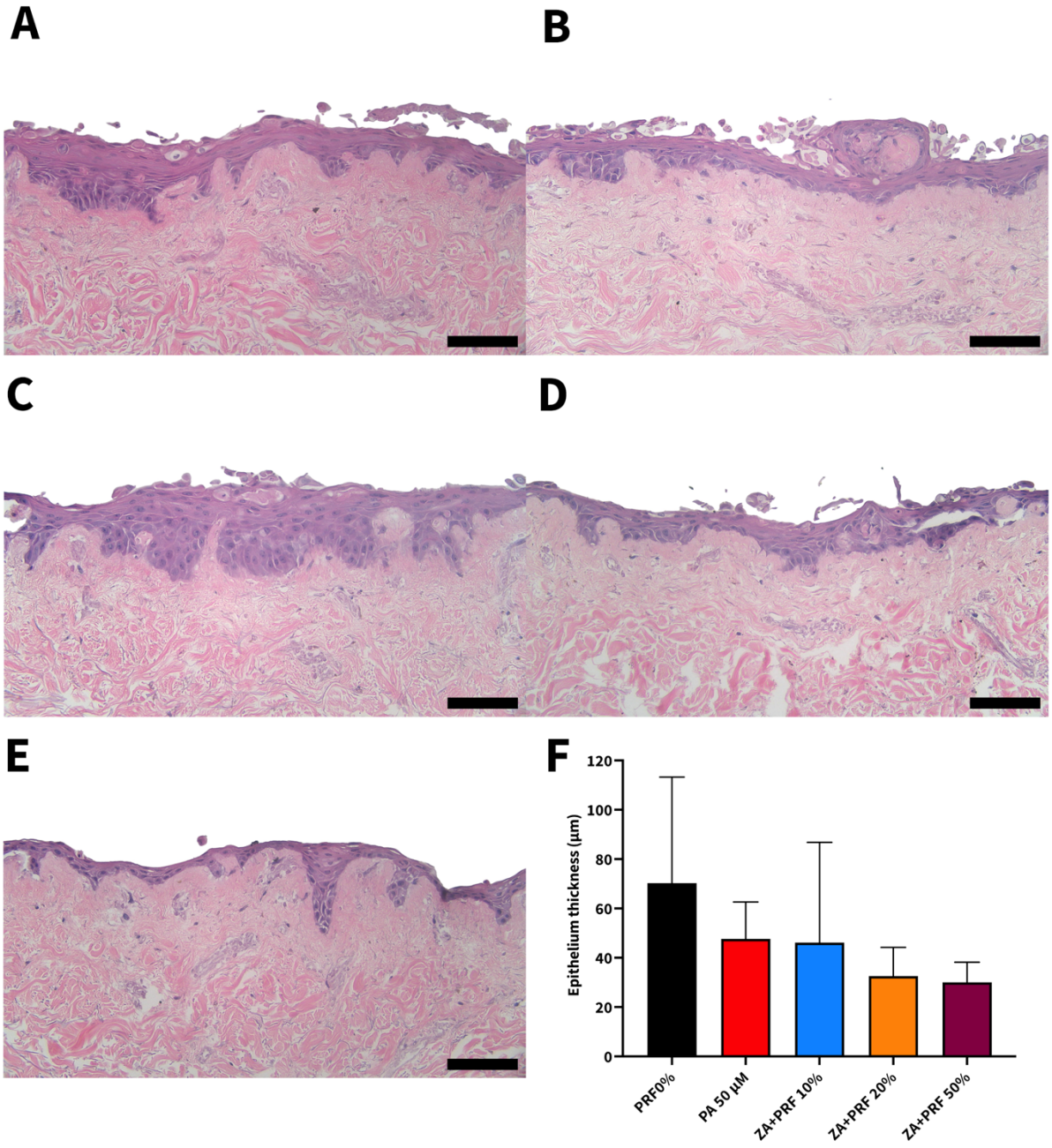

Figure 6.32 | ***H&E-stained sections of tissue-engineered oral mucosa (TEOM) treated with 50 µM PA and I-PRF-derived conditioned medium for 14 days.*** *Panels display TEOM sections cultured in conditioned medium containing (A) PRF 0%, (B) PA 50 µM, (C) PA+PRF 10%, (D) PA+PRF 20% and (E) PA+PRF 50% for 14 days. (F) demonstrates the epithelium thickness of TEOM after 14 days of culture. Representative images from three independent experiments (N=3, n=1) were used. Scale bar = 100 µm (20x magnification). A one-way ANOVA followed by Dunnett's multiple comparison was carried out on the data in (F) to test the statistical significance against the 50 µM PA. Abbreviations: H&E, haematoxylin and eosin; TEOM, tissue-engineered oral mucosa; PRF, platelet-rich fibrin; PA, pamidronate; ANOVA, analysis of variance.*

6.4.10 I-PRF did not affect the established epithelium of ZA-treated TEOM

To study the effect of I-PRF on established epithelium, TEOM was cultured in Green's medium at ALI for 7 days before the medium was replaced with either the basal medium (PRF 0%) or the conditioned medium containing ZA alone or I-PRF with ZA (Section 6.3.8). TEOM was cultured for an additional 7 days. Only the experiments on ZA-treated TEOM were carried out based on the previous results of our group. Our data has previously shown that 30 µM ZA reduced the metabolic activity of TEOM on day 14, while PA did not produce any effect [7].

Figure 6.33 shows the metabolic activity of TEOM after treating with ZA and I-PRF-conditioned medium. On day 10, there was no significant change in the metabolic activity between any conditions, including the ZA treatment alone without I-PRF. Data was supported by histological images, shown in Figure 6.34B, as the multi-layered epithelium was still present compared to the control TEOM (Figure 6.34A). Figure 6.34C, D, E, and F demonstrate that the addition of I-PRF to ZA-treated TEOM did not affect the epithelial morphology and thickness of TEOM after 10 days of culture.

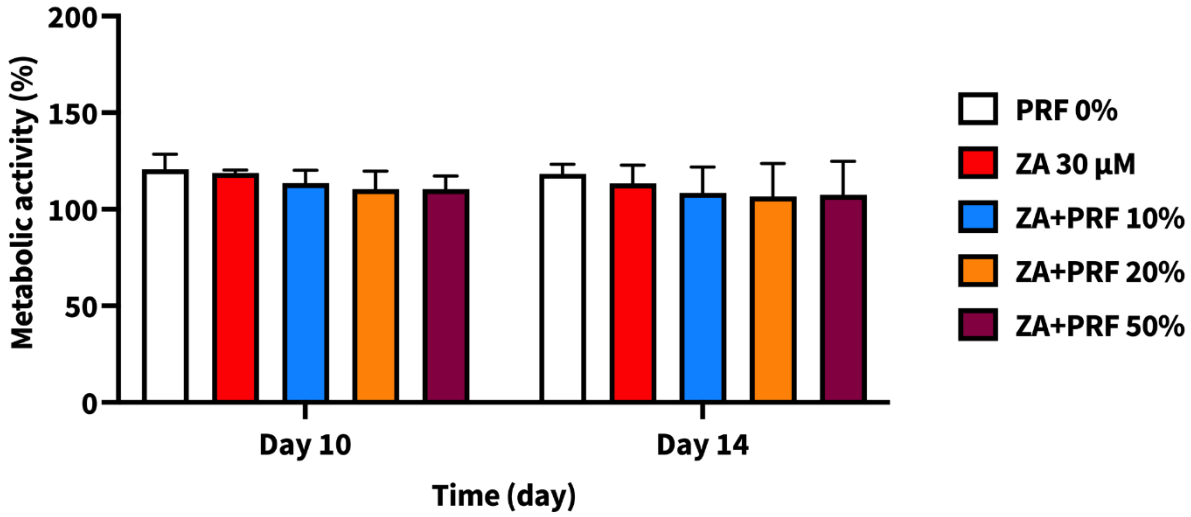

Figure 6.33 | Metabolic activity of tissue-engineered oral mucosa (TEOM) treated with Green's medium and I-PRF-derived conditioned medium with 30 µM ZA over 14 days. *TEOM was incubated with Green's medium at an air-liquid interface for the first 7 days, then cultured in varying concentrations of I-PRF-derived condition medium combined with 30 µM ZA for an additional 7 days (total of 14 days). Metabolic activity was assessed on days 10 and 14 using the resazurin assay. Data are presented as the mean ± standard deviation from three independent experiments (N=3, n=1). Statistical significance was determined using a one-way ANOVA followed by Dunnett's multiple comparison against the 30 µM ZA at each time point. Abbreviations: TEOM, tissue-engineered oral mucosa; PRF, platelet-rich fibrin; ZA, zoledronate; ANOVA, analysis of variance.*

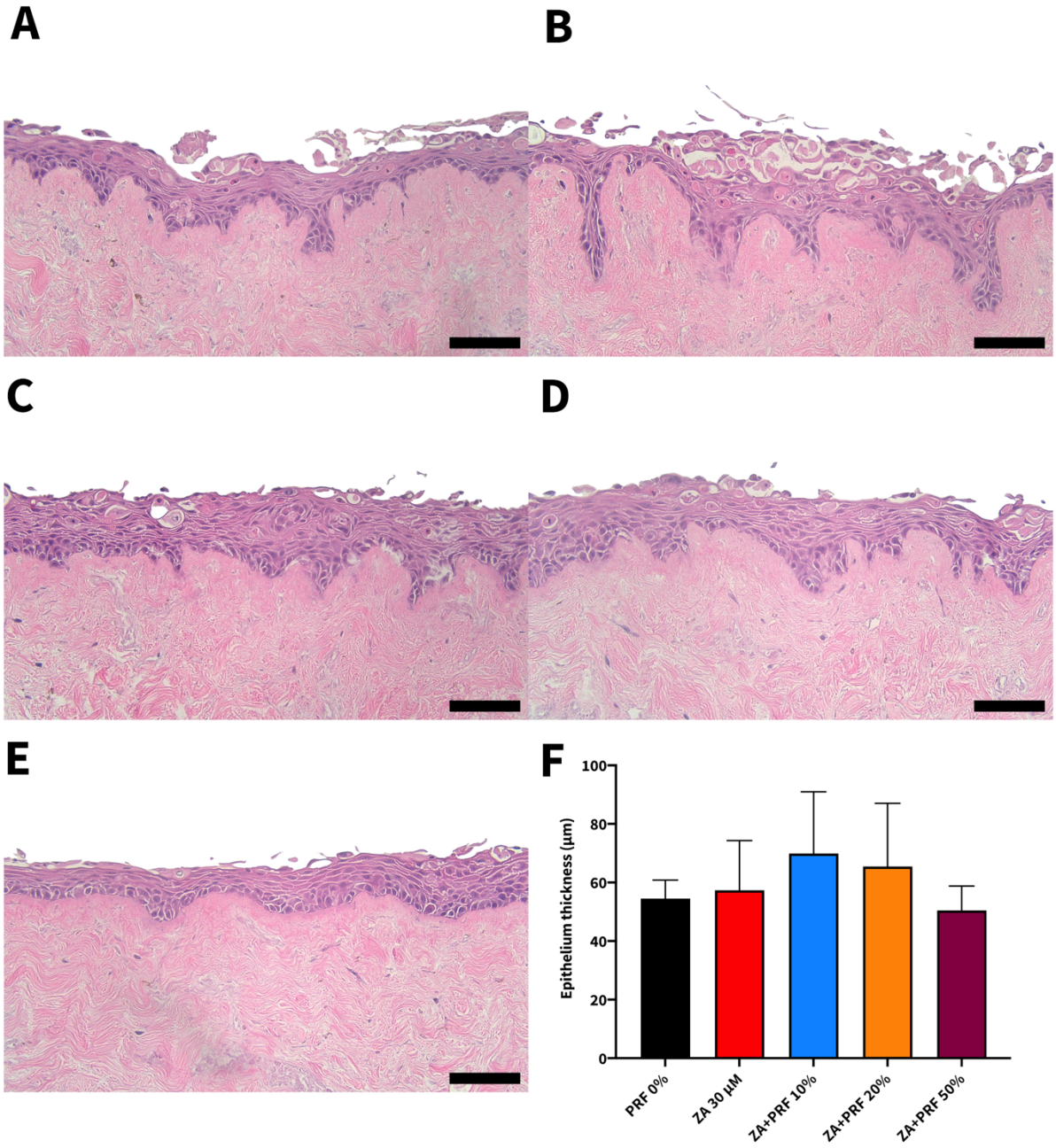

***Figure 6.34* | H&E-stained sections of tissue-engineered oral mucosa (TEOM) treated with Green's medium and I-PRF-derived conditioned medium with 30 µM ZA for 10 days.** *Panels display TEOM sections cultured in Green's medium at an air-liquid interface for 7 days, then cultured condition medium containing (A) PRF 0%, (B) ZA 30 µM, (C) ZA+PRF 10%, (D) ZA+PRF 20% and (E) ZA+PRF 50% for an additional 3 days (total of 10 days). (F) demonstrates the epithelium thickness of TEOM after 10 days of culture. Representative images from three independent experiments (N=3, n=1) were used. Scale bar = 100 µm (20x magnification). A one-way ANOVA followed by Dunnett's multiple comparison was carried out on the data in (F) to test the statistical significance against the 30 µM ZA. Abbreviations: TEOM, tissue-engineered oral mucosa; PRF, platelet-rich fibrin; ZA, zoledronate; ANOVA, analysis of variance.*

At day 14, the metabolic activity of TEOM was unaffected by either ZA treatment alone or the combination treatment of ZA and I-PRF, as shown in Figure 6.33. Figure 6.35A demonstrates the stratified epithelium of control TEOM after 14 days. A disrupted epithelium with only one layer thick was observed after culturing TEOM with 30 μM ZA, shown in Figure 6.35B. No changes were found when I-PRF was added, as shown in Figure 6.35C, D, and E, since the disrupted epithelium and shredded cells were still visible. This was supported by the thickness measurement, shown in Figure 6.35F, since there was a thinner epithelium thickness from ZA-treated conditions compared to the control. In addition, no significant difference was detected between any PRF conditions with ZA-treated TEOM alone.

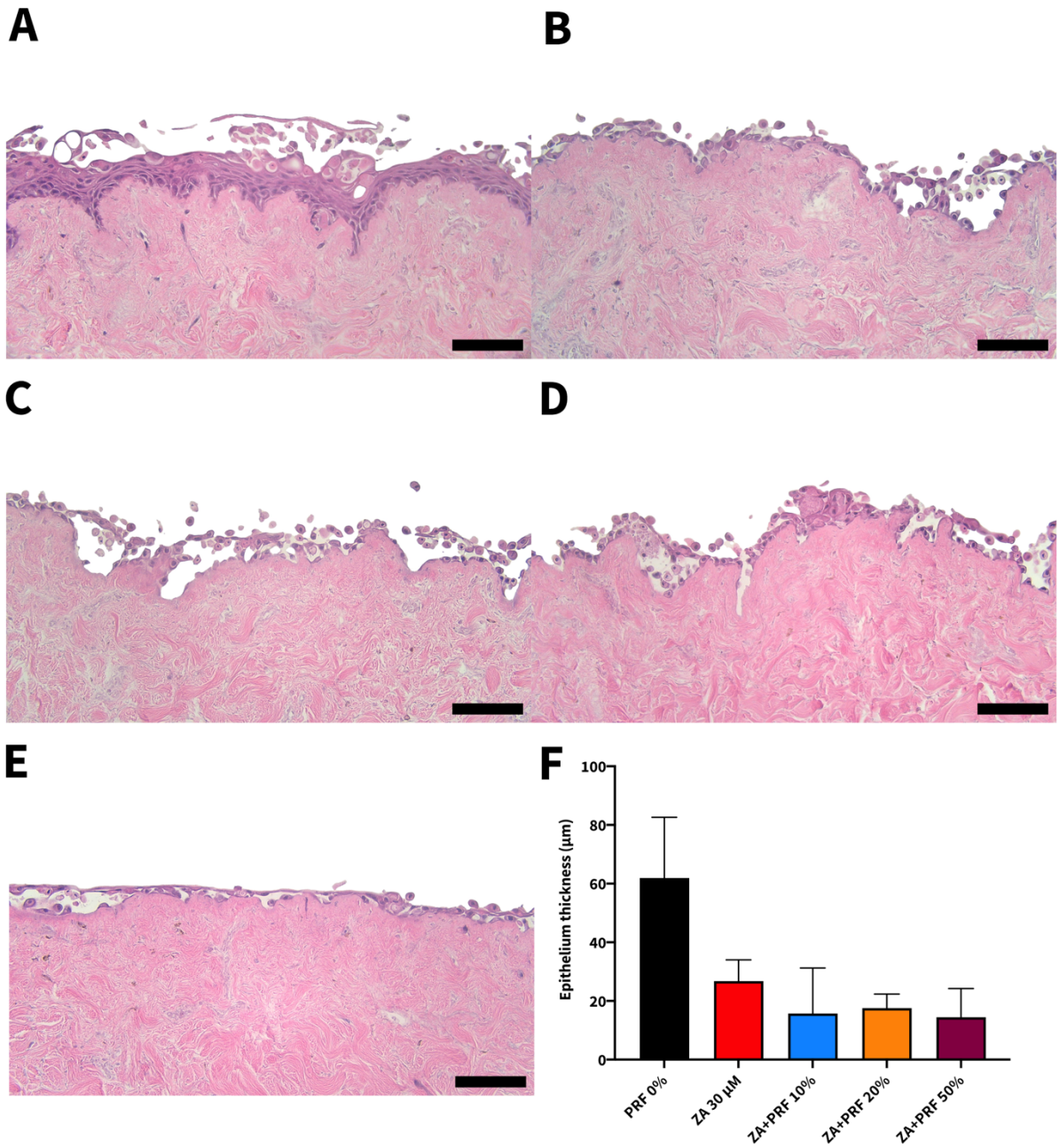

***Figure 6.35* | H&E-stained sections of tissue-engineered oral mucosa (TEOM) treated with Green's medium and I-PRF-derived conditioned medium with 30 µM ZA for 14 days.** *Panels display TEOM sections cultured in Green's medium at an air-liquid interface for 7 days, then cultured with condition medium containing (A) PRF 0%, (B) ZA 30 µM, (C) ZA+PRF 10%, (D) ZA+PRF 20% and (E) ZA+PRF 50% for an additional 7 days (total of 14 days). (F) demonstrates the epithelium thickness of TEOM after 14 days of culture. Representative images from three independent experiments (N=3, n=1) were used. Scale bar = 100 µm (20x magnification). A one-way ANOVA followed by Dunnett's multiple comparison was carried out on the data in (F) to test the statistical significance against the 30 µM ZA. Abbreviations: TEOM, tissue-engineered oral mucosa; PRF, platelet-rich fibrin; ZA, zoledronate; ANOVA, analysis of variance.*

6.5 Discussion

The management of MRONJ is still an ongoing concern for clinicians since there is no universal treatment approach and the outcomes of the existing therapies are also questionable [7]. Soft tissue reconstruction is considered to be one of the key elements to resolve the disease as it can prevent infection and support a vascularisation network needed for the healing of underlying bone [146], [199]. Investigations have been carried out on several possible options to improve the treatment for MRONJ patients, including using PRF.

PRF is an autologous blood fraction containing supraphysiological concentrations of factors released from platelets and leukocytes, first developed by Choukroun *et al.*, in 2001 [258]. An injectable formulation of PRF, or I-PRF, has been developed with the aim to obtain higher cellular contents and prolonged growth factor release compared to PRP [274]. In the previous chapter, we validated the I-PRF preparation method and investigated the composition of I-PRF, which contains a variety of growth factors, cytokines, and chemokines. We also demonstrated how I-PRF influences oral mucosa cell behaviour and demonstrated some improvements on oral wound healing *in vitro*.

Clinical applications of PRF to enhance the healing of MRONJ wounds have been studied [8]; however, the strength of evidence is weak as most studies were reported cases. In addition, the effect of PRF alone without other interventions on the wound healing of MRONJ remains unclear. Investigations into the effectiveness of PRF, particularly I-PRF which has been unaddressed in MRONJ, and understanding the cellular responses is important to support the potential use of PRF as a treatment of choice to reduce soft tissue toxicity in MRONJ patients. Therefore, we investigated the effect of I-PRF on oral mucosa cell activities in the presence of bisphosphonates using assays as previously described in Chapter 5.

To the best of our knowledge, we have shown for the first time that I-PRF can reduce some bisphosphonate induced toxicity in oral mucosa cells and can improve wound healing behaviours in 2D and 3D *in vitro* models of MRONJ.

This study used two nitrogen-containing bisphosphonates, ZA and PA, as both drugs have been frequently reported as associated with MRONJ development [2]. Both bisphosphonates act by inhibiting the farsenyl pyrophosphate enzyme in the mevalonate

pathway resulting in the loss of the prenylation process on the small GTPase molecules such as Ras, Rac, and Rho [107]. These molecules are essential for controlling cell growth, proliferation, and migration which are involved in the wound healing process [76]. Therefore, investigations on these cellular activities were carried out to evaluate whether PRF can improve the wound healing of oral mucosa, which is negatively affected by bisphosphonates.

Bisphosphonate concentrations should be carefully chosen as they possibly influence the outcomes observed. The clinically relevant concentrations of bisphosphonates that produce toxicity on the oral mucosa *in vitro* were selected based on the literature and previously reported data from our group [2], [301].

Cellular metabolic activity was first evaluated since both bisphosphonates have been reported to have an inhibitory effect on the metabolism of oral fibroblasts and keratinocytes [2]. Here, we found that I-PRF successfully increased fibroblast metabolism, which was negatively affected by both ZA and PA. Our data were partially in line with a study by Steller *et al.*, where they demonstrated that 5% PRF-derived conditioned medium increased the metabolic activity of ZA-treated fibroblasts after 24 hours. However, our results during a 72-hour time point differ from their work. They observed that the addition of PRF was unable to improve the metabolic activity after 72 hours of treatment , indicating the toxic effect of ZA on fibroblasts [252]. Different ZA concentrations were used between two studies with a lower dose of ZA (10 µM) in our study compared to the previous work (80 µM), suggesting the success of PRF in reducing toxicity may depend on ZA concentrations.

The underlying mechanisms of how I-PRF successfully restored the metabolic activity of ZA-treated fibroblasts possibly occur from the paracrine effect of growth factors and mediators released from PRF into the culture medium. The role of TGF-β1 is well-known in regulating the growth, proliferation, migration, and differentiation of fibroblasts [42]. A study by Zang *et al.*, demonstrated a decrease of TGF-β expression from gingival tissues obtained from MRONJ patients [199]. This was supported by Zhao *et al.*, who showed that ZA suppressed the expression of TGF-β1 protein in mouse fibroblasts [355]. Komatsu *et al.*, also demonstrated the inhibitory effect of ZA on TGF-β-mediated fibroblast viability [208]. The addition of PRF containing TGF-β, demonstrated by the antibody array assays shown

in Figure 5.13, suggests that TGF-β could partly influence an increase in the metabolic activity of fibroblasts in the presence of ZA.

Contrarily, both bisphosphonates only produced a slight decrease in the metabolic activity of keratinocytes, although the selected doses previously demonstrated significant toxic effects [78]. The possible explanation may involve the different keratinocyte cell lines used between the studies. Our work used FNB6/TERT keratinocytes originally obtained from buccal mucosa, while the previous work used OKF6/TERT-2, which was derived from the floor of mouth. Different sources of cells may play a part in the susceptibility of keratinocytes to bisphosphonate toxicity.

When PRF was added to either ZA- or PA-treated keratinocytes, our data showed that PRF did not increase metabolic activity. This is the first time that the *in vitro* effects of PRF with bisphosphonates on keratinocytes have been investigated. Previous studies have only examined the responses of human epithelial cells to individual growth factors in the presence of bisphosphonates. Wang *et al.*, examined the viability of keratinocytes after treating with EGF (10 ng/mL) and ZA 5 µM for 72 hours on a culture plate [209], while Pansani *et al.*, investigated the effects of EGF-coated titanium discs on keratinocytes treated with 5 µM after 48 hours [356]. Both demonstrated a significant increase in the metabolic activity of keratinocytes after being exposed to EGF with ZA, suggesting the therapeutic role of EGF in protecting cell viability. However, our results were not in agreement with both studies. The differences in the outcomes may be due to ZA concentrations, as our work used higher ZA doses to induce toxicity (10 µM).

Wound healing comprises several stages involving the interplay between cells and signalling mediators [335]. Evidence has shown that ZA administration in osteolytic bone cancer patients markedly reduced the levels of growth factors such as EGF and TGF-β1 in serum [357]. The loss of these growth factors and cytokines could lead to the delay and impaired wound healing, which is a primary clinical feature of MRONJ. Cell migration and proliferation are two important cellular events that play a significant role in wound closure [38]. Investigations on whether I-PRF can improve these cellular activities in the presence of bisphosphonates will provide more understanding of the bioactive role of I-PRF on the healing of MRONJ wounds.

Both ZA and PA have been shown to inhibit the proliferation of oral mucosa cells *in vitro* [2]. In this study, we showed that I-PRF produced a dose-dependent increase in cell proliferation of both fibroblasts and keratinocytes in the presence of ZA after 72 hours of treatment. This was consistent with a work by Stellar *et al.*, who reported the positive impacts of PRF on fibroblast proliferation [252]. This may have occurred as a result of PDGF-BB and TGF-β1 which are present at relatively high concentrations in the I-PRF-derived conditioned medium (Figure 5.13). These mediators have demonstrated their mitogenic effect on both oral fibroblasts and keratinocytes [208], [350]. Work by Zhao *et al.*, showed that ZA-inhibited fibroblast proliferation was mediated through the TGF-β1 pathway [355]. The potential role of PDGF-BB is supported by Cozin *et al.*, who showed that PDGF-BB partially restored the proliferation of fibroblasts after 72 hours [9]. It should be noted that the study by Cozin *et al.* used 3-(4,5-dimethylthiazol-2-yl)-5-(3-carboxymethoxyphenyl)-2-(4-sulfophenyl)-2H-tetrazolium) in the presence of phenazine methosulfate, known as MTS/PMS assay which measures mitochondrial activity. In this case, the assay was used indirectly to represent cell proliferation. As described in the previous chapter, the method, in fact, estimates the metabolic activity rather than measuring the proliferative capacity.

There is a lack of information on the role of EGF on oral mucosa cell proliferation in the presence of bisphosphonates. However, EGF has also been suggested to be a potent mitogen for keratinocytes [37]. Therefore, we hypothesise that increased cell proliferation after receiving the combination treatment of ZA and PRF could be as a result of EGF found in I-PRF, as shown in the cytokine array results in Figure 5.13.

We suggest that the addition of I-PRF-derived conditioned medium containing growth factors (PDGF-BB, TGF-β1, and EGF) released from I-PRF could possibly improve the healing of MRONJ wounds caused by ZA by increasing the proliferation of oral mucosa cells.

The migratory activity of oral mucosa cells in the presence of bisphosphonates was next examined to investigate the effectiveness of I-PRF on the healing process of MRONJ wounds. Sub-toxic concentrations of both ZA and PA were used to prevent any possible cytotoxic effect, which can negatively affect the migration activity of oral mucosa cells.

Here, we showed that I-PRF promoted oral mucosa cell migration in the presence of either ZA or PA, with a more pronounced effect observed on keratinocytes. This was consistent with Stellar *et al.*, who also investigated the bioactivity of PRF on cell migration of ZA-treated gingival fibroblasts using a scratch assay. The combination treatment of PRF with ZA increased fibroblast migration, resulting in better gap closure than the treatment with ZA alone after 72 hours [252]. However, the positive effect shown in their work could be due to an increase in cell proliferation as a method for stopping cell proliferation was not mentioned. Mitomycin C treatment used in our work led to more accurate data on the migratory responses of oral mucosa cells to I-PRF in the presence of bisphosphonates. In addition, it should be noted that various parameters, including ZA doses, I-PRF concentrations, I-PRF preparation procedures, and assays were different between the two studies.

Our promising results were also supported by studies demonstrating the powerful effect of mediators found in PRF. Wang *et al.*, showed a significant increase in keratinocyte migration after incubating with EGF and 5 µM ZA using a scratch wound assay [209]. Besides EGF, TGF-β1 has been commonly reported for its role in enhancing both fibroblast and keratinocyte migration [37], [358]. A work by Komatsu *et al.*, observed a slight improvement in fibroblast migration after being treated with ZA 1.47 µM and TGF-β1 5 ng/mL, supporting the possible therapeutic function of TGF-β1 on cell migration.

Our data have shown a higher level of TGF-β1 and EGF in I-PRF-derived conditioned medium compared to the basal DMEM, as shown in Figure 5.13. Therefore, we suggest that TGF-β1 and EGF possibly mediate the improvement of oral mucosa cell migration which is negatively affected by bisphosphonates.

Literature has shown that bisphosphonates can induce fibroblast and keratinocyte apoptosis [113]. Since we hypothesised that I-PRF could protect oral mucosa cells from bisphosphonate toxicity, examining whether I-PRF could prevent cell apoptosis induced by bisphosphonates is important.

Our data showed that although there was a significant reduction of the metabolic activity of fibroblasts after being treated with 10 μM ZA, the number of apoptotic cells was only slightly increased. This indicates that the doses that negatively affected the metabolic activity were insufficient to induce cell apoptosis. No difference was observed in the number of viable and apoptotic fibroblasts between conditions when I-PRF was added. Conversely, 100 μM PA markedly reduced the number of viable fibroblasts and increased fibroblast apoptosis after 72 hours of treatment. The addition of I-PRF-derived conditioned medium dose-dependently decreased the number of fibroblasts in late apoptotic stages, while the number of viable cells was increased across all I-PRF concentrations. Though the positive effect of PA-treated fibroblast in preventing cell apoptosis has never been mentioned before, the anti-apoptotic effect of platelet-derived products has been studied. Fukaya *et al.*, demonstrated that PRP reduced the number of apoptotic preadipocytes induced by TNF-α and cycloheximide [359]. Work by Vasina *et al.*, showed that platelet microparticles inhibited the apoptosis of human leukaemia monocytic cell line (THP-1) [360]. Evidence suggests the possible role of platelet concentrates, particularly for our work I-PRF, in preventing the apoptosis of oral fibroblasts.

Despite an increase in viable cells, we also observed that the number of necrotic cells also increased when treating cells with I-PRF and bisphosphonates. We did not observe these responses when I-PRF was added alone without bisphosphonates (Figure 5.16 and 5.17), this finding suggests the possible influence of bisphosphonates on increasing the proportion of necrotic cells. However, the underlying mechanism is still unknown and this was beyond our scope of research. Further investigations are needed to clarify the role of I-PRF on the cell death pathway.

Regarding keratinocytes, both ZA and PA had no significant effect on keratinocyte apoptosis and necrosis. There was no difference between conditions after I-PRF was added. These findings correlated well with our metabolic activity results. This could indicate that

the mechanism of action of bisphosphonates may not be associated with the apoptotic pathway or that the conditions in our experiments were not suitable to observe any effects.

Although 2D cell culture has proven to be a useful tool for investigating the effect of PRF on the oral mucosa, cells were cultured separately. The coordination between several cell types, including fibroblasts and keratinocytes, under the control of growth factors and mediators, is essential to maintain the integrity of oral mucosa. To evaluate the bioactivity of I-PRF in a more representative situation of the clinical scenario, TEOM was cultured with I-PRF-derived conditioned medium with either ZA or PA. This is the first time the effect of I-PRF in 3D oral mucosa MRONJ constructs have been investigated.

Two clinical features of the oral epithelium, which can be affected by the toxicity of bisphosphonates in MRONJ, were examined: (i) the formation of the epithelium layer and (ii) the already formed epithelium, mimicking the healthy epithelium of the tissues surrounding the wounds.

The first part of the 3D experiments focused on how I-PRF affected epithelium formation. TEOM was cultured with the medium conditioned with I-PRF and bisphosphonates immediately after lifting to an ALI. The re-epithelialisation process occurs around 3 to 4 days after tissue injury and lasts almost two weeks [39]. The responses were then observed from days 4 to 14. Our data showed a reduction of the metabolic activity of TEOM from ZA treatment but not from PA, linking to the higher potency of ZA than PA [97]. Our data was partly aligned with the previous results from our group where both ZA 10 µM and PA 50 µM produced a significant decrease in the metabolic activity after 10 days [120]. Although the toxic concentrations of bisphosphonates were chosen from the literature, differences in keratinocyte cell lines (OKF6/TERT-2 and FNB6/TERT) used for model construction in the two studies may be why PA was unable to induce toxicity in this study.

The addition of I-PRF-derived conditioned medium slightly improved the metabolic activity of ZA-treated TEOM in a dose-dependent fashion after 7 days. A similar trend was also observed on days 10 and 14. However, there was large variability across all conditions. This may be due to patient-to-patient variability of I-PRF and cells for model construction used between the three biological replicates (N=3). In addition, a limited amount of blood collected from donors to prepare I-PRF and the number of cells ready to be used also played a part, limiting the number of technical repeats to one (n=1).

Histological analysis of TEOM was performed to evaluate the effect of I-PRF on mucosal healing. This was used to rule out the possibility that the increase of metabolic activity was due to stress and stimuli rather than cell viability. Here, we have demonstrated that I-PRF reduced the toxicity of ZA on the epithelium formation of TEOM. Promising results were observed on day 10 as the epithelium of TEOM was completely diminished after receiving ZA treatment. The addition of I-PRF partially maintained the forming epithelium and preserved more viable cells, confirmed by the TUNEL labelling assay.

A randomised controlled study by Giudice *et al.*, observed good mucosal integrity in patients receiving A-PRF with surgical treatment compared to the non-PRF-treated group [242]. Correspondingly in our *in vitro* results, we observed the presence of forming epithelium layers in ZA-treated models that were treated with I-PRF. Data from the literature and our results here suggest the potential benefit of I-PRF on oral mucosa healing in the presence of ZA.

Contrarily, there was no difference in the metabolic activity of TEOM when treated with PA in combination with I-PRF compared to PA treatment alone. This outcome potentially involves PA doses used in the 3D experiments, which might not be high enough to induce toxicity. Thus, any potential effects of I-PRF may not have been measurable under these conditions.

The concentration of PA (50 µM) was chosen based on the previous findings from our group. This dose significantly lowered the metabolic activity of TEOM in their study and also reduced the epithelial thickness after 10 days, where only one or two layers of the epithelium was visible [120]. It is important to note that OKF6/TERT-2 keratinocytes were utilised to construct TEOM in the previous study, while this study used FNB6/TERT cells. It was observed here that models constructed from these two different cells types did not demonstrate the same effects following PA treatment. We observed a multi-layered epithelium in the TEOM after exposure with PA 50 µM at the same time points (Figure 6.31B). Only a slight decrease of epithelium thickness was noticed from PA-treated TEOM after 7 days [120]. Based on the evidence, it appears that the different cell lines of keratinocytes used to construct TEOM might be responsible for these varied responses.

This hypothesis was supported by the histological variations of TEOM in the absence of bisphosphonate treatment. Bullock G. and this study developed oral mucosa equivalent

models by using OKF6/TERT-2 cells and FNB6/TERT cells, respectively [64], [77]. Bullock G. demonstrated a thin epithelium with OKF6-based TEOM, consisting of only three or four layers thick [77]. This contrasts with TEOM made from FNB6/TERT in this work or the native oral mucosa where more layers of stratified epithelium were observed [64].

Our 3D data partly correlated with the 2D results where only fibroblasts, not keratinocytes, were negatively affected by PA toxicity, and the addition of I-PRF did not produce any remarkable effects on the epithelium. These events may be influenced by the different PA concentrations used and the behaviour of cells in 2D and 3D cultures. Testing with higher doses of PA is needed to confirm the toxicity of PA and to enable us to test the bioactivity of PRF on PA-treated TEOM.

We also studied the effect of I-PRF on the healthy epithelium, to model the mucosa surrounding a wounded area that can also be affected by bisphosphonate toxicity. Our findings showed that either ZA alone or combined with I-PRF did not affect the metabolic activity of TEOM at any time. This was inconsistent with work by Bullock *et al.*, who reported a significant reduction of the metabolic activity of TEOM after culturing in Green's medium containing ZA 30 µM for 7 days before replacing with the medium containing ZA 30 µM for a further week. However, the epithelium damage caused by ZA was still observed from the histological sections on day 14, as previously demonstrated [78]. The addition of I-PRF was unable to protect the epithelium and maintain integrity.

Over the years, the therapeutic potential of platelet concentrates on the healing process of MRONJ wounds has been focused mainly on the gel formulation (either PRP, L-PRF, or A-PRF) in animal models and clinical practice. Toro *et al.*, demonstrated an improvement in epithelial and connective tissue repair at the extraction sites when PRP was applied compared to the group solely treated with ZA [253]. Favourable mucosal healing was also observed in most MRONJ patients treated with PRF [8]. A study by Giudice *et al.,* showed complete healing of MRONJ wounds and an extraoral fistula in a severe osteoporotic patient treated with a combination of I-PRF and A-PRF [297]. However, these clinical findings are mostly case reports which often tend to demonstrate patients with successful outcomes. Thereby, data should be interpreted with caution due to the low strength of evidence and potential high-risk biases.

Taken together, our 2D results demonstrated that I-PRF is likely to improve oral wound healing in the presence of bisphosphonates through stimulation of cell proliferation and migration of oral mucosa cells. We also showed that I-PRF, which contains abundant growth factors, partially protects the epithelium integrity of TEOM from the toxicity of ZA, resulting in epithelium healing observed in 3D models.

Apart from the detrimental effects on oral mucosa cells, bisphosphonates have been shown to impair angiogenesis, which is one of the contributing mechanisms of MRONJ development [1]. Previous *in vitro* studies have demonstrated that both ZA and PA reduced the viability and migration, and increase apoptosis of endothelial cells [127], [133], [135]. Our cytokine analysis (Figure 5.13C) showed that angiogenin was present in high amounts. Given that angiogenin has been reported for its role in modulating endothelial cell function and stimulating blood vessel formation [349], this suggests that the application of I-PRF might also enhance the healing of MRONJ wounds by promoting angiogenesis and supporting sufficient blood supply for tissue repair. Although our findings did not identify a substantial amount of VEGF (a potent stimulator for angiogenesis [335]) in our I-PRF, a study conducted by Dohle *et al.*, demonstrated that I-PRF treatment enhanced the release of VEGF in co-cultures of endothelial cells and osteoblasts [361]. This finding suggests a potential benefit where I-PRF might influence tissue repair and wound healing and is an interesting area for future investigation.

Bisphosphonates have been shown, *in vitro* and *in vivo,* to increase inflammatory cell infiltration and stimulate the expression of several pro-inflammatory cytokines such as IL-1, IL-6, or TNF-α [253], [362]. These pro-inflammatory signals are believed to significantly contribute to the development of MRONJ [1]. Thus, the presence of specific interleukins in I-PRF may possibly be involved in the regulation of inflammation which may in turn support the healing of MRONJ wounds.

Our findings revealed elevated amounts of all tested interleukin subtypes in the conditioned medium derived from I-PRF compared to the baseline level in basal DMEM. It is worth noting that IL-8, IL-10, and IL-13 exhibited the highest levels (Figure 5.13B). IL-8 is recognised as a pro-inflammatory cytokine while IL-10 and IL-13 primarily exert anti-inflammatory properties as previously described, indicating that I-PRF contains a variety of both pro- and anti-inflammatory cytokines.

Our findings provide an overview of cytokine contents within I-PRF which is slightly different from prior research, which mostly highlight the anti-inflammatory effects of platelet concentrates. For instance, Wang *et al.*, demonstrated that L-PRF decreased the release of inflammatory cytokines from Schwann cells [363]. This is supported by work by Toro *et al.*, showing a reduction in IL-1β and TNF-α expression in rats after treatment with ZA in combination with PRP [253]. Data from clinical studies, summarised in Table 2.9, also showed that patients receiving PRF treatment experienced favourable wound healing with no prominent symptoms of inflammation. A possible explanation could be involved with the type and preparation procedures of PRF used or how the combination of factors within the platelet concentrates interacts with one another and endogenous signals once administered.

These are beyond the scope of our research and we cannot draw definitive conclusions on the role of I-PRF in angiogenesis or inflammation during the healing process of MRONJ wounds however this is an interesting area. Further investigations into the effects of I-PRF on endothelial cells or inflammatory models would be useful to further evaluate the potential benefits of I-PRF on soft tissue repair through these mechanisms.

Though we observed some improvements in oral wound healing from our *in vitro* model when treated with I-PRF, the main limitation of this work is that we are unable to definitively pinpoint which growth factors or cytokines primarily mediate these observed effects. The presented data only allows us to hypothesise that these outcomes occur as a result of the paracrine effect from highly represented growth factors and cytokines in I-PRF, identified from the cytokine array analysis. Further examination of the downstream signalling should be carried out to confirm whether these cytokines indeed regulate the observed effects on oral mucosa.

Another limitation of this work comes from the design of our *in vitro* studies. Specifically, our protocols involved feeding of models with fresh conditioned medium containing bisphosphonate and I-PRF every 3-4 days. This procedure may not accurately represent the real clinical situation especially for PRF where it is typically applied once during a surgical operation. Given that bisphosphonates can reside in the bone for several years, with their half-life of up to 10 years [106], the continual replenishment of bisphosphonates may lead to persistent toxicity in soft tissues.

The large disparities in outcomes between experimental repetitions are also another challenge to our work. This inconsistency is probably due to the limited number of models tested in each individual experiment as previously discussed. Moreover, our *in vitro* models were only evaluated using a specific concentration of bisphosphonates. The doses selected in this work were within the range of clinically relevant doses and had been reported in the literature to cause significant toxicity *in vitro*. However, in this model (cultured with alternative oral mucosa cells) toxicity was insufficient to see changes from I-PRF administration. It is also still a challenge to determine the local concentration of bisphosphonates to best model the clinical situation as it is difficult to accurately measure in MRONJ patients and local release is dependent on many factors. Future investigations should focus on developing methodologies to accurately quantify bisphosphonate concentration in the oral cavity, as this would enhance the translational relevance of our work to a clinic context.

In addition, our *in vitro* models still have limitations and cannot fully replicate the clinical scenario which is affected by several contributing factors. These factors including the severity of MRONJ disease, a patient's medical conditions, potency of bisphosphonates or duration of bisphosphonate therapy; all of which could collectively impact on the efficacy of platelet concentrate treatment. For example, patients with early-stage MRONJ and those having a lower potency bisphosphonate therapy often exhibit better treatment outcomes compared to patients with advanced stage MRONJ receiving higher potency bisphosphonates [248].

The observed differences and variability from our *in vitro* models in some ways represent the patient variability observed in clinical studies investigating the effectiveness of I-PRF on oral wound healing. In this study, the effects we observed from I-PRF were predominantly positive and indicated the potential of I-PRF to stimulate oral mucosa wound healing. This is in agreement with the positive cases reported in the clinical literature (summarised in Table 2.8 and 2.9).

Taken together, I-PRF has been demonstrated to be able to positively affect oral mucosa cells; however, the strength of this effect may be limited and suggests that I-PRF may need to be combined with additional treatments (such as materials or additional growth factors) to generate a minimal clinically important change. It would be interesting

in the future to further investigate whether characteristics of a patient's PRF correlates with treatment outcomes and whether variability seen in these outcomes can be attributed to particular growth factors or cytokines.

6.6 Summary

In conclusion, this is the first time that the therapeutic effect of I-PRF has been studied using *in vitro* oral mucosa models in combination with bisphosphonates. I-PRF improved the wound healing process of MRONJ-like conditions in both 2D and 3D cultures. Not all conditions tested were positive and there was inconsistency in the results from cells treated with PA and ZA; however, where effects were observed these were positive indicating PRF based therapies have potential. Results varied between PRF donors which may be illustrative of the patient-to-patient variability seen in clinical studies. The paracrine effect of growth factors and mediators in I-PRF possibly plays a role in promoting oral soft tissue healing mostly through an increase in cell migration and proliferation but further study is required.

Chapter 7

Conclusions

7. Conclusions

While MRONJ continues to present significant challenges for clinicians and the disease detrimentally impacts patient well-being, there is an urgent need to develop effective treatments that could restore the soft tissue barrier, which is pivotal for the resolution of the disease. In this thesis, we investigated the potential of two therapeutic approaches: GGOH and I-PRF, on bisphosphonate-induced toxicity in *in vitro* models of oral mucosa. We found some improvements on cellular activities related to oral wound healing process from both interventions.

The exploration into GGOH, as shown in Chapter 4, demonstrated its narrow therapeutic effect. While GGOH was able to reduce the toxicity of ZA on oral fibroblasts, those same doses were ineffective for keratinocytes. We also found that keratinocytes were more susceptible to GGOH toxicity than fibroblasts since a slightly elevated dose of GGOH produced toxicity in keratinocytes. In addition, the negative effects on the metabolic activity of oral mucosa cells were intensified when GGOH was combined with bisphosphonates. This part of our work indicates the limited potential of GGOH in the soft tissue repair of MRONJ wounds and raises a significant concern on its use in other applications.

Following our work determining the failure of GGOH to mitigate the toxicity of bisphosphonate on oral mucosa, our focus shifted to another alternative therapy, I-PRF. In chapter 5, we defined a valid preparation protocol and the cytokine profile of I-PRF. We showed that PDGF, TGF-β1 and EGF were the most abundant growth factors found in I-PRF. Our findings demonstrated encouraging results as I-PRF enhanced cell proliferation and epithelium formation in oral mucosa models during early time points. I-PRF was also shown to stimulate the migration of keratinocytes in both 2D cultures and 3D wound models. The pivotal role of paracrine factors released from either I-PRF or FBS has been highlighted since we found a comparable effect of these blood-derived materials on the healing process of oral mucosa.

In chapter 6, we demonstrated the potential of I-PRF to reduce ZA-induced mucosa toxicity. Our findings showed improvements in cell metabolism, proliferation, and migration in 2D cultures and demonstrated its ability to support the formation of a stratified

epithelium in TEOM. I-PRF partially increased the epithelial thickness and maintained epithelium integrity which was disrupted following ZA treatment. The mechanism of action remains unclear as our results could not pinpoint the exact growth factors and cytokines responsible for these effects, however, we propose possible mechanisms *via* the PDGF, TGF-β1 and EGF pathways.

In conclusion, this work indicates that GGOH is not a suitable option for MRONJ treatment whilst I-PRF demonstrate the potential benefits to support soft tissue healing in MRONJ treatment. Our work highlights the complexity of biological responses and emphasises the need for continued research to optimise and further develop the clinical translation of I-PRF for oral wound healing for MRONJ and other conditions.

Chapter 8

Future work

8. Future work

We have demonstrated that I-PRF offers the potential for improving the healing of oral wounds caused by bisphosphonates, whereas GGOH only showed limited efficacy. Thereby, future research should focus primarily towards I-PRF. As our observations only provided a broad overview of cytokine expression in I-PRF, we cannot conclude which bioactive factors are responsible for the effects observed in the oral mucosa. Future research to assess the impacts of each of these growth factors and cytokines individually or in combination should be performed. This will provide supportive evidence on whether these factors are indeed mediating the cellular responses observed in this work. The evaluation of downstream signalling pathways activated by these cytokines is also needed to gain deeper insights into their roles in wound healing.

I-PRF supplies a variety of paracrine factors which are essential for mucosal healing so it is also possible that these cytokines could stimulate the production of wound healing related cytokines from fibroblasts or keratinocytes in the tissue it is used to treat. For example, PDGF, TGF-β, EGF, KGF or bFGF have been reported in previous studies to be synthesised in fibroblasts and keratinocytes [37]. This process could potentially influence the behaviour of the oral mucosa in an autocrine manner. Therefore, future studies should focus on quantifying the levels of these growth factors in the culture medium following I-PRF treatment. Additionally, it would be interesting to explore gene and protein expression profiles of key factors. Having this information at the molecular level, we could also gain a more understanding into the mechanisms through which I-PRF contributes to oral wound healing.

Our study demonstrated an increase of cell proliferation in both 2D and 3D cultures, as evidenced by flow cytometry and Ki-67 immunostaining. However, wound healing is a complex process with a variety of cellular processes working in a coordinated manner [37], thereby additional immunostaining of key markers for other stages of the healing process could be considered. For instance, collagen staining could be used to assess the formation of ECM during the remodelling phase of wound closure. In addition, investigations on cytokeratin proteins to evaluate the effect on keratinocyte differentiation or other markers

such as VEGF, TGF-β or MMPs could also be considered. These all would provide a comprehensive view of the impact of I-PRF on the wound healing.

Additionally, it is also important to perform further quantitative analysis on specific highly expressed growth factors in the conditioned medium to confirm its presence in I-PRF. Given that VEGF is produced from platelets and has been reported in previous studies to be present in I-PRF [37], [274], [327], investigations on VEGF should also be conducted even though our current data did not demonstrate expression.

While soft tissue restoration is a pivotal compartment in the resolution of MRONJ treatment, the disease develops from complex multifactorial mechanisms. These include the inhibition of bone resorption and angiogenesis, and the presence of inflammation and infection [1]. A significant limitation of our current work is the simplified mucosa models which currently include only fibroblasts and keratinocytes. As a result, these models do not fully replicate the complexity of native environment of MRONJ wounds which involves other cell types including bone cells, immune cells, and endothelial cells. Advancements in tissue engineering have enabled the incorporation of these cells into the oral mucosa construct models [364], [365]; however, these models still have to be modified and optimised to be used as *in vitro* models for MRONJ. If this is successful, it would be another interesting area to explore the effect of I-PRF on more complex models of oral mucosa so we can obtain a more holistic view of the effectiveness of I-PRF on the healing of MRONJ wounds *in vitro* and understand the mechanistic regulation which occurs in the real-world clinical situation.

Given that angiogenin was identified as the most highly expressed cytokine in I-PRF, future research should also focus on the effects of I-PRF on endothelial cells and angiogenesis since angiogenin plays a crucial role in this process. Considering that bisphosphonates have been shown to negatively affect endothelial cells, exploring the role of angiogenin could offer more insights into the underlying mechanisms that could facilitate the healing of MRONJ wounds.

Previous studies have shown that the administration of ZA in bone cancer patients led to a reduction in serum levels of growth factors such as EGF and TGF-β [357]. Given that our study utilised I-PRF from healthy volunteers, obtaining I-PRF from patients with MRONJ could yield a different concentration of growth factors, which may, in turn, affect its efficacy

in wound healing. A comparative analysis of growth factor levels in I-PRF from healthy individuals and MRONJ patients could be another interesting research direction.

Our findings demonstrated inconsistencies particularly in the outcomes from our 3D models, in part due to the limited supply of cells and I-PRF samples. It would be sensible to narrow down the experimental conditions to enable more repeats and to maximise our chances of observing effects. This would also enhance the robustness of our data and potentially reveal more important differences. Furthermore, exploring the cellular response to I-PRF obtained from individual donors, as was done in our study, compared to pooled samples would be interesting to evaluate whether there is any impact from patient-to-patient variability.

Future exploration should also involve re-evaluating the impact of different concentrations of PA on oral mucosa, particularly in 3D culture models. Since our findings did not demonstrate any significant toxic effect of PA on oral mucosa, it may be worthwhile to test higher PA doses to determine the toxic threshold. Following this, subsequent experiments to assess whether I-PRF can mitigate the PA should be carried out to conclude whether I-PRF has a protective effect.

In addition to injectable forms, exploring other formulations of PRF, either L-PRF or A-PRF, is another interesting avenue for future research. Given that most *in vitro* and *in vivo* studies (Table 2.6, 2.8, and 2.9) have utilised this gel formulation, investigations with this formulation would enable us to compare our results more broadly and examine potential variations in cellular contents, cytokine expression, and cellular responses across different types of PRF.

Another promising avenue for future research is the integration of I-PRF with biomaterials scaffolds, such as collagen membranes or matrices. The combination of I-PRF with these biomaterials has the potential to enhance a scaffold's effectiveness in promoting tissue repair and regeneration. Scaffolds infused with I-PRF could provide a three-dimensional framework that facilitates cellular migration and proliferation while delivering growth factors and cytokines which are necessary for wound healing. While previous studies have primarily investigated the histological appearance [293], [366], a variety of investigations could be carried out following biomaterial fabrication. The physicochemical properties of these combined materials including porosity, mechanical strength, or

degradation rate could be examined. Additionally, evaluating the biocompatibility and cellular responses to these materials using 2D cultures and 3D wound models would be interesting for the field.

These proposed future investigations would not only broaden the understanding in the role of I-PRF in tissue repair and regeneration but also extend its potential applications beyond MRONJ to a wider range of oral soft tissue defects.

Chapter 9

References

9. References

[1] S. L. Ruggiero, T. B. Dodson, T. Aghaloo, E. R. Carlson, B. B. Ward, and D. Kademani, "American Association of Oral and Maxillofacial Surgeons' Position Paper on Medication-Related Osteonecrosis of the Jaw – 2022 Update," *J. Oral Maxillofac. Surg.*, 2022, doi: 10.1016/j.joms.2022.02.008.

[2] G. Bullock, C. A. Miller, A. McKechnie, and V. Hearnden, "A Review Into the Effects of Pamidronic Acid and Zoledronic Acid on the Oral Mucosa in Medication-Related Osteonecrosis of the Jaw," *Frontiers in Oral Health*, vol. 2. 2022. doi: 10.3389/froh.2021.822411.

[3] T. L. Aghaloo, A. L. Felsenfeld, and S. Tetradis, "Osteonecrosis of the jaw in a patient on Denosumab," *J Oral Maxillofac Surg*, vol. 68, no. 5, pp. 959–963, 2010, doi: 10.1016/j.joms.2009.10.010.

[4] V. Guarneri *et al.*, "Bevacizumab and osteonecrosis of the jaw: incidence and association with bisphosphonate therapy in three large prospective trials in advanced breast cancer," *Breast Cancer Res Treat*, vol. 122, no. 1, pp. 181–188, 2010, doi: 10.1007/s10549-010-0866-3.

[5] F. P. Koch, C. Walter, T. Hansen, E. Jager, and W. Wagner, "Osteonecrosis of the jaw related to sunitinib," *Oral Maxillofac Surg*, vol. 15, no. 1, pp. 63–66, 2011, doi: 10.1007/s10006-010-0224-y.

[6] S. N. Rogers, N. O. A. Palmer, D. Lowe, and C. Randall, "United Kingdom nationwide study of avascular necrosis of the jaws including bisphosphonate-related necrosis," *Br J Oral Maxillofac Surg*, vol. 53, no. 2, pp. 176–182, 2015, doi: 10.1016/j.bjoms.2014.11.008.

[7] S.-W. On, S.-W. Cho, S.-H. Byun, and B.-E. Yang, "Various Therapeutic Methods for the Treatment of Medication-Related Osteonecrosis of the Jaw (MRONJ) and Their Limitations: A Narrative Review on New Molecular and Cellular Therapeutic Approaches," *Antioxidants* , vol. 10, no. 5. 2021. doi: 10.3390/antiox10050680.

[8] M. Fabbro, S. Taschieri, and F. Goker, "Platelet concentrates as an adjunctive therapy for medication-related osteonecrosis of the Jaw: A systematic review and meta-analysis," *Int. J. Growth Factors Stem Cells Dent.*, vol. 1, p. 48, Jan. 2018, doi: 10.4103/GFSC.GFSC_19_18.

[9] M. Cozin *et al.*, "Novel therapy to reverse the cellular effects of bisphosphonates on primary human oral fibroblasts," *J Oral Maxillofac Surg*, vol. 69, no. 10, pp. 2564–2578, 2011, doi: 10.1016/j.joms.2011.03.005.

[10] A. M. Pabst, M. Krüger, T. Ziebart, C. Jacobs, K. Sagheb, and C. Walter, "The influence of geranylgeraniol on human oral keratinocytes after bisphosphonate treatment: An in vitro study.," *J. Craniomaxillofac. Surg.*, vol. 43, no. 5, pp. 688–695, 2015, doi: 10.1016/j.jcms.2015.03.014.

[11] H. K. Datta, W. F. Ng, J. A. Walker, S. P. Tuck, and S. S. Varanasi, "The cell biology of bone metabolism," *J. Clin. Pathol.*, vol. 61, no. 5, pp. 577–587, May 2008, doi: 10.1136/jcp.2007.048868.

[12] D. B. Burr and O. Akkus, "Bone Morphology and Organization," in *Basic and Applied Bone Biology*, Elsevier Inc., 2013, pp. 3–25. doi: 10.1016/B978-0-12-416015-6.00001-0.

[13] J. S. Kenkre and J. H. D. Bassett, "The bone remodelling cycle," *Ann. Clin. Biochem.*, vol. 55, no. 3, pp. 308–327, Mar. 2018, doi: 10.1177/0004563218759371.

[14] A. Nanci, *Ten Cate's oral histology: development, structure, and function*. St. Louis: Mosby, 2013.

[15] R. Florencio-Silva, G. Sasso, E. Sasso-Cerri, M. Simoes, and P. Cerri, "Biology of Bone Tissue: Structure, Function, and Factors That Influence Bone Cells," *Biomed Res. Int.*, vol. 2015, p. 421746, Aug. 2015, doi: 10.1155/2015/421746.

[16] B. Clarke, "Normal bone anatomy and physiology.," *Clin. J. Am. Soc. Nephrol.*, vol. 3 suppl 3,

no. s3, pp. S131–S139, 2008, doi: 10.2215/CJN.04151206.
[17] D. J. Hadjidakis and I. I. Androulakis, “Bone remodeling,” in *Annals of the New York Academy of Sciences*, 2006. doi: 10.1196/annals.1365.035.
[18] R. L. Jilka, “Biology of the basic multicellular unit and the pathophysiology of osteoporosis,” in *Medical and Pediatric Oncology*, Sep. 2003, pp. 182–185. doi: 10.1002/mpo.10334.
[19] E. Eriksen, “Cellular mechanisms of bone remodeling,” *Rev. Endocr. Metab. Disord.*, vol. 11, no. 4, pp. 219–227, 2010, doi: 10.1007/s11154-010-9153-1.
[20] J. C. Gallagher and A. J. Sai, “Molecular biology of bone remodeling: Implications for new therapeutic targets for osteoporosis,” *Maturitas*, vol. 65, no. 4. pp. 301–307, Apr. 2010. doi: 10.1016/j.maturitas.2010.01.002.
[21] W. J. Boyle, W. S. Simonet, and D. L. Lacey, “Osteoclast differentiation and activation,” *Nature*, vol. 423, no. 6937, p. 337, 2003, doi: 10.1038/nature01658.
[22] G. Stenbeck, “Formation and function of the ruffled border in osteoclasts,” *Semin. Cell Dev. Biol.*, vol. 13, no. 4, pp. 285–292, 2002, doi: 10.1016/S1084952102000587.
[23] J. Gasser and M. Kneissel, “Bone Physiology and Biology,” 2017, pp. 27–94. doi: 10.1007/978-3-319-56192-9_2.
[24] E. A. Imel, L. A. DiMeglio, and D. B. Burr, “Chapter 16 - Metabolic Bone Diseases,” D. B. Burr and M. R. B. T.-B. and A. B. B. Allen, Eds., San Diego: Academic Press, 2014, pp. 317–344. doi: https://doi.org/10.1016/B978-0-12-416015-6.00016-2.
[25] K. Turksen, *Wound Healing: Stem Cells Repair and Restorations, Basic and Clinical Aspects*. 2018. doi: 10.1002/9781119282518.
[26] C. A. Squier and M. J. Kremer, “Biology of oral mucosa and esophagus,” *J Natl Cancer Inst Monogr*, no. 29, pp. 7–15, 2001, doi: 10.1093/oxfordjournals.jncimonographs.a003443.
[27] J. E. Glim, M. van Egmond, F. B. Niessen, V. Everts, and R. H. Beelen, “Detrimental dermal wound healing: what can we learn from the oral mucosa?,” *Wound Repair Regen*, vol. 21, no. 5, pp. 648–660, 2013, doi: 10.1111/wrr.12072.
[28] A. R. Hand, *Fundamentals of oral histology and physiology*. Ames, Iowa: Ames, Iowa : John Wiley & Sons Inc., 2014, 2014.
[29] G. Campisi, C. Paderni, R. Saccone, O. Di Fede, A. Wolff, and L. Giannola, “Human Buccal Mucosa as an Innovative Site of Drug Delivery,” *Curr. Pharm. Des.*, vol. 16, pp. 641–652, Feb. 2010, doi: 10.2174/138161210790883778.
[30] X. Xiong, T. Wu, and S. He, “Physical forces make rete ridges in oral mucosa,” *Med. Hypotheses*, vol. 81, no. 5, pp. 883–886, 2013, doi: https://doi.org/10.1016/j.mehy.2013.07.005.
[31] A. Cruchley and L. Bergmeier, “Structure and Functions of the Oral Mucosa,” in *Oral Mucosa in Health and Disease: A Concise Handbook*, 2018, pp. 1–18. doi: 10.1007/978-3-319-56065-6_1.
[32] V. Hearnden *et al.*, “Diffusion Studies of Nanometer Polymersomes Across Tissue Engineered Human Oral Mucosa,” *Pharm. Res.*, vol. 26, no. 7, pp. 1718–1728, 2009, doi: 10.1007/s11095-009-9882-6.
[33] H. Larjava, *Oral Wound Healing: An Overview*. John Wiley & Sons, Incorporated, 2013. doi: 10.1002/9781118704509.ch1.
[34] A. Sculean, R. Gruber, and D. D. Bosshardt, “Soft tissue wound healing around teeth and dental implants,” *J. Clin. Periodontol.*, vol. 41, no. s15, pp. S6–S22, Apr. 2014, doi: 10.1111/jcpe.12206.
[35] P. C. Smith, M. Cáceres, C. Martínez, A. Oyarzún, and J. Martínez, “Gingival Wound Healing: An Essential Response Disturbed by Aging?,” *J. Dent. Res.*, vol. 94, no. 3, pp. 395–402, Dec. 2014, doi: 10.1177/0022034514563750.
[36] M. Waasdorp, B. P. Krom, F. J. Bikker, P. P. M. van Zuijlen, F. B. Niessen, and S. Gibbs, “The

bigger picture: Why oral mucosa heals better than skin," *Biomol. (Basel, Switzerland)*, vol. 11, no. 8, p. 1165, 2021, doi: 10.3390/biom11081165.
[37] S. Barrientos, O. Stojadinovic, M. S. Golinko, H. Brem, and M. Tomic-Canic, "Growth factors and cytokines in wound healing," *Wound Repair Regen*, vol. 16, no. 5, pp. 585–601, 2008, doi: 10.1111/j.1524-475X.2008.00410.x.
[38] P. Smith and C. Martinez, "Wound Healing in the Oral Mucosa," in *Oral Mucosa in Health and Disease: A Concise Handbook*, 2018, pp. 77–90. doi: 10.1007/978-3-319-56065-6_6.
[39] C. Politis, J. Schoenaers, R. Jacobs, and J. O. Agbaje, "Wound Healing Problems in the Mouth," *Front. Physiol.*, vol. 7, p. 507, 2016, [Online]. Available: https://www.frontiersin.org/article/10.3389/fphys.2016.00507
[40] S. Ellis, E. J. Lin, and D. Tartar, "Immunology of Wound Healing," *Curr Dermatol Rep*, vol. 7, no. 4, pp. 350–358, 2018, doi: 10.1007/s13671-018-0234-9.
[41] J. M. Reinke and H. Sorg, "Wound repair and regeneration," *European Surgical Research*. 2012. doi: 10.1159/000339613.
[42] S. Werner and R. Grose, "Regulation of Wound Healing by Growth Factors and Cytokines," *Physiol Rev*, vol. 83, no. 3, pp. 835–870, 2003, doi: 10.1152/physrev.2003.83.3.835.
[43] N. Landén, D. Li, and M. Ståhle, "Transition from inflammation to proliferation: a critical step during wound healing," *Cell. Mol. Life Sci.*, vol. 73, no. 20, pp. 3861–3885, 2016, doi: 10.1007/s00018-016-2268-0.
[44] G. C. Gurtner, S. Werner, Y. Barrandon, and M. T. Longaker, "Wound repair and regeneration," *Nature*, vol. 453, no. 7193, p. 314, 2008, doi: 10.1038/nature07039.
[45] H. Larjava, L. Häkkinen, and L. Koivisto, *Re-Epithelialization of Wounds*. John Wiley & Sons, Incorporated, 2013. doi: 10.1002/9781118704509.ch5.
[46] P. Rousselle, F. Braye, and G. Dayan, "Re-epithelialization of adult skin wounds: Cellular mechanisms and therapeutic strategies," *Adv. Drug Deliv. Rev.*, vol. 146, pp. 344–365, 2019, doi: 10.1016/j.addr.2018.06.019.
[47] I. Pastar *et al.*, "Epithelialization in Wound Healing: A Comprehensive Review," *Adv. Wound Care*, vol. 3, no. 7, pp. 445–464, Mar. 2014, doi: 10.1089/wound.2013.0473.
[48] K. A. Lygoe, I. Wall, P. Stephens, and M. P. Lewis, "Role of vitronectin and fibronectin receptors in oral mucosal and dermal myofibroblast differentiation," *Biol Cell*, vol. 99, no. 11, pp. 601–614, 2007, doi: 10.1042/BC20070008.
[49] N. Bagul, A. Ganjre, S. N. Goryawala, R. Kathariya, and S. Dusane, "Dynamic role of myofibroblasts in oral lesions," *World J Clin Oncol*, vol. 6, no. 6, pp. 264–271, 2015, doi: 10.5306/wjco.v6.i6.264.
[50] A. Turabelidze *et al.*, "Intrinsic differences between oral and skin keratinocytes.," *PLoS One*, vol. 9, no. 9, pp. e101480–e101480, 2014, doi: 10.1371/journal.pone.0101480.
[51] P. Stephens *et al.*, "Skin and oral fibroblasts exhibit phenotypic differences in extracellular matrix reorganization and matrix metalloproteinase activity," *Br. J. Dermatol.*, vol. 144, no. 2, pp. 229–237, 2001, doi: 10.1046/j.1365-2133.2001.04006.x.
[52] C. Rodrigues Neves *et al.*, "Human saliva stimulates skin and oral wound healing in vitro," *J. Tissue Eng. Regen. Med.*, vol. 13, no. 6, pp. 1079–1092, Jun. 2019, doi: 10.1002/term.2865.
[53] M. E. Schrementi, A. M. Ferreira, C. Zender, and L. A. Dipietro, "Site-specific production of TGF-β in oral mucosal and cutaneous wounds," *Wound Repair Regen.*, vol. 16, no. 1, pp. 80–86, 2008, doi: 10.1111/j.1524-475X.2007.00320.x.
[54] S. Meran *et al.*, "Involvement of Hyaluronan in Regulation of Fibroblast Phenotype," *J Biol Chem*, vol. 282, no. 35, pp. 25687–25697, 2007, doi: 10.1074/jbc.M700773200.
[55] N. Ganapathy, S. S. Venkataraman, R. Daniel, R. J. Aravind, and V. B. Kumarakrishnan, "Molecular biology of wound healing," *J Pharm Bioallied Sci*, vol. 4, no. Suppl 2, pp. S334–S337, 2012, doi: 10.4103/0975-7406.100294.
[56] S. Jimson, S. Murali, S. Zunt, L. Goldblatt, and M. Srinivasan, "Epithelial expression of

keratinocytes growth factor in oral precancer lesions," *Dent Res J*, vol. 13, no. 3, pp. 199–205, 2016, doi: 10.4103/1735-3327.182148.
[57] Z. Garoufalia *et al.*, "Insulin-like growth factor-I and wound healing, a potential answer to non-healing wounds: A systematic review of the literature and future perspectives," *Biomed. reports*, vol. 15, no. 2, pp. 1–66, 2021, doi: 10.3892/br.2021.1442.
[58] L.-L. Wang, R.-C. Wang, L.-Z. Wang, L.-R. Sun, and X.-M. Qi, "Expression of keratinocyte growth factor and its receptor in oral lichen planus," *Int J Clin Exp Pathol*, vol. 11, no. 2, pp. 757–764, 2018.
[59] K. Schenck, O. Schreurs, K. Hayashi, and K. Helgeland, "The role of nerve growth factor (NGF) and its precursor forms in oral wound healing," *Int J Mol Sci*, vol. 18, no. 2, p. 386, 2017, doi: 10.3390/ijms18020386.
[60] M. G. Araújo, C. O. Silva, M. Misawa, and F. Sukekava, "Alveolar socket healing: what can we learn?," *Periodontol. 2000*, vol. 68, no. 1, pp. 122–134, 2015, doi: 10.1111/prd.12082.
[61] R. Farina and L. Trombelli, "Wound healing of extraction sockets," *Endod. Top.*, vol. 25, no. 1, pp. 16–43, 2011, doi: 10.1111/etp.12016.
[62] N. Cohen and J. Cohen-Lévy, "Healing processes following tooth extraction in orthodontic cases," *J. Dentofac. Anomalies Orthod.*, vol. 17, no. 3, 2014, doi: 10.1051/odfen/2014006.
[63] P. de S. Gomes, P. Daugela, L. Poskevicius, L. Mariano, and M. H. Fernandes, "Molecular and Cellular Aspects of Socket Healing in the Absence and Presence of Graft Materials and Autologous Platelet Concentrates: a Focused Review," *eJournal Oral Maxillofac. Res.*, vol. 10, no. 3, p. e2, 2019, doi: 10.5037/jomr.2019.10302.
[64] L. R. Jennings *et al.*, "Development and Characterization of In Vitro Human Oral Mucosal Equivalents Derived from Immortalized Oral Keratinocytes," *Tissue Eng. Part C. Methods*, vol. 22, no. 12, pp. 1108–1117, 2016, doi: 10.1089/ten.tec.2016.0310.
[65] W. M. S. Russell and R. L. Burch, *The principles of humane experimental technique*. Methuen, 1959.
[66] D. J. Geer, D. D. Swartz, and S. T. Andreadis, "In vivo model of wound healing based on transplanted tissue-engineered skin," *Tissue Eng*, vol. 10, no. 7–8, pp. 1006–1017, 2004, doi: 10.1089/1076327041887727.
[67] A. A. Almansoori, B. Kim, J.-H. Lee, and S. D. Tran, "Tissue engineering of oral mucosa and salivary gland: Disease modeling and clinical applications," *Micromachines (Basel)*, vol. 11, no. 12, pp. 1–13, 2020, doi: 10.3390/mi11121066.
[68] K. Moharamzadeh *et al.*, "Tissue-engineered Oral Mucosa," *J. Dent. Res.*, vol. 91, no. 7, pp. 642–650, 2012, doi: 10.1177/0022034511435702.
[69] I. Masuda, "An in vitro Oral Mucosal Model Reconstructed from Human Normal Gingival Cells," *J. Stomatol.*, vol. 63, no. 2, pp. 334–353, 1996, doi: 10.5357/koubyou.63.334.
[70] K. Moharamzadeh, I. M. Brook, R. Van Noort, A. M. Scutt, and M. H. Thornhill, "Tissue-engineered oral mucosa: A review of the scientific literature," *J. Dent. Res.*, vol. 86, no. 2, pp. 115–124, 2007, doi: 10.1177/154405910708600203.
[71] I. C. Mackenzie and N. E. Fusenig, "Regeneration of Organized Epithelial Structure," *J Invest Dermatol*, vol. 81, no. 1, pp. S189–S194, 1983, doi: 10.1111/1523-1747.ep12541093.
[72] O. K. Vintermyr, D. E. Costea, L. L. Loro, E. A. O. Dimba, and A. C. Johannessen, "Crucial Effects of Fibroblasts and Keratinocyte Growth Factor on Morphogenesis of Reconstituted Human Oral Epithelium," *J Invest Dermatol*, vol. 121, no. 6, pp. 1479–1486, 2003, doi: 10.1111/j.1523-1747.2003.12616.x.
[73] N. P. Yadev, C. Murdoch, S. P. Saville, and M. H. Thornhill, "Evaluation of tissue engineered models of the oral mucosa to investigate oral candidiasis," *Microb Pathog*, vol. 50, no. 6, pp. 278–285, 2011, doi: 10.1016/j.micpath.2010.11.009.
[74] M. A. Dickson *et al.*, "Human keratinocytes that express hTERT and also bypass a p16(INK4a)-enforced mechanism that limits life span become immortal yet retain normal

growth and differentiation characteristics.," *Mol. Cell. Biol.*, vol. 20, no. 4, pp. 1436–1447, 2000, doi: 10.1128/MCB.20.4.1436-1447.2000.
[75] M. Irfan Maqsood, M. M. Matin, A. R. Bahrami, and M. M. Ghasroldasht, "Immortality of cell lines: challenges and advantages of establishment: Immortality of cell lines," *Cell Biol. Int.*, vol. 37, no. 10, pp. 1038–1045, 2013, doi: 10.1002/cbin.10137.
[76] M. Hasmim, G. Bieler, and C. Ruegg, "Zoledronate inhibits endothelial cell adhesion, migration and survival through the suppression of multiple, prenylation-dependent signaling pathways," *J Thromb Haemost*, vol. 5, no. 1, pp. 166–173, 2007, doi: 10.1111/j.1538-7836.2006.02259.x.
[77] A. Dongari-Bagtzoglou and H. Kashleva, "Development of a highly reproducible three-dimensional organotypic model of the oral mucosa," *Nat Protoc*, vol. 1, no. 4, pp. 2012–2018, 2006, doi: 10.1038/nprot.2006.323.
[78] G. Bullock, C. Miller, A. Mckechnie, and V. Hearnden, "Synthetic Hydroxyapatite Inhibits Bisphosphonate Toxicity to the Oral Mucosa In Vitro.," *Mater. (Basel, Switzerland)*, vol. 13, no. 9, 2020, doi: 10.3390/ma13092086.
[79] N. M. H. McLeod FRCS(OMFS), FDS, MRCS, K. A. Moutasim BDS, MSc, PhD, P. A. Brennan MD, FRCS(OMFS), FRCS, FDS, G. Thomas MScD, PhD, and V. Jenei MSc, PhD, "In Vitro Effect of Bisphosphonates on Oral Keratinocytes and Fibroblasts," *J Oral Maxillofac Surg*, vol. 72, no. 3, pp. 503–509, 2014, doi: 10.1016/j.joms.2013.08.007.
[80] K. Izumi, H. Terashi, C. L. Marcelo, and S. E. Feinberg, "Development and Characterization of a Tissue-engineered Human Oral Mucosa Equivalent Produced in a Serum-free Culture System," *J Dent Res*, vol. 79, no. 3, pp. 798–805, 2000, doi: 10.1177/00220345000790030301.
[81] F. Berthod, D. Hayek, O. Damour, and C. Collombel, "Collagen synthesis by fibroblasts cultured within a collagen sponge," *Biomaterials*, vol. 14, no. 10, pp. 749–754, 1993, doi: 10.1016/0142-9612(93)90039-5.
[82] A. F. Black, C. Bouez, E. Perrier, K. Schlotmann, F. Chapuis, and O. Damour, "Optimization and Characterization of an Engineered Human Skin Equivalent," *Tissue Eng*, vol. 11, no. 5–6, pp. 723–733, 2005, doi: 10.1089/ten.2005.11.723.
[83] B. Kinikoglu *et al.*, "Reconstruction of a full-thickness collagen-based human oral mucosal equivalent," *Biomaterials*, vol. 30, no. 32, pp. 6418–6425, 2009, doi: 10.1016/j.biomaterials.2009.08.010.
[84] J. W. Haycock, *3D Cell Culture [electronic resource]: Methods and Protocols*, 1. Totowa, NJ: Totowa, NJ : Humana Press : Imprint: Humana, 2011, 2011.
[85] H. E. Colley *et al.*, "Development of tissue-engineered models of oral dysplasia and early invasive oral squamous cell carcinoma," *Br J Cancer*, vol. 105, no. 10, pp. 1582–1592, 2011, doi: 10.1038/bjc.2011.403.
[86] Z. Said, C. Murdoch, J. Hansen, L. Siim Madsen, and H. E. Colley, "Corticosteroid delivery using oral mucosa equivalents for the treatment of inflammatory mucosal diseases," *Eur J Oral Sci*, vol. 129, no. 2, pp. e12761-n/a, 2021, doi: 10.1111/eos.12761.
[87] P. Zwicker, M. Zumpe, A. Kramer, and G. Müller, "A 3D Model of Human Buccal Mucosa for Compatibility Testing of Mouth Rinsing Solutions," *Pharmaceutics*, vol. 15, no. 3, p. 721, 2023, doi: 10.3390/pharmaceutics15030721.
[88] B. Ollington, H. E. (orcid:0000-0003-0053-7468) Colley, and C. (orcid:0000-0001-9724-122X) Murdoch, "Immuno-responsive tissue engineered oral mucosal equivalents containing macrophages," 2021.
[89] R. G. Russell, "Bisphosphonates: mode of action and pharmacology," *Pediatrics*, vol. 119 Suppl, pp. S150-62, 2007, doi: 10.1542/peds.2006-2023H.
[90] R. G. Russell, "Bisphosphonates: from bench to bedside," *Ann N Y Acad Sci*, vol. 1068, pp. 367–401, 2006, doi: 10.1196/annals.1346.041.
[91] M. T. Drake, B. L. Clarke, and S. Khosla, "Bisphosphonates: mechanism of action and role in

clinical practice," *Mayo Clin Proc*, vol. 83, no. 9, pp. 1032–1045, 2008, doi: 10.4065/83.9.1032.
[92] R. G. Russell, "Bisphosphonates: the first 40 years," *Bone*, vol. 49, no. 1, pp. 2–19, 2011, doi: 10.1016/j.bone.2011.04.022.
[93] A. Reszka and G. Rodan, "Bisphosphonate mechanism of action," *Curr. Rheumatol. Rep.*, vol. 5, no. 1, pp. 65–74, 2003, doi: 10.1007/s11926-003-0085-6.
[94] L. Rasmusson and J. Abtahi, "Bisphosphonate associated osteonecrosis of the jaw: an update on pathophysiology, risk factors, and treatment," *Int J Dent*, vol. 2014, p. 471035, 2014, doi: 10.1155/2014/471035.
[95] R. G. Russell *et al.*, "Bisphosphonates: an update on mechanisms of action and how these relate to clinical efficacy," *Ann N Y Acad Sci*, vol. 1117, pp. 209–257, 2007, doi: 10.1196/annals.1402.089.
[96] K. McLeod *et al.*, "XPS and bioactivity study of the bisphosphonate pamidronate adsorbed onto plasma sprayed hydroxyapatite coatings," *Appl. Surf. Sci. $V 253*, no. 5, pp. 2644–2651, 2006.
[97] M. J. Rogers, J. C. Crockett, F. P. Coxon, and J. Monkkonen, "Biochemical and molecular mechanisms of action of bisphosphonates," *Bone*, vol. 49, no. 1, pp. 34–41, 2011, doi: 10.1016/j.bone.2010.11.008.
[98] P. K. Piper Jr. and U. Gruntmanis, "Management of osteoporosis in the aging male: focus on zoledronic acid.," *Clin. Interv. Aging*, vol. 4, pp. 289–303, 2009.
[99] J. B. Catterall and T. E. Cawston, "Drugs in development: Bisphosphonates and metalloproteinase inhibitors," *Arthritis Res. Ther.*, vol. 5, no. 1, pp. 12–24, 2003.
[100] S. Cremers, R. Sparidans, H. J. den, N. Hamdy, P. Vermeij, and S. Papapoulos, "A pharmacokinetic and pharmacodynamic model for intravenous bisphosphonate (pamidronate) in osteoporosis," *Eur J Clin Pharmacol*, vol. 57, no. 12, pp. 883–890, 2002, doi: 10.1007/s00228-001-0411-8.
[101] T. Chen *et al.*, "Pharmacokinetics and Pharmacodynamics of Zoledronic Acid in Cancer Patients with Bone Metastases," *J. Clin. Pharmacol.*, vol. 42, no. 11, pp. 1228–1236, 2002, doi: 10.1177/009127002762491316.
[102] S. Khosla *et al.*, "Benefits and risks of bisphosphonate therapy for osteoporosis," *J Clin Endocrinol Metab*, vol. 97, no. 7, pp. 2272–2282, 2012, doi: 10.1210/jc.2012-1027.
[103] D. Marolt, M. Cozin, G. Vunjak-Novakovic, S. Cremers, and R. Landesberg, "Effects of Pamidronate on Human Alveolar Osteoblasts In Vitro," *J. Oral Maxillofac. Surg.*, vol. 70, no. 5, pp. 1081–1092, 2012, doi: 10.1016/j.joms.2011.05.002.
[104] S. Otto *et al.*, "Osteonecrosis of the jaw: effect of bisphosphonate type, local concentration, and acidic milieu on the pathomechanism," *J Oral Maxillofac Surg*, vol. 68, no. 11, pp. 2837–2845, 2010, doi: 10.1016/j.joms.2010.07.017.
[105] S. Cremers and S. Papapoulos, "Pharmacology of bisphosphonates," *Bone*, vol. 49, no. 1, pp. 42–49, 2011, doi: 10.1016/j.bone.2011.01.014.
[106] J. Lin, "Bisphosphonates: A review of their pharmacokinetic properties," *Bone*, vol. 18, no. 2, pp. 75–85, 1996, doi: 10.1016/8756-3282(95)00445-9.
[107] V. Kumar and R. K. Sinha, "Bisphosphonate Related Osteonecrosis of the Jaw: An Update," *J Maxillofac Oral Surg*, vol. 13, no. 4, pp. 386–393, 2014, doi: 10.1007/s12663-013-0564-x.
[108] S. Paulo *et al.*, "Bisphosphonate-related osteonecrosis of the jaw: specificities," *Oncol Rev*, vol. 8, no. 2, p. 254, 2014, doi: 10.4081/oncol.2014.254.
[109] G. Hampson and I. Fogelman, "Clinical role of bisphosphonate therapy," *Int J Womens Heal.*, vol. 4, pp. 455–469, 2012, doi: 10.2147/IJWH.S24783.
[110] K. Abe *et al.*, "Effects of bisphosphonates on osteoclastogenesis in RAW264.7 cells," *Int J Mol Med*, vol. 29, no. 6, pp. 1007–1015, 2012, doi: 10.3892/ijmm.2012.952.
[111] T. Bellido and L. I. Plotkin, "Novel actions of bisphosphonates in bone: Preservation of osteoblast and osteocyte viability," *Bone*, vol. 49, no. 1, pp. 50–55, 2011, doi:

https://doi.org/10.1016/j.bone.2010.08.008.
[112] A. M. Pabst *et al.*, “Angiogenesis in the Development of Medication-Related Osteonecrosis of the Jaws: An Overview,” *Dent J*, vol. 5, no. 1, 2016, doi: 10.3390/dj5010002.
[113] M. A. Scheper, A. Badros, R. Chaisuparat, K. J. Cullen, and T. F. Meiller, “Effect of zoledronic acid on oral fibroblasts and epithelial cells: a potential mechanism of bisphosphonate-associated osteonecrosis,” *Br. J. Haematol.*, vol. 144, no. 5, pp. 667–676, 2009, doi: 10.1111/j.1365-2141.2008.07504.x.
[114] S. Zafar, D. E. Coates, M. P. Cullinan, B. K. Drummond, T. Milne, and G. J. Seymour, “Zoledronic acid and geranylgeraniol regulate cellular behaviour and angiogenic gene expression in human gingival fibroblasts,” *J. Oral Pathol. Med.*, vol. 43, no. 9, pp. 711–721, 2014, doi: 10.1111/jop.12181.
[115] A. M. Pabst, T. Ziebart, F. P. Koch, K. Y. Taylor, B. Al-Nawas, and C. Walter, “The influence of bisphosphonates on viability, migration, and apoptosis of human oral keratinocytes—in vitro study,” *Clin. Oral Investig.*, vol. 16, no. 1, pp. 87–93, 2012, doi: 10.1007/s00784-010-0507-6.
[116] R. Landesberg *et al.*, “Inhibition of oral mucosal cell wound healing by bisphosphonates,” *J Oral Maxillofac Surg*, vol. 66, no. 5, pp. 839–847, 2008, doi: 10.1016/j.joms.2008.01.026.
[117] N. Taniguchi *et al.*, “Bisphosphonate-induced reactive oxygen species inhibit proliferation and migration of oral fibroblasts: A pathogenesis of bisphosphonate-related osteonecrosis of the jaw,” *J. Periodontol.*, vol. 91, no. 7, pp. 947–955, 2020, doi: 10.1002/JPER.19-0385.
[118] K. Walker and M. F. Olson, “Targeting Ras and Rho GTPases as opportunities for cancer therapeutics,” *Curr Opin Genet Dev*, vol. 15, no. 1, pp. 62–68, 2005, doi: 10.1016/j.gde.2004.11.001.
[119] A. Hall and S. Etienne-Manneville, “Rho GTPases in cell biology,” *Nature*, vol. 420, no. 6916, pp. 629–635, 2002, doi: 10.1038/nature01148.
[120] G. Bullock, “Tissue engineering approaches to the treatment of bisphosphonate-related osteonecrosis of the jaw,” The University of Sheffield, 2019. [Online]. Available: http://etheses.whiterose.ac.uk/24529/
[121] S. S. Soydan *et al.*, “Effects of alendronate and pamidronate on apoptosis and cell proliferation in cultured primary human gingival fibroblasts,” *Hum Exp Toxicol*, vol. 34, no. 11, pp. 1073–1082, 2015, doi: 10.1177/0960327115569808.
[122] T. Hemmi, K. Yusa, S. Ishikawa, H. Takano, M. Fukuda, and M. Iino, “Synergistic effect of zoledronate and compressive force suppresses proliferation and differentiation of human gingival fibroblasts,” *Br J Oral Maxillofac Surg*, 2023, doi: 10.1016/j.bjoms.2023.10.018.
[123] H. Ohnuki *et al.*, “Zoledronic acid induces S-phase arrest via a DNA damage response in normal human oral keratinocytes,” *Arch. Oral Biol.*, vol. 57, no. 7, pp. 906–917, 2012, doi: https://doi.org/10.1016/j.archoralbio.2011.11.015.
[124] R. H. Kim *et al.*, “Bisphosphonates induce senescence in normal human oral keratinocytes,” *J Dent Res*, vol. 90, no. 6, pp. 810–816, 2011, doi: 10.1177/0022034511402995.
[125] F. J. Manzano-Moreno *et al.*, “Impact of bisphosphonates on the proliferation and gene expression of human fibroblasts.,” *Int. J. Med. Sci.*, vol. 16, no. 12, pp. 1534–1540, 2019, doi: 10.7150/ijms.36994.
[126] M. Lang *et al.*, “Influence of zoledronic acid on proliferation, migration, and apoptosis of vascular endothelial cells,” *Br J Oral Maxillofac Surg*, vol. 54, no. 8, pp. 889–893, 2016, doi: 10.1016/j.bjoms.2016.05.030.
[127] J. Jung *et al.*, “Effects of an oral bisphosphonate and three intravenous bisphosphonates on several cell types in vitro,” *Clin. Oral Investig.*, vol. 22, no. 7, pp. 2527–2534, 2018, doi: 10.1007/s00784-018-2349-6.
[128] B. S. Kim, S. S. Yang, C. S. Kim, and J. Lee, “Zoledronate suppresses VEGF-induced capillary tube formation and inhibits expression of interferon-induced transmembrane protein-1 in

human umbilical vein endothelial cells," *Int. J. Mol. Med.*, 2018, doi: 10.3892/ijmm.2018.3497.
[129] G. Misso *et al.*, "Evaluation of the in vitro and in vivo antiangiogenic effects of denosumab and zoledronic acid," *Cancer Biol Ther*, vol. 13, no. 14, pp. 1491–1500, 2012, doi: 10.4161/cbt.22274.
[130] C. Walter, A. Pabst, T. Ziebart, M. Klein, and B. Al-Nawas, "Bisphosphonates affect migration ability and cell viability of HUVEC, fibroblasts and osteoblasts in vitro," *Oral Dis*, vol. 17, no. 2, pp. 194–199, 2011, doi: 10.1111/j.1601-0825.2010.01720.x.
[131] V. Stresing *et al.*, "Nitrogen-containing bisphosphonates can inhibit angiogenesis in vivo without the involvement of farnesyl pyrophosphate synthase," *Bone*, vol. 48, no. 2, pp. 259–266, 2011, doi: 10.1016/j.bone.2010.09.035.
[132] J. Wood *et al.*, "Novel Antiangiogenic Effects of the Bisphosphonate Compound Zoledronic Acid," *J. Pharmacol. Exp. Ther.*, vol. 302, pp. 1055–1061, Oct. 2002, doi: 10.1124/jpet.102.035295.
[133] T. Ziebart *et al.*, "Bisphosphonates: Restrictions for vasculogenesis and angiogenesis: Inhibition of cell function of endothelial progenitor cells and mature endothelial cells in vitro," *Clin. Oral Investig.*, vol. 15, no. 1, pp. 105–111, 2011, doi: 10.1007/s00784-009-0365-2.
[134] Y. Lu, Z. Wang, W. Han, and H. Li, "Zoledronate induces autophagic cell death in human umbilical vein endothelial cells via Beclin-1 dependent pathway activation," *Mol Med Rep*, vol. 14, no. 5, pp. 4747–4754, 2016, doi: 10.3892/mmr.2016.5834.
[135] C. Walter, M. Klein, A. Pabst, B. Al-Nawas, H. Duschner, and T. Ziebart, "Influence of bisphosphonates on endothelial cells, fibroblasts, and osteogenic cells," *Clin. Oral Investig.*, vol. 14, no. 1, pp. 35–41, 2010, doi: 10.1007/s00784-009-0266-4.
[136] J. Compston *et al.*, "UK clinical guideline for the prevention and treatment of osteoporosis," *Arch. Osteoporos.*, vol. 12, no. 1, pp. 1–24, 2017, doi: 10.1007/s11657-017-0324-5.
[137] O. Nicolatou-Galitis *et al.*, "Medication-related osteonecrosis of the jaw: definition and best practice for prevention, diagnosis, and treatment," *Oral Surg Oral Med Oral Pathol Oral Radiol*, vol. 127, no. 2, pp. 117–135, 2019, doi: 10.1016/j.oooo.2018.09.008.
[138] B. Abrahamsen, "Adverse Effects of Bisphosphonates," *Calcif. Tissue Int.*, vol. 86, no. 6, pp. 421–435, 2010, doi: 10.1007/s00223-010-9364-1.
[139] K. A. Kennel and M. T. Drake, "Adverse Effects of Bisphosphonates: Implications for Osteoporosis Management," *Mayo Clin. Proc.*, vol. 84, no. 7, pp. 632–638, 2009, doi: 10.4065/84.7.632.
[140] T. Tanvetyanon and P. J. Stiff, "Management of the adverse effects associated with intravenous bisphosphonates," *Ann. Oncol.*, vol. 17, no. 6, pp. 897–907, 2006, doi: 10.1093/annonc/mdj105.
[141] M. Aapro *et al.*, "Guidance on the use of bisphosphonates in solid tumours: recommendations of an international expert panel," *Ann. Oncol.*, vol. 19, no. 3, pp. 420–432, 2008, doi: 10.1093/annonc/mdm442.
[142] E. M. Lewiecki, "Bisphosphonates for the treatment of osteoporosis: insights for clinicians," *Ther. Adv. Chronic Dis.*, vol. 1, no. 3, pp. 115–128, 2010, doi: 10.1177/2040622310374783.
[143] B. Mehrotra, "Safety Profile of Intravenous Bisphosphonates," *Semin. Oncol.*, vol. 34, pp. S24–S27, 2007, doi: https://doi.org/10.1053/j.seminoncol.2007.10.007.
[144] M. Schiodt *et al.*, "Workshop of European task force on medication-related osteonecrosis of the jaw-Current challenges," *Oral Dis*, vol. 25, no. 7, pp. 1815–1821, 2019, doi: 10.1111/odi.13160.
[145] S. Kalra and V. Jain, "Dental complications and management of patients on bisphosphonate therapy: A review article," *J Oral Biol Craniofac Res*, vol. 3, no. 1, pp. 25–30, 2013, doi: 10.1016/j.jobcr.2012.11.001.

[146] I. R. Reid, M. J. Bolland, and A. B. Grey, “Is bisphosphonate-associated osteonecrosis of the jaw caused by soft tissue toxicity?,” *Bone*, vol. 41, no. 3, pp. 318–320, 2007, doi: 10.1016/j.bone.2007.04.196.
[147] H. Kishimoto, K. Noguchi, and K. Takaoka, “Novel insight into the management of bisphosphonate-related osteonecrosis of the jaw (BRONJ),” *Jpn. Dent. Sci. Rev.*, vol. 55, no. 1, pp. 95–102, 2019, doi: 10.1016/j.jdsr.2018.09.002.
[148] S. Kuhl, C. Walter, S. Acham, R. Pfeffer, and J. T. Lambrecht, “Bisphosphonate-related osteonecrosis of the jaws--a review,” *Oral Oncol*, vol. 48, no. 10, pp. 938–947, 2012, doi: 10.1016/j.oraloncology.2012.03.028.
[149] S. L. Ruggiero *et al.*, “American Association of Oral and Maxillofacial Surgeons Position Paper on Medication-Related Osteonecrosis of the Jaw—2014 Update,” *J. Oral Maxillofac. Surg.*, vol. 72, no. 10, pp. 1938–1956, 2014, doi: 10.1016/j.joms.2014.04.031.
[150] A. A. Khan *et al.*, “Diagnosis and management of osteonecrosis of the jaw: a systematic review and international consensus,” *J Bone Min. Res*, vol. 30, no. 1, pp. 3–23, 2015, doi: 10.1002/jbmr.2405.
[151] A. Bamias *et al.*, “Osteonecrosis of the jaw in cancer after treatment with bisphosphonates: incidence and risk factors,” *J Clin Oncol*, vol. 23, no. 34, pp. 8580–8587, 2005, doi: 10.1200/JCO.2005.02.8670.
[152] D. H. Henry *et al.*, “Randomized, double-blind study of denosumab versus zoledronic acid in the treatment of bone metastases in patients with advanced cancer (excluding breast and prostate cancer) or multiple myeloma,” *J Clin Oncol*, vol. 29, no. 9, pp. 1125–1132, 2011, doi: 10.1200/JCO.2010.31.3304.
[153] J. C. Lo MD *et al.*, “Prevalence of Osteonecrosis of the Jaw in Patients With Oral Bisphosphonate Exposure,” *J Oral Maxillofac Surg*, vol. 68, no. 2, pp. 243–253, 2010, doi: 10.1016/j.joms.2009.03.050.
[154] D. M. Black *et al.*, “The Effect of 6 versus 9 Years of Zoledronic Acid Treatment in Osteoporosis: A Randomized Second Extension to the HORIZON-Pivotal Fracture Trial (PFT),” *J Bone Min. Res*, vol. 30, no. 5, pp. 934–944, 2015, doi: 10.1002/jbmr.2442.
[155] T. Ikebe, “Pathophysiology of BRONJ: Drug-related osteoclastic disease of the jaw,” *Oral Sci. Int.*, vol. 10, no. 1, pp. 1–8, 2013, doi: https://doi.org/10.1016/S1348-8643(12)00045-6.
[156] T. Shibahara, “Antiresorptive Agent-Related Osteonecrosis of the Jaw (ARONJ): A Twist of Fate in the Bone,” *Tohoku J Exp Med*, vol. 247, no. 2, pp. 75–86, 2019, doi: 10.1620/tjem.247.75.
[157] F. Saad *et al.*, “Incidence, risk factors, and outcomes of osteonecrosis of the jaw: integrated analysis from three blinded active-controlled phase III trials in cancer patients with bone metastases,” *Ann Oncol*, vol. 23, no. 5, pp. 1341–1347, 2012, doi: 10.1093/annonc/mdr435.
[158] Y.-G. Kim, B.-S. Lee, Y.-D. Kwon, J.-H. Suh, and S.-M. Jeen, “Study on bisphosphonate-related osteonecrosis of the jaw (BRONJ): case report and literature review,” *J Korean Assoc Oral Maxillofac Surg*, vol. 36, no. 4, pp. 291–302, 2010, [Online]. Available: http://synapse.koreamed.org/DOIx.php?id=10.5125%2Fjkaoms.2010.36.4.291
[159] I. Giovannacci *et al.*, “Medication-Related Osteonecrosis of the Jaw Around Dental Implants: Implant Surgery-Triggered or Implant Presence-Triggered Osteonecrosis?,” *J Craniofac Surg*, vol. 27, no. 3, pp. 697–701, 2016, doi: 10.1097/SCS.0000000000002564.
[160] K. Niibe, T. Ouchi, R. Iwasaki, T. Nakagawa, and N. Horie, “Osteonecrosis of the jaw in patients with dental prostheses being treated with bisphosphonates or denosumab,” *J Prosthodont Res*, vol. 59, no. 1, pp. 3–5, 2015, doi: 10.1016/j.jpor.2014.08.001.
[161] A. Kyrgidis *et al.*, “Bisphosphonate-related osteonecrosis of the jaws: a case-control study of risk factors in breast cancer patients,” *J Clin Oncol*, vol. 26, no. 28, pp. 4634–4638, 2008, doi: 10.1200/JCO.2008.16.2768.
[162] S. Otto *et al.*, “Tooth extraction in patients receiving oral or intravenous bisphosphonate

administration: A trigger for BRONJ development?," *J Craniomaxillofac Surg*, vol. 43, no. 6, pp. 847–854, 2015, doi: 10.1016/j.jcms.2015.03.039.
[163] S. Soutome *et al.*, "Factors affecting development of medication-related osteonecrosis of the jaw in cancer patients receiving high-dose bisphosphonate or denosumab therapy: Is tooth extraction a risk factor?," *PLoS One*, vol. 13, no. 7, p. e0201343, 2018, doi: 10.1371/journal.pone.0201343.
[164] M. Kos, "Association of dental and periodontal status with bisphosphonate-related osteonecrosis of the jaws. A retrospective case controlled study," *Arch Med Sci*, vol. 10, no. 1, pp. 117–123, 2014, doi: 10.5114/aoms.2014.40738.
[165] D. E. Hughes *et al.*, "Bisphosphonates promote apoptosis in murine osteoclasts in vitro and in vivo," *J. Bone Miner. Res.*, vol. 10, no. 10, pp. 1478–1487, Oct. 1995, doi: 10.1002/jbmr.5650101008.
[166] M. R. Allen and D. B. Burr, "The Pathogenesis of Bisphosphonate-Related Osteonecrosis of the Jaw: So Many Hypotheses, So Few Data," *J. Oral Maxillofac. Surg.*, vol. 67, no. 5 SUPPL., pp. 61–70, May 2009, doi: 10.1016/j.joms.2009.01.007.
[167] V. Viereck *et al.*, "Bisphosphonates pamidronate and zoledronic acid stimulate osteoprotegerin production by primary human osteoblasts," *Biochem. Biophys. Res. Commun.*, vol. 291, no. 3, pp. 680–686, 2002, doi: 10.1006/bbrc.2002.6510.
[168] T. Kaiser, K. Geiger, D. Wallwiener, G. Klein, and T. N. Fehm, "Effects of bisphosphonates on human osteoblasts as an important constituent of the bone marrow microenvironment.," *J. Clin. Oncol.*, vol. 28, no. 15_suppl, pp. e13620–e13620, May 2010, doi: 10.1200/jco.2010.28.15_suppl.e13620.
[169] D. Santini *et al.*, "Zoledronic acid induces significant and long-lasting modifications of circulating angiogenic factors in cancer patients.," *Clin. Cancer Res.*, vol. 9, no. 8, pp. 2893–2897, 2003.
[170] T. Hansen, M. Kunkel, A. Weber, and C. James Kirkpatrick, "Osteonecrosis of the jaws in patients treated with bisphosphonates – histomorphologic analysis in comparison with infected osteoradionecrosis," *J. Oral Pathol. Med.*, vol. 35, no. 3, pp. 155–160, 2006, doi: 10.1111/j.1600-0714.2006.00391.x.
[171] P. P. Sedghizadeh, S. K. S. Kumar, A. Gorur, C. Schaudinn, C. F. Shuler, and J. W. Costerton, "Microbial Biofilms in Osteomyelitis of the Jaw and Osteonecrosis of the Jaw Secondary to Bisphosphonate Therapy," *J. Am. Dent. Assoc.*, vol. 140, no. 10, pp. 1259–1265, 2009, doi: 10.14219/jada.archive.2009.0049.
[172] R. C. Boff, F. G. Salum, M. A. Figueiredo, and K. Cherubini, "Important aspects regarding the role of microorganisms in bisphosphonate-related osteonecrosis of the jaws," *Arch Oral Biol*, vol. 59, no. 8, pp. 790–799, 2014, doi: 10.1016/j.archoralbio.2014.05.002.
[173] S. Panya *et al.*, "Role of microbiological culture and polymerase chain reaction (PCR) of actinomyces in medication-related osteonecrosis of the jaw (MRONJ)," *J Craniomaxillofac Surg*, vol. 45, no. 3, pp. 357–363, 2017, doi: 10.1016/j.jcms.2017.01.006.
[174] X. Wei *et al.*, "Molecular profiling of oral microbiota in jawbone samples of bisphosphonate-related osteonecrosis of the jaw," *Oral Dis.*, vol. 18, no. 6, pp. 602–612, 2012, doi: 10.1111/j.1601-0825.2012.01916.x.
[175] F. Hallmer, T. Bjørnland, G. Andersson, J. P. Becktor, A. K. Kristoffersen, and M. Enersen, "Bacterial diversity in medication-related osteonecrosis of the jaw," *Oral Surg. Oral Med. Oral Pathol. Oral Radiol.*, vol. 123, no. 4, pp. 436–444, 2017, doi: 10.1016/j.oooo.2016.11.011.
[176] P. P. Sedghizadeh, S. K. S. Kumar, A. Gorur, C. Schaudinn, C. F. Shuler, and J. W. Costerton, "Identification of Microbial Biofilms in Osteonecrosis of the Jaws Secondary to Bisphosphonate Therapy," *J. Oral Maxillofac. Surg.*, vol. 66, no. 4, pp. 767–775, 2008, doi: 10.1016/j.joms.2007.11.035.
[177] J. I. Aguirre *et al.*, "Oncologic doses of zoledronic acid induce osteonecrosis of the jaw-like

lesions in rice rats (Oryzomys palustris) with periodontitis," *J Bone Min. Res*, vol. 27, no. 10, pp. 2130–2143, 2012, doi: 10.1002/jbmr.1669.
[178] H. Katsarelis, N. P. Shah, D. K. Dhariwal, and M. Pazianas, "Infection and medication-related osteonecrosis of the jaw," *J Dent Res*, vol. 94, no. 4, pp. 534–539, 2015, doi: 10.1177/0022034515572021.
[179] M. Kos, A. Junka, D. Smutnicka, P. Szymczyk, K. Gluza, and M. Bartoszewicz, "Bisphosphonates enhance bacterial adhesion and biofilm formation on bone hydroxyapatite," *J. Cranio-Maxillo-Facial Surg.*, vol. 43, no. 6, pp. 863–869, 2015, doi: 10.1016/j.jcms.2015.04.018.
[180] S. Kalyan *et al.*, "Systemic immunity shapes the oral microbiome and susceptibility to bisphosphonate-associated osteonecrosis of the jaw," *J. Transl. Med.*, vol. 13, no. 1, p. 212, 2015, doi: 10.1186/s12967-015-0568-z.
[181] W. Zhang *et al.*, "The Role of the Immune Response in the Development of Medication-Related Osteonecrosis of the Jaw," *Front Immunol*, vol. 12, p. 606043, 2021, doi: 10.3389/fimmu.2021.606043.
[182] T. Soma *et al.*, "Tooth extraction in mice administered zoledronate increases inflammatory cytokine levels and promotes osteonecrosis of the jaw," *J Bone Min. Metab*, vol. 39, no. 3, pp. 372–384, 2021, doi: 10.1007/s00774-020-01174-2.
[183] R. S. de Molon *et al.*, "Rheumatoid Arthritis Exacerbates the Severity of Osteonecrosis of the Jaws (ONJ) in Mice. A Randomized, Prospective, Controlled Animal Study: RHEUMATOID ARTHRITIS EXACERBATES SEVERITY OF OSTEONECROSIS OF THE JAW," *J. bone Miner. Res.*, vol. 31, no. 8, pp. 1596–1607, 2016, doi: 10.1002/jbmr.2827.
[184] G. Yang *et al.*, "SIRT1/HERC4 Locus Associated With Bisphosphonate-Induced Osteonecrosis of the Jaw: An Exome-Wide Association Analysis," *J Bone Min. Res*, vol. 33, no. 1, pp. 91–98, 2018, doi: 10.1002/jbmr.3285.
[185] K. H. Lee *et al.*, "Identifying genetic variants underlying medication-induced osteonecrosis of the jaw in cancer and osteoporosis: a case control study," *J Transl Med*, vol. 17, no. 1, p. 381, 2019, doi: 10.1186/s12967-019-2129-3.
[186] S. Otto, C. Pautke, T. Van den Wyngaert, D. Niepel, and M. Schiodt, "Medication-related osteonecrosis of the jaw: Prevention, diagnosis and management in patients with cancer and bone metastases," *Cancer Treat Rev*, vol. 69, pp. 177–187, 2018, doi: 10.1016/j.ctrv.2018.06.007.
[187] O. Di Fede *et al.*, "The dental management of patients at risk of medication-related osteonecrosis of the jaw: New paradigm of primary prevention," *BioMed Research International*. 2018. doi: 10.1155/2018/2684924.
[188] S. L. Ruggiero and S. Bin Woo, "Biophosphonate-Related Osteonecrosis of the Jaws," *Dent. Clin. North Am.*, vol. 52, no. 1, pp. 111–128, 2008, doi: 10.1016/j.cden.2007.09.002.
[189] S. Y. Jung, H. S. Suh, J. W. Park, and J. W. Kwon, "Drug holiday patterns and bisphosphonate-related osteonecrosis of the jaw," *Oral Dis*, vol. 25, no. 2, pp. 471–480, 2019, doi: 10.1111/odi.12966.
[190] D. Rosella, P. Papi, R. Giardino, E. Cicalini, L. Piccoli, and G. Pompa, "Medication-related osteonecrosis of the jaw: Clinical and practical guidelines," *J Int Soc Prev Community Dent*, vol. 6, no. 2, pp. 97–104, 2016, doi: 10.4103/2231-0762.178742.
[191] UK Chemotherapy Board., "Medication-related osteonecrosis of the jaw. Guidance for the oncology multidisciplinary team. Report of a working party on behalf of the UK Chemotherapy Board.," 2019. [Online]. Available: https://www.rcplondon.ac.uk/guidelines-policy/medication-related-osteonecrosis-jaw-guidance-oncology-multidisciplinary-team
[192] T. Lombard, V. Neirinckx, B. Rogister, Y. Gilon, and S. Wislet, "Medication-Related Osteonecrosis of the Jaw: New Insights into Molecular Mechanisms and Cellular Therapeutic Approaches.," *Stem Cells Int.*, vol. 2016, p. 8768162, 2016.

[193] J. Abtahi, F. Agholme, and P. Aspenberg, “Prevention of osteonecrosis of the jaw by mucoperiosteal coverage in a rat model,” *Int. J. Oral Maxillofac. Surg.*, vol. 42, no. 5, pp. 632–636, 2013, doi: 10.1016/j.ijom.2013.02.007.
[194] D. Holzinger *et al.*, “Long-term success of surgery in bisphosphonate-related osteonecrosis of the jaws (BRONJs),” *Oral Oncol*, vol. 49, no. 1, pp. 66–70, 2013, doi: 10.1016/j.oraloncology.2012.07.008.
[195] E. R. Carlson and J. D. Basile, “The Role of Surgical Resection in the Management of Bisphosphonate-Related Osteonecrosis of the Jaws,” *J. Oral Maxillofac. Surg.*, vol. 67, no. 5, pp. 85–95, 2009, doi: 10.1016/j.joms.2009.01.006.
[196] F. Wilde *et al.*, “The role of surgical therapy in the management of intravenous bisphosphonates-related osteonecrosis of the jaw,” *Oral Surgery, Oral Med. Oral Pathol. Oral Radiol. Endodontology*, vol. 111, no. 2, pp. 153–163, Feb. 2011, doi: 10.1016/j.tripleo.2010.04.015.
[197] Y. Li *et al.*, “Allogeneic Mesenchymal Stem Cell Therapy for Bisphosphonate-Related Jaw Osteonecrosis in Swine,” *Stem Cells Dev.*, vol. 22, no. 14, pp. 2047–2056, Mar. 2013, doi: 10.1089/scd.2012.0615.
[198] T. Kikuiri *et al.*, “Cell-based immunotherapy with mesenchymal stem cells cures bisphosphonate-related osteonecrosis of the jaw-like disease in mice,” *J. Bone Miner. Res.*, 2010, doi: 10.1002/jbmr.37.
[199] X. Zang, L. He, L. Zhao, Y. He, E. Xiao, and Y. Zhang, “Adipose-derived stem cells prevent the onset of bisphosphonate-related osteonecrosis of the jaw through transforming growth factor beta-1-mediated gingival wound healing,” *Stem Cell Res Ther*, vol. 10, no. 1, p. 169, 2019, doi: 10.1186/s13287-019-1277-y.
[200] S. Altowity, A. Abdel-Rahm, R. Kasem, and M. Elsebaie, “Role of Mesenchymal Stem Cells in Bone Healing of Rat Bisphosphonate-induced Osteonecrosis of the Jaw,” *J. Med. Sci.*, vol. 18, pp. 87–95, Feb. 2018, doi: 10.3923/jms.2018.87.95.
[201] L. Cella *et al.*, “Autologous bone marrow stem cell intralesional transplantation repairing bisphosphonate related osteonecrosis of the jaw.,” *Head Face Med.*, vol. 7, no. 1, p. 16, 2011, doi: 10.1186/1746-160X-7-16.
[202] E. Alonso-Rodriguez *et al.*, “Bisphosphonate-related osteonecrosis. Application of adipose-derived stem cells in an experimental murine model,” *Med. Oral Patol. Oral Cir. Bucal*, vol. 24, no. 4, pp. e529–e536, Jul. 2019, doi: 10.4317/medoral.22959.
[203] P. Barba-Recreo *et al.*, “Adipose-derived stem cells and platelet-rich plasma for preventive treatment of bisphosphonate-related osteonecrosis of the jaw in a murine model,” *J. Cranio-Maxillo-Facial Surg.*, vol. 43, no. 7, pp. 1161–1168, 2015, doi: 10.1016/j.jcms.2015.04.026.
[204] M. Del Fabbro, G. Gallesio, and M. Mozzati, “Autologous platelet concentrates for bisphosphonate-related osteonecrosis of the jaw treatment and prevention. A systematic review of the literature,” *Eur. J. Cancer*, vol. 51, no. 1, pp. 62–74, 2015, doi: 10.1016/j.ejca.2014.10.015.
[205] F. Longo *et al.*, “Platelet rich plasma in the treatment of bisphosphonate-related osteonecrosis of the jaw: personal experience and review of the literature.,” *Int. J. Dent.*, vol. 2014, no. 2014, p. 298945, 2014, doi: 10.1155/2014/298945.
[206] R. Mauceri *et al.*, “Conservative Surgical Treatment of Bisphosphonate-Related Osteonecrosis of the Jaw with Er,Cr:YSGG Laser and Platelet-Rich Plasma: A Longitudinal Study.,” *Biomed Res. Int.*, vol. 2018, p. 3982540, 2018, doi: 10.1155/2018/3982540.
[207] V. Pavlovic, M. Ciric, V. Jovanovic, and P. Stojanovic, “Platelet Rich Plasma: a short overview of certain bioactive components,” *Open Med. (Warsaw, Poland)*, vol. 11, no. 1, pp. 242–247, Aug. 2016, doi: 10.1515/med-2016-0048.
[208] Y. Komatsu *et al.*, “Zoledronic acid suppresses transforming growth factor-β-induced

fibrogenesis by human gingival fibroblasts," *Int. J. Mol. Med.*, vol. 38, no. 1, pp. 139–147, Jul. 2016, doi: 10.3892/ijmm.2016.2582.
[209] Q. Wang, J. Liu, T. Guo, D. Liu, and J. Pan, "Epidermal Growth Factor Reverses the Inhibitory Effects of the Bisphosphonate, Zoledronic Acid, on Human Oral Keratinocytes and Human Vascular Endothelial Cells In Vitro via the Epidermal Growth Factor Receptor (EGFR)/Akt/Phosphoinositide 3-Kinase (PI3K) Signaling Pathway," *Med. Sci. Monit.*, vol. 25, pp. 700–710, Jan. 2019, doi: 10.12659/MSM.911579.
[210] J. B. B. Weber, R. S. Camilotti, and M. E. Ponte, "Efficacy of laser therapy in the management of bisphosphonate-related osteonecrosis of the jaw (BRONJ): a systematic review," *Lasers Med. Sci.*, vol. 31, no. 6, pp. 1261–1272, 2016, doi: 10.1007/s10103-016-1929-4.
[211] C. Walter, A. M. Pabst, and T. Ziebart, "Effects of a low-level diode laser on oral keratinocytes, oral fibroblasts, endothelial cells and osteoblasts incubated with bisphosphonates: An in vitro study.," *Biomed. reports*, vol. 3, no. 1, pp. 14–18, 2015, doi: 10.3892/br.2014.389.
[212] F. G. Basso *et al.*, "Biostimulatory effects of low-level laser therapy on epithelial cells and gingival fibroblasts treated with zoledronic acid," *Laser Phys.*, vol. 23, no. 5, 2013, doi: 10.1088/1054-660X/23/5/055601.
[213] P. Vescovi, E. Merigo, M. Meleti, M. Manfredi, C. Fornaini, and S. Nammour, "Surgical Approach and Laser Applications in BRONJ Osteoporotic and Cancer Patients," *J. Osteoporos.*, vol. 2012, p. 585434, 2012, doi: 10.1155/2012/585434.
[214] E. B. Bermúdez-Bejarano *et al.*, "Prophylaxis and antibiotic therapy in management protocols of patients treated with oral and intravenous bisphosphonates," *J. Clin. Exp. Dent.*, 2017, doi: 10.4317/jced.53372.
[215] T. Ikeda, J. Kuraguchi, Y. Kogashiwa, H. Yokoi, T. Satomi, and N. Kohno, "Successful treatment of Bisphosphonate-Related Osteonecrosis of the Jaw (BRONJ) patients with sitafloxacin: New strategies for the treatment of BRONJ," *Bone*, vol. 73, pp. 217–222, 2015, doi: https://doi.org/10.1016/j.bone.2014.12.021.
[216] G. D. Çapar *et al.*, "Preventive effect of doxycycline sponge against bisphosphonate-related osteonecrosis of the jaws: an animal study," *Biotechnol. Biotechnol. Equip.*, vol. 30, no. 4, pp. 752–761, 2016, doi: 10.1080/13102818.2016.1174078.
[217] S. Paulo *et al.*, "Synthetic Calcium Phosphate Ceramics as a Potential Treatment for Bisphosphonate-Related Osteonecrosis of the Jaw," *Mater.*, vol. 12, no. 11, 2019, doi: 10.3390/ma12111840.
[218] P. Siri *et al.*, "Calcium Phosphate Ceramics Can Prevent Bisphosphonate-Related Osteonecrosis of the Jaw," *Materials (Basel).*, vol. 13, no. 8, p. 1955, 2020, doi: 10.3390/ma13081955.
[219] H.-J. Ho, H. Shirakawa, P. E. Giriwono, A. Ito, and M. Komai, "A novel function of geranylgeraniol in regulating testosterone production," *Biosci. Biotechnol. Biochem. Spec. Issue Recent Adv. isoprenoid Stud.*, vol. 82, no. 6, pp. 956–962, 2018, doi: 10.1080/09168451.2017.1415129.
[220] N. Nualkaew, W. De-Eknamkul, T. M. Kutchan, and M. H. Zenk, "Geranylgeraniol formation in Croton stellatopilosus proceeds via successive monodephosphorylations of geranylgeranyl diphosphate," *Tetrahedron Lett.*, vol. 46, no. 50, pp. 8727–8731, 2005, doi: 10.1016/j.tetlet.2005.10.048.
[221] N. C. for B. Information, "Geranylgeraniol," *PubChem Database*. https://pubchem.ncbi.nlm.nih.gov/compound/Geranylgeraniol (accessed Mar. 01, 2020).
[222] R. M. Fliefel, S. A. Entekhabi, M. Ehrenfeld, and S. Otto, "Geranylgeraniol (GGOH) as a Mevalonate Pathway Activator in the Rescue of Bone Cells Treated with Zoledronic Acid: An In Vitro Study.," *Stem Cells Int.*, vol. 2019, p. 4351327, 2019, doi: 10.1155/2019/4351327.
[223] N. Hagelauer, T. Ziebart, A. Pabst, and C. Walter, "Bisphosphonates inhibit cell functions of

HUVECs, fibroblasts and osteogenic cells via inhibition of protein geranylgeranylation," *Clin. Oral Investig.*, vol. 19, no. 5, pp. 1079–1091, 2015, doi: 10.1007/s00784-014-1320-4.
[224] T. Ziebart *et al.*, "Geranylgeraniol – A new potential therapeutic approach to bisphosphonate associated osteonecrosis of the jaw," *Oral Oncol.*, vol. 47, no. 3, pp. 195–201, 2011, doi: 10.1016/j.oraloncology.2010.12.003.
[225] A. Pabst *et al.*, "The influence of geranylgeraniol on microvessel sprouting after bisphosphonate substitution in an in vitro 3D-angiogenesis assay," *Clin. Oral Investig.*, vol. 21, no. 3, pp. 771–778, 2017, doi: 10.1007/s00784-016-1842-z.
[226] S. Zafar, D. E. Coates, M. P. Cullinan, B. K. Drummond, T. Milne, and G. J. Seymour, "Effects of zoledronic acid and geranylgeraniol on the cellular behaviour and gene expression of primary human alveolar osteoblasts," *Clin Oral Investig*, vol. 20, no. 8, pp. 2023–2035, 2016, doi: 10.1007/s00784-015-1706-y.
[227] F. Koneski *et al.*, "In vivo effects of geranylgeraniol on the development of bisphosphonate-related osteonecrosis of the jaws," *J. Cranio-Maxillo-Facial Surg.*, vol. 46, no. 2, pp. 230–236, 2018, doi: 10.1016/j.jcms.2017.11.007.
[228] Y. Nagaoka, H. Kajiya, S. Ozeki, T. Ikebe, and K. Okabe, "Mevalonates Restore Zoledronic Acid–induced Osteoclastogenesis Inhibition," *J. Dent. Res.*, vol. 94, no. 4, pp. 594–601, 2015, doi: 10.1177/0022034514564187.
[229] Y. Inoue, T. Hada, A. Shiraishi, K. Hirose, H. Hamashima, and S. Kobayashi, "Biphasic effects of geranylgeraniol, teprenone, and phytol on the growth of Staphylococcus aureus," *Antimicrob Agents Chemother*, vol. 49, no. 5, pp. 1770–1774, 2005, doi: 10.1128/AAC.49.5.1770-1774.2005.
[230] N. Togashi, H. Hamashima, A. Shiraishi, Y. Inoue, and A. Takano, "Antibacterial Activities Against Staphylococcus aureus of Terpene Alcohols With Aliphatic Carbon Chains," *J. Essent. Oil Res.*, vol. 22, no. 3, pp. 263–269, 2010, doi: 10.1080/10412905.2010.9700321.
[231] A. Marcuzzi, A. Tommasini, S. Crovella, and A. Pontillo, "Natural isoprenoids inhibit LPS-induced-production of cytokines and nitric oxide in aminobisphosphonate-treated monocytes," *Int Immunopharmacol*, vol. 10, no. 6, pp. 639–642, 2010, doi: 10.1016/j.intimp.2010.03.008.
[232] Y. Ohsaki *et al.*, "Vitamin K suppresses the lipopolysaccharide-induced expression of inflammatory cytokines in cultured macrophage-like cells via the inhibition of the activation of nuclear factor κB through the repression of IKKα/β phosphorylation," *J. Nutr. Biochem.*, vol. 21, no. 11, pp. 1120–1126, 2010, doi: 10.1016/j.jnutbio.2009.09.011.
[233] P. Giriwono *et al.*, "Geranylgeraniol Suppresses the Expression of IRAK1 and TRAF6 to Inhibit NFB Activation in Lipopolysaccharide-Induced Inflammatory Responses in Human Macrophage-Like Cells," *Int. J. Mol. Sci.*, vol. 20, no. 9, 2019, doi: 10.3390/ijms20092320.
[234] P. E. Giriwono *et al.*, "Dietary supplementation with geranylgeraniol suppresses lipopolysaccharide-induced inflammation via inhibition of nuclear factor-kappaB activation in rats," *Eur J Nutr*, vol. 52, no. 3, pp. 1191–1199, 2013, doi: 10.1007/s00394-012-0429-y.
[235] T. Kawase, S. Mubarak, and C. F. Mourão, "The Platelet Concentrates Therapy: From the Biased Past to the Anticipated Future," *Bioeng.*, vol. 7, no. 3, p. 82, 2020, doi: 10.3390/bioengineering7030082.
[236] R. E. Marx, E. R. Carlson, R. M. Eichstaedt, S. R. Schimmele, J. E. Strauss, and K. R. Georgeff, "Platelet-rich plasma: Growth factor enhancement for bone grafts," *Oral Surg Oral Med Oral Pathol Oral Radiol Endod*, vol. 85, no. 6, pp. 638–646, 1998, doi: 10.1016/S1079-2104(98)90029-4.
[237] P. Lopez-Jornet, A. Sanchez Perez, R. Amaral Mendes, and A. Tobias, "Medication-related osteonecrosis of the jaw: Is autologous platelet concentrate application effective for prevention and treatment? A systematic review," *J Craniomaxillofac Surg*, vol. 44, no. 8, pp.

1067–1072, 2016, doi: 10.1016/j.jcms.2016.05.004.
[238] A. Albanese, M. E. Licata, B. Polizzi, and G. Campisi, “Platelet-rich plasma (PRP) in dental and oral surgery: From the wound healing to bone regeneration,” *Immun Ageing*, vol. 10, no. 1, p. 23, 2013, doi: 10.1186/1742-4933-10-23.
[239] G. Maluf, R. J. Caldas, and P. S. Silva Santos, “The use of leukocyte-and platelet-rich fibrin (LPRF) in the treatment of medication-related osteonecrosis of the jaws (MRONJ),” *J Oral Maxillofac Surg*, vol. 76, no. 1, pp. 88–96, 2017, doi: 10.1016/j.joms.2017.06.004.
[240] T. Asaka *et al.*, “Platelet-rich fibrin may reduce the risk of delayed recovery in tooth-extracted patients undergoing oral bisphosphonate therapy: a trial study,” *Clin Oral Investig*, vol. 21, no. 7, pp. 2165–2172, 2017, doi: 10.1007/s00784-016-2004-z.
[241] J.-H. Park DDS, PhD, J.-W. Kim DDS, PhD, and S.-J. Kim DDS, PhD, “Does the addition of bone morphogenetic protein-2 to platelet-rich fibrin improve healing after treatment for medication-related osteonecrosis of the jaw?,” *J Oral Maxillofac Surg*, vol. 75, no. 6, pp. 1176–1184, 2016, doi: 10.1016/j.joms.2016.12.005.
[242] A. Giudice, S. Barone, C. Giudice, F. Bennardo, and L. Fortunato, “Can platelet-rich fibrin improve healing after surgical treatment of medication-related osteonecrosis of the jaw? A pilot study,” *Oral Surg Oral Med Oral Pathol Oral Radiol*, vol. 126, no. 5, pp. 390–403, 2018, doi: 10.1016/j.oooo.2018.06.007.
[243] A. Pispero, I. Bancora, A. Khalil, D. Scarnò, and E. M. Varoni, “Use of Platelet Rich Fibrin (PRF)-Based Autologous Membranes for Tooth Extraction in Patients under Bisphosphonate Therapy: A Case Report,” *Biomedicines*, vol. 7, no. 4, p. 89, Nov. 2019, doi: 10.3390/biomedicines7040089.
[244] C. Fernando de Almeida Barros Mourão *et al.*, “The use of Platelet-rich Fibrin in the management of medication-related osteonecrosis of the jaw: A case series,” *J Stomatol Oral Maxillofac Surg*, vol. 121, no. 1, pp. 84–89, 2020, doi: 10.1016/j.jormas.2019.02.011.
[245] M. C. Adornato, I. Morcos, and J. Rozanski, “The treatment of bisphosphonate-associated osteonecrosis of the jaws with bone resection and autologous platelet-derived growth factors,” *J. Am. Dent. Assoc.*, vol. 138, no. 7, pp. 971–977, 2007, doi: 10.14219/jada.archive.2007.0294.
[246] M. M. Curi *et al.*, “Treatment of Avascular Osteonecrosis of the Mandible in Cancer Patients With a History of Bisphosphonate Therapy by Combining Bone Resection and Autologous Platelet-Rich Plasma: Report of 3 Cases,” *J. Oral Maxillofac. Surg.*, vol. 65, no. 2, pp. 349–355, 2007, doi: 10.1016/j.joms.2005.12.051.
[247] S. S. Soydan DDS, PhD and S. Uckan DDS, PhD, “Management of Bisphosphonate-Related Osteonecrosis of the Jaw With a Platelet-Rich Fibrin Membrane: Technical Report,” *J Oral Maxillofac Surg*, vol. 72, no. 2, pp. 322–326, 2014, doi: 10.1016/j.joms.2013.07.027.
[248] J.-W. Kim, S.-J. Kim, and M.-R. Kim, “Leucocyte-rich and platelet-rich fibrin for the treatment of bisphosphonate-related osteonecrosis of the jaw: a prospective feasibility study,” *Br J Oral Maxillofac Surg*, vol. 52, no. 9, pp. 854–859, 2014, doi: 10.1016/j.bjoms.2014.07.256.
[249] O. Dincă *et al.*, “Clinical and histopathological studies using fibrin-rich plasma in the treatment of bisphosphonate-related osteonecrosis of the jaw,” *Rom. J. Morphol. Embryol.*, vol. 55, pp. 961–964, Oct. 2014.
[250] S. E. Nørholt and J. Hartlev, “Surgical treatment of osteonecrosis of the jaw with the use of platelet-rich fibrin: a prospective study of 15 patients,” *Int. J. Oral Maxillofac. Surg.*, vol. 45, no. 10, pp. 1256–1260, 2016, doi: 10.1016/j.ijom.2016.04.010.
[251] Z. B. Gönen and C. Yılmaz Asan, “Treatment of bisphosphonate-related osteonecrosis of the jaw using platelet-rich fibrin,” *Cranio*, vol. 35, no. 5, pp. 332–336, 2017.
[252] D. Steller, N. Herbst, R. Pries, D. Juhl, and S. G. Hakim, “Positive impact of Platelet-rich plasma and Platelet-rich fibrin on viability, migration and proliferation of osteoblasts and

fibroblasts treated with zoledronic acid," *Sci. Rep.*, vol. 9, no. 1, 2019, doi: 10.1038/s41598-019-43798-z.
[253] L. F. Toro *et al.*, "Application of Autologous Platelet-Rich Plasma on Tooth Extraction Site Prevents Occurence of Medication-Related Osteonecrosis of the Jaws in Rats," *Sci. Rep.*, vol. 9, no. 1, 2019, doi: 10.1038/s41598-018-37063-y.
[254] F. Sarkarat, M. H. K. Motamedi, J. Jahanbani, D. Sepehri, R. Kahali, and Z. Nematollahi, "Platelet-rich plasma in treatment of zoledronic acid-induced bisphosphonate-related osteonecrosis of the jaws," *Trauma Mon.*, vol. 19, no. 2, 2014, doi: 10.5812/traumamon.17196.
[255] F. S. Al-Hamed, M. Mahri, H. Al-Waeli, J. Torres, Z. Badran, and F. Tamimi, "Regenerative Effect of Platelet Concentrates in Oral and Craniofacial Regeneration," *Front. Cardiovasc. Med.*, vol. 6, no. August, p. 126, 2019, doi: 10.3389/fcvm.2019.00126.
[256] C. Kia, J. Baldino, R. Bell, A. Ramji, C. Uyeki, and A. Mazzocca, "Platelet-Rich Plasma: Review of Current Literature on its Use for Tendon and Ligament Pathology," *Curr Rev Musculoskelet Med*, vol. 11, no. 4, pp. 566–572, 2018, doi: 10.1007/s12178-018-9515-y.
[257] D. Kardos *et al.*, "Biological and mechanical properties of platelet-rich fibrin membranes after thermal manipulation and preparation in a single-syringe closed system," *Int J Mol Sci*, vol. 19, no. 11, p. 3433, Nov. 2018, doi: 10.3390/ijms19113433.
[258] D. M. Dohan Ehrenfest, L. Rasmusson, and T. Albrektsson, "Classification of platelet concentrates: from pure platelet-rich plasma (P-PRP) to leucocyte- and platelet-rich fibrin (L-PRF)," *Trends Biotechnol.*, vol. 27, no. 3, pp. 158–167, 2009, doi: 10.1016/j.tibtech.2008.11.009.
[259] T. Bielecki, D. M. Dohan Ehrenfest, P. A. Everts, and A. Wiczkowski, "The role of leukocytes from L-PRP/L-PRF in wound healing and immune defense: new perspectives.," *Curr. Pharm. Biotechnol.*, vol. 13, no. 7, pp. 1153–1162, Jun. 2012, doi: 10.2174/138920112800624373.
[260] D. M. Dohan Ehrenfest *et al.*, "Do the fibrin architecture and leukocyte content influence the growth factor release of platelet concentrates? An evidence-based answer comparing a pure platelet-rich plasma (P-PRP) gel and a leukocyte- and platelet-rich fibrin (L-PRF).," *Curr. Pharm. Biotechnol.*, vol. 13, no. 7, pp. 1145–1152, Jun. 2012, doi: 10.2174/138920112800624382.
[261] T. Kawase, "Platelet-rich plasma and its derivatives as promising bioactive materials for regenerative medicine: basic principles and concepts underlying recent advances," *Odontology*, vol. 103, no. 2, pp. 126–135, 2015, doi: 10.1007/s10266-015-0209-2.
[262] O. Ezzatt, "Autologous Platelet Concentrate Preparations in Dentistry," *Biomed. J. Sci. Tech. Res.*, vol. 8, Sep. 2018, doi: 10.26717/BJSTR.2018.08.001706.
[263] M. Cáceres, R. Hidalgo, A. Sanz, J. Martínez, P. Riera, and P. C. Smith, "Effect of Platelet-Rich Plasma on Cell Adhesion, Cell Migration, and Myofibroblastic Differentiation in Human Gingival Fibroblasts," *J Periodontol*, vol. 79, no. 4, pp. 714–720, 2008, doi: 10.1902/jop.2008.070395.
[264] K. Rattanasuwan, S. Rassameemasmaung, S. Kiattavorncharoen, A. Sirikulsathean, J. Thorsuwan, and W. Wongsankakorn, "Platelet-rich plasma stimulated proliferation, migration, and attachment of cultured periodontal ligament cells," *Eur J Dent*, vol. 12, no. 4, pp. 469–474, 2018, doi: 10.4103/ejd.ejd_255_17.
[265] E. Kobayashi *et al.*, "Effects of platelet rich plasma (PRP) on human gingival fibroblast, osteoblast and periodontal ligament cell behaviour," *BMC Oral Health*, vol. 17, no. 1, p. 91, 2017, doi: 10.1186/s12903-017-0381-6.
[266] P. A. Nguyen and T. A. V. Pham, "Effects of platelet-rich plasma on human gingival fibroblast proliferation and migration in vitro," *J Appl Oral Sci*, vol. 26, pp. e20180077–e20180077, 2018, doi: 10.1590/1678-7757-2018-0077.
[267] S. V. Khiste and R. Naik Tari, "Platelet-Rich Fibrin as a Biofuel for Tissue Regeneration," *ISRN*

Biomater., vol. 2013, 2013, doi: 10.5402/2013/627367.
[268] R. J. Miron, M. Fujioka-Kobayashi, M. Bishara, Y. Zhang, M. Hernandez, and J. Choukroun, "Platelet-Rich Fibrin and Soft Tissue Wound Healing: A Systematic Review," *Tissue Eng Part B Rev*, vol. 23, no. 1, pp. 83–99, 2017, doi: 10.1089/ten.teb.2016.0233.
[269] R. Landesberg *et al.*, "Activation of platelet-rich plasma using thrombin receptor agonist peptide," *J Oral Maxillofac Surg*, vol. 63, no. 4, pp. 529–535, 2005, doi: 10.1016/j.joms.2004.12.007.
[270] J. CHOUKROUN *et al.*, "Platelet-rich fibrin (PRF) : A second-generation platelet concentrate. Part V: Histologic evaluations of PRF effects on bone allograft maturation in sinus lift," *Oral Surg Oral Med Oral Pathol Oral Radiol Endod*, vol. 101, no. 3, pp. 299–303, 2006, doi: 10.1016/j.tripleo.2005.07.012.
[271] R. J. Miron, J. Chai, S. Zheng, M. Feng, A. Sculean, and Y. Zhang, "A novel method for evaluating and quantifying cell types in platelet rich fibrin and an introduction to horizontal centrifugation," *J. Biomed. Mater. Res. - Part A*, vol. 107, no. 10, 2019, doi: 10.1002/jbm.a.36734.
[272] G. Kasnak *et al.*, "Regulatory effects of PRF and titanium surfaces on cellular adhesion, spread, and cytokine expressions of gingival keratinocytes," *Histochem Cell Biol*, vol. 152, no. 1, pp. 63–73, 2019, doi: 10.1007/s00418-019-01774-8.
[273] F.-J. Strauss, J. Nasirzade, Z. Kargarpoor, A. Staehli, and R. Gruber, "Effect of platelet-rich fibrin on cell proliferation, migration, differentiation, inflammation, and osteoclastogenesis: a systematic review of in vitro studies," *Clin Oral Investig*, vol. 24, no. 2, pp. 569–584, 2020, doi: 10.1007/s00784-019-03156-9.
[274] R. J. Miron *et al.*, "Injectable platelet rich fibrin (i-PRF): opportunities in regenerative dentistry?," *Clin. Oral Investig.*, vol. 21, no. 8, 2017, doi: 10.1007/s00784-017-2063-9.
[275] X. Wang, Y. Yang, Y. Zhang, and R. J. Miron, "Fluid platelet-rich fibrin stimulates greater dermal skin fibroblast cell migration, proliferation, and collagen synthesis when compared to platelet-rich plasma," *J. Cosmet. Dermatol.*, vol. 18, no. 6, 2019, doi: 10.1111/jocd.12955.
[276] V. Pavlovic, M. Ciric, V. Jovanovic, M. Trandafilovic, and P. Stojanovic, "Platelet-rich fibrin: Basics of biological actions and protocol modifications.," *Open Med. (Warsaw, Poland)*, vol. 16, no. 1, pp. 446–454, 2021, doi: 10.1515/med-2021-0259.
[277] E. Kobayashi *et al.*, "Comparative release of growth factors from PRP, PRF, and advanced-PRF," *Clin Oral Investig*, vol. 20, no. 9, pp. 2353–2360, 2016, doi: 10.1007/s00784-016-1719-1.
[278] M. Fujioka-Kobayashi *et al.*, "Improved growth factor delivery and cellular activity using concentrated platelet-rich fibrin (C-PRF) when compared with traditional injectable (i-PRF) protocols," *Clin. Oral Investig.*, vol. 24, no. 12, 2020, doi: 10.1007/s00784-020-03303-7.
[279] R. J. Miron and Y. Zhang, "Autologous liquid platelet rich fibrin: A novel drug delivery system," *Acta Biomater*, vol. 75, pp. 35–51, 2018, doi: 10.1016/j.actbio.2018.05.021.
[280] D. M. Dohan Ehrenfest *et al.*, "The impact of the centrifuge characteristics and centrifugation protocols on the cells, growth factors, and fibrin architecture of a leukocyte- and platelet-rich fibrin (L-PRF) clot and membrane," *Platelets*, vol. 29, no. 2, pp. 171–184, 2018, doi: 10.1080/09537104.2017.1293812.
[281] T. Burnouf *et al.*, "Human blood-derived fibrin releasates: Composition and use for the culture of cell lines and human primary cells," *Biologicals*, vol. 40, no. 1, pp. 21–30, 2012, doi: 10.1016/j.biologicals.2011.09.017.
[282] S. Vahabi, S. Vaziri, M. Torshabi, and Z. Rezaei Esfahrood, "Effects of Plasma Rich in Growth Factors and Platelet-Rich Fibrin on Proliferation and Viability of Human Gingival Fibroblasts.," *J. Dent. (Tehran).*, vol. 12, no. 7, 2015.
[283] M. Fujioka-Kobayashi, R. J. Miron, M. Hernandez, U. Kandalam, Y. Zhang, and J. Choukroun, "Optimized Platelet-Rich Fibrin With the Low-Speed Concept: Growth Factor Release, Biocompatibility, and Cellular Response," *J. Periodontol.*, vol. 88, no. 1, 2017, doi:

10.1902/jop.2016.160443.
[284] L. Pitzurra, I. D. C. Jansen, T. J. Vries, M. A. Hoogenkamp, and B. G. Loos, “Effects of L-PRF and A-PRF+ on periodontal fibroblasts in in vitro wound healing experiments,” *J Periodontal Res*, vol. 55, no. 2, pp. 287–295, 2020, doi: 10.1111/jre.12714.
[285] X. Wang, Y. Zhang, J. Choukroun, S. Ghanaati, R. J. Miron, and J. R. Miron, “Behavior of Gingival Fibroblasts on Titanium Implant Surfaces in Combination with either Injectable-PRF or PRP,” *Int. J. Mol. Sci.*, vol. 18, no. 2, p. 331, 2017, doi: 10.3390/ijms18020331.
[286] A. A. Danastri, S. Suryono, and K. Murdiastuti, “THE INFLUENCE BETWEEN INJECTABLE PLATELET-RICH FIBRIN AND PLATELET-RICH PLASMA TOWARDS GINGIVAL FIBROBLAST CELL PROLIFERATION,” *ODONTO Dent. J.*, vol. 8, no. 2, p. 25, 2021, doi: 10.30659/odj.8.2.25-31.
[287] R. Narayanaswamy *et al.*, “Evolution and Clinical Advances of Platelet-Rich Fibrin in Musculoskeletal Regeneration,” *Bioeng.*, vol. 10, no. 1, p. 58, 2023, doi: 10.3390/bioengineering10010058.
[288] S. Ghanaati *et al.*, “Advanced Platelet-Rich Fibrin: A New Concept for Cell-Based Tissue Engineering by Means of Inflammatory Cells,” *J. Oral Implantol.*, vol. 40, no. 6, pp. 679–689, Dec. 2014, doi: 10.1563/aaid-joi-D-14-00138.
[289] M. Simões-Pedro, P. M. B. P. S. Tróia, N. B. M. Dos Santos, A. M. G. Completo, R. M. Castilho, and G. V. de Oliveira Fernandes, “Tensile Strength Essay Comparing Three Different Platelet-Rich Fibrin Membranes (L-PRF, A-PRF, and A-PRF+): A Mechanical and Structural In Vitro Evaluation.,” *Polymers (Basel).*, vol. 14, no. 7, Mar. 2022, doi: 10.3390/polym14071392.
[290] S. Ravi and M. Santhanakrishnan, “Mechanical, chemical, structural analysis and comparative release of PDGF-AA from L-PRF, A-PRF and T-PRF - an in vitro study.,” *Biomater. Res.*, vol. 24, p. 16, 2020, doi: 10.1186/s40824-020-00193-4.
[291] J. Choukroun and S. Ghanaati, “Reduction of relative centrifugation force within injectable platelet-rich-fibrin (PRF) concentrates advances patients’ own inflammatory cells, platelets and growth factors: the first introduction to the low speed centrifugation concept,” *Eur. J. Trauma Emerg. Surg.*, vol. 44, no. 1, 2018, doi: 10.1007/s00068-017-0767-9.
[292] S. Wend *et al.*, “Reduction of the relative centrifugal force influences cell number and growth factor release within injectable PRF-based matrices,” *J Mater Sci Mater Med*, vol. 28, no. 12, pp. 1–11, 2017, doi: 10.1007/s10856-017-5992-6.
[293] S. Al-Maawi *et al.*, “Biologization of collagen-based biomaterials using liquid-platelet-rich fibrin: New insights into clinically applicable tissue engineering,” *Materials (Basel).*, vol. 12, no. 23, 2019, doi: 10.3390/ma12233993.
[294] P. Thanasrisuebwong, S. Kiattavorncharoen, R. Surarit, C. Phruksaniyom, and N. Ruangsawasdi, “Red and yellow injectable platelet-rich fibrin demonstrated differential effects on periodontal ligament stem cell proliferation, migration, and osteogenic differentiation,” *Int. J. Mol. Sci.*, vol. 21, no. 14, 2020, doi: 10.3390/ijms21145153.
[295] M. de A. N. C. Pascoal, N. B. M. Dos Santos, A. M. G. Completo, and G. V. de O. Fernandes, “Tensile strength assay comparing the resistance between two different autologous platelet concentrates (leucocyte-platelet rich fibrin versus advanced-platelet rich fibrin): a pilot study.,” *Int. J. Implant Dent.*, vol. 7, no. 1, p. 1, Jan. 2021, doi: 10.1186/s40729-020-00284-w.
[296] S. Dashore, K. Chouhan, S. Nanda, and A. Sharma, “Preparation of platelet-rich plasma: National IADVL PRP taskforce recommendations,” *Indian Dermatol Online J*, vol. 12, no. 7, pp. 12–23, 2021, doi: 10.4103/idoj.idoj_269_21.
[297] A. Giudice, A. Antonelli, D. Muraca, and L. Fortunato, “Usefulness of advanced-platelet rich fibrin (A-PRF) and injectable-platelet rich fibrin (i-PRF) in the management of a massive medication-related osteonecrosis of the jaw (MRONJ): A 5-years follow-up case report,” *Indian J. Dent. Res.*, vol. 31, no. 5, pp. 813–818, 2020, doi: 10.4103/ijdr.IJDR_689_19.

[298] B. Law, H. Y. Soh, S. Nabil, R. K. Rajandram, A. J. Nazimi, and R. Ramli, “Autologous platelet-rich fibrin (Prf) as an adjunct in the management of osteoradionecrosis and medication-related osteonecrosis of jaws. case series in a single centre,” *Appl. Sci.*, vol. 11, no. 8, p. 3365, 2021, doi: 10.3390/app11083365.
[299] R. A. Miksad *et al.*, “Quality of life implications of bisphosphonate-associated osteonecrosis of the jaw,” *Oncologist*, vol. 16, no. 1, pp. 121–132, 2011, doi: 10.1634/theoncologist.2010-0183.
[300] R. E. Marx, “Pamidronate (Aredia) and zoledronate (Zometa) induced avascular necrosis of the jaws: a growing epidemic,” *J Oral Maxillofac Surg*, vol. 61, no. 9, pp. 1115–1117, 2003, doi: 10.1016/s0278-2391(03)00720-1.
[301] M. Scheper, R. Chaisuparat, K. Cullen, and T. Meiller, “A novel soft-tissue in vitro model for bisphosphonate-associated osteonecrosis,” *Fibrogenes. Tissue Repair*, vol. 3, p. 6, 2010, doi: 10.1186/1755-1536-3-6.
[302] W. Singhatanadgit, W. Hankamolsiri, and W. Janvikul, “Geranylgeraniol prevents zoledronic acid-mediated reduction of viable mesenchymal stem cells via induction of Rho-dependent YAP activation,” *R. Soc. Open Sci.*, vol. 8, no. 6, p. 202066, Aug. 2021, doi: 10.1098/rsos.202066.
[303] Y. Takeda *et al.*, “Geranylgeraniol, an Intermediate Product in Mevalonate Pathway, Induces Apoptotic Cell Death in Human Hepatoma Cells: Death Receptor-independent Activation of Caspase-8 with Down-regulation of Bcl-xL Expression,” *Jpn J Cancer Res*, vol. 92, no. 9, pp. 918–925, 2001, doi: 10.1111/j.1349-7006.2001.tb01181.x.
[304] N. Fernandes *et al.*, “Geranylgeraniol suppresses the viability of human DU145 prostate carcinoma cells and the level of HMG CoA reductase,” *Exp. Biol. Med. (Maywood).*, vol. 238, Sep. 2013, doi: 10.1177/1535370213492693.
[305] N. Yoshikawa *et al.*, “Plaunotol and Geranylgeraniol Induce Caspase-Mediated Apoptosis in Colon Cancer,” *J. Surg. Res.*, vol. 153, no. 2, pp. 246–253, May 2009, doi: 10.1016/j.jss.2008.04.021.
[306] A. Jaśkiewicz, B. Pająk, A. Litwiniuk, K. Urbańska, and A. Orzechowski, “Geranylgeraniol Prevents Statin-Dependent Myotoxicity in C2C12 Muscle Cells through RAP1 GTPase Prenylation and Cytoprotective Autophagy,” *Oxid. Med. Cell. Longev.*, vol. 2018, p. 6463807, 2018, doi: 10.1155/2018/6463807.
[307] A. M. Wojtowicz, S. Oliveira, M. W. Carlson, A. Zawadzka, C. F. Rousseau, and D. Baksh, “The importance of both fibroblasts and keratinocytes in a bilayered living cellular construct used in wound healing,” *Wound Repair Regen.*, vol. 22, no. 2, pp. 246–255, Mar. 2014, doi: https://doi.org/10.1111/wrr.12154.
[308] A. Van Tonder, A. M. Joubert, and A. D. Cromarty, “Limitations of the 3-(4,5-dimethylthiazol-2-yl)-2,5-diphenyl-2H-tetrazolium bromide (MTT) assay when compared to three commonly used cell enumeration assays,” *BMC Res. Notes*, vol. 8, no. 1, 2015, doi: 10.1186/s13104-015-1000-8.
[309] N. W. C. J. van de Donk, H. M. Lokhorst, E. H. J. Nijhuis, M. M. J. Kamphuis, and A. C. Bloem, “Geranylgeranylated Proteins are Involved in the Regulation of Myeloma Cell Growth,” *Clin. Cancer Res.*, vol. 11, no. 2, pp. 429 LP – 439, Jan. 2005, [Online]. Available: http://clincancerres.aacrjournals.org/content/11/2/429.abstract
[310] R. J. Miron, J. Chai, M. Fujioka-Kobayashi, A. Sculean, and Y. Zhang, “Evaluation of 24 protocols for the production of platelet-rich fibrin,” *BMC Oral Health*, vol. 20, no. 1, p. 310, 2020, doi: 10.1186/s12903-020-01299-w.
[311] G. Serafini *et al.*, “Platelet Rich Fibrin (PRF) and Its Related Products: Biomolecular Characterization of the Liquid Fibrinogen,” *J. Clin. Med.*, vol. 9, no. 4, 2020, doi: 10.3390/jcm9041099.
[312] N. Farshidfar *et al.*, “The application of injectable platelet-rich fibrin in regenerative

dentistry: A systematic scoping review of In vitro and In vivo studies," *Jpn Dent Sci Rev*, vol. 58, pp. 89–123, 2022, doi: 10.1016/j.jdsr.2022.02.003.
[313] T. Scholzen and J. Gerdes, "The Ki-67 protein: From the known and the unknown," *J. Cell. Physiol*, vol. 182, no. 3, pp. 311–322, 2000, doi: 10.1002/(SICI)1097-4652(200003)182:3<311::AID-JCP1>3.0.CO.
[314] S. S. Birajdar, M. Radhika, K. Paremala, M. Sudhakara, M. Soumya, and M. Gadivan, "Expression of Ki-67 in normal oral epithelium, leukoplakic oral epithelium and oral squamous cell carcinoma," *J Oral Maxillofac Pathol*, vol. 18, no. 2, pp. 169–176, 2014, doi: 10.4103/0973-029X.140729.
[315] V. M. C. Quent, D. Loessner, T. Friis, J. C. Reichert, and D. W. Hutmacher, "Discrepancies between metabolic activity and DNA content as tool to assess cell proliferation in cancer research," *J Cell Mol Med*, vol. 14, no. 4, pp. 1003–1013, 2010, doi: 10.1111/j.1582-4934.2010.01013.x.
[316] M. Roederer, "Interpretation of cellular proliferation data: Avoid the panglossian," *Cytom. A*, vol. 79A, no. 2, pp. 95–101, 2011, doi: 10.1002/cyto.a.21010.
[317] K. I. Hulkower and R. L. Herber, "Cell Migration and Invasion Assays as Tools for Drug Discovery," *Pharmaceutics*, vol. 3, no. 1, pp. 107–124, Mar. 2011, doi: 10.3390/pharmaceutics3010107.
[318] Q.-M. Zhou, X.-F. Wang, X.-J. Liu, H. Zhang, Y.-Y. Lu, and S.-B. Su, "Curcumin enhanced antiproliferative effect of mitomycin C in human breast cancer MCF-7 cells in vitro and in vivo," *Acta Pharmacol. Sin.*, vol. 32, no. 11, pp. 1402–1410, 2011, doi: 10.1038/aps.2011.97.
[319] D. Y. Lee *et al.*, "Review of the Current Research on Fetal Bovine Serum and the Development of Cultured Meat," *Food Sci. Anim. Resour.*, vol. 42, no. 5, pp. 775–799, 2022, doi: 10.5851/kosfa.2022.e46.
[320] T. Kawase *et al.*, "Platelet-rich fibrin extract: A promising fetal bovine serum alternative in explant cultures of human periosteal sheets for regenerative therapy," *Int J Mol Sci*, vol. 20, no. 5, p. 1053, 2019, doi: 10.3390/ijms20051053.
[321] M. A. Saeed, M. A. El-Rahman, M. E. Helal, A. R. Zaher, and M. E. Grawish, "Efficacy of human platelet rich fibrin exudate vs fetal bovine serum on proliferation and differentiation of dental pulp stem cells," *Int J Stem Cells*, vol. 10, no. 1, pp. 38–47, 2017, doi: 10.15283/ijsc16067.
[322] W. Albatal, T. Qasem, and Y. A. Tolibah, "Evaluation of the Effect of Injectable Platelet-rich Fibrin on Palatal Wound Healing: A Two-arm Randomized Controlled Clinical Trial," *J. Contemp. Dent. Pract.*, vol. 24, no. 4, pp. 214–220, 2023, doi: 10.5005/jp-journals-10024-3496.
[323] A. Sharma *et al.*, "Influence of platelet-rich fibrin on wound healing and bone regeneration after tooth extraction: A clinical and radiographic study," *J Oral Biol Craniofac Res*, vol. 10, no. 4, pp. 385–390, 2020, doi: 10.1016/j.jobcr.2020.06.012.
[324] G. Ustaoğlu, D. Göller Bulut, and K. Ç. Gümüş, "Evaluation of different platelet-rich concentrates effects on early soft tissue healing and socket preservation after tooth extraction," *J. Stomatol. oral Maxillofac. Surg.*, vol. 121, no. 5, pp. 539–544, 2020, doi: 10.1016/j.jormas.2019.09.005.
[325] C. F. de Almeida Barros Mourão, R. C. de Mello-Machado, K. Javid, and V. Moraschini, "The use of leukocyte- and platelet-rich fibrin in the management of soft tissue healing and pain in post-extraction sockets: A randomized clinical trial," *J Craniomaxillofac Surg*, vol. 48, no. 4, pp. 452–457, 2020, doi: 10.1016/j.jcms.2020.02.020.
[326] G. Nicoletti, M. Saler, L. Villani, A. Rumolo, M. M. Tresoldi, and A. Faga, "Platelet Rich Plasma Enhancement of Skin Regeneration in an ex-vivo Human Experimental Model," *Front Bioeng Biotechnol*, vol. 7, p. 2, 2019, doi: 10.3389/fbioe.2019.00002.
[327] P. Thanasrisuebwong, R. Surarit, S. Bencharit, and N. Ruangsawasdi, "Influence of

fractionation methods on physical and biological properties of injectable platelet-rich fibrin: An exploratory study," *Int. J. Mol. Sci.*, vol. 20, no. 7, 2019, doi: 10.3390/ijms20071657.
[328] S. A. Eming, T. Krieg, and J. M. Davidson, "Inflammation in Wound Repair: Molecular and Cellular Mechanisms," *J. Invest. Dermatol.*, vol. 127, no. 3, pp. 514–525, 2007, doi: https://doi.org/10.1038/sj.jid.5700701.
[329] P. Everts, K. Onishi, P. Jayaram, J. F. Lana, and K. Mautner, "Platelet-Rich Plasma: New Performance Understandings and Therapeutic Considerations in 2020," *Int J Mol Sci*, vol. 21, no. 20, p. 7794, 2020, doi: 10.3390/ijms21207794.
[330] G. Eren, A. Gürkan, H. Atmaca, A. Dönmez, and G. Atilla, "Effect of centrifugation time on growth factor and MMP release of an experimental platelet-rich fibrin-type product," *Platelets*, vol. 27, no. 5, pp. 427–432, 2016, doi: 10.3109/09537104.2015.1131253.
[331] L. Hermida-Nogueira *et al.*, "Deciphering the secretome of leukocyte-platelet rich fibrin: towards a better understanding of its wound healing properties," *Sci Rep*, vol. 10, no. 1, p. 14571, 2020, doi: 10.1038/s41598-020-71419-7.
[332] R. E. Roberts, J. Cavalcante-Silva, R. D. Kineman, and T. J. Koh, "Liver is a primary source of insulin-like growth factor-1 in skin wound healing," *J Endocrinol*, vol. 252, no. 1, pp. 59–70, 2021, doi: 10.1530/JOE-21-0298.
[333] H. A. Varela *et al.*, "Injectable platelet rich fibrin: cell content, morphological, and protein characterization," *Clin Oral Investig*, vol. 23, no. 3, pp. 1309–1318, 2019, doi: 10.1007/s00784-018-2555-2.
[334] T. Fernández-Medina, C. Vaquette, and S. Ivanovski, "Systematic Comparison of the Effect of Four Clinical-Grade Platelet Rich Hemoderivatives on Osteoblast Behaviour," *Int J Mol Sci*, vol. 20, no. 24, p. 6243, 2019, doi: 10.3390/ijms20246243.
[335] A. Ridiandries, J. T. M. Tan, and C. A. Bursill, "The Role of Chemokines in Wound Healing.," *Int. J. Mol. Sci.*, vol. 19, no. 10, Oct. 2018, doi: 10.3390/ijms19103217.
[336] R. Sabat *et al.*, "Biology of interleukin-10," *Cytokine Growth Factor Rev.*, vol. 21, no. 5, pp. 331–344, 2010, doi: 10.1016/j.cytogfr.2010.09.002.
[337] W. E. N. G. JIANG, A. J. SANDERS, F. RUGE, and K. G. HARDING, "Influence of interleukin-8 (IL-8) and IL-8 receptors on the migration of human keratinocytes, the role of PLC-γ and potential clinical implications," *Exp Ther Med*, vol. 3, no. 2, pp. 231–236, 2012, doi: 10.3892/etm.2011.402.
[338] M. Akdis MD, PhD *et al.*, "Interleukins (from IL-1 to IL-38), interferons, transforming growth factor β, and TNF-α: Receptors, functions, and roles in diseases," *J Allergy Clin Immunol*, vol. 138, no. 4, pp. 984–1010, 2016, doi: 10.1016/j.jaci.2016.06.033.
[339] K. L. Kroeze, M. A. Boink, S. C. Sampat-Sardjoepersad, T. Waaijman, R. J. Scheper, and S. Gibbs, "Autocrine regulation of re-epithelialization after wounding by chemokine receptors CCR1, CCR10, CXCR1, CXCR2, and CXCR3.," *J. Invest. Dermatol.*, vol. 132, no. 1, pp. 216–225, Jan. 2012, doi: 10.1038/jid.2011.245.
[340] J. Steude, R. Kulke, and E. Christophers, "Interleukin-1-stimulated secretion of interleukin-8 and growth-related oncogene-alpha demonstrates greatly enhanced keratinocyte growth in human raft cultured epidermis.," *J. Invest. Dermatol.*, vol. 119, no. 6, pp. 1254–1260, Dec. 2002, doi: 10.1046/j.1523-1747.2002.19616.x.
[341] S. A. Khurram, L. Bingle, B. M. McCabe, P. M. Farthing, and S. A. Whawell, "The chemokine receptors CXCR1 and CXCR2 regulate oral cancer cell behaviour.," *J. oral Pathol. Med. Off. Publ. Int. Assoc. Oral Pathol. Am. Acad. Oral Pathol.*, vol. 43, no. 9, pp. 667–674, Oct. 2014, doi: 10.1111/jop.12191.
[342] A. King, S. Balaji, L. D. Le, T. M. Crombleholme, and S. G. Keswani, "Regenerative Wound Healing: The Role of Interleukin-10.," *Advances in wound care*, vol. 3, no. 4. United States, pp. 315–323, Apr. 2014. doi: 10.1089/wound.2013.0461.
[343] J. K. Nguyen, E. Austin, A. Huang, A. Mamalis, and J. Jagdeo, "The IL-4/IL-13 axis in skin

fibrosis and scarring: mechanistic concepts and therapeutic targets," *Arch Dermatol Res*, vol. 312, no. 2, pp. 81–92, 2020, doi: 10.1007/s00403-019-01972-3.
[344] S. Shibata *et al.*, "Adiponectin regulates cutaneous wound healing by promoting keratinocyte proliferation and migration via the ERK signaling pathway," *J Immunol*, vol. 189, no. 6, pp. 3231–3241, 2012, doi: 10.4049/jimmunol.1101739.
[345] O. G. Rossler and G. Thiel, "Brain-derived neurotrophic factor-, epidermal growth factor-, or A-Raf-induced growth of HaCaT keratinocytes requires extracellular signal-regulated kinase," *Am J Physiol Cell Physiol*, vol. 286, no. 5, pp. 1118–1129, 2004, doi: 10.1152/ajpcell.00301.2003.
[346] C. R. Rho, M. Park, and S. Kang, "Effects of Granulocyte-Macrophage Colony-Stimulating (GM-CSF) Factor on Corneal Epithelial Cells in Corneal Wound Healing Model," *PLoS One*, vol. 10, no. 9, pp. e0138020–e0138020, 2015, doi: 10.1371/journal.pone.0138020.
[347] Z. Wang, Y. Wang, N. Bradbury, C. Gonzales Bravo, B. Schnabl, and A. Di Nardo, "Skin wound closure delay in metabolic syndrome correlates with SCF deficiency in keratinocytes," *Sci Rep*, vol. 10, no. 1, p. 21732, 2020, doi: 10.1038/s41598-020-78244-y.
[348] F. Tortelli, M. Pisano, P. S. Briquez, M. M. Martino, and J. A. Hubbell, "Fibronectin binding modulates CXCL11 activity and facilitates wound healing.," *PLoS One*, vol. 8, no. 10, p. e79610, 2013, doi: 10.1371/journal.pone.0079610.
[349] L. M. Cucci, C. Satriano, T. Marzo, and D. La Mendola, "Angiogenin and Copper Crossing in Wound Healing," *Int. J. Mol. Sci.*, vol. 22, no. 19, p. 10704, 2021, doi: 10.3390/ijms221910704.
[350] J. Wang, L. Yang, J. You, D. Wen, B. Yang, and C. Jiang, "Platelet-Derived Growth Factor Regulates the Biological Behavior of Oral Mucosal Fibroblasts by Inducing Cell Autophagy and Its Mechanism," *J. Inflamm. Res.*, vol. 14, pp. 3405–3417, 2021, doi: 10.2147/JIR.S313910.
[351] M. Morikawa, R. Derynck, and K. Miyazono, "TGF-β and the TGF-β Family: Context-Dependent Roles in Cell and Tissue Physiology," *Cold Spring Harb Perspect Biol*, vol. 8, no. 5, p. a021873, 2016, doi: 10.1101/cshperspect.a021873.
[352] H.-W. Jeong and I.-S. Kim, "TGF-β1 enhances βig-h3-mediated keratinocyte cell migration through the α3β1 integrin and PI3K," *J. Cell. Biochem*, vol. 92, no. 4, pp. 770–780, 2004, doi: 10.1002/jcb.20110.
[353] A. I. Bracher, N. Vig, J.-P. Burkhard, B. Schaller, and F. Schlittler, "The application of platelet rich fibrin in patients presenting with osteonecrosis of the jaw: A systematic literature review," *Adv. Oral Maxillofac. Surg.*, vol. 2, p. 100076, 2021, doi: https://doi.org/10.1016/j.adoms.2021.100076.
[354] C. Lebon, G. V. Rodriguez, I. El Zaoui, I. Jaadane, F. Behar-Cohen, and A. Torriglia, "On the use of an appropriate TdT-mediated dUTP-biotin nick end labeling assay to identify apoptotic cells.," *Anal. Biochem.*, vol. 480, pp. 37–41, Jul. 2015, doi: 10.1016/j.ab.2015.04.007.
[355] Z. Zhao *et al.*, "Zoledronate inhibits fibroblasts' proliferation and activation via targeting TGF-β signaling pathway," *Drug Des Devel Ther*, vol. 12, pp. 3021–3031, 2018, doi: 10.2147/DDDT.S168897.
[356] T. Pansani, L. Cardoso, L. Augusto, I. Ribeiro, C. Costa, and F. Basso, "Effects of EGF-coated titanium surfaces on adhesion and metabolism of bisphosphonate-treated human keratinocytes and gingival fibroblasts," *Clin. Oral Investig.*, vol. 25, pp. 1–10, Oct. 2021, doi: 10.1007/s00784-021-03880-1.
[357] D. Steller, R. Simon, R. Von Bialy, S. G. Hakim, and R. Pries, "Impact of Zoledronic Acid and Denosumab Treatment on Growth Factor Concentration in Platelet Rich Fibrin of Patients With Osteolytic Bone Metastases.," *Anticancer Res.*, vol. 41, no. 8, pp. 3917–3923, Aug. 2021, doi: 10.21873/anticanres.15187.
[358] S. Liarte, Á. Bernabé-García, and F. J. Nicolás, "Role of TGF-β in Skin Chronic Wounds: A

Keratinocyte Perspective.," *Cells*, vol. 9, no. 2, Jan. 2020, doi: 10.3390/cells9020306.
[359] Y. Fukaya *et al.*, "Platelet-rich plasma inhibits the apoptosis of highly adipogenic homogeneous preadipocytes in an in vitro culture system," *Exp Mol Med*, vol. 44, no. 5, pp. 330–339, 2012, doi: 10.3858/emm.2012.44.5.037.
[360] E. M. Vasina *et al.*, "Aging- and activation-induced platelet microparticles suppress apoptosis in monocytic cells and differentially signal to proinflammatory mediator release," *Am J Blood Res*, vol. 3, no. 2, pp. 107–123, 2013.
[361] E. Dohle, K. El Bagdadi, R. Sader, J. Choukroun, C. James Kirkpatrick, and S. Ghanaati, "Platelet-rich fibrin-based matrices to improve angiogenesis in an in vitro co-culture model for bone tissue engineering," *J Tissue Eng Regen Med*, vol. 12, no. 3, pp. 598–610, 2018, doi: 10.1002/term.2475.
[362] M. Morita *et al.*, "Elevation of pro-inflammatory cytokine levels following anti-resorptive drug treatment is required for osteonecrosis development in infectious osteomyelitis," *Sci Rep*, vol. 7, no. 1, p. 46322, 2017, doi: 10.1038/srep46322.
[363] Z. Wang *et al.*, "The Effects of Leukocyte-Platelet Rich Fibrin (L-PRF) on Suppression of the Expressions of the Pro-Inflammatory Cytokines, and Proliferation of Schwann Cell, and Neurotrophic Factors," *Sci Rep*, vol. 10, no. 1, p. 2421, 2020, doi: 10.1038/s41598-020-59319-2.
[364] F. Tabatabaei, M. Rasoulianboroujeni, A. Yadegari, S. Tajik, K. Moharamzadeh, and L. Tayebi, "Osteo-mucosal engineered construct: In situ adhesion of hard-soft tissues," *Mater. Sci. Eng. C*, vol. 128, p. 112255, 2021, doi: 10.1016/j.msec.2021.112255.
[365] B. Ollington, H. E. Colley, and C. Murdoch, "Immunoresponsive Tissue-Engineered Oral Mucosal Equivalents Containing Macrophages," *Tissue Eng. Part C. Methods*, vol. 27, no. 8, pp. 462–471, 2021, doi: 10.1089/ten.tec.2021.0124.
[366] S. E. Udeabor, C. Herrera-Vizcaíno, R. Sader, C. J. Kirkpatrick, S. Al-Maawi, and S. Ghanaati, "Characterization of the cellular reaction to a collagen-based matrix: An in vivo histological and histomorphometrical analysis," *Materials (Basel).*, vol. 13, no. 12, 2020, doi: 10.3390/ma13122730.